Author:
Attard, Sean-Paul

Title:
The Use of Auxetic Laminates as a Construction Material

A study on the behaviour of confined concrete columns using Prepreg CFRP Auxetic Jackets

The Use of Auxetic Laminates as a Construction Material

A study on the behaviour of confined concrete columns using Prepreg CFRP Auxetic Jackets

By

Sean-Paul Attard

Advanced Composites Collaboration for Innovation and Science (ACCIS),
UNIVERSITY OF BRISTOL

A dissertation submitted to the University of Bristol in accordance with the requirements of the degree of DOCTOR OF PHILOSOPHY in the Faculty of Engineering

July 2018

Abstract

The increasing use of Fibre Reinforced Plastics (FRPs) as retrofitting or repairing materials to structural elements, has led to advances in the development of in-situ techniques allowing flexibility in the application and choice of FRP type using either pre-impregnated resin or manually impregnating epoxy resin into the FRP laminae. Extensive work was carried out on reinforced concrete columns where FRP jackets, when wound around the surface of the columns, enhance the strength and ductility of these columns. Developments have shown that FRP laminates with particular stacking sequences exhibit auxetic behaviour. This was noted to occur in symmetric balanced angle-ply laminates, particularly with angles varying between 20° and 25°, where a negative Poisson's ratio (NPR) was discovered to be either negative in-plane or through-thickness Poisson's ratio.

In this research study, design oriented and analysis oriented confinement models were used to examine the behaviour of confinement jackets. These results were compared to compression tests carried out using a Force Control mechanism at a rate of 1kN/s. The SE70 CFRP prepreg, having a curing temperature of 70°C for 16 hours, was used for manufacturing the jackets using the conventional vacuum bagging system. The $[\pm 20]_{2s}$ and $[\pm 25]_{2s}$ configurations were chosen to inspect auxetic behaviour. To provide a suitable means of comparison to the auxetic jackets, other stacking sequences were tested, more precisely $[\pm 35,0_2]_s$ and $[\pm 16,\pm 45]_s$, that have the same Young's modulus as the auxetic laminates tested, yet with a different Poisson's ratio value. Confinement jackets holding the maximum and minimum Young's modulus of elasticity respectively i.e. $[0_8]$ and $[90_8]$, were also examined. All confinement jackets, except $[90_8]$, failed in an explosive manner. From the experimental tests, it was deduced that the auxetic confinement jackets performed best. This resulted due to the improved fracture toughness and increase in energy storage instigated by the through thickness expansion that were achieved with the presence of a negative Poisson's ratio, that in turn contributed in enhancing the strength of a confined concrete column. In fact, the auxetic stacking sequence $[\pm 20]_{2s}$ having NPR value of -0.403 and mean value failure stress of 148.24MPa showed gains of 387% in terms of compressive strength when compared with the control concrete cylinder. Similarly, a 351% gain was obtained for the auxetic stacking sequence $[\pm 25]_{2s}$ having NPR value of -0.468, and a mean value failure stress of 134.15MPa.

To my parents and
grandmother

First of all, I would like to express my special appreciation to Prof. Fabrizio Scarpa my principal supervisor, for his support throughout the past years, unreserved sharing of knowledge and availability.

My sincere gratitude also goes to Dr. Wendel Sebastian my co-supervisor, who has been available with his replies to my questions.

I have found great support from the Technical staff at the Aerospace Engineering and civil engineering Laboratory especially Mr. Ian Chorley, the composites technician, Mr. Peter Whereat Faculty Research Technician, Mr. Guy Pearn – Senior Engineering Research Technician and Mr. Dave Cooper, for their great assistance.

MGSS (Maltese Government Scholarship Scheme) for granting me a scholarship and partly financing my studies fees.

Sincere thanks go also to all my close friends for their constant encouragement, availability and support. My thanks go to Dr. Marc Bonello, Professor Duncan Camilleri, Dr. Nicholas De Battista, Dr. Svetlana Sammut, Petra Sapiano and Mario Pirotta.

Last but definitely not least, I thank my family without whom, this long journey would not have been possible – for supporting me during all this time and for their constant encouragement in all my pursuits. I can never thank you enough.

Declaration

I, Sean-Paul Attard, declare that the work in this dissertation was carried out in accordance with the requirements of the University's Regulations and Code of Practice for Research Degree Programmes and that it has not been submitted for any other academic award. Except where indicated by specific reference in the text, the work is the candidate's own work. Work done in collaboration with, or with the assistance of, others, is indicated as such. Any views expressed in the dissertation are those of the author.

SIGNED: DATE: 27th July 2018

Contents:

List of Figures

List of Tables

Abbreviations

CCFT – Confined concrete filled tube;

CFRP – Carbon Fibre Reinforced Polymer;

CLT – Classical Laminate Theory;

CM – Confinement Model;

FRP – Fibre Reinforced Polymer;

GFRP – Glass Fibre Reinforced Polymer;

MD – multiple directional laminae;

NPR – Negative Poisson's Ratio;

PAN - polyacrylonitrile;

PTFE – polytetrefluorethylene;

S1-S40 – Individual Cylinders tested for compression;

SG1– Strain Gauge positioned 50mm away from the cylinder's top surface;

SG2– Strain Gauge positioned at the centre of the cylinder;

SG3– Strain Gauge positioned 50mm away from the cylinder's bottom surface;

SR1 – Strain Rosette positioned 75mm away from the cylinder's surface;

SR2 – Strain Rosette positioned at the centre of the cylinder;

ST1 – Stacking sequence configuration - $[\pm 20]_{2s}$;

ST2 – Stacking sequence configuration - $[\pm 25]_{2s}$;

ST3 – Stacking sequence configuration - $[\pm 35,0]_{s}$;

ST4 – Stacking sequence configuration - $[\pm 16,\pm 45]_{s}$;

ST5 – Stacking sequence configuration - $[0_8]$;

ST6 – Stacking sequence configuration - $[90_8]$ configuration;

UD – unidirectional laminae.

Glossary of Terms

Auxetic materials: Auxetic polymeric materials are special kind of materials that exhibit negative Poisson's ratio (NPR) effect. They get fatter when stretched and thinner when compressed. Auxetic behaviour is a scale independent property which can be achieved at different structural levels from molecular to macroscopic levels. (1)

Anisotropic: Materials which have mechanical properties which are not the same in different directions at a point or materials whose properties vary with rotation at a point. (2)

Isotropic: Materials which have the same mechanical properties in all directions at an arbitrary point or materials whose properties are invariant upon rotation of axes at a point. (2)

Young's modulus of elasticity (E): The quantity that describes a material's response to stresses applied normal to opposite faces. It defines the relationship between stress (force per unit area) and strain (proportional deformation) in a material. (3)

Shear modulus of elasticity (G): The coefficient that relates shear stress to shear strain is called the shear modulus or the rigidity modulus. (3)

Bulk modulus (K): The coefficient that relates stress to strain under uniform compression is known as bulk modulus or compression modulus. It is the proportion of volumetric stress related to the volumetric strain of a specified material, while the material deformation is within elastic limit. (3)

Poisson's ratio (ν): Poisson's ratio is defined as the negative of the ratio of the lateral strain to the axial strain for a uniaxial stress state. Tensile deformation is considered positive and compressive deformation is considered negative. (4)

Ductility: The ductility of a material is defined by its ability to be loaded beyond the elastic limit and then demonstrate some permanent strain upon unloading. Ductile materials can be reloaded without loss of stiffness. This behaviour is not usually exhibited by composite materials. (5)

Pseudo Ductile Behaviour: In this study, the pseudo-ductile behaviour is dependent on the relative thickness of the 0^o and $\pm\theta$ plies, as well as the absolute thickness of the 0^o plies. (5)

Symmetric laminate: A laminate is called symmetric when the material, angle and thickness of the layers are the same above and below the mid-plane. (6)

Anti-symmetric laminate: A laminate is called anti-symmetric when the material and thickness of the plies are same above and below the mid-plane but the orientation of the plies at same distance above and below the mid-plane have opposite signs. (6)

Cross-ply laminate: A laminate is called cross-ply laminate if all the plies used to fabricate the laminate are only 0^o and 90^o. (6)

Balanced laminate: A laminate is called a balanced laminate when it has pairs of plies with same thickness and material and the angles of plies are $+\theta$ and $-\theta$. (6)

Angle-ply laminate: A laminate is called angle-ply laminate if it has plies of the same thickness and material and are oriented at $+\theta$ and $-\theta$. (6)

Bidirectional laminate: A fibre-reinforced material in which the fibres are laid in two different directions, typically in the length and width directions. (7)

Unidirectional lamina: A unidirectional lamina is a thin layer (ply) of composite and is normally treated as a two-dimensional problem. It contains parallel, continuous fibres and provides extremely high directional properties. (8)

Static Indentation Testing: This is one of the oldest and most widely used methods for characterizing materials properties. The technique has been used extensively for determining hardness, which has been related to mechanical properties of materials (e.g., yield stress, tensile strength, work-hardening rate, wear resistance, and fracture toughness of brittle materials), for evaluating the effectiveness of heat treatment processes and surface modification techniques, and for measuring the adhesive strength of thick films and surface coatings. (9)

Re-entrant structures: These are the most commonly used auxetic structures. The first investigated re-entrant structure was a 2D re-entrant. When it is subjected to an axial extension, its diagonal ribs will rotate to the horizontal direction, which leads to a transverse expansion of the structure. Therefore, the NPR effect is achieved. (10)

Pyrolysis: the application of heat to chemical compounds in order to cause decomposition. (11)

Telecentric lens: This has the unique property of maintaining a constant magnification over a specific range of object distanced. It gives an image of constant perspective which helps to remove measurement errors caused by the tests sample moving nearer or further away from the lens. (12)

Stacking Sequence Notation

A laminated composite consists of a number of plies stacked at various angles relative to the x axis of the laminate. It is designated using a special nomenclature. The following points summarise the main steps to designate a laminate:

1. The stacking sequence is enclosed in square brackets symbol, [].
2. The distinct layers or groups are separated with a slash symbol, /.
3. The ply orientations, θ, are listed from top to bottom. The stacking sequence gives the orientation of the fibres with respect to global axis in degrees.
4. The repetition of a ply or plies is denoted by subscript indicating the total number of repetitions. For instance $[90_8]$ refers to 8 layers of 90° plies.
5. The subscript s denotes that the stacking sequence is repeated symmetrically about the laminate centreline. For instance $[\pm 25]_{2s}$ refers to a stacking sequence configuration of 8 plies with angles of +25° and -25° that are repeated twice and are symmetrical about the laminate centreline.
6. The subscript T denoted that the sequence accounts for the total number of layers. However, in general, this is not used. (13, 14).

Symbol Notations

A_{ij}: the extensional stiffnesses;

B_{ij}: the bending-extension coupling stiffnesses;

C_{ij}: the stiffness matrix where the properties of each individual layer is defined;

D_{ij}: the bending stiffnesses;

D: Diameter of the cylinder;

E: Young's modulus of elasticity;

E_1: longitudinal Young's modulus of elasticity (in direction 1);

E_2: transverse Young's modulus of elasticity (in direction 2);

E_{xx}: Young's modulus of elasticity of the composite jacket in the hoop direction;

E_{yy}: Young's modulus of elasticity of the composite jacket in the longitudinal direction;

E_{long}: Young's modulus of elasticity of the FRP shell material in the longitudinal direction;

E_{hoop}: Young's modulus of elasticity of the FRP shell material in the hoop direction;

E_{FRP}: Elastic Modulus of elasticity of the CFRP in the hoop direction;

E_c: Elastic Modulus of elasticity of the unconfined concrete, defined as $4730\sqrt{f'_{co}}$;

E_2: The slope of the second linear portion;

E_{f1}: the Young's Modulus of elasticity for the fibre in the x_1 direction;

F_i, F_{ij} and F_{ijk}: lamina strengths in the principal directions;

f_l: Confining pressure provided by the FRP jacket until it fails by rupture due to hoop tensile forces;

f'_{co}: Average value of unconfined concrete strength;

f_l/f'_{co}: Confinement ratio ;

f'_{cc}: Compressive strength at rupture;

f'_{cu}: the axial stress at ultimate axial strain of FRP-confined concrete;

f'_{co} :the compressive strength of unconfined concrete;

G: Shear modulus of elasticity;

G_{ij}: plane shear modulus of elasticity (in direction i-j);

h: the thickness of the laminate;

K: bulk modulus;

K_{12}, K_{13}, K_{23}: strength coefficients depending on the material;

$m_{\sigma f}$: the mean stress magnification factor for the fibres in the x_2 direction;

N: the number of plies;

N_x : the stress resultant in the x direction;

Q_{ij}: reduced stiffness coefficients;

R: Radius of the cylinder;

R_{vv}^{A} : the fracture resistance of the action plane against its fracture due to transverse/transverse shear stressing;

S_{ij}: the compliance transformation constants;

S_{21}: the shear stress of a uni-directional layer transverse and parallel to the fibre direction;

t^k: individual thickness of k layer;

t: thickness of FRP;

$\varepsilon_{h,rup}$: Hoop rupture strain of FRP jacket;

ε_{co}: Axial strain of unconfined concrete;

ε_t: Transition point;

ε_d: Pseudo ductile strain;

ε_{cu}: Ultimate axial strain at failure;

ε_{1T}: the tensile failure strain of a unidirectional layer in the x_1 direction;

ε_{1C}: the compressive failure strain of a uni-directional layer in the $x_1$direction;

ε_1: the normal strain of a unidirectional layer;

ε_{eff}: effective strain;

ρ_K : confinement stiffness ratio;

ρ_f: FRP volumetric ratios;

p_{vp}^{+}, p_{vp}^{-}, p_{vv}^{-}: the fracture plane angle dependent parameters;

v: Poisson's ratio ;

v'_f : minor Poisson's ratio of the FRP;

v_f : major Poisson's ratio of the FRP;

v_c: the elastic Poisson coefficient of the concrete core;

v_{f12}: the Poisson's ratio for the fibre in the x_1 direction;

σ_c: Axial stress;

σ_i, σ_j and σ_k : stresses in the principal directions;

σ^u_1, σ^u_2, and σ^u_3: normal strength of the lamina in the 1,2 and 3 directions;

σ^u_{12}, σ^u_{13}, and σ^u_{23}: shear strength of the material in the 12,13 and 23 planes;

σ^u_{1T} : the tensile strength along the fibres;

σ^u_{2T} : the tensile strength in the direction transverse to the fibres;

σ^u_{12}: the shear stress along the fibres;

σ^u_{13}: the shear stress transverse to the fibres;

σ^u_{1C} : the compressive strength along the fibres;

σ^u_{2C} : the compressive strength in the direction transverse to the fibres;

σ_{11} ,σ_{22}: the normal stresses in a unidirectional layer;

σ_{11D}: the stress value for linear degradation;

γ_{21}: the shear strain of a uni-directional layer in the elastic symmetry direction;

τ_{21C} : the shear stress at the turning point of the (σ_{22},τ_{21}) fracture curve;

τ_{21}: the shear stress of a uni-directional layer in the elastic symmetry direction;

$\Delta\sigma_{long}$: incremental longitudinal stress in the shell;

$\Delta\sigma_{hoop}$: incremental hoop stress in the shell;

$\Delta\varepsilon_1$ and $\Delta\varepsilon_2$: incremental principal strains in the concrete.

Chapter 1. Introduction

1.1 Introduction

The application of externally-bonded fibre reinforced polymers (FRPs) is considered as a widely accepted system for retrofitting structural concrete members, since they contribute to an efficient and economical way of enhancing the structure's integrity**.** The use of confinement jackets applied to members in compression (i.e. columns) has been successfully used to increase the load carrying capacity of an existing structure, repair corrosion-related problems or, in the case of seismic upgrading, increase their structural ductility. This type of structural member can be described as a 'hybrid column', since it consists of two materials that are working together in resisting stresses and strains induced by forces and conditions external to the column. The techniques implemented to manufacture and apply the jackets play a vital role in providing an impeccable confinement. In fact, improvements have been carried out both in the methodology by improving bonding between the concrete surface and the jacket, as well as in its application, where with the introduction of suitable equipment, various types of FRPs (i.e. including pre-pregs) can be implemented on site.

To date a number of auxetic applications have been successfully introduced in the biomedical, military and sport sectors. Materials exhibiting a Negative Poisson's ratio were first introduced in the late 1800's, but their actual breakthrough began with the works carried out by Ken Evans (15) in 1991, who gave them the name 'Auxetics', derived from the word *auxetikos* i.e. 'that tends to increase'. The auxetic effect plays a vital role in modifying the mechanical properties of a structure to provide an enhanced performance. Generally, the elastic behaviour of a material is expressed by four constants: Young's modulus of elasticity (E), shear modulus of elasticity (G), bulk modulus (K) and Poisson's ratio (ν). For a constant E but decreasing ν towards -1, the microstructure of the material changes in such a way that a very high shear modulus of elasticity relative to the bulk modulus is obtained. In addition, when ν reaches -1, the shear modulus of elasticity tends to infinity, which

implies that it is difficult to shear the material yet, it is easier to deform volumetrically. Materials having a negative Poisson's ratio are considerably more flexible than the actual solids from which they are made, because they require space for 'hinges' to bend or 'nodules' to spread.

1.2 Aims and Objectives

The aim of this study is to investigate the behaviour of auxetic confinement jackets and, by means of experimental tests provide an understanding of its improved effect, if any, on the concrete's confinement. In fact, the main objective of the research study is to make use of the beneficial properties that auxetics offer and observe the behaviour of confinement stresses when auxetic prepreg CFRP jackets are applied on concrete columns. High NPR values are achieved when using high anisotropic materials (16), such as carbon fibre polymer materials (CFRP). Thus, it is interesting to apply these findings by investigating the behaviour of auxetic laminates when in contact with other materials such as concrete.

This study focuses on the use of auxetic CFRP laminates acting as confinement jackets, with through thickness expansion being minimal in dimension due to the nature of the material. By exploiting this through thickness expansion caused by particular stacking sequences, it is possible to introduce the advantageous properties of auxetic materials in the construction field.

CFRPs consist of two distinctly different components, the fibres and the matrix material. Even though they are considered as brittle materials, their distinctive properties of adaptability, high strength-to-weight ratio and chemical inertness are suitable for retrofitting structural members. Their ease of manufacture and their effortlessness in encompassing any shape allow composite laminates to be applied in a variety of circumstances. Furthermore, it is also worth mentioning that impressive advancements were made in the prepreg sector where CFRPs are cured at ambient temperature, thus, increasing the spectrum of applications.

Tangible auxetic materials have been introduced in various industrial sectors, where successful systems were implemented particularly in the military and

biomedical fields. Yet, this study describes the advantageous applications of FRPs that were carried out on existing structures, concentrating mainly on the retrofitting techniques of reinforced concrete columns. Only circular columns and the use of carbon fibres will be discussed. The fibre orientation of the individual layers is a predominant factor that affects the properties of a laminate. Different works have shown that symmetric balanced ply laminates having stacking sequence configurations of $[\pm 20]_{2s}$ and $[\pm 25]_{2s}$ contain auxetic behaviour. In fact, this study will focus mainly on the auxetic behaviour of confinement jackets.

The objectives of this thesis are achieved through experimental work carried out in the laboratory and analytical analysis. These can be summarised as follows:

- To conduct tensile tests and determine the Poisson's ratio for auxetic stacking sequences and compare their values with conventional analytical systems.
- To create a suitable system for manufacturing confinement jackets using prepregs and investigate their behaviour when placed in contact with concrete cylinders.
- To conduct compression tests and determine the confinement stresses of auxetic confinement jackets.

- To compare and investigate whether auxetic confinement jackets provide a better performance than jackets having 0°plies or jackets containing a positive Poisson's ratio.

1.3 Scope of Research

The research work reported in the next chapters is based on the testing of prepreg carbon fibre reinforced laminates with a negative ν_{13}, through thickness Poisson's ratio. To obtain an efficient auxetic effect, it is advisable that a uniform distribution of resin is transferred between the individual CFRP layers and the optimal way in order to achieve this, is by using a prepreg. In fact, the confinement jackets tested in this study were manufactured using a prepreg.

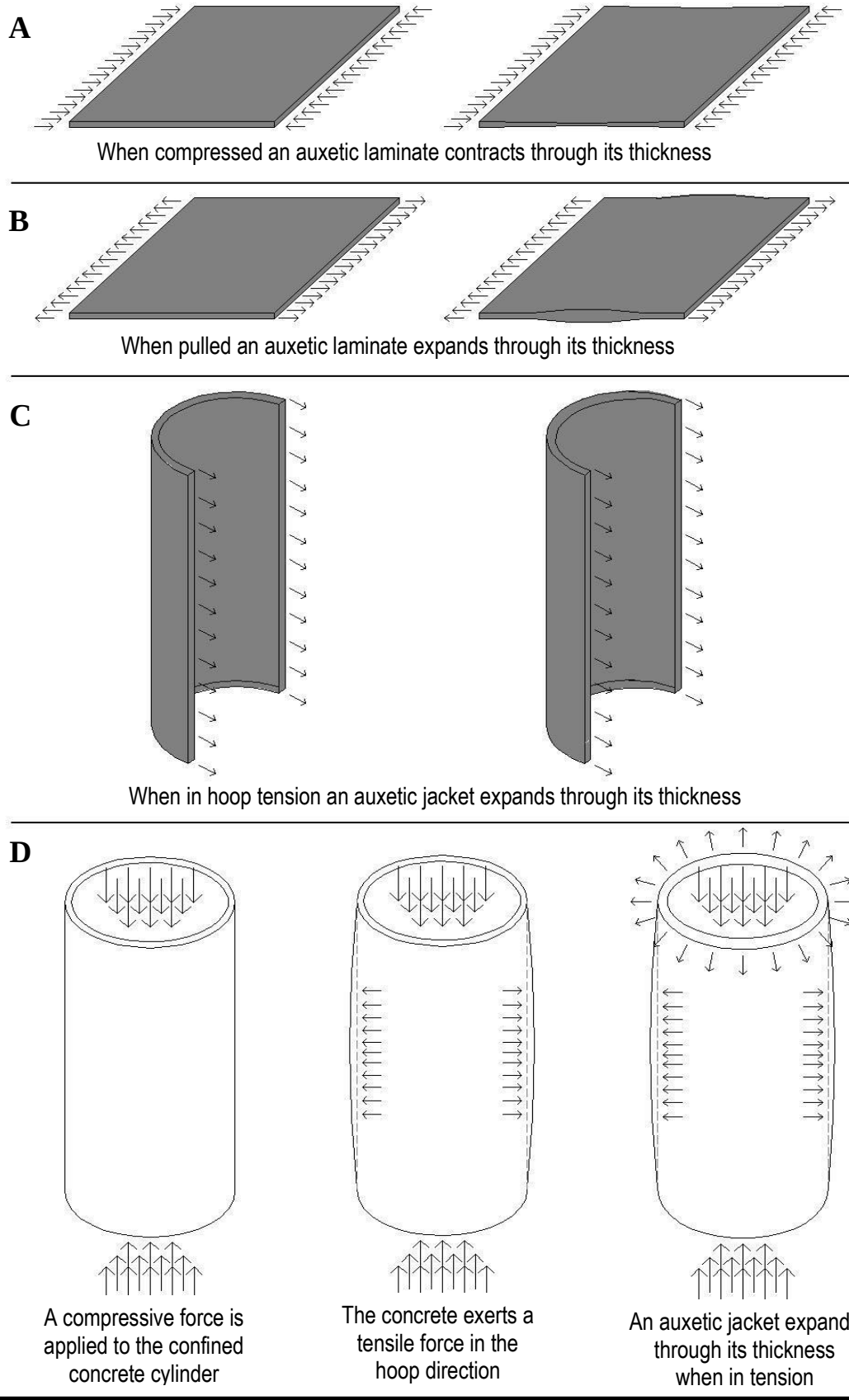

Figure 1.1: Diag. A depicts the through thickness contraction of an auxetic laminate when compressed whereas Diag. B shows its expansion when pulled.
Diag. C represents the through thickness expansion of a cylindrically shaped auxetic laminate when in tension i.e. similar behaviour of a confined jacket when cylinder is compressed.
Diag. D depicts the confinement process of an auxetic jacket.

Figure 1.1 depicts a diagrammatic representation outlining the auxetic behaviour of CFRP as a laminate and consequently as a confined jacket. Diagram A illustrates an auxetic laminate, which when pushed from its ends, i.e. compressed, results in a through thickness contraction. In a similar way, as shown in Diagram B, when pulled from its ends, a through thickness expansion occurs. Likewise, as shown in Diagram C a through thickness expansion is also bound to occur for a laminate placed in a 'cylindrical' shape and pulled from its ends. This auxetic behaviour can be applied to a confined jacket as outlined in Diagram D.

When a concrete cylinder is subjected to an axial compressive stress, it tends to expand laterally. For a confined cylinder, this lateral expansion is resisted by the lateral pressure induced by the jacket, which is loaded in tension in the circumferential (hoop) direction. In the case of an auxetic laminate, the tensile hoop stress subjected on the confinement jacket triggers a through thickness expansion that in turn creates further confinement.

The best auxetic effect occurs when the hoop stress exerts an equal tensile force along the cylinder's circumference such that a uniform through thickness expansion occurs within the jacket. This improved confinement provides an increase in the ultimate strength of the confined column. Thus, by utilising conventional systems that are commonly used in manufacturing the confinement jackets for retrofitting concrete columns and implementing stacking sequences that provide a negative Poisson's ratio, it will be shown that auxetic behaviour does improve the confinement stress. In fact, the scope is to compare auxetic confinement jackets wrapped around concrete columns with other confinement jackets that have the same through thickness Young's modulus of elasticity value E_{xx}, having a positive or near zero Poisson's ratio. In this way, any difference in structural behaviour in this direction is solely due to the Poisson's ratio.

1.4 Methodology

Tensile tests were carried out for the auxetic stacking sequences using Instron 1342, where, by means of a video gauge, the Poisson's ratios were obtained. To determine the confinement stresses, compression tests were carried out using the

Losenhousen 6,000kN compression machine operating with Servocon software, where all cylinders were tested to failure. The vacuum bagging technique was adopted to wrap the prepreg around the concrete cylinders. The SE 70 prepreg carbon-epoxy is used to manufacture auxetic confinement jackets having $[\pm 20]_{2s}$ and $[\pm 25]_{2s}$ configurations. As a means of comparison, other confinement jackets, more precisely $[\pm 35,0_2]_s$, $[\pm 16,\pm 45]_s$, $[0_8]$ and $[90_8]$, were also manufactured and tested. An SA 70 resin was included between the concrete surface and the first CFRP layer. It can be said, that the presence of the resin created a perfect bond and this was vital to transfer the stresses/strains. These experiments were carried out using a force-control system, where all cylinders were compressed at a rate of 1kN/sec.

The basic principles of classical laminate theory were necessary to calculate the Poisson's ratio of the laminate. Using methodologies proposed by other researchers, it was possible to evaluate the through thickness Poisson's ratios for the various stacking sequences tested in this study. Confinement models are categorised into analysis-oriented or design-oriented models, where both approaches provide a systematic methodology to obtain an initial analysis of the confinement stresses present within the FRP jacket. An analysis-oriented confinement model proposed by Becque (17), Becque et al. (18) and a design-oriented confinement model proposed by Lam et al. (19), Teng et al. (20) were chosen to study the behaviour of the SE70 laminates. Graphs of stress versus strain were plotted to compare both models. Their results were also used as a means of comparison with the experimental tests carried out. Using the Tsai-Hill failure criterion, a set of graphs is plotted providing an indication of auxetic behaviour.

1.5 Structure of thesis

The research work presented herein is compiled in seven chapters, where the main focus is that of explaining in detail the behaviour of auxetic confinement jackets.

Chapter 2 provides a thorough description of the developments carried out to date in the auxetic field. The initial part of this chapter describes the advantageous applications of FRPs that were carried out on existing structures, concentrating mainly on the retrofitting techniques of reinforced concrete columns.

Chapter 3 incorporates the techniques adopted for the 'in-situ' strengthening of reinforced concrete columns. The wrapping of prepregs around a concrete column is made possible through adequate systems and appropriate equipment described in this chapter. A summary of the confinement models presented by different researchers is presented. The failure criteria that are most commonly used when designing FRP laminates, such as the Tsai Hill, Tsai-Wu and Puck failure criteria, are outlined.

Chapter 4 groups together all preliminary analysis related to the confinement jackets manufactured by using the SE70 CFRP prepreg. Both design oriented and analysis oriented confinement models are discussed, explaining their methodologies. These were used to examine the behaviour of confinement jackets. Two models were chosen to study the behaviour of the SE70 laminates, mainly, an analysis-oriented confinement model proposed by Becque (17), Becque et al. (18) and a design-oriented confinement model proposed by Lam et al. (19), Teng et al. (20).

Chapter 5 describes all the experimental tests. The system used to roll the cylinder, the methodology adopted to create the laminate as well as all problems encountered during experimentation are described. The experiments were carried out in two sets, yet, the first set of experiments are presented in the appendix of this study since the results achieved were not adequate. Nevertheless, these tests still contributed to this research study, since the confinement jackets tested provided satisfactory results and resisted a relatively large amount of load before failing.

Chapter 6 demonstrates all the experimental results, i.e. both the tensile and compressive tests. The graphs of force versus time and stress versus strain are also shown. An explanation of the outcome of the experimental results, being compared with the confinement models presented in Chapter 4, is outlined.

Finally, in Chapter 7, the salient conclusions of this research study together with the details regarding the possibility of future research work, implementing the use of auxetics in the construction field, are also provided.

Chapter 2.
Literature Review I: The Use of FRPs for Retrofitting Concrete Structures & The Applications of Auxetic Materials

2.1 FRPs in Construction

Over the last few decades, the acceptance of fibre reinforced polymer (FRP) composites as a construction material has grown rapidly. In construction, the applications of FRPs are associated with enhancing of the load-carrying capacity of the structure. Studies (20, 21) have shown the superior properties these materials comprise with regards to the strengthening and retrofitting of structural members, especially when applied externally to reinforced concrete columns, beams or walls. FRP reinforcing gave satisfactory results in improving the flexural strength of damaged wall and-slabs, the seismic resistance of columns and the shear resistance of damaged beams (20). It is evident that their advantageous properties are appropriate in civil engineering applications for various types of reasons including: high tensile strength-to-weight ratio, high stiffness, low electrical conductivity, low thermal expansion, corrosion resistance, high fatigue endurance, optimal design, reduction in maintenance, possibility of adapting to any shape, and preservation of properties at elevated temperatures (21). These properties make FRP composite a good alternative for innovative construction, not only for upgrading the existing structures, but also for new buildings. A few case studies are presented in Figures 2.1-2.5 demonstrating the application of FRPs wrapped around different structural members.

In the repair sector of construction, externally-bonded FRP reinforcement is considered to be a technically-superior and economical substitute to traditional systems (22). As a general rule, the FRPs are manually-fixed to the structural member in concern with an adhesive, typically an epoxy adhesive. The need to repair and to maintain or increase the structural member's load-carrying capacity emerged from several elements, mainly:

- Changes in the use and functionality of the structure;
- Damage due to mechanical actions (impact, explosions, earthquakes, vibration from nearby construction sites);

- Environmental effects which include corrosion of steel, variation in temperature, freeze-thaw cycles and exposure to ultra-violet radiation;
- The need to extend the service life of a structure, while minimising costs, environmental impact and disruption in economic activity;
- Lack of detailing, design and construction errors.

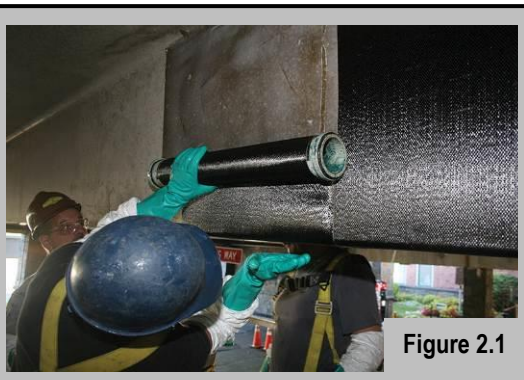

Figure 2.1

Figure 2.2

Figure 2.3

Figure 2.4

Figure 2.5

Figures 2.1-2.5: Applications of FRPs on various structural elements, more precisely:

Figure 2.1 – CFRP wrapped around beams (23:p.18).
Figure 2.2 – CFRP wrapped around columns (23:p.18).
Figure 2.3 – CFRP placed below concrete slabs (23:p.19).
Figure 2.4 – CFRP used on bridges (24:p.41).
Figure 2.5 – CFRP applied on masonry walls (25).

The retrofitting techniques can be considered as novel, since most of the current research work is related to the short term behaviour of reinforced concrete structural elements strengthened with FRPs. Even though in other fields, such as marine and aerospace engineering, FRPs and epoxy adhesives have shown positive results when used for mass production of mechanical and structural components, more research is vital within the civil engineering field to further study the durability and

long term performance of FRPs for retrofitting structures. This is due to environmental effects such as the presence of water in epoxy resin, which can cause degradation and possible failure of the FRP material. In fact, Correia et al. (26) have experimented the durability of RC slabs strengthened with prestressed CFRP laminate strips under different environmental and loading conditions. Other research work concerning further development of FRP composite code specifications (27) as well as improvements in their behaviour in extreme and particular conditions, such as fire resistance (28) is currently being carried out.

Glass, aramid and carbon are among the most common FRP material composites used in civil and structural engineering. FRPs have been used in structural members (20) to enhance load carrying capacities, structural ductility, structural rigidity, fatigue life and durability against harsh environments. This research study will focus mainly upon reinforced concrete columns wrapped with carbon fibre reinforced polymers (CFRP).

Undoubtedly, one of the main FRP composite applications is the enhancement in the compressive strength and the structural ductility of concrete in columns provided by jacket confinement. Reinforced concrete columns are compression members that need to be accurately detailed, especially in seismic areas, where ductile columns may cause collapse of the entire structure. In fact, in order to reduce ductility, it is customary that spiral or rectangular links, depending on the column configuration, are placed at regular intervals along its length. These avoid the buckling of the longitudinal bars, confine the compressed concrete, and prevent shear failure. As a general rule, when an axial load is applied on a reinforced concrete column, the load will cause the concrete to expand laterally. By means of suitable codes (29), both the steel reinforcement and the concrete itself have to be adequately designed and calculated to withstand the load and to transfer it to its respective foundation. Yet, due to particular circumstances, the concrete column may need to be reinforced further in order to withstand more load or repaired when damaged. In such situations, an external reinforcement is implemented enhancing further confinement. The lateral expansion caused by the concrete column is resisted by the hoop action of the jacket that is wound around the column. This confinement affects the stress-strain behaviour of the concrete.

The structural behaviour of confined concrete columns has been under study for quite a few decades. To date, it has been discovered that lateral confinement in columns improves not only its ductility, but also the compressive strength and energy absorption capacity of the concrete. The on-going improvements in the characteristics and properties of CFRP stimulate researchers to explore further the capabilities of this material. For instance, tests have recently been carried out to study the behaviour of FRPs when subjected to blast and impact resistance of structures. Buchan et al. (30) give a clear explanation of the encouraging results in blast resistance obtained by FRP strengthened structures. Similarly, Pham et al. (31) provide a review on the structures' strength to resist impact loads and their energy absorption capacity.

2.2 Properties of CFRP

Carbon fibres are a type of high-performance fibre that gained popularity over the past 50 years in the civil engineering field. Yet, the first application of carbon fibres dates back to 1880 when Thomas Edison patented their use as filaments in electrical lamps. This fibre was very fragile and was made of cotton or rayon fibres by pyrolysis. The introduction of the FRP composites to marine structures dates back to the early 1940s (i.e. World War II) when the UK Royal navy was pursuing to manufacture ship hulls for a warship (32). In 1958, Roger Bacon was the next researcher that developed a high-performance carbon fibre in Ohio in the USA. From the 1970s onwards, carbon fibres began to be extensively used in the aerospace industry (21). Initially, these fibres were too expensive to produce. By the late 1980s and the early stages of 1990s, when the defence market was no longer at its best, FRP manufacturers provided cost reductive alternatives to continue improving the growth of the FRP industry (33). Great advancements were visible with the introduction of the Boeing 787 Dreamliner and the Airbus A380 (34). The use of carbon fibres offered reduction in assembly as well as improvements in the aerodynamic and aesthetic finishing. Boeing (35) stated that a single-piece carbon fibre structure of fuselage substitutes 1,500 aluminium sheets and 40,000-50,000 fasteners per section. These benefits led to companies like BMW to partner with Boeing, providing further advancements in carbon fibre developments (35). FRP materials are currently applicable in the conservative infrastructure construction industry. Kim (35) believes

that carbon fibres represent an interesting future especially for rapid fabrication and customisation. Carbon fibres are flexible, can be easily erected and are recommended to be used for large span structures. One promising fabrication uses cable robots (36). Yet, further research is necessary to be able to introduce systems that can make on-site fibre construction possible (36).

Carbon fibres are similar to graphite; in a single carbon crystal the atoms are in the form of hexagonal arrays and are held together with covalent bonds. The first fibres containing high strength values were created using polyacrylonitrile (PAN) at Rolls Royce and the Royal Aircraft Establishment in Farnborough in the UK. There are typically four main types of carbon fibres: cellulose-based carbon fibres, PAN-based fibres, pitch-based fibres and vapour-grown carbon fibres. Table 2.1 gives an indication of their main properties. All these production technologies, with the exception of the vapour-grown fibres, are very similar and consist of three stages: oxidation, carbonisation and graphitisation. To date, different types of CFRPs have been manufactured by various companies, each having their own properties (21).

Type	Cellulose Based Carbon Fibres	PAN-based fibres	Pitch based fibres
Density (kg/m^3)	1350-1450	1750-1870	1900-2200
Tensile Strength (kN/mm^2)	0.66-0.82	0.9-6.37	1.38-4.05
Young's Modulus (kN/mm^2)	34-41	40-588	159-966
Elongation (%)	-	0.7-2.2	0.27-1.21
Filament Diameter (µm)	-	4.4-7.2	6.0-11.0

Table 2.1: Types of Carbon Fibres & their main properties (21)

Carbon fibres are renowned for their high tensile strength, high Young's modulus of elasticity and fatigue strength. Moreover, they have a high chemical resistance as well as a high temperature tolerance with low thermal expansion and corrosion resistance. When compared to steel, carbon fibres have shown to give astounding results with respect to strength and stiffness. Furthermore, studies (21)

have also shown that the service life of carbon fibre reinforced polymers is much better when compared to glass and aramid fibres. On the other hand, the main drawback of CFRPs is that they are still considered to be expensive materials when compared to other structural materials, approximately three times more expensive than steel. The CFRPs performance is considered to be quite low since its behaviour is greatly dependent on the type of resin. However, CFRP strengthening is not applicable for high reinforced beams and slabs, where fragile failure might develop in the compressed zone of concrete (21).

Carbon fibre plates can be considered to be thin, strong and flexible. These offer the possibility of encompassing any shape and can be installed in a cost-effective solution without causing any visual impacts to the original design of the structure. Carbon fibres are said to give better results under tension loads, and they can easily be applied to the structure by gluing them in the direction of main tensile stresses. Table 2.2 provides a general view of typical tensile properties for carbon firbres.

Carbon	Elastic Modulus (GPa)	Ultimate strength (N/mm^2)	Rupture Strain (%)
General Purpose	220-240	2050-3790	1.2
High Strength	220-240	3790-4820	1.4
Ultra high Strength	220-240	4820-6200	1.5
High Modulus	340-520	1720-3100	0.5
Ultra high modulus	520-690	1380-2400	0.2

Table 2.2: Tensile Properties for Carbon Fibres (21)

Nevertheless, it is also worth mentioning that CFRPs have not only been used as a strengthening structure in conjunction with timber, masonry, concrete and steel, but have also been applied in other fields. In fact, CFRPs have been used widely in aerospace engineering, where their high strength-to-weight ratio with values reaching 2457 kN/kg, were used for aircraft components. In the sporting industry, CFRPs were adapted for the stiffening of running shoes and as protective crash helmets for

climbers, horse riders as well as for motor cyclists. CFRPs have also been used in ice hockey sticks, tennis racquets and golf clubs. Military applications range from planes and missiles to protective helmets or small flapping wings on miniaturised drones used in surveillance missions. Last but not least, carbon fibres were used in the medical field, mainly in the imaging equipment structures. Yet, the most popular application of all is in the production of artificial limbs i.e. prosthetics (37).

2.3 The Importance of Fibre Orientation Angles

The use of CFRP laminates as a structural material is increasing in popularity due to its various applications in this field. A composite is a combination of the reinforcing phase, i.e. the constituent which, in this case, is in the form of carbon fibres and the matrix is usually a polymer resin that is necessary to give shape to the composite. The resin forming the laminate creates the bond between the individual carbon fibre sheets, providing a unique balance of chemical and mechanical properties (38). The most common gluing materials are vinyl-ether, polyether and epoxy resins. For good cohesion, it is recommended that the concrete surface should be smooth finished. Pre-impregnated CFRPs, i.e. composite fibres with epoxy present in the fibres, have also been introduced and were used in a number of engineering applications (39).

The most important issues determining the physical properties of carbon fibres are the degree of carbonisation and orientation of the layered carbon planes. The carbon fibre orientations are a determining factor of the properties of the laminate and, during the preparation of the composite, the fibres can be arranged in various orientations. CFRPs show different rigidities and strengths depending on the difference that lies in the properties of fibre and matrix materials.

It has been shown that the behaviour of CFRP jackets wrapped around the column at 0° is linear-elastic. To date, satisfactory results were obtained for the enhancement of a reinforced Concrete (RC) column strength under uni-axial compression when CFRPs were wrapped at 0° to the RC column. For seismic design and strengthening, it is ideal to use FRPs with particular angle orientations so as to provide enhancement of column ductility. CFRPs wrapped with particular angle

orientations have also given better results in strength and ductility than 0° fibre angles for certain applications, such as eccentric compression loading or combinations of axial load and bending moment (40).

As shown in Figure 2.6, generally, the CFRP sheet orientation in a strengthened beam, column or slab is applied perpendicularly to the loading direction. In such cases, the CFRP fibres will resist the loading by stretching through its principal direction. On the other hand, in the case of reinforced concrete walls, the CFRPs fibre orientation is placed parallel to the structural member.

Experimental tests and analysis were carried out so as to study the behaviour of CFRP orientation in reinforced concrete columns. It was shown that, when a layer of CFRP was applied horizontally (i.e. orientation of fibres at 0°) around a square column, a 6% enhancement in ultimate strength was achieved (41).

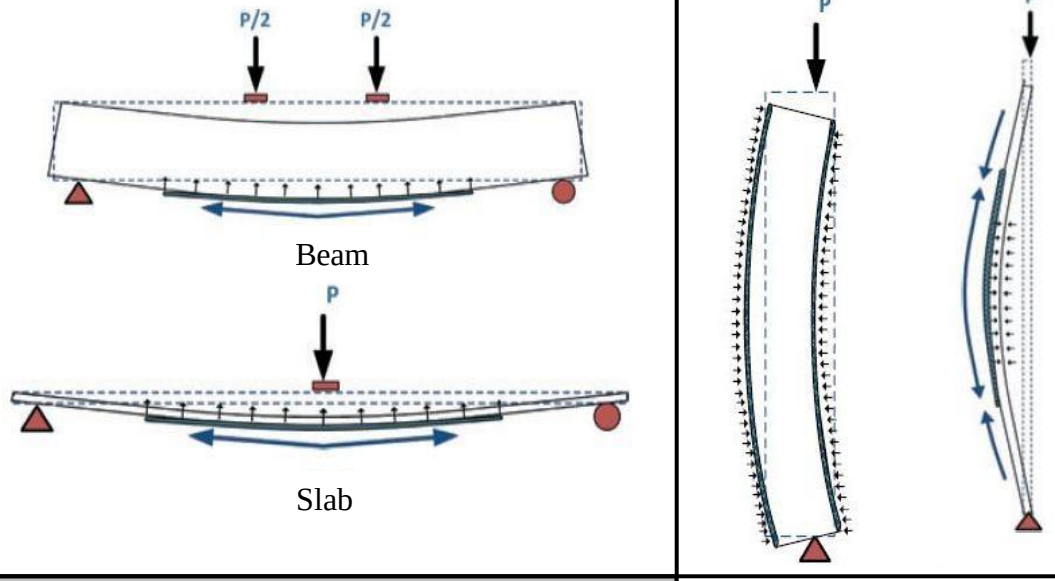

Figure 2.6: Loading Direction & CFRP Orientation (41:p.764)

The virtually limitless combinations of ply orientations and ply stacking sequences enhance the design flexibility providing different strengths and results. Multiple laminae, or plies or layers, are said to be oriented in different directions and bonded in an integral structural unit. Both uni-directional (UD) laminae and multi-directional (MD) laminae have been extensively used in a number of experiments. Due to poor matrix properties, uni-directional composites resulted to be weak in the

direction transverse to the fibres. On the other hand, the mechanical characteristics of multiple laminae composites tend to be more complex. MD composites are more complex to analyse, mainly due to the multi-axial stress state that occurs in the laminate (42). In addition, MD laminates are preferable mostly to uni-directional (UD) laminates due to their higher inter-laminar fracture resistance observed through experiments, where it is believed to be due to extrinsic toughening mechanisms, such as blunted crack tip and some in-ply energy absorption (42).

2.4 Symmetric Balanced Angle-Ply Laminates

2.4.1 Pseudo Ductile Behaviour

As described in the previous section, the properties of carbon fibres are undoubtedly remarkable and suitable for the construction industry. By varying the resin type, fibre type, and the fibre arrangement within the resin matrix, the designer is allowed to explore a variety of possibilities. In addition, the ply thickness and the type of carbon fibre together have an impact on the results. Researchers (43-45) have shown that composites with particular stacking sequences exhibit behaviours that can improve the efficiency of the composite when exploited appropriately. In fact, this study will focus on works related to symmetric balanced angle-ply laminates, with particular reference to works carried out by Fuller et al. (43), Fuller et al. (44) and Harkati et al. (45). These angle-ply laminates are considered to be symmetric with respect to the stacking sequence about the centre of the laminate and balanced as they are made from an equal number of layers oriented at $\pm\theta$ to a reference direction (46, 47). The findings outlined in their works can be relevant to enhancing confinement and CFRP failure. These research papers give a fair understanding of the auxetic or ductile behaviour to adapt or engage in an engineering field. A brief description of these behaviours will be outlined in the next sections.

CFRPs are suitable retrofitting materials that have been proved to excel in strength and stiffness. Yet, their lack of ductility leads to a material, where failure is sudden and catastrophic. Researchers have worked on improving the pseudo ductile or ductile properties in high performance composites. Fuller et al. (43) and Fuller et al. (44) have experimentally shown that CFRP composites having stacking sequence

configurations of $[\pm 25_5]_s$ result in a pseudo ductile strain, ε_d of 1.22%**.** The high pseudo ductile strains and strengths were obtained through fibre rotation and matrix plasticity on thin ply angle-ply laminates with ply thicknesses in the region of 0.03mm. Fuller et al. (48) studied further the possibility of improving the ductility in CFRP composites by inserting a central 0° ply in the symmetrical stacking sequence configuration. In fact, it was experimentally shown that consistent results were achieved for CFRP composites having stacking configurations of $[\pm 26_5/0]_s$ reaching a mean pseudo ductile strain of 2.2% (48). It was revealed that the zero layer predominates the layup and consequently the failure of the composite. In the analysis and experimentation, it was shown that the ductility value is largely dependent on the thickness of the zero layer. In addition, to achieve better pseudo-ductility, the researchers (48) have stated that the manufacturing of the laminate's layup is such that the -26° plies are to be placed adjacent to the 0° central ply. Thus, the concept of combining fibre rotations and fibre fragmentation via the application of angle-ply laminates with central zero plies achieved high performance, metal-like stress-strain responses. Yet, the best ductile strain results were discovered mainly in low thickness prepreg laminates described by the researchers as fragile to handle. It is possible that, due to the thin layer required for the 0° ply, it is not ideal to adopt this system for manufacturing confinement jackets. The ply thickness limits the choice of CFRP as well as the curing times and resin matrix. Consequently, it limits the options of application in retrofitting works and thus, further research work is necessary.

2.4.2 Negative Poisson's Ratio

It is interesting to note that the same stacking sequence configuration used by Fuller et al. (43) has led to a different discovery, more precisely the presence of Negative Poisson's ratio in CFRPs. In the last few decades, the presence of auxetics in composite laminates has been discovered to be either negative in-plane (i.e. on the free edge of the laminates) or through-thickness Poisson's ratio (49, 50). Both the fibre orientation and fibre type play an important role in obtaining a high negative Poisson's ratio. Auxetic values were revealed in symmetric balanced angle-ply laminates, particularly with angles of θ varying between 20° and 25°, with the peak value achieved when θ=20°. Even though, it was shown that auxetics can be achieved

in different fibre types (45), the carbon/epoxy laminates, being highly anisotropic, provide better results than Kevlar/epoxy or glass/epoxy ones. It was actually shown by Harkati et al. (45) that glass reinforced laminates do not exhibit a negative Poisson's ratio. In fact, it can be stated that the main requisite to obtain an auxetic composite is when the individual plies forming the laminate are highly anisotropic (45, 49). The magnitude of the out-of-plane Poisson's ratio depends mainly on the anisotropy of the composite material. Hence, researchers have inspected the possibility of obtaining a negative Poisson's ratio by using prepreg plies with a stiffer fibre or a higher volume fraction (i.e. increased anisotropy). Similar to the works carried out by Fuller et. al (44), Harkati et al. (45) also included a 0° layer in the stacking sequence configuration, i.e. $[0_2,\pm\theta]_s$. Yet, in this case, the ply was not centrally placed and its addition did not give a negative Poisson's ratio, since it decreased the value of v_{13}.

The auxetic evidence present in laminates has intrigued a number of researchers. A few experimental studies have been carried out using IM7/5882 uni-directional carbon epoxy prepreg (49, 51) to give an understanding of the behaviour related to auxetic composites. The static indentation testing has shown that their damage is characterised by highly localised fibre breakage directly under the indentor with very few delaminations**.** This type of response was also noted in auxetic foams and the suppression of delamination noted in the composite laminates gives a better distribution of strain. Similarly, the low velocity impact testing showed that the initial damage was localised with a distinct lack of large delaminations. Experiments have proved that auxetic laminates showed higher loads to first failure with enhanced energy absorption (49, 51). Figures 2.7-2.9 show the damages obtained when carrying out flexural indentations tests on laminates having a positive and negative through thickness Poisson's ratio. Further work on indentation testing was carried out by the same researchers to study the effects of indentor geometry on the mechanisms of failure of auxetic CFRP. Indentors of 2mm, 12.7mm as well as 20mm were used and, similar to their previous tests, the auxetic laminates were compared to laminates having a near zero Poisson's ratio and a positive Poisson's ratio. It was shown that auxetic CFRPs gave enhanced mechanical properties for the 12.7mm and 20mm indentors, where delaminations through the thickness were observed in all layers (52).

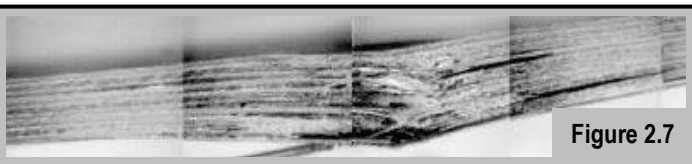

Figure 2.7

'Damage induced in the specimen with ν_{13} = 0.086 by the flexural indentation test'

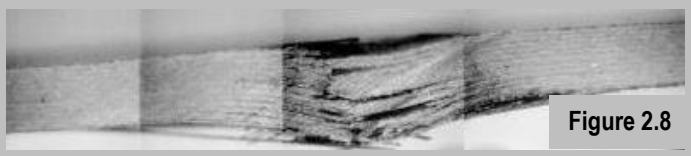

Figure 2.8

'Damage induced in the specimen with ν_{13} = -0.156 by the flexural indentation test'

Figure 2.9

'Damage induced in the specimen with ν_{13} = 0.187 by the flexural indentation test'

Figures 2.7 – 2.9: Abstract of the flexural indentation test carried out. (51:p.494)

Experiments of auxetic laminates using Hexcel prepreg T300/914 carbon/epoxy were carried out on laminates having stacking sequences of $[\pm 20]_{2s}$, $[\pm 25]_{2s}$ and $[\pm 30]_{2s}$ to investigate their behaviour when subjected to three-point bending in static and cyclic fatigue loading (53)**.** Figures 2.10-2.12 give an indication of the results obtained after carrying out a three point bending test. It resulted that $[\pm 20]_{2s}$ feature the highest failure loads, smallest displacements and larger delamination when compared to the $[\pm 25]_{2s}$ and $[\pm 30]_{2s}$ layups. Fatigue tests using the N_5 criterion (i.e. corresponding to reductions of 5% of the load in relation to the initial load) were carried out and it resulted that $[\pm 20]_{2s}$ performed better to cyclic fatigue than other layups.

Due to the practicality and ease of manufacturing most of the research work accomplished to date was carried out using an elastic analysis. The interest in auxetic CFRP laminates has even led to interesting analytical studies, where researchers (54) investigated the negative through thickness Poisson's ratio in the elastic viscoplastic behaviour. By modelling symmetric balanced angle-ply CFRP laminates with microstructures consisting of carbon fibres and a matrix material, it was shown that the increasing negativity in Poisson' ratio was a consequence on the interaction between $+\theta$ and $-\theta$ laminae. In addition, high negative Poisson' ratio were reached for stacking sequence configurations between $[\pm 15]$ and $[\pm 40]$ where the values became increasingly negative as the viscoplastic deformation progressed in the laminates (54).

Figure 2.10

Figure 2.11

Figure 2.12

Figures 2.10 – 2.12: 'Observation of the fracture topographies of the studied laminates after three-point bending for laminates: $[\pm 20]_{2s}$, $[\pm 25]_{2s}$ & $[\pm 30]_{2s}$' (53:p.2104)

2.5 Auxetic Materials & Applications

The auxetic phenomenon has captivated a number of researchers that have taken advantage of their properties to introduce novel concepts and materials in various engineering fields. In fact, auxetic behaviour has not only been discovered in composite laminates, but also in foams (open-celled, metallic, etc.), polymer gels, ceramics, textiles, microporous polymers, filaments and fibres (See Table 2.4). This research study focuses on the use of auxetic composite laminates wrapped around columns to examine and exploits the through thickness effect in confinement stresses. To date, little, if any, research concerning auxetics has been used in structural engineering. It is beyond the scope of this study to report in detail all the progress achieved in the auxetic field. Yet, a brief description of the properties and findings in other fields is necessary to help give a better understanding of auxetic behaviour.

Auxetic behaviour does not necessarily depend on scale and its deformation can occur at the macro, micro or molecular level (55). Thus, both auxetic materials and auxetic structures can be created. The principal phenomenon of auxetics is that of expanding in the transverse direction when pulled longitudinally and similarly, getting shorter in the transverse direction when compressed longitudinally (Figures 2.13 and 2.14). A number of auxetic molecular materials were designed and synthesised using particular microstructure geometry configurations and honeycomb topologies to produce novel properties. It is rather impossible to describe in detail all the work

carried out by researchers with respect to the various honeycomb topologies and geometrical configurations. Re-entrant, multi re-entrant, chiral, star and double arrow head are a few honeycomb topologies that were experimented. A summary of the auxetic honeycomb configurations created to date is provided in Table 2.3.

Auxetic materials are attracting interest since they are providing an alternative route obtaining extreme (high or low) values of material properties that are not easily achieved when using conventional materials. A common feature is that their honeycomb structure is not of a conventional type; hence, when stretched, it expands, 'closing up' any potential cracks, obtaining, as a result, a fracture resistant material. In fact, unlike other materials, the drilling or punching of holes are not considered as weak points. Other properties include synclastic (dome-shape) curvature when subject to a bending moment (Figure 2.15), enhanced indentation resistance (Figure 2.16) and vibration damping.

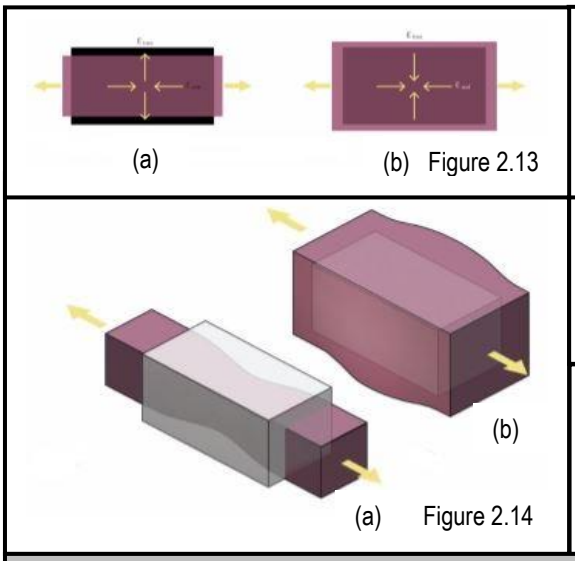

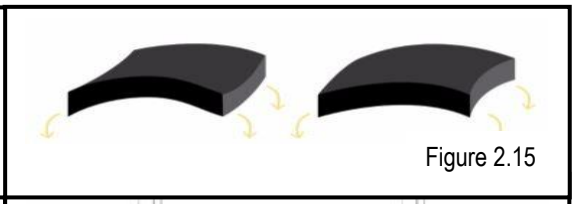

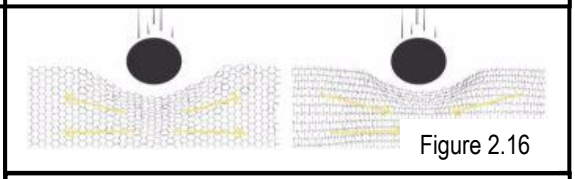

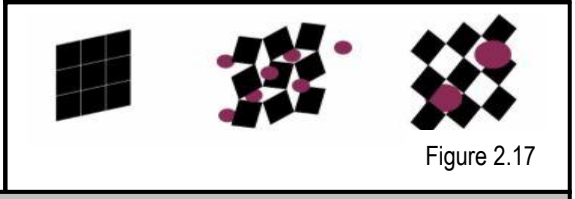

Figures 2.13 – 2.17: Depict the main properties of auxetic materials (56).

Figure 2.13 – Comparison between conventional (a) & auxetic materials (b) [plan view] – Equal strains but different behaviours;
Figure 2.14 – Comparison between conventional (a) & auxetic materials (b) [3D view] – When pulled in tension an auxetic material expands;
Figure 2.15 – Comparison between a conventional Anitclastic and auxetic Synclastic curvature;
Figure 2.16 – Indentation Resistance;
Figure 2.17 - Depicts Variable Permeability.

Table 2.3: Different Types of Auxetic Structures & Models (57)

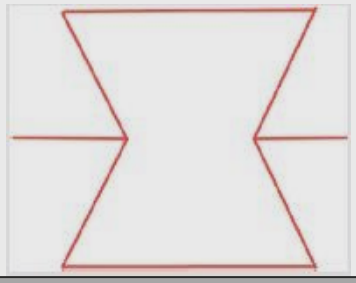	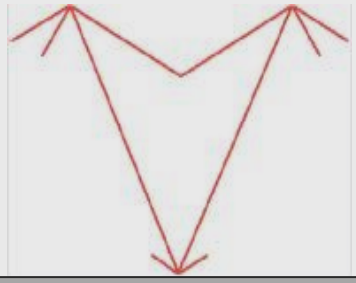	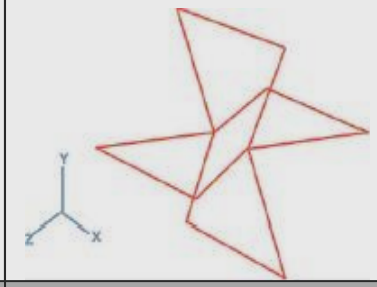
Re-entrant Type - 2D Re-entrant Evans	Re-entrant Type - 2D Re-entrant Triangular	Re-entrant Type - 3D Re-entrant Variant 1
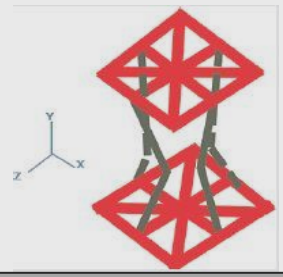	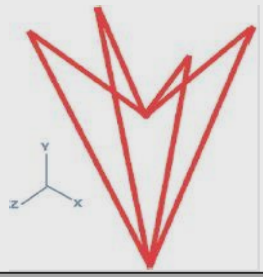	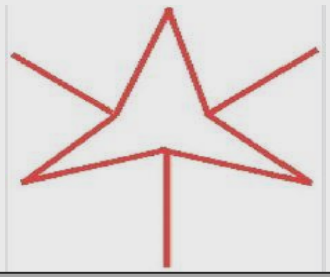
Re-entrant Type - 3D Re-entrant Variant 2	Re-entrant Type - 3D Re-entrant Triangular	Re-entrant Type - Re-entrant Stars Variant 1
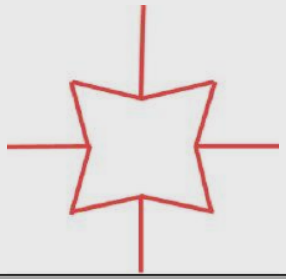	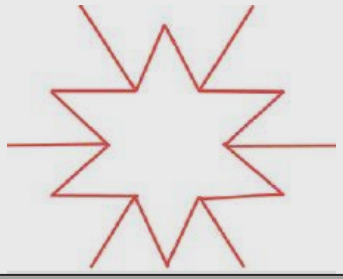	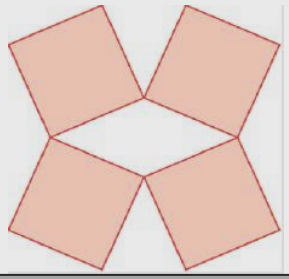
Re-entrant Type - Re-entrant Stars Variant 2	Re-entrant Type - Re-entrant Stars Variant 3	Rotating Polygons – Rotating Squares
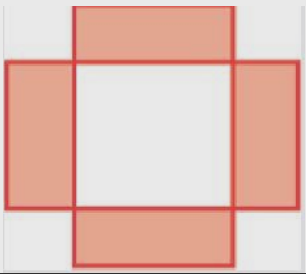	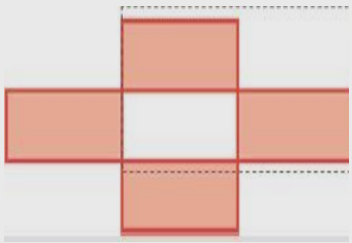	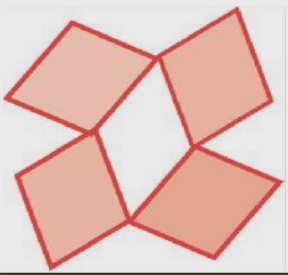
Rotating Polygons - Rotating Rectangles Variant 1	Rotating Polygons - Rotating Rectangles Variant 2	Rotating Polygons - Rotating Rhombi
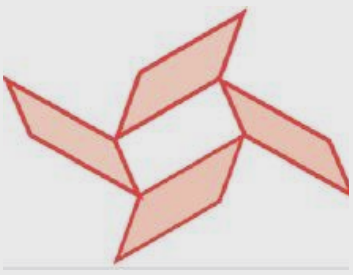	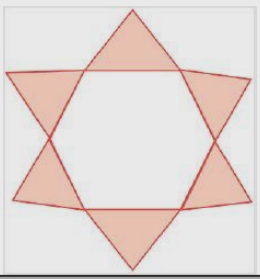	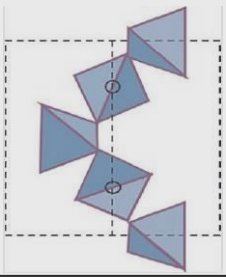
Rotating Polygons - Rotating Parallelogram	Rotating Polygons - Rotating Triangles	Rotating Polygons - Rotating Tetrahedral

Table 2.3ctd. : Different Types of Auxetic Structures & Models (57)

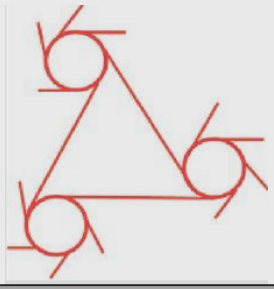	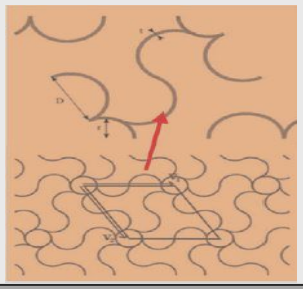	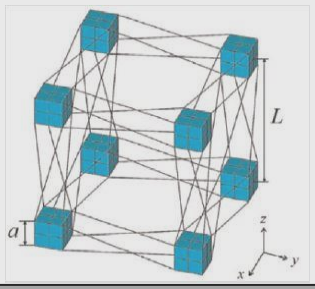
Chiral Type - Chiral Circular	Chiral Type - Rotachiral Type	Chiral Type - 3D Chiral
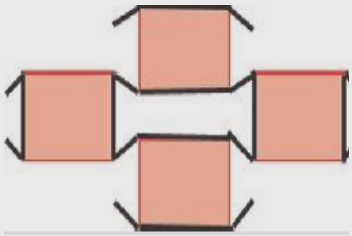		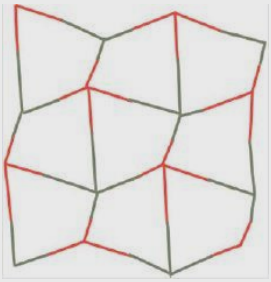
Nodule Fibral Model	Hexatruss	Egg Rack Structure
	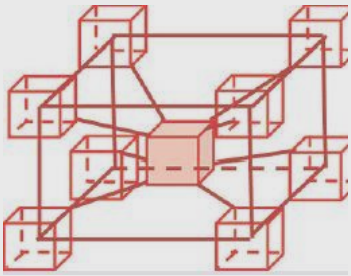	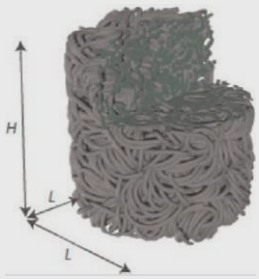
Missing Rib Model	Generalize Tethered Nodule Model	Entangled Single Wire Auxetics
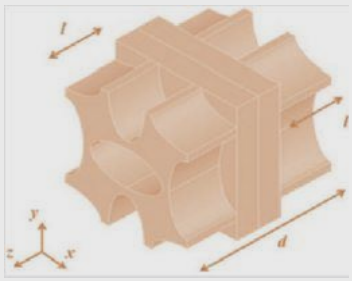		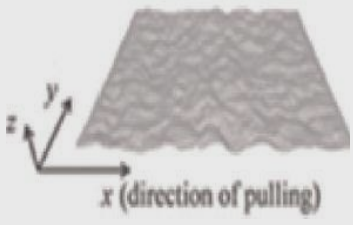
Grooved Block of Metal as Single Material Auxetic	Crumpled Sheets – Aluminium Thin Foils	Crumpled Sheets – Graphene Sheet
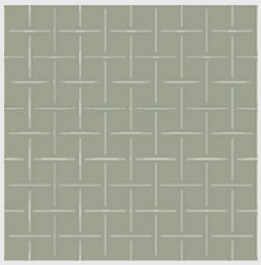	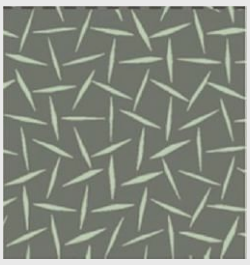	
Perforated Sheets – Perpendicular Oriented Cuts	Perforated Sheets – Random Oriented Cuts	Perforated Sheets – Diamond Perforations

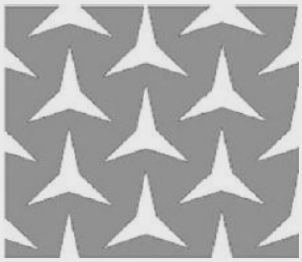	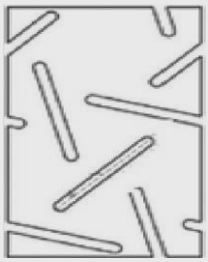	
Perforated Sheets – Star Perforations	2D sheets containing holes arranged in a hexagonal pattern	

Table 2.3 ctd.: Different Types of Auxetic Structures & Models (57)

Re-entrant honeycomb structures have proved to lead to optimal combined mechanical and dielectric properties for radome applications (58), whereas both hexagonal and chiral honeycombs, made from shape memory alloy ribbon material, are adaptable for thermally-activated and deployable structures. Moreover, besides its beneficial auxetic properties, the chiral honeycomb structure has great potential due to the particular structural features that are characteristic of its geometry. The cylinders, in particular, provide improved out-of-plane compressive strength, whereas the ligaments provide resistance to out-of-plane shear bending (58).

One of the first auxetic discoveries, that was tangibly created and where exhaustive works have been produced and studied in detail, is related to foams. Auxetic foams exhibiting isotropic and anisotropic mechanical properties were created (59, 60). It is beyond the scope of this study to explain all the advances made in the manufacture and characteristics of auxetic foams. The microcellular foams as well as the closed-cell foams have both been successfully converted into auxetic form. Hence, it is evident that researchers (59, 60) were and are still investing their time to improve the efficiency of the material due to their advantageous properties. Polyurethane, polytetrafluorethylene (PTFE), polyethylene, metallic and copper foams are typical auxetic foams that have been developed and are considered to be a potential as robust shock absorbers, air filters as well as several other applications (59-70). In addition, foams with curved or convoluted ribs were found to provide dispersion of acoustic waves and cut-off frequencies that might lead to an application involving the absorption of sound. Foam slabs having a few 10s of centimetres in dimension were manufactured and used in the aerospace industry (70).

Auxetic materials are either formed by manipulating existing polymers or by creating them from scratch. Due to their advantageous properties, mainly the compressive strength, shear stiffness, indentation resistance, resilience, sound and damping absorption, auxetic polymeric materials have been recognised in a number of applications in biomedical, textiles, protection, sensors and other fields (1). A few of these applications are presented in Figures 2.18 - 2.24. In addition, Figure 2.25 depicts a diagrammatic representation where various auxetic materials are grouped together pointing out their valuable properties as well as their applications and industrial sector. Table 2.4 summarises most of the auxetic applications and studies carried out to date explaining the benefits their behaviour provide to the different industries. As depicted, a number of research studies have been done in the aerospace, biomedical, military/defence, smart/intelligent systems and others sectors.

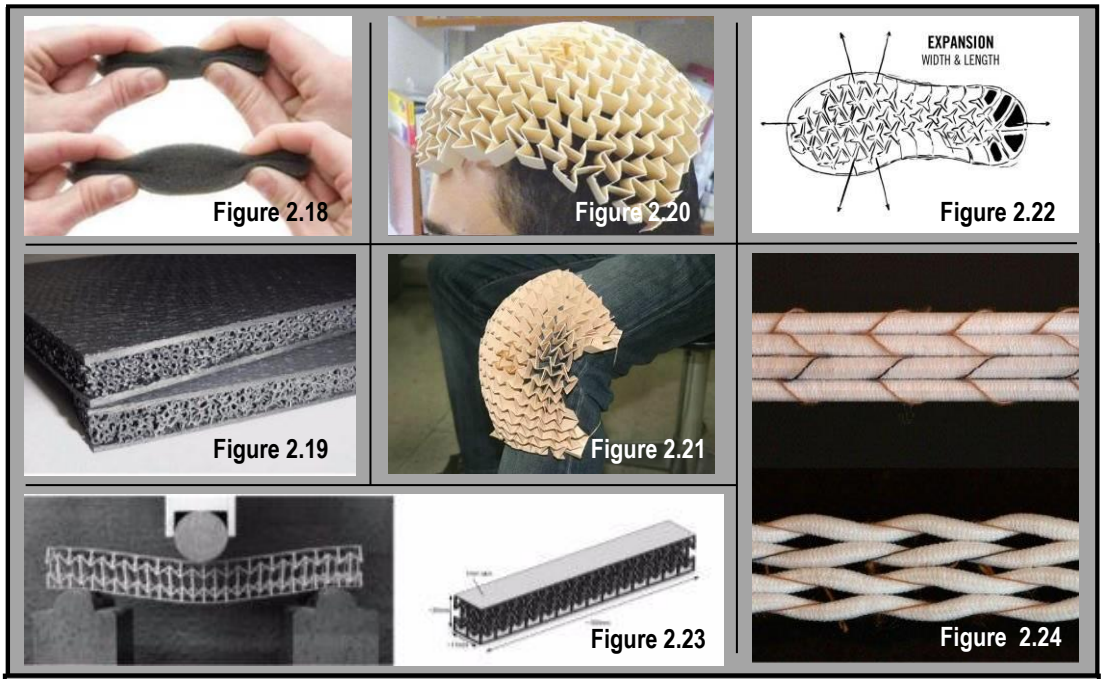

Figures 2.18 – 2.24: Depict different types of auxetic materials that have been manufactured over the years.

Figure 2.18 – Auxetic Foam (71),
Figure 2.19 – Isolating panel filled with metallic auxetic foam (72),
Figure 2.20 – Auxetic Helmet (73),
Figure 2.21 – Auxetic knee pad (74),
Figure 2.22 - Nike midsole (75),
Figure 2.23 – Auxetic Sandwich Panel (76),
Figure 2.24 – Auxetic Textile Rope (77)

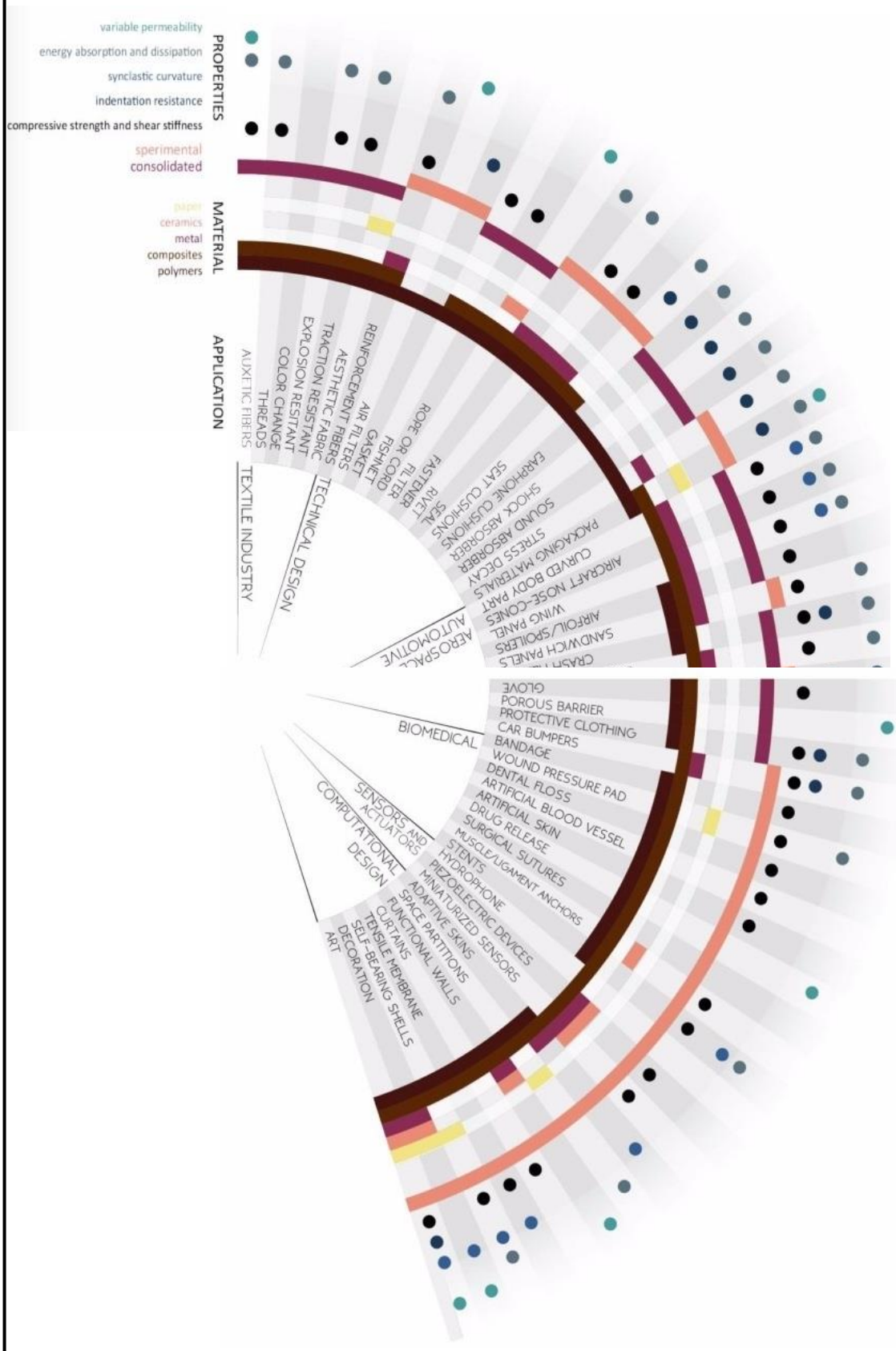

Figure 2.25: Applications of auxetics depending on areas of interest. (78:p.82-83)

Auxetic Type	Auxetic Applications	Industrial Sector	Description
Foam	Midsole (75)	Sports	The renowned company of Nike has recently introduced a new pair of shoes that features a progressive geometric auxetic midsole. Upon impact, the shock is absorbed, accounting for the dual plane expansion in foot size - approximately one size in length and two sizes in width.
	Dilator (79)	Medical	The dilator consists of an auxetic hollow rod of expanded polytetrafluorethylene (PTFE). When placed in the coronary artery at the desired location, it is pulled lengthwise, expanding radially outwardly, applying pressure to there atheroma in the artery , reshaping and redistributing the accumulated material opening the lumen of the artery.
	Surgical Implants (80)	Medical	Relatively rigid re-entrant structures are useful for the construction of devices to be surgically implanted into the musculoskeletal system. It is useful for the construction of orthopadic implant devices. The re-entrant material can be made from any biocompatible substance including but not limited to pure metals, metal alloys, polymer, composites and the like.
Textile	Zetix - Blast Curtain -helical auxetic fibre technology (81)	Blast	Zetix comprises a series of auxetic yarns, each yarn wrapped using S or Z twist with a high strength cord and woven by weft insertion across the warp. When a force is applied, the yarns deform, opening thousands of small pores in the fabric's surface absorbing the peak pressure from the blast wave and allowing the rest to go through.
Textile	Medical Sutures (Stitches) (82)	Medical	Auxetic sutures are a part braided, part wound system that have a core that can be soaked in an agent. When the yarn is stretched, the outer cover expands, opening a number of pores and contemporarily squeezes the core forcing the agent out.
Textile	Filtration (82)	Industrial Filtration Market	Auxetic filters can be used to prevent blockages of debris. A specific pore size could be set and maintained by controlled stretching allowing the pore sizes to open and prevent any form of blockages.

Table 2.4 : Auxetic Applications in various fields.

Auxetic Type	Auxetic Applications	Industrial Sector	Description
Textile	Seat Belts & Safety Harnesses (83)		When a car brakes suddenly, the forces involved between the passenger and the seat belt are quite high. At impact, when using an auxetic seat belt, this expands, spreading the force over a larger surface area reducing injuries.
Textile	Dental Floss (83)	Medical	Auxetic dental floss offers the ability to expand so as to fit the widely differing gaps between human teeth and the ability to deliver chemotherapeutics, florides or flavours directly the gum line.
Foam	Ballistic Protection (84)	Military	Mitsubishi patented a bullet design where one component is made of auxetic material, in an attempt to create an overall Poisson's ratio of zero. By achieving a negative Poisson's ratio, lateral expansion would be reduced when travelling down the gun barrel.
Foam	Wrestling Mat (84)		Due to the enhanced indentation and energy distribution mechanismsof negative Poisson's ratio materials, auxetic foam would offer a better performance than rubber.
Composites	Drive Unit (55)		Toyota patented a manufacturing route for auxetic composites and a drive unit for feed gear rotation formed from auxetic materials.
Composites	Skis (55)	Sports	Auxetic fibre-reinforced composites have been desinged with a lower resistance to motion. These have been patented by Yamaha
	Stent (85)	Biomedical	Auxetic stent is a tool made up with biocompatible polymers shaped into a tube which can be shrinked once introuced into the obstructed veins and dilate once arrived at the needed position.
	Piezoelectric sensors & actuators (78)		Auxetic metals can be used as electrodes sandwiching a piezoelectric polymer or piezoelectric ceramic rods embedded with an auxetic polymer matric. These are expected to increse piezoelectric device sensitivity by at lest a factor of two and possibly by ten or hundred times.

Table 2.4 ctd.: Auxetic Applications in various fields.

Auxetic Type	Auxetic Applications	Industrial Sector	Description
	Scaffolds (86)	Biomedical	In some applications in tissue engineering auxetic scaffolds are more suitable for emulating the behaviour of native tissues and accommodating and transmitting forces to the host tissue site. Auxetic scaffold could be effective for chondrocyte proliferation with compressive load simulation.
	Prosthetic linings (86)		The synclastic (dome shape) curvature when subjected to out of plane bending and the high change in volume under mechanical loading have been studied in depth to produce lining materials for prosthetic limb sockets.
	Force Sensors for hand rehabilitation (87)		Using a melt electrospinning technique, stretchable forse sensors were designed for use in an application of hand rehabilitation. A typical rehabitative robotic device consists of an actuator system to power designed prosthetic hands, a control mechanism to mimic human tendon driven actuation system and a sensor system to detect the position of the subtrate.
	Compression Bandage (78)		By using an auxetic spacer fabric it was possible to attain high levels of compression with a soft, comfortable padding structure. This invention provides a multi layered bandage comprising an inner wound facing layer made in viscose or cotton.
	Morphing Structures (88)		Structural configurations presenting auxetic behaviour offer interesting advantages for the development of a deformable internal structure of a morphing aerodynamic surface, since negative Poisson's ratios involve high shear moduli and inherent resistance to local shape variations. Morphing structural concepts have been studied on aileron, flaps, wings, rudders and spoilers.
Foam	Cushions (84)		Car and wheel chair seats with auxetic cushion foam might be beneficial in reducing pressure inducing discomfort for people who remain seated for a long period of time

Table 2.4 ctd.: Auxetic Applications in various fields.

Auxetic Type	Auxetic Applications	Industrial Sector	Description
Textile	Protective Clothing & Sport Safety Equipment (56, 89)		Auxetic fabrics can be used in protective clothing and equipment because of there good energy absorption properties and shape fitting. Protective clothing and equipment are indispensable for dangerous sports such as riding, racing and skating to protect wearers from injuries by impact forces. The work presented by Allen et al. (74) has indicated the potential of auxetic foam to be applied for sports safety equipment. Further work is recommended, particularly if crash barriers are to be investigated or if prototype protective equipment is used.
	Structural Damper for wind turbine blades (90)	Wind Turbine Technology	A structural composite damper for wind turbines using the topology of auxetic chiral configuration has been simulated and tested under compressive cyclic loading. The auxetic behaviour of his damper allows it to dissipate energy in the edgewise/shear modes.

Table 2.4 ctd.: Auxetic Applications in various fields.

2.6 Auxetics in Construction

Auxetic behaviour can also be exploited in the civil and structural engineering field. To date, the research papers encountered in these fields are related to deployable and seismic designs. The use of auxetic geometric configurations in deployable structures has been studied from an architectural aspect by Mirante (78) & Borg Bonnici (91). The thesis by Borg Bonnici has studied the auxetic behaviour and applied this to deployable structures indicating the benefits, which this material may provide in the engineering field. As part of her study, she devised an auxchiball which, on application of a force, unfolds/deploys exhibiting also auxetic properties (91). The sphere is a tri-symmetric sphere, which is composed of hexagonal and pentagonal plates joined together with line elements, which are pin-jointed on each end. The line elements join the plates together in such a way that chirality (i.e. the property of having rotational symmetry without having mirror-symmetry) is observed. This spherical model has shown that the auxetic behaviour may be applied to deployable structures. Likewise, as shown in Figures 2.26-2.29, Mirante (78) has also discussed the possible chiral configurations that can be adopted as deployable structures. In both situations, the chiral configurations being discussed were studied

from a practical/design aspect. No analysis was carried out to study the nodal forces. Their concepts are still in their primary stages and further research work still has to be done in this field before actual buildings may be erected. As shown, the architectural auxetic configurations presented provide an alternative solution to deployable structures. Yet, the configurations do not produce any improved structural efficiency when compared to the conventional deployable structures constructed to date, other than their shape and nodal force distribution.

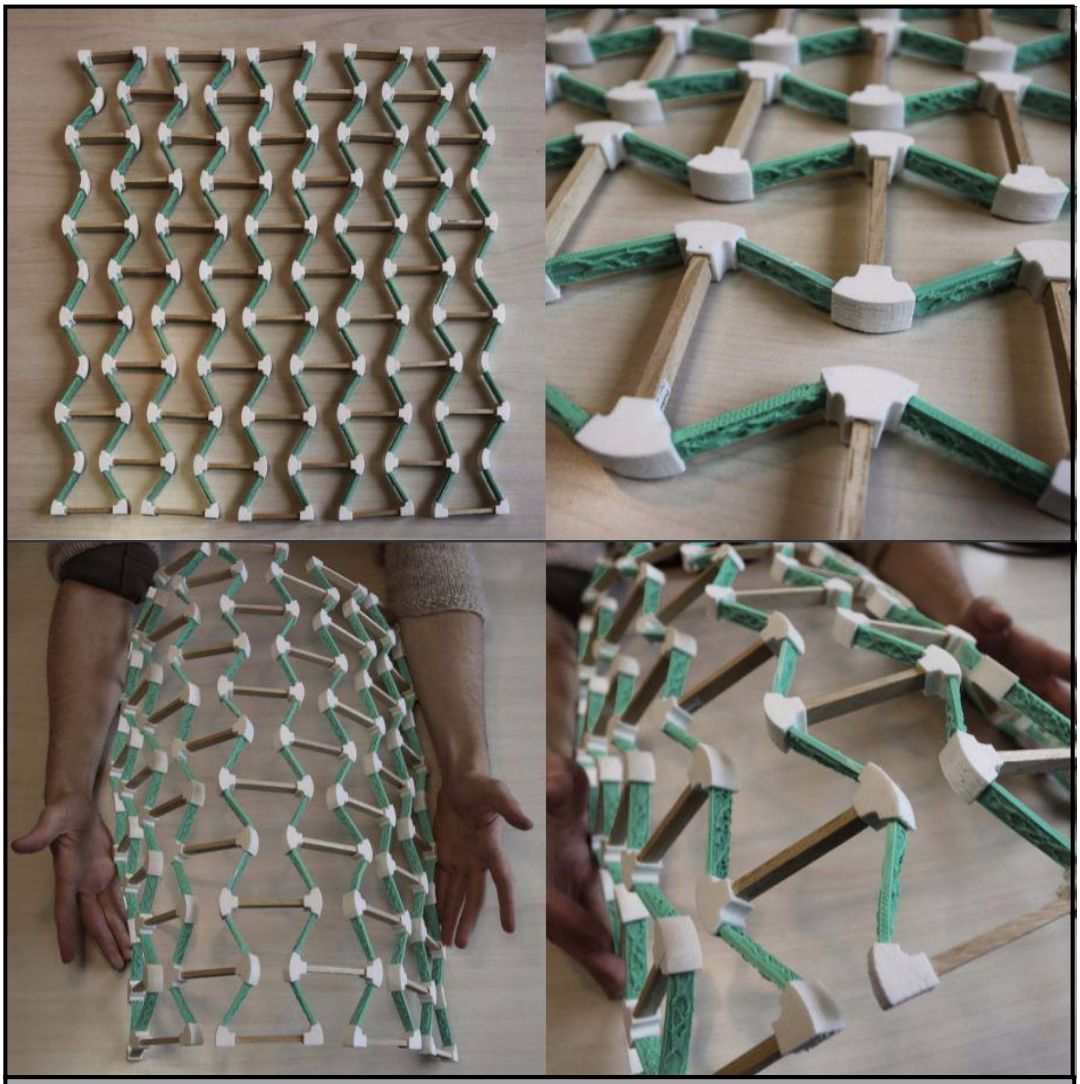

Figures 2.26 – 2.29: Depict the deployable structure presented by Mirante (78:p.170-173) in planar and bent configuration. The model consists of rigid polymers (PLA) for the joints, a flexible experimental polymer for the inclined rods and wooden bars for the parallel rods.

On the other hand, auxetics have proved to be beneficial in the seismic field. A number of methodologies and systems have been tested over the years to dampen

the vibrations caused by earthquakes with the aim of preventing possible collapses or failure of buildings especially when high Richter scale values of 7 and above are achieved. Magneto rheological fluids (92, 93), elastomeric bearings and flexible plates are a few examples of the systems applied at foundation level so as to dissipate energy and dampen the earthquake vibrations.

Lord (USA) is the world's only manufacturer of commercialised magneto-rheological (MR) fluid (92). The magnetic materials they produce are oils that are very densely filled with iron particles. They flow as a very viscous fluid under normal conditions, but, when subjected to a magnetic field, even to a simple magnet, the fluid freezes into its shape and becomes a solid with a yield stress where the magnitude depends solely upon the strength of the magnetism. Thus, such a material could be put into a bag, pumped into place, and then frozen in shape. On removal of the magnetism the material would return back to a liquid state. The material has been utilised for several projects, such as the Notre Dame University and San Waa Tekki Corporation (Japan) where, the material is capable of reducing building vibrations during earthquakes. Both projects have built working seismic dampers using MR fluid. (92)

In a similar way, the study of seismic wave protection based on spectral properties of auxetic-like metamaterials has been introduced providing positive outcomes in the seismic field (94). In this class of metamaterials, their elastic parameters provide negative values in elastic stop bands. The valuable study proposed by Ungureanu et al. (94) is detailed and presents a concept which would help in earthquake protection. In a nutshell, it was shown that the vibration representing the equivalent eigenmode at 17Hz of a building is completely supressed when the plate is structured with an auxetic-like metamaterial. The use of arrays of auxetic cells to perform elastic bands gaps for prevention of seismic propagation over specific frequency ranges is regarded as an innovative concept for earthquake resistant structures. Nevertheless, it was also found that 'the very strong impedance mismatch between the elastic wave velocity within the homogeneous bulk of concrete and that within the auxetic metamaterial enables suppression of wave transmission over a very large frequency range'(94:p.7). This too, can provide further openings in the earthquake damage protection field.

The possibility of exploiting auxetic behaviour in construction has recently been one of the main topics of engineers and they have studied various possibilities to improve the efficiency of a structure. For instance, finite element models were built to test the possibility of increasing the strength in concrete by using an auxetic reinforcement system (95). Auxetix Ltd. have mentioned the possibility of installing smart sensor yarns that can be utilised as monitoring devices in a variety of masonry and composite structures (83). They have also proposed the possibility of using an auxetic rod-cladding to improve the bonding between the steel reinforcement and the concrete. Debonding in reinforced concrete structures is visible via permanent cracks that occur in the individual structural elements. Hence, the use of an auxetic composite structure would greatly help in this respect providing a lighter material that is capable of withstanding greater loads. Even though it is theoretically feasible, there is no tangible information to date related to the response or reaction of auxetics when in contact with concrete.

Most of the research conducted on auxetics related to construction did not involve experimental testing. In certain situations, it is also not economically feasible to manufacture or test auxetic components. As described in Section 2.2, the use of CFRPs as a retrofitting material is increasing in popularity and, to a certain extent, it is also becoming a necessity for strengthening structural elements. In addition, the use of particular symmetric balanced angle-ply laminates exhibit auxetic behaviour. Their ease of manufacture and their effortlessness in encompassing any shape allow composite laminates to be applied in a variety of circumstances. Furthermore, it is also worth mentioning that impressive advancements were made in the prepreg sector where CFRPs are cured at ambient temperature, thus, increasing the spectrum of applications.

It can be deduced that auxetics are providing innovative and alternative solutions in different industries. The majority gave optimistic results in their respective sectors. The auxetic through thickness behaviour in CFRP laminates also was examined and interesting results were obtained. Hence, the aim of this research study is to take this a step further and observe thoroughly the behaviour of auxetic jackets when in contact with concrete. The research work reported in the next

chapters is based on the testing of prepreg carbon fibre reinforced laminates with a negative ν_{13}, through thickness Poisson's ratio. The scope is to compare auxetic confinement jackets wrapped around concrete columns with other confinement jackets to investigate whether they indeed provide improvements in withstanding higher confinement stresses.

Chapter 3
Literature Review II : Confinement Models & Failure of Composites

3.1 Introduction

Auxetic laminates are considered to be innovative materials, where the potential for applications was shown noticeably in the aerospace sector. As outlined in the previous chapter, the negative Poisson's ratio effect provides interesting characteristics that can be exploited in various fields. Construction materials, mainly concrete, steel or masonry, are harsh in nature and it would be interesting to examine the behaviour of auxetic laminates when in contact with such media. As an initial study, this chapter discusses the behaviour of the confinement stresses exerted by CFRPs enclosed around circular concrete columns when subjected to compression loading. In this way, it would be possible to inspect the unusual effect created by a negative Poisson's ratio CFRP, which is being transferred in a through thickness variation and stress confinement enhancement. It is evident that, due to the nature of the material, the expansion or contraction is minimal in dimension; nonetheless, it can still be effective. This is dependent on the actual negative Poisson's ratio which, in turn, is dependent on the laminate's properties and, to a certain extent, also on the number of layers forming the laminate. It was experimentally shown that auxetic behaviour is visible in laminates having particular stacking sequence configurations (51-53). Hence, the practicality and methodology of application of auxetic CFRPs is identical to the standard methods adopted for wrapping concrete columns.

Most of the research studies carried out to date with respect to auxetic laminates focus on the characteristics and stacking sequence configurations with the aim of obtaining optimal/higher negative values of Poisson's ratio (45)**.** In addition, it is also important to note that all studies and applications using auxetic laminates were carried out using a prepreg system. This is understandable because minimal error is necessary to obtain an efficient auxetic system and prepregs have the advantage of providing an evenly applied resin between the individual plies. Yet, pre-impregnated resins require high temperatures for curing. Thus, it is fundamental to create a

balance between the curing temperature of the chosen CFRP prepreg and the actual negative Poisson's ratio attained for the CFRPs properties. The application of a prepreg laminate wrapped around reinforced concrete columns is an innovative concept and is worth testing.

3.2 Properties of Concrete & its Behaviour in High Temperatures

Concrete is undoubtedly one of the most common construction materials in use. It is considered to be a non-linear, non-elastic and quasi-brittle material with high compressive properties. The development of micro-cracks in concrete either due to uni-axial tension or compression results in a progressive degradation of the elastic stiffness of the material. The degraded elastic operator evolves with micro-cracking and gradually causes the concrete material to change from an isotropic material to an anisotropic material, a phenomenon known as damaged induced anisotropy (96). The individual ply materials forming the CFRP laminate have to be highly anisotropic so as to obtain an auxetic effect. In the research work presented by Miki & Murotsu (97) it is indicated that high negative Poisson's ratios are obtained for unbalanced bi-directional laminates. These are laminates with two orientation angles θ_1 and θ_2, and ply ratios p_1 and p_2 whose values are not equal. Hence, it can be stated that, at a particular point, both the concrete column and the wrapped auxetic CFRP are anisotropic.

A number of studies were carried out to examine the behaviour of concrete when subjected to high temperatures and a brief summary of the main properties are outlined below. At normal ambient conditions, Poisson's ratio for concrete is in the range of 0.11 to 0.32, yet, on average, it is assumed to be in the region of 0.15 to 0.20. In addition, it was shown that the Poisson's ratio has a tendency of increasing with the age of concrete within the first two years. This is lower for higher strength concrete (98). The Young's modulus of elasticity of concrete varies widely, since the value is a consequence of various factors. The major contributing variables that affect the Young's modulus of elasticity include: water/cement ratio (where, high values of water/cement ratio result in a lower Young's modulus of elasticity); age (the Young's

modulus of elasticity, increases at a relatively fast rate in the first few months and keeps on increasing for approximately up to 3 years); the richness of the mix (the

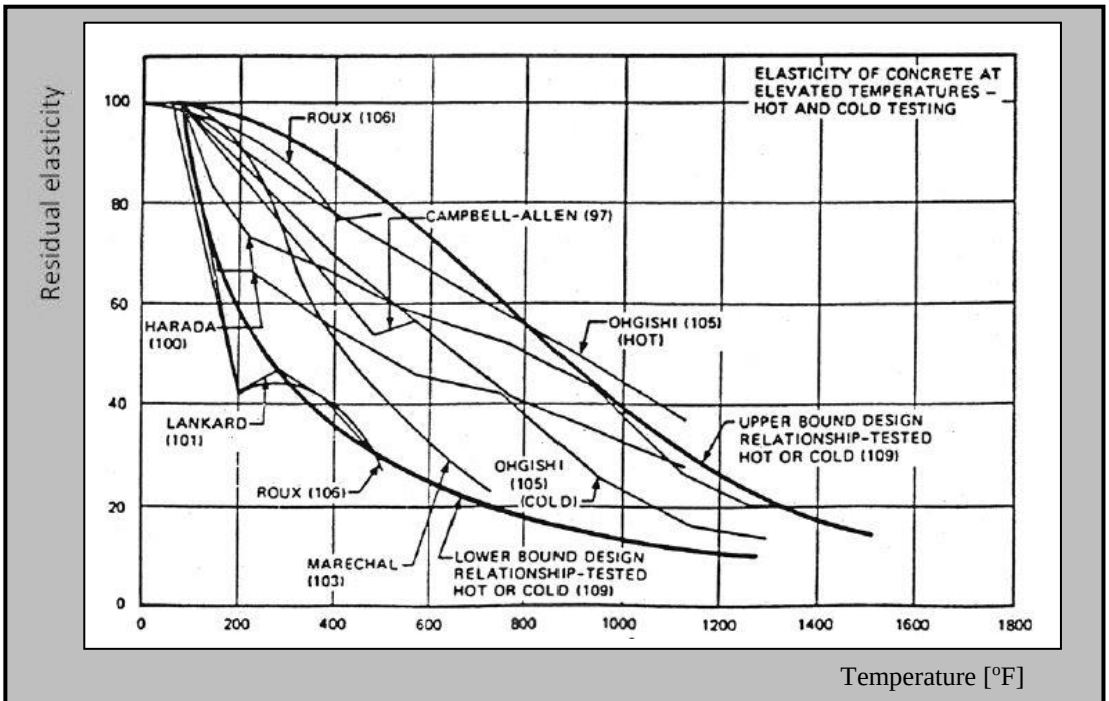

Figure 3.1 Graph showing the effect of temperature on the modulus of elasticity of concrete : hot and cold results. (99:p.19)

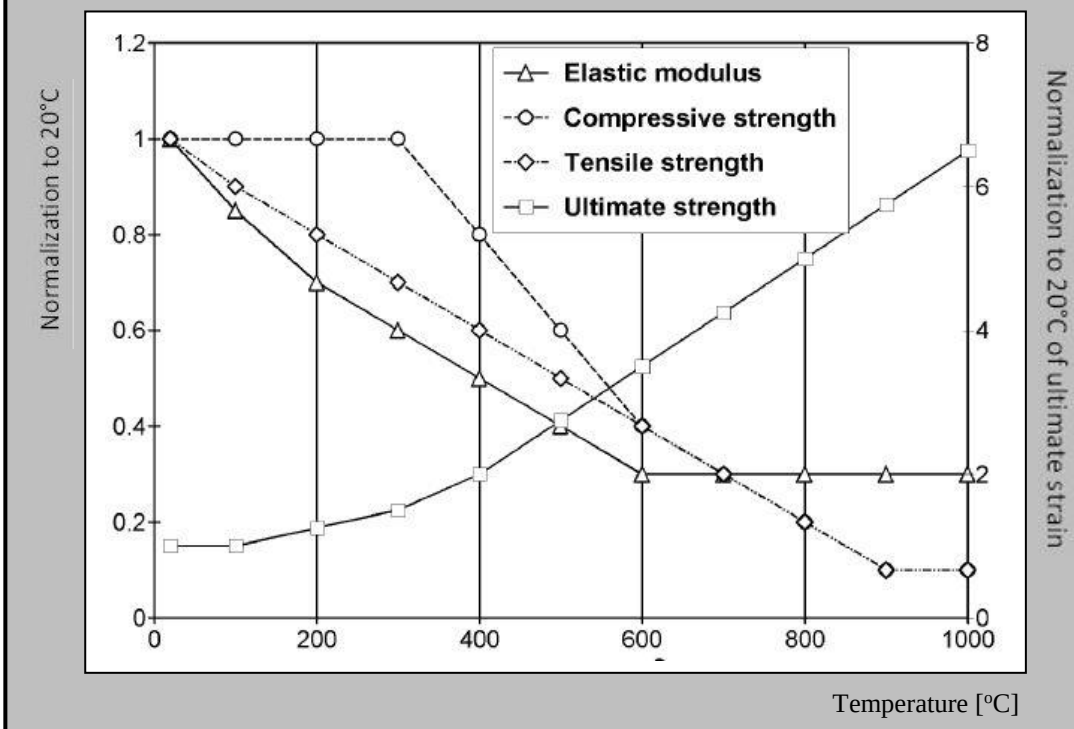

Figure 3.2: Normalisation of mechanical properties of concrete with temperature. (100:p.10)

richer the mix, the greater the modulus increase with age); type and grade of aggregate (stiffer aggregates yield higher Young's modulus of elasticity); moisture content at time of set (where, wet specimens yield a higher Young's modulus of elasticity) (99). The graphs presented in Figures 3.1 and 3.2, give an indication of the changes in the effects on the concrete behaviour that occur at elevated temperatures. It was shown that the critical temperature of concrete is in the region of 550°C (100). In fact, it can be said that concrete is considered to be a material that is resistant to very high temperatures and prepregs with ambient or low curing temperatures cause minimal, if any, changes to the actual concrete properties.

3.3 Techniques for External FRP Strengthening of Columns

To date, FRP strengthening is undoubtedly an established system being used for lateral confinement of concrete columns enhancing its axial compressive strength and ductility. At present, the most common composite materials commercially-available for strengthening of civil engineering structures are either thin uni-directional strips made by pultrusion or flexible sheets or fabrics in turn made of either dry fibres or pre-impregnated resin fibres, in one or at least two different directions (101). Over the years, a number of techniques were developed to facilitate and enhance the in-situ wrapping of FRPs around concrete columns. Xiao (102) describes a number of these systems and takes a step forward where the author also describes the possibility of a new hybrid column system known as CCFT i.e. confined concrete filled tube. The techniques described briefly in this section give an appropriate classification and a generic idea of the main commercially-used systems, whereby it can consequently be shown that prepreg CFRPs are a viable solution for the strengthening of concrete columns. Figure 3.3 groups together the most common methods used for strengthening RC columns.

'Any successful structural repair involves namely four basic elements: concepts used in system design; compatibility and composite behaviour of existing members with upgraded system; field application methods and design details' (103:p.27). An FRP strengthened concrete column is subjected to axial compression, where the jackets are loaded mainly in hoop tension, whereas the concrete is subjected to tri-axial compression. In this way, both materials are being used to their utmost

potentials (104). It is important to note that the concrete substrate has to be appropriately prepared since this can affect the overall behaviour of the FRP strengthened columns, where it is likely that the delamination of the FRP system occurs before achieving the designed load transfer. As a general rule, prior to externally reinforcing the column with FRP, its surface is to be thoroughly cleaned from any loose concrete or coating by sandblasting, grinding or water jet blasting. It is also vital that the column's surface is kept dry. In addition, if the concrete surface has a lower temperature than that proposed by the manufacturer, then, the column has to be heated to raise the temperature. Finally, a repair mortar is placed over the crevices and holes until a smooth surface is obtained.

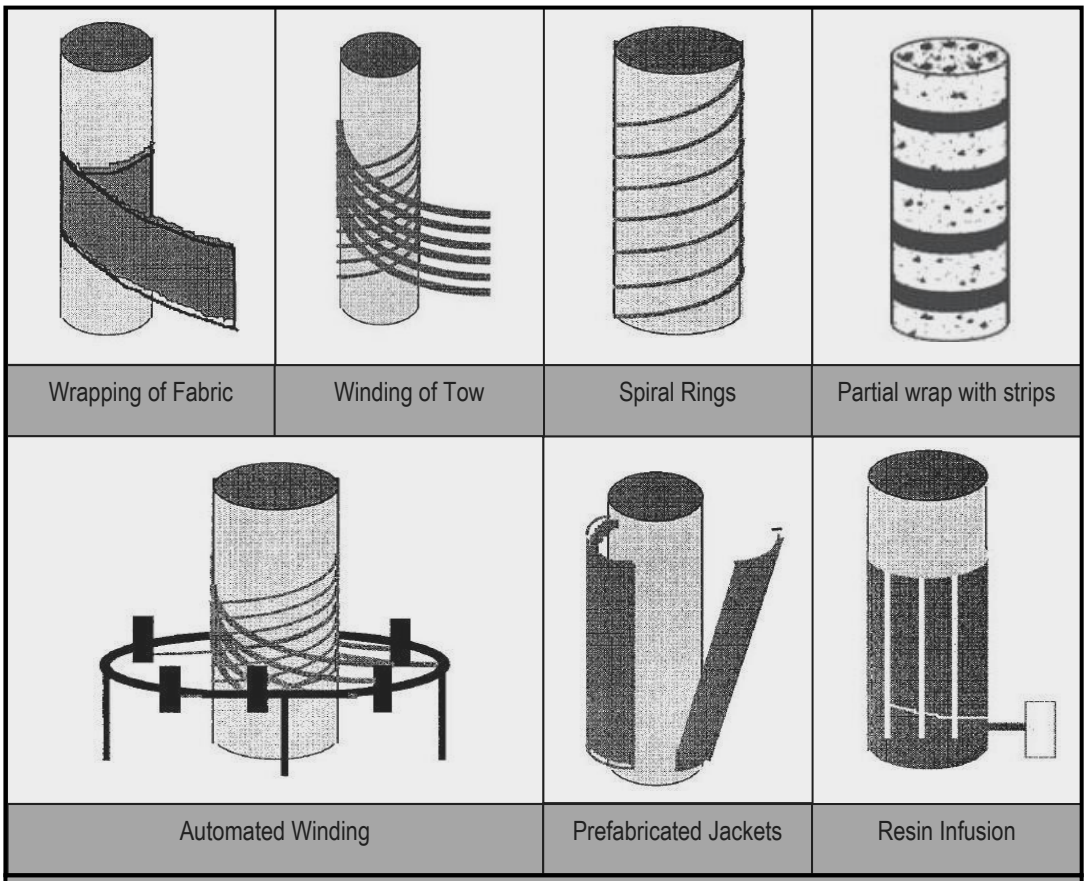

Figure 3.3: Methods of FRP strengthening for RC columns (104:p.16)

3.3.1 Wrapping of the column with fabric – Wet lay up Process

This is one of the most common manual applied FRP strengthening techniques. It is also known as the wet lay up system. The primer coating is applied

either by brush or spray around the concrete column, followed by the wrapping of the FRP layer/s placed around the column. At the end, a protective coating is applied on the jacket. This process affords maximum flexibility and is photographically represented in Figures 3.4-3.6. On the other hand, the main drawback to this system is undoubtedly the presence of human errors that cannot be easily controlled on site. In fact, it is difficult for workmen on site to be in full control of the quality of the resin mix and attain good wet-out of fibres with uniform resin impregnation without entrapment of excessive voids. In addition, it is not so straightforward to obtain good compaction of fibres without excessive wrinkling of the predominantly hoop directed fibres and to control the curing kinetics as well as the achievement of the full cure (103, 105, 106).

Figure 3.4

Figure 3.5

Figure 3.6

Wrapping of column with CFRP (107:p.132-133)

Figure 3.4: A primary coating is first applied around the column.

Figure 3.5: Wrapping of CFRP around the reinforced concrete column

Figure 3.6: The column was fully wrapped with CFRP

3.3.2 Partial Wrapping of the Column with FRP Strips

Another system involves partially wrapping of the column with strips spaced at set distances to each other, whilst keeping a constant FRP volumetric strain. The individual strips are applied in a similar way as the wet lay-up technique. In the studies presented by Ghanem (107), it was concluded that a particular number of strips can satisfy the necessary design requirements. Yet, it is recommended that this method is preferably adopted only in situations where there is limited access to the column. Hence, a fully-wrapped column provides efficient results. Figure 3.7 groups together a set of columns with varying FRP volumetric ratios (ρ_f) used to evaluate the influence of different parameters on the confined concrete stress, axial strain and lateral strain.

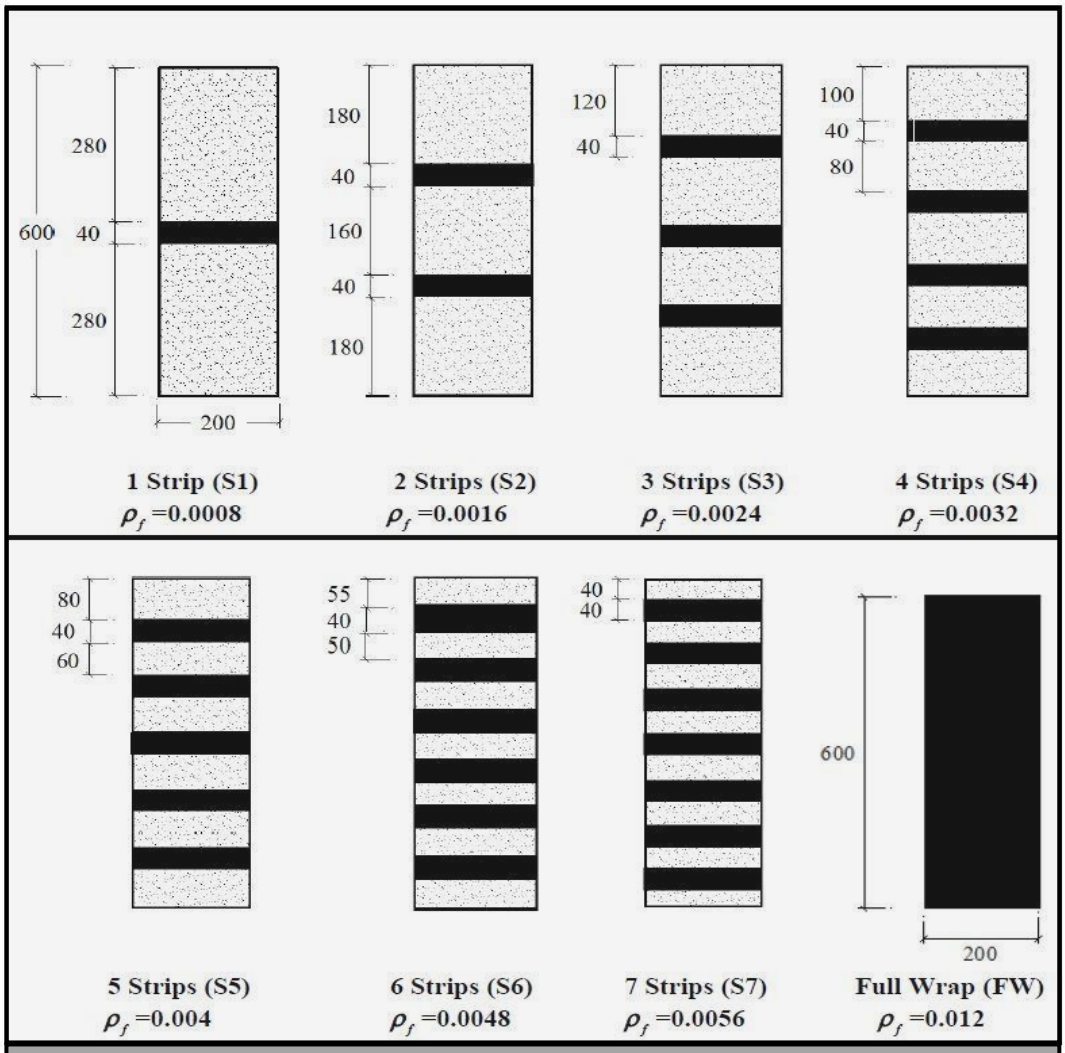

Figure 3.7: Ghanem (107:p.80) has carried out a study where a set of columns were wrapped with strips spaced at particular distances and it was concluded that this system is not effective.

3.3.3 Prefabricated Jackets

As its name implies, this system involves the manufacturing of a jacket prior to retrofitting a column. When using prefabricated FRPs, the installation time is reduced and a better quality control is achieved. To summarise, these prefabricated shells are either made from single-layer cylindrical shells with a longitudinal slit or designed as a multi-layer roll. These are clamped around the column and the composite is then bonded by means of an adhesive. To avoid the formation of weak seams, it is recommended to place the slits of the individual shells in a staggered position (102). In the case of multiple layers, they must be accurately positioned to ensure the desired collaboration of the entire jacket system (105).

3.3.4 Resin Infusion Processes – Vacuum Infusion

The Resin Infusion Process is a system that is operated by means of a vacuum pressure that infuses resin into a laminate. The reinforcing fabric is first formed into a preform and is attached to the substrates using a vacuum bag. This has two holes, one is used for injecting the resin, whereas the other hole is used for the application of vacuum pressure. Once a complete vacuum is achieved, the resin is infused into the fibres via tubing placed with precision. The vacuum infusion provides a number of improvements and benefits including: less wasted resin, better fibre-to-resin ratio, unlimited set up time, consistent resin usage, and is cleaner than a wet lay up system. This technique is more time consuming and one of its drawbacks is that this process has the potential to leave dry spots or probably does not completely fill the preform due to local irregularities, surface conditions or the inability to hold full vacuum (106, 108).

3.3.5 Automated Wrapping

This process makes use of an automated wrapping machine that was first developed in Japan in the 1980's. As shown in Figures 3.8 and 3.9, this device is set up around the column and consists of a wrapping machine used for automatically-winding the fibres around the column. The fibres, wound on reels and placed in the

fibres winding head, are pre-impregnated with resin. The winding angle, fibre volume fraction and thickness are computer-controlled. Starting from the bottom and wrapping its way to the top, the column is completely wrapped with fibres. After the winding is complete, a curing blanket is placed to cure the resin.

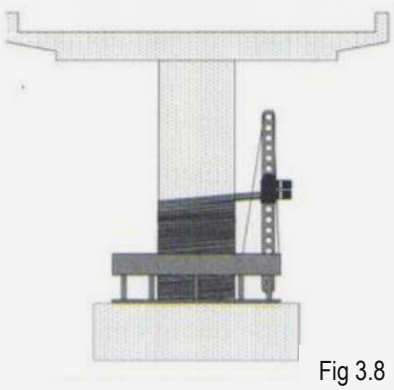

Figures 3.8 & 3.9: Automated Wrapping System (105:p.67-68)

3.3.6 Prepreg Laminates Wrapped around Concrete Columns

The use of prepregs for the retrofitting of concrete columns is another feasible system. The wrapping of the prepregs around the column can be manually-applied or using adequate equipment, such as lifting/positioning devices, winding machines and sprayers. As explained in detail in Chapter 5, the concrete cylinder specimens used for experimentation are wrapped with prepreg auxetic CFRP laminates using the bagging system. This technique can be adapted on a larger scale for retrofitting existing columns on site using appropriate equipment. Heating devices for curing are readily available, and take the form of electrical heaters, IR (infrared) heating systems or heating blankets. For instance, JR Technology Ltd. (109, 110) is a company that specialises in the production of hot bonding controllers, flexible rubber heater mats, as well as insulated jackets that are specifically designed for the manufacture and repair of adhesive metal bonded/composite applications (refer to Figures 3.10 and 3.11). Vacuum bags, similar to those used for the resin infusion system can also be used to remove the air and firmly tighten the layers to the concrete column. The main disadvantage of this system is that it can be considered to be complicated and not so cost-effective.

For the scope of this study, it can be stated that, unlike other auxetic materials, auxetic laminates can be manufactured using the conventional composite manufacturing techniques. In fact, theoretically any of the above-mentioned systems can be implemented. Yet, for the creation of efficient auxetic laminates, minimal errors are required and systems that spread the resin uniformly between the fibres are strongly recommended.

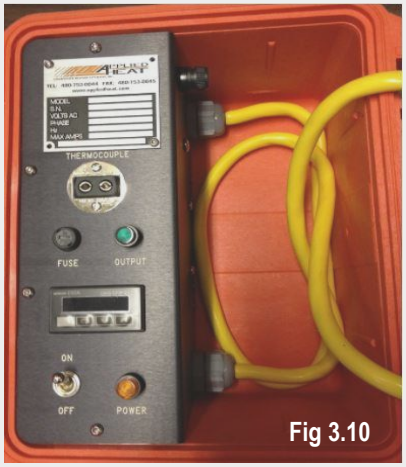

Figures 3.10 & 3.11: Different types of hot bonding controllers offered by JR Technology Ltd. (109, 110)

3.4 FRP Confined Concrete Columns

Reinforced concrete columns are compression members that need to be detailed carefully, especially in seismic areas, if not they may cause collapse of the structure. At times, they are also considered as axial-flexural members due to moments at rigid connections or eccentric axial load (111). It is customary to provide links in the form of spirals or circular hoops or of rectangular arrangement, depending on the column configuration, so as to confine the compressed concrete, prevent buckling of the longitudinal bars and also shear failure. When a column is loaded axially, it expands laterally where it tends to be subjected to an axial strain ε_v and a lateral strain $\varepsilon = \nu_c \times \varepsilon_v$ (where, ν_c is the elastic Poisson coefficient of the concrete core). These values are partially reduced in the presence of an FRP sheet wrapped externally around the concrete column, where confinement pressures arise, resulting in an effective strain of $\varepsilon_{eff} = \varepsilon - \varepsilon_1$ (where, ε_1 is a 'fictitious' lateral strain) (112). So, the lateral expansion will be resisted by the hoop action of the shell, where the

presence of a 3D compressive state of stress has a favourable effect by delaying the loss of strength and stiffness of the concrete, preventing volumetric dilation and keeping the concrete fragments together. As the confinement jacket is subjected to a tensile force along the hoop direction, the confining pressure increases proportionately with the lateral expansion until subsequent failure of the system occurs i.e. when the FRP jacket ruptures.

3.5 Confinement Behaviour – Dilation

Confinement is a term relating to the restriction of the lateral dilation of concrete. In fact, it can be stated that the accuracy of a confinement model relies on the ability it has to capture the dilation tendency of concrete. When an unconfined concrete column is under axial compression, its initial Poisson's ratio varies from 0.15 to 0.22 and consequently follows a volumetric reduction or compaction of 90% at the peak stress. Following this, the concrete begins to show volumetric expansion or dilation that occurs due to the rapidly increasing lateral to axial strain ratio (113). When the concrete column is externally-confined with a linear-elastic restraining member such as a CFRP, then the hoop elongation is imposed on the FRP by Poisson's effect in concrete, achieving a strain reversal that results in containment of dilation (114). Unstable dilation occurring after the initial compaction has also been observed in actively-confined concrete in tri-axial compression tests, although, the volumetric expansion is less prominent at a higher confining pressure (113).

Confinement changes the stress-strain behaviour of the concrete enhancing its compressive strength and deformability. The confining pressure of an FRP jacket wrapped around a column subjects the core concrete to a tri-axial stress state. The initial part of the stress-strain response is similar in behaviour to that of unconfined concrete. A change in behaviour is noted the moment the unconfined concrete strength is reached. In fact, the FRP confined concrete either exhibits a bi-linear behaviour until complete failure of the FRP jacket, or the softening response of the FRP confined concrete, is visible as a localised descending branch that stabilises while dilation of the concrete core progresses. (115).

3.6 Confinement Models

Over the last few decades, several FRP confinement models have been presented and it is beyond the scope of this study to elaborate or discuss these models in detail. Furthermore, a number of guidelines have also been developed, such as ACI-440 (116) and FIB technical report-bulletin 14 (101), that provide a basis for evaluating the confinement stresses that arise between the externally wrapped FRP and the concrete column. Guler et al. (117) have also presented an interesting study by comparing seven guidelines that are currently being used and discussed their efficiency, where it resulted that the FRP confinement models presented in these guidelines are generally more effective on low strength concrete rather than high- or ultra-high strength concrete cylinders.

A brief history as well as a generic description of the significant discoveries are outlined in this section. These methods are appropriate to analyse the confinement stresses of laminates and a few of these methodologies are selected for further exploration. The earliest models are attributed to Hognestad (118), Popovics (119), Sargin (120), and Sargin et al. (121); these researchers proposed a mathematical fractional function for the stress-strain relationship. Further developments were then followed by Wang et al. (122), Kent and Park (123), Sheikh and Uzumeri (124), and Saatcioglu and Ravzi (125). Yet, one of the most popular models is the one proposed by Mander (126, 127) who designed models using stress-strain relationships for concrete columns confined with steel tubes or stirrups and adapted them to predict the behaviour of concrete confined with FRP. The researchers suggested the use of a single equation to be adopted for the entire range of concrete compressive strains. The model was based on an equation proposed by Popovics (119) and is valid for both circular and rectangular shaped columns. The assumption of keeping a constant value for the confining pressure throughout the loading history is not effective mainly because FRPs are elastic until failure and the inward pressure increases continuously (128). In the modified models, the lateral confining pressure on concrete is estimated by assuming strain compatibility between the shell and the concrete core at the interface. Other research studies involved an energy balance equation, where it was

shown that the energy stored in the shell is equal to the difference in the energy of the confined and unconfined concrete. Yet, this approach was not successful (17).

A number of experimental as well as analytical studies have evolved the aim of developing reliable and accurate stress-strain models that predict the overall response of FRP-confined concrete until failure**.** Various researchers, such as Monti (129 – 131), Campione (112, 132–134), Lam and Teng (19, 20, 135, 136), and Ozbakkaloglu (137-140) have carried out extensive research on column behaviour when wrapped with FRPs. To create an appropriate confinement model, it is essential to identify the parameters that exert an influence on the tensile failure of the material. Every model incorporates particular parameters and these vary from tie spacing, reinforcement, columns shape and concrete strength. Experimental studies determined that most concrete cylinders fail when the FRP confining jacket ruptures in hoop tension. In addition, it can be stated that the experimental value of the hoop strain in the FRP at tensile failure for wrapped cylinders is lower than the FRP ultimate strain in uni-axial tension. At times, 'premature' tension failure of the confining device was experienced in the wrapped specimen and this can be the result of the quality of execution (i.e. presence of voids, local protrusions, etc.) or possibly due to the multi-axial stress state present in the FRP even when loaded uni-directionally (141).

In one of their recent studies, Ozbakkaloglu and Lim (137) explored the field of high strength concrete proposing a model of FRP confinement. Ready-mixed high strength concretes have wide spread applications and this too intrigued researchers to investigate the behaviour of confinement (142). In fact, in their work (137), they grouped together a total of 739 axial compression test results for FRP confined 'normal strength concrete' and also collected 237 axial compression test results for FRP-confined high strength concrete columns, covering specimens with unconfined concrete strengths ranging from 6.2 MPa to 169.7MPa.

3.6.1 Design-Oriented & Analysis-Oriented Models

A number of proposed models on FRP-confined concrete have evolved over the years, proposing systems relating to the study of axial stress-strain relationships.

Two main approaches prevail and these can be summarised as follows: one method uses a predefined explicit equation for the stress-strain law of concrete and its parameters are related to the confining FRP properties through regression analysis of experimental results, i.e. design-oriented models; the alternative approach obtains the concrete response by solving step by step, a number of equations that model the essential physical phenomena, i.e. analysis-oriented models (131). It is also necessary to make a distinction between passive and active confinement. The former occurs when the confining pressure from the jacket is induced by and increases with the expansion of the concrete core, whereas, in the latter case, the confining pressure is externally-applied and remains constant as the axial stress increases (143). Ozbakkaloglu et al. (139), classifies the design-oriented models into three categories, namely parabolic, bi-linear or combination of both, depending on the geometric form of the curves. Most of the design-oriented confinement models that emerged were mainly developed from uniformly-reinforced circular columns and recognised the bi-linear stress-strain behaviour of FRP-confined concrete (144). These models consider the FRP and the concrete as a single 'composite' material, whereas analysis-oriented models make use of an iterative approach where the use of stress-strain curves of actively-confined concrete are employed as base curves. 'The axial stress-strain curve of FRP-confined concrete is obtained through an incremental approach, with the resulting curve crossing a family of stress-strain curves for the same concrete under different levels of active confinement pressure' (139:p.1080). This approach features the dilation relationship of FRP- confined concrete as an input. A number of these models predict the behaviour during the loading phase of the column (136, 145-146), whereas other models predict the stress-strain relationship during the loading and unloading phases (146).

Teng et al. (143) categorises the concrete confinement into three main types:

- Weakly-confined concrete – stress-strain curves feature a descending branch;
- Moderately-confined concrete – stress-strain curves feature a bi-linear ascending branch and have an f'_{cu}/f'_{co} ratio less than 2;
- Heavily-confined concrete – stress-strain curves feature a bi-linear ascending branch and have an f'_{cu}/f'_{co} ratio greater or equal to 2.

(where, f'_{cu} is the axial stress at ultimate axial strain of FRP-confined concrete and f'_{co} is the compressive strength of unconfined concrete.)

Analysis-oriented models consist of incremental iterative numerical procedures used to solve the force equilibrium and strain compatibility that occurs between the concrete and the FRP jacket. These models are able to predict the behaviour of concrete confined with different materials as long as appropriate constitutive relationships are used for the confining material. The main advantage of the analysis-oriented approach is that the behaviour of weakly, moderately or heavily-confined concrete can be predicted by the same model without any difficulty and, the stress in the FRP can be explicitly evaluated throughout the loading process and related to the condition of the FRP rupture (128). Research carried out by Mirmiran and Shahawy (114, 147), Spoelstra and Monti (129), Fam and Tizkalla (148), and Becque (18) are typical examples of analysis-oriented models.

Huang et al. (144) have examined 64 design-oriented models and 12 analysis-oriented models to compare and evaluate which type of models perform better. The difference in performance noted between these models is namely in the prediction of the ultimate strain enhancement ratios. The majority of the models obtaining satisfactory results engage rupture strain efficiency factors in their expressions. In addition, it was observed that design-oriented models give more accurate results in predicting the ultimate strength of CFRP-confined concrete specimens since the values obtained for the coefficient of determination (R^2) and the root mean square error (RMSE) are smaller with lower degree of data dispersing compared to the corresponding values obtained from analysis-oriented models. It was concluded from this study that analysis-oriented models are adopted from existing models and are often suitable in evaluating the interaction between the FRP and concrete core theoretically. Lam et al. (19) state that design-oriented models are suitable for direct application in design calculations.

In a similar way, Jiang et al. (143) grouped together 48 analysis-oriented tests, where it was recommended that these models are precise in areas that involve cumbersome analysis. For instance, they are adequate for incorporating computer-

based numerical analysis, such as non-linear finite element analysis of concrete structures with FRP confinement. At times, they are used for generating numerical results that are implemented in the formation of a design-oriented model. The models examined capture the dilatation properties of FRP-confined concrete. It was shown that analysis-oriented models are also suitable in predicting the axial stress at ultimate axial strain, although they are quite inaccurate in predicting the ultimate axial strain.

3.7 Through Thickness Compressive & Tensile Tests

Auxetic CFRP laminates are manufactured using standard methods and the confinement models discussed in the previous section, being design-oriented or analysis-oriented, are suitable for evaluating the stresses present within the laminate. The in-plane or out-of-plane (i.e. through thickness) negative Poisson's ratio are the properties that characterise an auxetic laminate. Harkati et al. (149) investigated the effect of Poisson's ratio ν_{13} for different types of carbon fibres in various resins with fibre volume fractions V_f ranging between 65% and 80%. It resulted that the carbon fibre type significantly affects the through thickness Poisson's ratio, contributing to the anisotropy of the laminas and negative Poisson's ratios. It was noted that stacking sequences $[\pm 20]_{2s}$, $[\pm 22]_{2s}$ and $[\pm 25]_{2s}$ exhibit a negative Poisson's ratio and, as a result, show an increase in the plate thickness. On the contrary, other stacking sequences having a positive Poisson's ratio result in a displacement through thickness equivalent to $U_z = 0$. It can be concluded that, to maximise the laminates' auxetic behaviour and exploit the through thickness NPR effect, it is necessary to opt for carbon fibres bonded with resins that give high values of NPR.

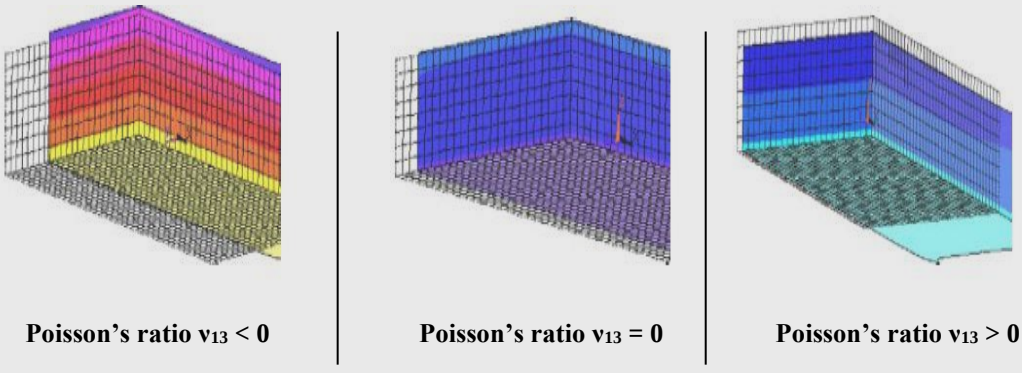

Figure 3.12: Deformations obtained for minimum values of ν_{13} obtained for laminates types $[\pm\theta]_{2s}$ and for different reinforcement carbon type. (149:p.214)

Composite laminates are anisotropic materials that are highly susceptible to delamination driven by secondary through-thickness stress. It is worth noting that methods using ultrasonic vibrations exist to insert z-pins (thin rods) that improve both the delamination resistance and in-plane properties of the laminate (150). The through thickness stresses in confined CFRP laminates play an important role in the overall failure and tests need to be carried out to examine the CFRP's auxetic behaviour. Through thickness compressive and tensile tests of carbon fibre laminates have been carried out using various testing methods. Items such as pressure vessels and submersible marine structures can be subjected to large through thickness compressive stresses. In addition, free-edge effects subjected to in-plane loading can generate out-of-plane stresses at the free-edges of multi-angled laminates. These inter-laminar stresses can be the cause of complete failure of the material due to local delaminations created between the layers of the laminates (151). Thompson (152) states that, due to the increase of CFRPs as primary structures, more research work needs to be done to understand the behaviour of through thickness compression. Even though it is rare to obtain pure compressive failure, it is recommended to provide reliable test methods available for the investigation of through thickness mechanical properties. Guo et al. (153) have studied the surface displacements of cross-ply sided specimens under through thickness compression, where it was shown that the transverse strains were small and constant across the surface of the specimens. It was also noted that, when the load was applied, the specimen had an undulated surface which was created due to the differing Poisson's ratio between the axial and transverse directions in the plies.

Through thickness tensile tests are necessary to evaluate the material properties of anisotropic materials such as CFRP. Speckle interferometry or digital image correlation are effective systems that are widely used. Yoneyama et al. (154) have investigated the possibility of measuring through thickness material properties using a curved beam composite specimen, where the displacement fields are measured using Moiré interferometry. Because of the shape and loading conditions it is possible to determine both the tensile and shear stresses. The through thickness material properties are identified from the measured displacement distributions using the virtual fields method.

3.8 Failure of Composites

3.8.1 Types of Failure

Failure mechanisms are rather complex because of their inhomogeneous structure composed of constituents. This is due to the different properties that remain distinct in a laminate's final composition. This section will focus mainly on the failure of CFRPs wrapped around RC columns outlining also other common failure modes due to the heterogeneous and anisotropic nature of CFRP laminates that give rise to four major modes of failure, namely: matrix damage, delamination damage, fibre damage and penetration. When loaded, the fibres forming the laminate begin to resist the load and defects, such as matrix cracks, fibre breakage, fibre/matrix debonding begin to arise within the laminate. These initial defects do not cause sudden collapse. Failure of the CFRP occurs as a result of an accumulation of these defects leading to the progressive degradation of the material properties.

A number of experimental studies have been carried out over the years to understand the reasons of failure of CFRPs. The failure of the laminate is reached when the hoop stress exerted by the column is larger than the laminate's rupture strength. Bouchelaghem et al. (155) have made a clear distinction between GFRP and CFRP-jacketed samples, where it was shown that the GFRP-jacketed samples follow a ductile failure, anticipated by cracks forming on the external reinforcement, whereas CFRP-jacketed samples have a brittle failure mode. Thus, the ability of CFRP to undergo plastic deformation is limited. As a result, the energy is more likely to be absorbed in creating large areas of fracture, and subsequently provide a reduction in both the strength and stiffness of the material (156). Carbon fibres have a high resistance and their constraining effect, that is dependent on the number of layers forming the laminate, is the main reason that causes this mode of failure. In addition, the reinforcement type, whether uni-directional or bi-directional, also has an effect on the failure mode. Rahai et al. (157) also experienced a brittle failure when testing a total of 23 concrete cylinders wrapped with CFRPs having different orientation angles. The failure was gradual, where initial cracking noises were heard until a sudden explosive failure was reached. It is evident that this demonstrates a sudden release of energy that occurs at the failure of the CFRP. In the experiments carried

out by Karabinis et al. (158), it was also shown that failure of the CFRP occurred at the overlap of the layers forming the laminate. Premature failure also occurred in some specimens due to local failure of the carbon FRP sheet.

Matrix damage is considered to be a critical type of failure, since it can reduce the load-bearing capacity of the composite by up to 50%. Generally, the cracking occurs parallel to the fibres due to compression, tension or shear. The tensile cracks occur when in-plane normal stresses exceed the transverse tensile strength of the ply, whereas shear cracks are formed by very high transverse shear stresses through the material. Matrix cracks caused by shear happen in the first layer impacted by the projectile because of the high, localised contact stresses, resulting in a pine tree pattern (159). Delamination is probably the main failure mechanism of laminates and is more likely to occur in composite structures under out-of-plane loading. This is caused by inter-laminar normal and/or shear stresses that may result in a detrimental effect on the failure mode of the laminate. Delamination is said to occur at interfaces between plies with different fibre orientations. Normally, they initiate by opening forces at matrix cracks, or transverse cracks in adjacent layers. Methods, namely, cohesive zone models, discrete cohesive crack model, the Virtual Crack Closure Technique (VCCT) and 3D Hashin-type failure criteria, have been used to predict both propagation and delamination initiation (160). Fibre breakage is bound to happen during through-thickness impact events or when there are high stress concentrations on local spots or possibly high bending stresses that occur in the surrounding areas. Under high level strains, carbon fibres begin to deform elastically, and consequently break. This mode of failure is likely to occur during the final stages of the fracture process, i.e. after the formation of matrix cracking and delamination. Figure 3.13 provides a schematic representation of three types of failure modes, whereas Figure 3.14 depicts a photographic representation of various CFRP specimen experimental failure modes.

Debonding is another issue that can occur when the wrapped concrete cylinders are compressed. This generally starts after the cracking of concrete, initiating at or near the cracks and propagates in both directions even when a stress gradient exists in the CFRP or concrete. When debonding occurs, the stress transfer capacity between the CFRP and concrete is highly or completely lost. In this instance,

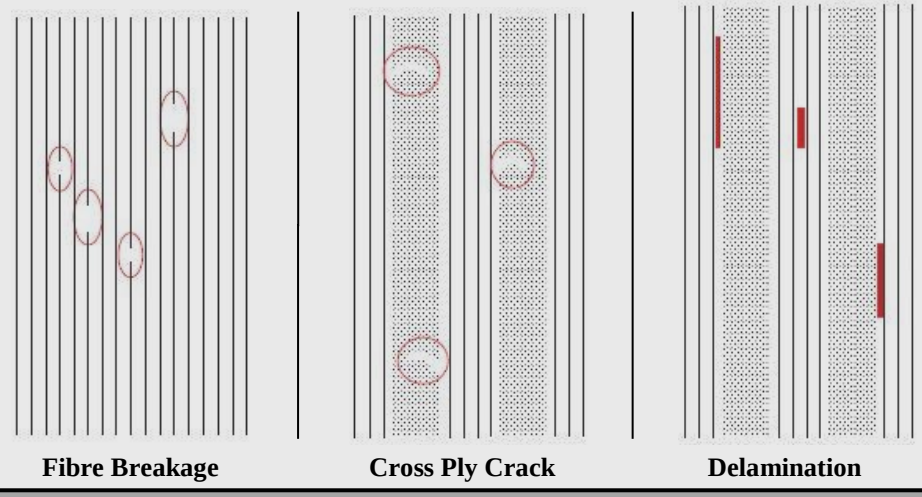

Figure 3.13: Schematic representation of fibre breakage, cross ply crack and delamination failure modes (161:p.13).

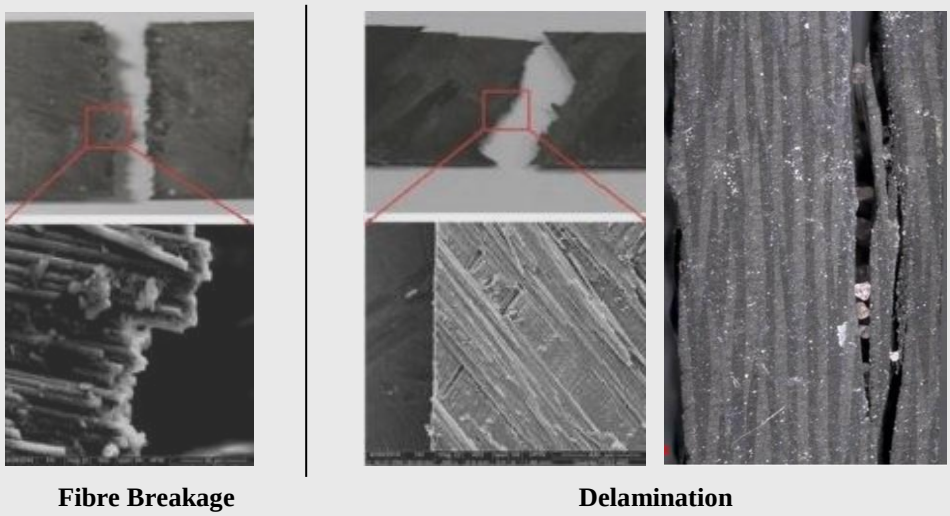

Figure 3.14: Experimental representation of fibre breakage &delamination failure modes (162:p.730).

the CFRP no longer acts as a strengthening medium (163). The debonding can happen not only between the concrete and the adhesive interface, but also between the CFRP strip and the adhesive or both (164). Dandapat et al. (165), have shown that the thickness of the laminate wrapped around the column has an influence on the laminate failure. The increase in wrap thickness has the tendency of increasing interfacial shear stresses. In addition, in the case of thick wraps, the damage in the bond fails earlier. Yet, the increased confining pressure formed by thicker laminates resists the opening of interfacial gaps and the tensile stresses in the surface concrete resulting therefrom. Other researchers have studied failure modes on thin laminates (162,166-167).

3.8.2 Failure Criteria

Failure criteria can be considered to be one of the main topics in the study of composites and they are well-established for homogeneous isotropic materials. By extending and making use of isotropic failure theories, macro-mechanical failure theories for composite materials were established to account for the strength of the composite and anisotropy in stiffness. There are still a number of factors and controversies that surround the subject of CFRPs failure. Several complexities can arise and it is not straight forward to understand the actual reason of laminate failure. The causes are a mix of a multitude of independent and interacting mechanisms, which include, matrix cavitation, de-wetting, filament breaks and micro-buckling, delamination and crack propagation. The initial fibre failure is the main design criterion to ensure the structural safety of a composite structure. In fact, the assumption of most failure criteria is that the laminate is said to fail the moment one of the layers forming the laminate has failed. It is evident that this will occur on the weakest angle or lamina (168). This approach is quite conservative and it is assumed that the failure of a single layer does not necessarily lead to the total failure of the laminate. The actual mechanisms of failures cannot be explained through an operationally-simple strength criterion (169). Hence, many mechanisms must be taken into account when studying failure as it is often a combination of several modes.

Generally, failure criteria are grouped into three different classes: interactive criteria, limit criteria and hybrid criteria. These failure criteria combine selected aspects of limit and interactive methods. None of these criteria can give accurate prediction of failure for all composite materials and loading conditions (170). The simplest of all classes is the limit criterion that comprises both the maximum stress criterion as well as the maximum strain criterion. These failure criteria will give different predictions in situations where the stress-strain relation is non-linear.

The interactive criteria take account of stress interactions. They are successful in predicting failure that is often confined to one fibre/resin combination subjected to a well-defined set of stresses. This group includes all tensorial and polynomial criteria, making use of mathematical expressions to define the failure surface as a

function of the material strengths. Several popular and well-known quadratic failure criteria have been used and a few of them are described in this section.

The Tsai-Wu failure criterion is considered to be one of the first failure criteria that made use of strength tensors. It was an improvement over most of the existing quadratic approximations of the yield surface. The Tsai-Wu failure criterion was originally designed for anisotropic materials using quadratic polynomial expression of stresses containing tensorial coefficients, and was based on conservative assumptions of homogeneity and linear elasticity up to failure.

The following polynomial failure criteria proposed by Tsai and Wu is expressed in tensor notation as (171):

$$F_i.\sigma_i + F_{ij}.\ \sigma_i.\ \sigma_j + F_{ijk}.\ \sigma_i.\ \sigma_j.\ \sigma_k \geq 1 \qquad (3.1)$$

where, σ_i, σ_j and σ_k – stresses in the principal directions;

F_i, F_{ij} and F_{ijk} – lamina strengths in the principal directions;

Due to large number of material constants required, the third-tensor F_{ijk} is usually neglected and hence, the general polynomial criterion can be written as a quadratic expression (171):

$$F_i.\sigma_i + F_{ij}.\ \sigma_i.\ \sigma_j\ \geq 1 \qquad (3.2)$$

The most familiar form of Tsai-Wu failure criterion employs the following failure function for orthotropic materials in their materials' principal axes:

$$F = F_{11}\,\sigma_1^2 + F_{22}\,\sigma_2^2 + F_{33}\,\sigma_3^2 + 2F_{23}\,\sigma_2\,\sigma_3 + 2F_{13}\,\sigma_1\,\sigma_3 + 2F_{12}\,\sigma_1\,\sigma_2 + F_1\,\sigma_1 + F_2\,\sigma_2 + F_3\,\sigma_3 + F_{44}\,\sigma_4^{\,2} + F_{55}\,\sigma_5^{\,2} + F_{66}\,\sigma_6^2 \qquad (3.3)$$

To deliver a failure criterion, it is claimed that the material is safe if $F<1$, whereas the critical condition for failure is predicted when $F=1$.

It can be assumed that the behaviour of uni-directional composites is best described as transverse isotropy. Thus, it can be stated that:

$$F_{33} = F_{22},\ F_{13} = F_{12},\ F_3 = F_2,\ F_{55} = F_{66},\ F_{23} = F_{22} - 1/2F_{44}$$

The Tsai-Wu failure criterion expression shown in Equation 3.3 can be reduced to:

$$F = F_{11}\sigma_1^2 + F_{22}(\sigma_2^2 + \sigma_3^2) + (2F_{22} - F_{44})\sigma_2\sigma_3 + 2F_{12}\sigma_1(\sigma_2+\sigma_3) + F_1(\sigma_1+\sigma_2) + F_2\sigma_3 + F_{44}\sigma_4^2 + F_{66}(\sigma_5^2 + \sigma_6^2) \quad (3.4)$$

where, most of the coefficients involved can be determined as follows:

$$F_{11} = \frac{1}{\sigma_{1T}^u \sigma_{1C}^u}, \quad F_{22} = \frac{1}{\sigma_{2T}^u \sigma_{2C}^u}, \quad F_1 = \frac{1}{\sigma_{1T}^u} - \frac{1}{\sigma_{1C}^u}, \quad F_2 = \frac{1}{\sigma_{2T}^u} - \frac{1}{\sigma_{2C}^u},$$

$$F_{44} = \frac{1}{(\sigma_{23}^u)^2} \text{ and } F_{66} = \frac{1}{(\sigma_{12}^u)^2}$$

where σ_{1T}^u and σ_{1C}^u are the tensile and compressive strengths along the fibres;

σ_{2T}^u and σ_{2C}^u are the tensile and compressive strength in the direction transverse to the fibres;

σ_{12}^u is the shear stress along the fibres;

σ_{13}^u is the shear stress transverse to the fibres.

It is interesting to point out that the way the value of F_{12} was obtained is empirically-supported by limited justifications. Ideally, its value can be determined through bi-axial stress tests. However, no experimental method can be used to achieve its value. This is due to the difficulties encountered in performing such tests as well as the lack of standard testing procedures. Li et al. (172) provided a systematic re-examination of the original quadratic equation proposed by Tsai and Wu (168) and offer one missing facet associated with the determination of the interactive coefficient F_{12}, on a rational basis to eliminate the empiricism. The researchers introduced a non-dimensional parameter $\partial = 4 - \frac{\sigma_{2T}^u \sigma_{2C}^u}{(\sigma_{23}^u)^2}$ that is completely determined by the materials' conventional strength properties. The parameter divides the UD composites into two categories, $\partial \geq 0$ and $\partial < 0$ and it was shown that a rational expression of F_{12} can be obtained.

Other well-known quadratic failure criteria include those proposed by Tsai-Hill (171), Azzi-Tsai (173), Hoffman (174) and Chamis (175). These failure criteria have been grouped together and summarised in Table 3.1.

Failure Criteria					
	Tsai-Wu	**Tsai-Hill**	**Azzi-Tsai**	**Hoffman**	**Chamis**
F_1	$\frac{1}{\sigma^u_{1T}\sigma^u_{1C}}$	0	0	$\frac{1}{\sigma^u_{1T}\sigma^u_{1C}}$	0
F_2	$\frac{1}{\sigma^u_{2T}\sigma^u_{2C}}$	0	0	$\frac{1}{\sigma^u_{2T}\sigma^u_{2C}}$	0
F_3	$\frac{1}{\sigma^u_{3T}\sigma^u_{3C}}$	0	0	$\frac{1}{\sigma^u_{3T}\sigma^u_{3C}}$	0
F_{12}	$\frac{-1}{2\sqrt{\sigma^u_{1T}\sigma^u_{1C}\sigma^u_{2T}\sigma^u_{2C}}}$	$-\frac{1}{2}\left(\frac{1}{\sigma_1^{u^2}}+\frac{1}{\sigma_2^{u^2}}-\frac{1}{\sigma_3^{u^2}}\right)$	$\frac{-1}{\sigma_1^{u^2}}$	$-\frac{1}{2}\left(\frac{1}{\sigma^u_{1T}\sigma^u_{1C}}+\frac{1}{\sigma^u_{2T}\sigma^u_{2C}}-\frac{1}{\sigma^u_{3T}\sigma^u_{3C}}\right)$	$\frac{-K_{12}}{\sigma^u_1\sigma^u_2}$
F_{13}	$\frac{-1}{2\sqrt{\sigma^u_{1T}\sigma^u_{1C}\sigma^u_{3T}\sigma^u_{3C}}}$	$-\frac{1}{2}\left(\frac{1}{\sigma_3^{u^2}}+\frac{1}{\sigma_1^{u^2}}-\frac{1}{\sigma_2^{u^2}}\right)$	0	$-\frac{1}{2}\left(\frac{1}{\sigma^u_{3T}\sigma^u_{3C}}+\frac{1}{\sigma^u_{1T}\sigma^u_{1C}}-\frac{1}{\sigma^u_{2T}\sigma^u_{2C}}\right)$	$\frac{-K_{13}}{\sigma^u_1\sigma^u_3}$
F_{23}	$\frac{-1}{2\sqrt{\sigma^u_{2T}\sigma^u_{2C}\sigma^u_{3T}\sigma^u_{3C}}}$	$-\frac{1}{2}\left(\frac{1}{\sigma_2^{u^2}}+\frac{1}{\sigma_3^{u^2}}-\frac{1}{\sigma_1^{u^2}}\right)$	0	$-\frac{1}{2}\left(\frac{1}{\sigma^u_{2T}\sigma^u_{2C}}+\frac{1}{\sigma^u_{3T}\sigma^u_{3C}}-\frac{1}{\sigma^u_{1T}\sigma^u_{1C}}\right)$	$\frac{-K_{23}}{\sigma^u_2\sigma^u_3}$
F_{11}	$\frac{1}{\sigma^u_{1T}\sigma^u_{1C}}$	$\frac{1}{\sigma_1^{u^2}}$	$\frac{1}{\sigma_1^{u^2}}$	$\frac{1}{\sigma^u_{1T}\sigma^u_{1C}}$	$\frac{1}{\sigma_1^{u^2}}$
F_{22}	$\frac{1}{\sigma^u_{2T}\sigma^u_{2C}}$	$\frac{1}{\sigma_2^{u^2}}$	$\frac{1}{\sigma_2^{u^2}}$	$\frac{1}{\sigma^u_{2T}\sigma^u_{2C}}$	$\frac{1}{\sigma_2^{u^2}}$
F_{33}	$\frac{1}{\sigma^u_{3T}\sigma^u_{3C}}$	$\frac{1}{\sigma_3^{u^2}}$	0	$\frac{1}{\sigma^u_{3T}\sigma^u_{3C}}$	$\frac{1}{\sigma_3^{u^2}}$
F_{44}	$\frac{1}{\sigma_{23}^{u^2}}$	$\frac{1}{\sigma_{23}^{u^2}}$	0	$\frac{1}{\sigma_{23}^{u^2}}$	$\frac{1}{\sigma_{23}^{u^2}}$
F_{55}	$\frac{1}{\sigma_{13}^{u^2}}$	$\frac{1}{\sigma_{13}^{u^2}}$	0	$\frac{1}{\sigma_{13}^{u^2}}$	$\frac{1}{\sigma_{13}^{u^2}}$
F_{66}	$\frac{1}{\sigma_{12}^{u^2}}$	$\frac{1}{\sigma_{12}^{u^2}}$	$\frac{1}{\sigma_{12}^{u^2}}$	$\frac{1}{\sigma_{12}^{u^2}}$	$\frac{1}{\sigma_{12}^{u^2}}$

F_i, F_{ij} and F_{ijk}	are related to the lamina strengths in the principal directions
$\sigma^u_1, \sigma^u_2, \sigma^u_3$	normal strength of the lamina in the 1,2 and 3 directions
$\sigma^u_{23}, \sigma^u_{13}, \sigma^u_{12}$	shear strengths of the material in the 23, 13 and 12 planes
$\sigma^u_1, \sigma^u_2, \sigma^u_3$: $\sigma^u_{1C}, \sigma^u_{2C}, \sigma^u_{3C}$ or $\sigma^u_{1T}, \sigma^u_{2T}, \sigma^u_{3T}$	depending on the sign of $\sigma_1, \sigma_2, \sigma_3$
K_{12}, K_{13} and K_{23}	strength coefficients depending on the material

Table 3.1: Different types of failure criteria have been grouped together showing the lamina strengths for all the principal directions. (171:p.3)

Yet, the Tsai-Hill failure criterion, which is an interactive failure criterion (i.e. it allows the interaction of multi-axial stresses) has been proven to be the most successful in a wide variety of circumstances. In its general form, the Tsai-Hill failure criterion can be defined as:

$$\left(\frac{\sigma_1}{\sigma_{1u}}\right)^2+\left(\frac{\sigma_2}{\sigma_{2u}}\right)^2-\left(\frac{\sigma_1\sigma_2}{\sigma_{1u}^2}\right)+\left(\frac{\tau_{12}}{\tau_{12u}}\right)^2\geq 1 \qquad (3.5)$$

The third term is comparably small and is generally neglected. The modified form of criterion is then defined as:

$$\left(\frac{\sigma_1}{\sigma_{1u}}\right)^2+\left(\frac{\sigma_2}{\sigma_{2u}}\right)^2+\left(\frac{\tau_{12}}{\tau_{12u}}\right)^2\geq 1 \qquad (3.6)$$

When using the above failure criteria, it is not possible to calculate the local failure in a region of the fibre and/or matrix under a particular stress combination. In fact, models were proposed, including a separate failure-criterion for fibre and matrix collapse, by making use of fracture plane-dependent stress components. Puck and Schurmann (176) proposed three kinds of fracture modes:

- 'Mode A – This incorporates inter-fibre failures under tensile stress on the plan perpendicular to the fibre direction and in-plane shear stress.
- Mode B - Failure due to a small compressive stress on the plane perpendicular to the fibre direction and large in-plane shear stress.
- Mode C - Failure due to a large compressive stress on the plane perpendicular to the fibre direction and small in-plane shear stress.' (176)

The Puck failure criterion (176) can be written as follows:

1. Fibre failure in tension:

$$\frac{1}{\varepsilon_{1T}}\left(\varepsilon_1+\frac{\nu_{f12}}{E_{f1}}m_{\sigma f}\sigma_{22}\right)=1 \qquad (3.7)$$

For $\varepsilon_1+\frac{\nu_{f12}}{E_{f1}}m_{\sigma f}\sigma_{22}\geq 0$

2. Fibre failure in compression:

$$\frac{1}{\varepsilon_{1C}}\left|\left(\varepsilon_1+\frac{\nu_{f12}}{E_{f1}}m_{\sigma f}\sigma_{22}\right)\right|+\left(10\gamma_{21}\right)^2=1 \qquad (3.8)$$

For $\varepsilon_1+\frac{\nu_{f12}}{E_{f1}}m_{\sigma f}\sigma_{22}<0$

3. Matrix failure in transverse tension:

$$\sqrt{\left(\frac{\tau_{21}}{s_{21}}\right)^2+(1-p^+_{vp}\frac{Y_T}{S_{21}})^2\left(\frac{\sigma_{22}}{Y_T}\right)^2}+p^+_{vp}\frac{\sigma_{22}}{S_{21}}+\frac{\sigma_{11}}{\sigma_{11D}}=1 \qquad (3.9)$$

For $\sigma_{22}\geq 0$

4. Matrix failure in moderate transverse compression:

$$\frac{1}{S_{21}}\left(\sqrt{\tau_{21}^2+(p^-_{vp}\sigma_{22})^2}+p^-_{vp}\sigma_{22}\right)+\frac{\sigma_{11}}{\sigma_{11D}}=1 \qquad (3.10)$$

$$\text{For } \sigma_{22}<0 \text{ and } 0 \leq \left|\frac{\sigma_{22}}{\tau_{21}}\right| \leq \frac{R^A_{vv}}{|\tau_{21C}|}$$

5. Matrix failure in large transverse compression:

$$\left[\left(\frac{\tau_{21}}{2(1+p^-_{vv})S_{21}}\right)^2+\left(\frac{\sigma_{22}}{Y_C}\right)^2\right]\frac{Y_C}{(-\sigma_{22})}+\frac{\sigma_{11}}{\sigma_{11D}}=1 \qquad (3.11)$$

$$\text{For } \sigma_{22}<0 \text{ and } 0 \leq \left|\frac{\tau_{21}}{\sigma_{22}}\right| \leq \frac{|\tau_{21C}|}{R^A_{vv}}$$

where, ε_{1T} – the tensile failure strain of a unidirectional layer in the x_1 direction

ε_{1C} – the compressive failure strain of a uni-directional layer in the $x_1$direction

ε_1 – the normal strain of a unidirectional layer

ν_{f12} – the Poisson's ratio for the fibre in the x_1 direction

E_{f1} – the Young's Modulus of elasticity for the fibre in the x_1 direction

$m_{\sigma f}$ – the mean stress magnification factor for the fibres in the x_2 direction

σ_{11} and σ_{22}– the normal stresses in a unidirectional layer

γ_{21} –the shear strain of a uni-directional layer in the elastic symmetry direction

τ_{21} –the shear stress of a uni-directional layer in the elastic symmetry direction

S_{21} –the shear stress of a uni-directional layer transverse and parallel to the fibre direction

p_{vp}^{+}, p_{vp}^{-}, p_{vv}^{-} – the fracture plane angle dependent parameters

σ_{11D} – the stress value for linear degradation

R_{vv}^{A} - the fracture resistance of the action plane against its fracture due to transverse/transverse shear stressing

τ_{21C} – the shear stress at the turning point of the (σ_{22},τ_{21}) fracture curve.

With the introduction of new inter-fibre fracture criteria, based on the brittle failure behaviour of composites, the Puck Failure criterion seems to offer a realistic approach. Using the Puck failure criterion, it is possible to evaluate the initial failure (i.e. the crack initiation in the fibre and/or matrix) as well as the progressive failure (i.e. the crack growth in the fibre and/or matrix) (176,177).

3.9 Conclusion

As discussed, it is not straightforward to quantify the rupture strength of a confined jacket, since, many mechanisms have to be taken into account when studying failure as in most situations it is a combination of several modes. A number of failure criteria were outlined. Yet, the Tsai Hill failure criterion has been proven to be successful in a wide variety of circumstances and thus, it is incorporated in this study.

The design and analysis oriented models described in this chapter are suitable to study the behaviour of auxetic jackets. Different systems have been discussed, where a number of these methodologies were adopted numerous times as preliminary analyses to study the behaviour of confinement jackets, giving satisfactory results. These analytical tools give adequate guidance on the failure stress of the confinement jackets. Therefore, by using the appropriate methods and CFRP, it is possible to explore and get an indication of the ultimate compressive strength and ultimate axial strain of the jackets.

Chapter 4.
Analysis of Negative Poisson's Ratio & Confinement Models

4.1 Introduction

In this chapter, a set of preliminary analyses is outlined to examine the confinement performance of auxetic laminates. As discussed in the previous chapter, a number of studies and models developed by researchers can be used to estimate the confinement and failure stresses of the CFRP jackets. An analysis-oriented model developed by Becque (17), Becque et al. (18) and a design-oriented model proposed by Lam et al. (19), Teng et al. (20) were chosen to test the stacking sequence configurations given in this study. The models are based on particular assumptions that are suitable for providing a preliminary analysis of the stresses encountered by the confinement jacket. It is important to note that these models can be utilised for evaluating auxetic laminates, since they are dependent on the properties of the individual laminae forming the jacket as well as their stacking sequence configuration. In fact, the equations presented in these models are, in most cases, reliant on the 2D classical laminate theory, that does not take into account the through thickness effect that occurs within an auxetic laminate. However, the expansion or contraction is minimal and, even though this effect will not be reflected in the overall failure strength of the laminate, these models still contribute to providing an adequate estimate for the jacket's failure stress.

4.2 SE70 CFRP Prepreg

As outlined in the previous chapter, most of the experimental research that studied confinement stresses made use of a wet lay up system, with the resin applied manually between the individual laminae. To study well the behaviour of wrapped auxetic laminates around RC columns, it is important to minimise human errors, since imperfections in the lay up can lead to their poor production. To enhance the Negative Poisson's ratio through thickness effect and test its effect on confinement, it is ideal that uniform properties are kept within the laminate. Thus, to achieve a uniform resin thickness between the individual layers and a better penetration of the resin, it is recommended to use a pre-impregnated CFRP. This choice affects the

manufacturing or lay-up methodology, which is considered to be more laborious when creating the required stacking sequences.

The curing temperature of the impregnated resin located within the fibres varies according to the selected type of prepreg. Likewise, even their mechanical properties have an impact on the actual value of the negative Poisson's ratio, which, in turn, also effects the expansion/contraction limit of the material. In addition, it is preferable to select a CFRP prepreg with a low curing temperature so as to minimise any adverse effects that high temperatures could cause to the concrete properties. The SE70 carbon prepreg provided by Gurit was used in this study for the manufacturing of confinement jackets. The cost and availability of the material also had an issue on the prepreg's choice. The SE70 is a hot melt epoxy prepreg recommended for the manufacturing of thick sections. It can be cured at temperatures as low as 70°C. However, rapid manufacture of components is possible where the prepreg is cured in 25-minutes at a temperature of 120°C. Table 4.1 gives an indication of the different curing temperatures and times that can be implemented for an SE70 prepreg. For a good balance of composite materials, it is best to cure the resin at a temperature of 70°C for 16 hours. This curing temperature is said to be quite low and does not cause any changes to the concrete properties. Furthermore, the material's properties seem to be adequate for the required purpose (Refer to Appendix A).

SE70 Prepreg Curing Temperatures & Times				
Typical Laminate	8 plies of 200g/cm^3 HEC UD carbon 37% resin content			
Curing Temperature	70°C	80°C	95°C	110°C
Cure Dwell Time	16 hours	8 hours	4 hours	50 min.
Cure Pressure	-1bar			

Table 4.1: Table showing the curing temperature & times of SE70 prepreg

4.3 Geometric Properties of Laminates

The SE70 CFRP prepreg was deliberately chosen for experimental purposes in this study. The material's properties and the resin's curing temperature have strongly influenced the choice of the material. The next step is to achieve the general properties of the SE70 prepreg laminates, evaluating the longitudinal and transversal Young's modulus of elasticity for every stacking sequence tested. In fact, this section groups together all the preliminary analysis required to confirm the characteristics of

the SE70 laminates when laid in specific stacking sequences or when subjected to particular loads. This analysis is carried out using both mathematical tools as well as aforementioned confinement models. The methodology implemented to wrap the concrete cylinders is discussed in detail in Chapter 5**.** The results obtained together with the experimental works tested in the laboratory will provide a better understanding of the auxetic confinement behaviour of confined cylindrical concrete specimens.

A number of experimental studies were carried out (155) using different types of FRPs, thicknesses or stacking sequence configurations. It can be stated that the performance of the laminate is dependent on its stiffness and axial rigidity. In addition, the thickness and the number of layers used to create the laminate are of utmost importance. It can be said that most stacking sequence configurations used for retrofitting RC columns consist of 0° fibre orientation angles (i.e. fibres are perpendicular to the applied/existing force).

By making use of suitable tools, it is possible to calculate both the failure strength of the CFRP and the number of layers deemed necessary for the laminate to withstand the compressive strength required. It is evident that the type of CFRP used has an effect on the compressive strength due to its mechanical properties. This too bears an impact on the number of layers required. The greater the number of layers, the greater is the gain in the axial load carrying capacity with respect to unconfined columns (128). Substantial increases in ductility were noted when increasing the number of wraps. Bearing in mind, the experimental works carried out by previous researchers and considering that the thickness of a single SE70 CFRP ply is equivalent to 0.2mm, in this research study, it was decided to proceed using a laminate containing a total of 8 layers, i.e. having a global thickness of 1.6mm.

Throughout this study, symmetric balanced angle-ply laminates having stacking sequence configurations of $[\pm 20]_{2s}$ and $[\pm 25]_{2s}$ will be used to create the auxetic laminates. Yet, so as to be able to confirm whether the negative Poisson's ratio through thickness effects are beneficial, it is necessary to provide a fair comparison with other stacking sequences. The criteria chosen were based on two approaches: the study of differences or improvements, if any, between auxetic

laminates that contain the major and minor Young's modulus of elasticity i.e. fibre orientation of 0° and 90°; and/or to compare the results of stacking sequences having the same Young's modulus of elasticity, but with different Poisson's ratios (i.e. negative and positive Poisson's ratios). In both situations, it is possible to show the differences in the stresses/strains, and consequently compare their load-carrying capacities. On site, the stacking sequences having fibre orientation angles at 0° are most commonly used as confinement jackets and so, it would be valuable to examine whether particular stacking sequences with a lower axial rigidity perform better than the ones with maximum axial rigidity. Compression tests were also carried out using confinement jackets having individual layers of 90°, i.e. whose fibres are parallel to the application of loading.

4.4 Classical Laminate Theory & Mechanics of Laminated Composites

Prior to testing or analysing the behaviour of auxetic laminates when wrapped around concrete columns, it is essential to have an initial prediction of the performance of FRP laminates, which can be done using suitable mathematical tools. Classical laminate theory (CLT) is frequently used to predict the in-plane performance of FRP composites. It provides the necessary tools to evaluate the properties of FRPs having different stacking sequence configurations. In addition, it is suitable for predicting the stress/strain distributions and failure mechanisms. Classical laminate theory neglects the out-of-plane components and is created on the plane stress assumption (178).

The Generalised Hooke's Law of stress and strain of any material is described as:

$$\sigma_i = C_{ij}\varepsilon_j \qquad (4.1)$$

In terms of strain

$$\varepsilon_j = S_{ij}\sigma_i \qquad (4.2)$$

where, C_{ij} is the stiffness matrix, S_{ij} is the compliance matrix, σ_i are the stress components and ε_j are the strain components.

The Generalised Hooke's Law for an orthotropic material reduces to (179):

$$\begin{bmatrix} \varepsilon_1 \\ \varepsilon_2 \\ \varepsilon_3 \\ \nu_{23} \\ \nu_{31} \\ \nu_{12} \end{bmatrix} = \begin{bmatrix} \frac{1}{E_1} & -\frac{\nu_{21}}{E_2} & -\frac{\nu_{31}}{E_3} & 0 & 0 & 0 \\ -\frac{\nu_{12}}{E_1} & \frac{1}{E_2} & -\frac{\nu_{32}}{E_3} & 0 & 0 & 0 \\ -\frac{\nu_{13}}{E_1} & -\frac{\nu_{23}}{E_2} & \frac{1}{E_3} & 0 & 0 & 0 \\ 0 & 0 & 0 & \frac{1}{G_{23}} & 0 & 0 \\ 0 & 0 & 0 & 0 & \frac{1}{G_{31}} & 0 \\ 0 & 0 & 0 & 0 & 0 & \frac{1}{G_{12}} \end{bmatrix} \begin{bmatrix} \sigma_1 \\ \sigma_2 \\ \sigma_3 \\ \tau_{23} \\ \tau_{31} \\ \tau_{12} \end{bmatrix} \quad (4.3)$$

CLT uses a number of assumptions and these include (180):

- 'The overall thickness of the laminate is very small when compared to its other dimensions;
- The individual layers forming the laminate are perfectly-bonded to one another;
- Lines perpendicular to the surface of the laminate remain straight and perpendicular to the surface after deformation;
- The individual laminae and laminate are linear-elastic;
- The through thickness stresses and strains are negligible;'

Since the thickness of the lamina is thin, and it is not able to carry out-of-plane loads, then, plane stress conditions can be assumed for the lamina. Therefore, taking σ_3 =0, τ_{31} =0, τ_{23} =0, the equation for orthotropic plane stress can be written as follows:

$$\begin{bmatrix} \varepsilon_1 \\ \varepsilon_2 \\ \gamma_{12} \end{bmatrix} = \begin{bmatrix} S_{11} & S_{12} & 0 \\ S_{12} & S_{22} & 0 \\ 0 & 0 & S_{66} \end{bmatrix} \begin{bmatrix} \sigma_1 \\ \sigma_2 \\ \tau_{12} \end{bmatrix} \quad (4.4)$$

Inverting equation (3.4), stress-strain relationship becomes,

$$\begin{bmatrix}\sigma_1\\ \sigma_2\\ \tau_{12}\end{bmatrix}=\begin{bmatrix}Q_{11} & Q_{12} & 0\\ Q_{12} & Q_{22} & 0\\ 0 & 0 & Q_{66}\end{bmatrix}\begin{bmatrix}\varepsilon_1\\ \varepsilon_2\\ \gamma_{12}\end{bmatrix} \quad (4.5)$$

where, Q_{ij} are the reduced stiffness coefficients.
These can be expressed in the following way:

$$Q_{11}=\frac{E_1}{1-\nu_{12}\nu_{21}};Q_{12}=\frac{\nu_{12}E_2}{1-\nu_{12}\nu_{21}};$$

$$Q_{22}=\frac{E_2}{1-\nu_{12}\nu_{21}};Q_{66}=G_{12}$$

where, E_1: longitudinal Young's modulus of elasticity (in direction 1);

E_2: transverse Young's modulus of elasticity (in direction2);

ν_{12}: major Poisson's ratio;

G_{12}: in plane shear modulus of elasticity (in plane 1-2).

It is very common for the lamina to be loaded at any other angle other than 0º or 90º. In this situation, the lamina is referred to as generally orthotropic, mainly because the loading direction does not coincide with the principal material directions. Thus, the stresses and strains are transformed into co-ordinated that do coincide with the principal material directions. This results in a new matrix, known as the lamina stiffness matrix, where (180):

$$[\bar{Q}]=[T]^{-1}[Q]\begin{bmatrix}1 & 0 & 0\\ 0 & 1 & 0\\ 0 & 0 & 2\end{bmatrix}[T], \quad (4.6)$$

And letting

m=cos θ and

n=sin θ,

the components are:

$$\overline{Q_{11}} = Q_{11}m^4 + 2(Q_{12} + 2Q_{66})m^2n^2 + Q_{22}n^4$$
$$\overline{Q_{12}} = (Q_{11} + Q_{22} - 4Q_{66})\, m^2n^2 + Q_{12}(m^4 + n^4)$$
$$\overline{Q_{22}} = Q_{11}n^4 + 2(Q_{12} + 2Q_{66})m^2n^2 + Q_{22}m^4$$
$$\overline{Q_{16}} = (Q_{11} - Q_{12} - 2Q_{66})\, m^3n + (Q_{12} - Q_{22} + 2Q_{66})mn^3$$
$$\overline{Q_{26}} = (Q_{11} - Q_{12} - 2Q_{66})\, n^3m + (Q_{12} - Q_{22} + 2Q_{66})nm^3$$
$$\overline{Q_{66}} = (Q_{11} + Q_{22} - 2Q_{12} - 2Q_{66})\, m^2n^2 + Q_{66}(m^4 + n^4) \quad (4.7)$$

The final stage of the CLT approach includes the characterisation of the relation of the laminate forces and moments to the strain and curvatures. A number of books and papers explain in detail all the theory related to the stresses and moments resultants of a laminate. (180-182). A diagrammatic representation is shown in Figure 4.1, where the loading N_x is a force per unit width of the cross section of the laminate and M_x is a moment per unit width acting on the laminate.

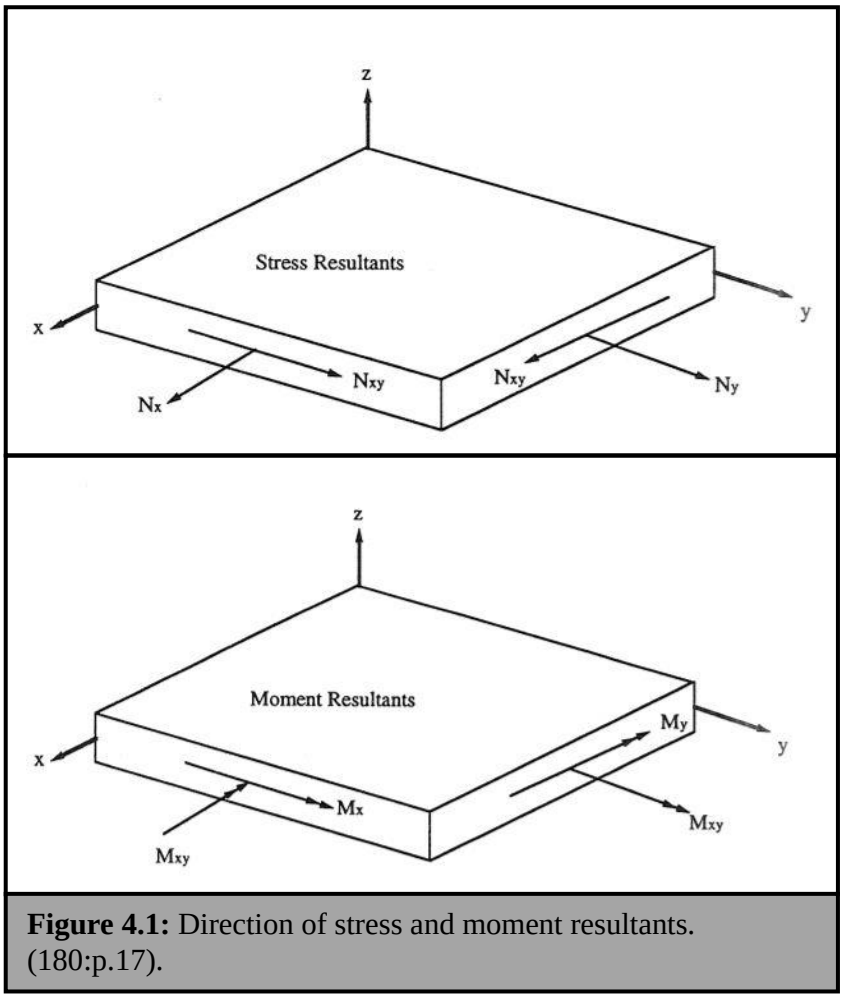

Figure 4.1: Direction of stress and moment resultants. (180:p.17).

Equations 4.8 – 4.10, denote the [A], [B] and [D] matrices that represent the extensional stiffnesses, bending-extension coupling stiffnesses and the bending stiffnesses respectively. The definitions of these matrices can be expressed as (180):

$$A_{ij} = \sum_{k=1}^{n} [\overline{Q_{ij}}]_k (h_k - h_{k-1}), \qquad (4.8)$$

$$B_{ij} = \frac{1}{2} \sum_{k=1}^{n} [\overline{Q_{ij}}]_k (h_k^2 - h_{k-1}^2), \qquad (4.9)$$

$$D_{ij} = \frac{1}{3} \sum_{k=1}^{n} [\overline{Q_{ij}}]_k (h_k^3 - h_{k-1}^3), \qquad (4.10)$$

The stacking sequences used in this study are symmetic laminates. This means that all elements forming part of the B_{ij} matrix are zero. This, in turn greatly simplifies finding the in-plane engineering constants of the laminate (180). In fact, the x direction Young's modulus of elasticity of the laminate can be expressed as:

$$E_{xx} = \frac{\sigma_x}{\epsilon_x} = \frac{N_{x/h}}{\epsilon_x} \qquad (4.11)$$

where h is the thickness of the laminate,

N_x is the stress resultant in the x direction,

The constitutive equations can be written as:

$$\begin{bmatrix} N_x \\ N_y \\ N_{xy} \end{bmatrix} = \begin{bmatrix} A_{11} & A_{12} & A_{16} \\ A_{12} & A_{22} & A_{26} \\ A_{16} & A_{26} & A_{66} \end{bmatrix} \begin{bmatrix} \varepsilon_x^0 \\ \varepsilon_y^0 \\ \gamma_{xy}^0 \end{bmatrix} \qquad (4.12)$$

A relationship between N_x and ϵ_x is sought, when a load is applied in the x direction, where the resultant equation is derived to be:

$$\frac{N_x}{\epsilon_x^0} = A_{11} + A_{12}\left(\frac{A_{26}A_{16} - A_{12}A_{66}}{A_{22}A_{66} - A_{26}^2}\right) + A_{16}\left(\frac{-A_{16}}{A_{66}} + \frac{A_{26}A_{12}A_{66} - A_{26}^2 A_{16}}{A_{22}A_{66}^2 - A_{26}^2 A_{66}}\right) \qquad (4.13)$$

Thus, E_{xx} is calculated by dividing equation 4.13 by the thickness of the laminate.

The same procedure is used to derive *Ey*, where:

$$\frac{N_x}{\epsilon_y^0} = A_{12}\left(\frac{A_{16}A_{26} - A_{12}A_{66}}{A_{11}A_{66} - A_{16}^2}\right) + A_{22} + A_{26}\left(\frac{-A_{26}}{A_{66}} + \frac{A_{16}A_{12}\,A_{66} - A_{16}^2A_{26}}{A_{11}A_{66}^2 - A_{16}^2A_{66}}\right) \tag{4.14}$$

E_{yy} is calculated by dividing equation 4.14 equation by the thickness of the laminate.

4.5 Calculation of Negative Poisson's Ratio ν_{13} and ν_{23}.

The through thickness effect caused by auxetic laminates is dependent on the values of ν_{13} and ν_{23}. Tessari (183) states that not many researchers have tackled this issue and there is not sufficient literature covering this topic. Only a few authors have studied its theoretical aspect (184-186). The classical laminate theory is widely used for the calculation of the properties of a composite material subjected to a given load condition. In most cases, when considering a composite to be subjected to in-plane tension, the tensions and deformations along the thickness are normally considered to be non-significant and are, therefore neglected. Yet, the values of these quantities, as well as the elastic constants that control them, at times, are of significant importance and their values need to be determined. In addition, the value of the laminate E_3 is often assumed to be equal to that of a single ply. This assumption is not completely correct, since the stiffening effects due to the coupling between the various planes are neglected. Recent studies (187) have concluded that more concise methodologies can be adapted to non-symmetrical, unbalanced laminates or even laminates made up of layers containing different materials.

With the increasing interest in materials exhibiting a negative Poisson's ratio, a number of studies carried out include a comparison between theoretical predictions and experimental measurements. The research methods proposed by Clarke et al. (188), Harkati et al. (45) and Tessari (183) were used to evaluate the values of ν_{13} and ν_{23} for the stacking sequences tested using an SE70 CFRP prepreg. All the three studies make use of classical laminate theory to provide the through thickness

Poisson's ratio. Tessari (183) gives an in-depth study on the behaviour of auxetic laminates with a thorough explanation on the fundamental principles required to examine the through thickness behaviour.

By subjecting the laminate to tension in the plane σ_1, and by finding the deformations that occur within the ply, i.e. both parallel and perpendicular to the direction of force, it is possible to derive the through thickness Poisson's ratio v_{13}. Likewise, when subjecting the laminate to tension in the plane σ_2, a similar procedure is to be followed so as to determine the value v_{23}.

Thus, the Poisson's ratio along the thickness of the laminate can be determined by the following summation:

$$v_{13} = \sum_j V_j \frac{\varepsilon_3^j}{\varepsilon_1} \qquad (4.15)$$

where *Vj*: the volume fraction of the jth ply;

Consequently, it can be said that:

$$v_{13} = \sum_j \frac{V_j}{1 - v_{12}^j v_{21}^j} (v_{13}^j (cos^2\theta^j (1 - v_{21}^j v_{12})) + sin^2\theta^j (v_{21}^j - v_{12})) + v_{23}^j (sin^2\theta^j (1 - v_{12}^j v_{12}) + cos^2\theta^j (v_{21}^j - v_{12}))) \qquad (4.16)$$

$$v_{23} = \sum_j \frac{V_j}{1 - v_{12}^j v_{21}^j} (v_{13}^j (sin^2\theta^j (1 - v_{21}^j v_{12})) + cos^2\theta^j (v_{21}^j - v_{12})) + v_{23}^j (cos^2\theta^j (1 - v_{12}^j v_{12}) + sin^2\theta^j (v_{21}^j - v_{12}))) \qquad (4.17)$$

In a similar way, by using a combination of classical laminate theory together with the appropriate 3-D constitutive equation, Harkati et al. (45) have derived the through-thickness Poisson's ratio for symmetric composite laminates subjected to axial loading. When using the stiffness and compliance coefficients as well as the inverse reduced stiffness matrix A_{ij}, the authors developed an equation that yields the through thickness Poisson's ratio of the laminate:

$$\nu_{13} = -\frac{1}{2h(A_{11})^{-1}} \begin{Bmatrix} (A_{11})^{-1} \\ (A_{12})^{-1} \\ (A_{16})^{-1} \end{Bmatrix} \left[\sum_{k=1}^{N} (S'_{31}S'_{32}S'_{36})^k \begin{pmatrix} Q'_{11} \\ Q'_{12} \\ Q'_{16} \end{pmatrix}^k t^k, \sum_{k=1}^{N} (S'_{31}S'_{32}S'_{36})^k \begin{pmatrix} Q'_{12} \\ Q'_{22} \\ Q'_{26} \end{pmatrix}^k t^k, \sum_{k=1}^{N} (S'_{31}S'_{32}S'_{36})^k \begin{pmatrix} Q'_{16} \\ Q'_{26} \\ Q'_{66} \end{pmatrix}^k t^k \right] \quad (4.18)$$

Using a similar approach, the following expression was obtained for ν_{23}:

$$\nu_{23} = -\frac{1}{2h(A_{22})^{-1}} \begin{Bmatrix} (A_{21})^{-1} \\ (A_{22})^{-1} \\ (A_{26})^{-1} \end{Bmatrix} \left[\sum_{k=1}^{N} (S'_{31}S'_{32}S'_{36})^k \begin{pmatrix} Q'_{11} \\ Q'_{12} \\ Q'_{16} \end{pmatrix}^k t^k, \sum_{k=1}^{N} (S'_{31}S'_{32}S'_{36})^k \begin{pmatrix} Q'_{12} \\ Q'_{22} \\ Q'_{26} \end{pmatrix}^k t^k, \sum_{k=1}^{N} (S'_{31}S'_{32}S'_{36})^k \begin{pmatrix} Q'_{16} \\ Q'_{26} \\ Q'_{66} \end{pmatrix}^k t^k \right] \quad (4.19)$$

where, N – the number of plies;

Q_{ij}^k – the stiffness coefficients;

t^k – individual thickness of k layer

$2h$ – the thickness of the laminate

S_{ij} – the Compliance transformation constants

Clarke et al. (188), have focused on symmetric balanced angle-ply laminates; i.e. balanced by being composed of an equal number of layers at ±θ to a reference direction and symmetric with respect to the stacking sequence about the centre of the laminate. Using the inverted stiffness matrix, it is possible to determine the compliance constants of the laminate, and consequently the engineering constants, i.e. Young's moduli of elasticity, shear moduli of elasticity and Poisson's ratio of the laminates. The Poisson's ratios are defined in Equation 4.20, whereas the Poisson's ratio of the laminate ν'_{ij} are defined using the stiffness constants C'_{ij} proposed in Equations 4.21.

$$\nu_{12} = -\left(\frac{S_{12}}{S_{22}}\right); \qquad \nu_{13} = -\left(\frac{S_{13}}{S_{33}}\right); \qquad \nu_{23} = -\left(\frac{S_{23}}{S_{33}}\right);$$

$$\nu_{21} = -\left(\frac{S_{21}}{S_{11}}\right); \qquad \nu_{31} = -\left(\frac{S_{31}}{S_{11}}\right); \qquad \nu_{32} = -\left(\frac{S_{32}}{S_{22}}\right) \quad (4.20)$$

The Poisson's ratio of the laminate can be expressed as (189):

$$\nu'_{12}=\left(\frac{C'_{12}C'_{33}-C'_{13}C'_{23}}{C'_{22}C'_{33}-C'_{23}C'_{23}}\right);\nu'_{21}=\left(\frac{C'_{12}C'_{33}-C'_{13}C'_{23}}{C'_{11}C'_{33}-C'_{13}C'_{13}}\right);\ \nu'_{13}=\left(\frac{C'_{22}C'_{13}-C'_{12}C'_{23}}{C'_{22}C'_{33}-C'_{23}C'_{23}}\right);$$

$$\nu'_{31}=\left(\frac{C'_{13}C'_{22}-C'_{12}C'_{23}}{C'_{11}C'_{22}-C'_{12}C'_{12}}\right);\ \nu'_{23}=\left(\frac{C'_{11}C'_{23}-C'_{12}C'_{13}}{C'_{11}C'_{33}-C'_{13}C'_{13}}\right);\ \nu'_{32}=\left(\frac{C'_{11}C'_{23}-C'_{12}C'_{13}}{C'_{11}C'_{22}-C'_{12}C'_{12}}\right)$$

(4.21)

Using the above-mentioned approaches, it is possible to determine the values of v_{13} and v_{23} for the different confinement jackets tested in this study. The only drawback encountered was that the SE70 data sheet provided by Gurit (Refer to Appendix A) did not source all the data necessary to evaluate them; mainly referring to the lamina values of v_{23} and G_{23}. The manufacturer confirmed that no testing was done on the prepreg to supply these values. So, in absence of these values, a study was carried out on other CFRPs. It can be said that a similar pattern or ratio was observed between the values of v_{13} and v_{23}. For instance, UM graphite/epoxy used in the studies of Harkati et al. (45) show that the values of ν_{23} is approximately 1.70 times the value of v_{13}, whereas the value of G_{13} is approximately 1.80 times the value of G_{23}. Likewise, the USN 150 carbon fibre-epoxy composite material (190) follows a similar pattern for the Poisson's ratios, where the values of v_{23} is approximately 1.75 times the value of ν_{13}, whereas the value of G_{13} is approximately 1.25 times the value of G_{23}. It is important to note that the value of G_{23} has no particular effect on the overall estimate of the through thickness Poisson's ratio of the laminate. On the contrary, the value of v_{23} does have a slight impact. Thus, a value of v_{23} = 0.56, whereas G_{23} was assumed to be equivalent to $1.65\text{x}10^9$ Pa.

Using these values for the SE70 CFRP lamina, a brief analysis was done for symmetric balanced angle-ply laminates, consisting of 8 plies with angles varying between 5° and 65°. As presented in Table 4.2, the behaviour of the through thickness Poisson's ratio for the various stacking sequence configurations was obtained. As was expected, the negative Poisson's ratios occurred with the angles in the region between 15° and 40°, with the peak values taking place between 20° and

30°. The maximum negative through thickness value achieved is approximately equal to -0.468 and occurred at stacking sequence configuration $[\pm25]_{2s}$. Only a 0.045 difference was noted between stacking sequence configurations $[\pm20]_{2s}$ and $[\pm25]_{2s}$. It is evident that the mechanical properties of the lamina have an impact on the behaviour of the laminate. If one had to compare the values obtained by other researchers (45, 183) where different laminates were tested, the negative through thickness Poisson's ratio was higher. Moreover, the peak value occurred for the $[\pm20]_{2s}$ stacking sequence configuration. In Table 4.3, the values calculated for the different stacking sequences tested in this study and manufactured using the SE70 CFRP prepreg are outlined accordingly.

$[\pm\theta]_{2s}$ [°]	±5	±10	±15	±18	±20	±22	±25	±28
	±30	±35	±40	±45	±50	±55	±60	±65
v_{13}	0.254	0.0602	-0.195	-0.333	-0.403	-0.448	-0.468	-0.435
	-0.392	-0.239	-0.072	0.0785	0.204	0.303	0.382	0.442
v_{23}	0.556	0.542	0.521	0.502	0.488	0.471	0.442	0.408
	0.382	0.303	0.203	0.0785	-0.072	-0.239	-0.392	-0.468

Table 4.2: Values of v_{13} and v_{23} for SE70 prepreg laminates

Using equations 4.13 and 4.14, it was possible to determine the Young's modulus of elasticity, E_{xx} of the laminates for the auxetic stacking sequence configurations $[\pm20]_{2s}$ and $[\pm25]_{2s}$. These were determined to be $8.40x10^{10}$ N/m^2 and $5.84x10^{10}$ N/m^2 respectively. Using an inverse function, the stacking sequences having the same axial rigidity i.e. Young's modulus of elasticity E_{xx} approximately equal to $8.40x10^{10}$ N/m^2 and $5.84x10^{10}$ N/m^2 were determined to be $[\pm35,0_2]_s$ and $[\pm16,\pm45]_s$ respectively. The Poisson's ratios ν_{13} and ν_{23} are determined for every stacking sequence. Thus, to summarise, as shown in Table 4.3, a total of six stacking sequence configurations are to be examined throughout this study. It resulted that $[\pm35,0_2]_s$ had a negative Poisson's ratio. Therefore, $[\pm20]_{2s}$, $[\pm25]_{2s}$ and $[\pm35,0_2]_s$ layouts are tested for auxetic confinement behaviour, whereas, the layouts $[\pm16, \pm45]_s$ $[0_8]$ and $[\pm90]_{2s}$ are to be used as a means of comparison as discussed.

Name	Stacking Sequence Configuration	Young's Modulus E_{xx} (N/m^2)	Poisson's Ratio ν_{13}	Poisson's Ratio ν_{23}
ST1	$[\pm 20]_{2s}$	8.40×10^{10}	-0.403	0.488
ST2	$[\pm 25]_{2s}$	5.84×10^{10}	-0.468	0.422
ST3	$[\pm 35, 0_2]_s$	8.40×10^{10}	-0.1078	0.475
ST4	$[\pm 16, \pm 45]_s$	5.84×10^{10}	0.007	0.399
ST5	$[0_8]$	13.7×10^{10}	0.56	0.324
ST6	$[90_8]$	0.781×10^{10}	0.324	0.56

Table 4.3: The table groups together the properties of the different stacking sequence configurations tested in this study.

4.4 Behaviour of Auxetic Laminates

The Tsai-Hill failure criterion is a conservative approach that is frequently used for checking the failure of the laminate. Similar to most other failure criteria methodologies, it assumes that the failure of the laminate occurs with the failure of the first lamina, which, in turn, is dependent on the weakest angle of the stacking sequence forming the laminate. As an initial study, using the Tsai-Hill failure criterion together with the available data and results achieved by Harkati et al. (45) and Tessari (183), it is interesting to obtain an idea of the failure strength behaviour of auxetic CFRP laminates. In these works, a systematic study of laminates with symmetric configuration $[\pm\beta/\pm\theta]_s$ (See Table 4.5) was conducted. Laminates consisting of eight layers having an overall thickness of 2mm were used, each having a volume fraction of 70% and an epoxy resin matrix. Increments of 5^o were tested, with finer increments of 1^o used within the range between 15^o and 25^o. An IM7 8552 prepreg was made use of with properties shown in Table 4.4. It was shown (45) that a negative Poisson's ratio was achieved when the values of θ varied between 0^o - 35^o, where the highest value of ν_{13} equivalent to -0.746 was obtained for ST1 having an angle of θ=20^o i.e. $[\pm 20]_s$. The values of ν_{13} and ν_{23} for stacking sequences with angles varying between 0^o - 35^o were calculated. Consequently, using classical laminate theory, it was possible to determine the stiffness matrices and eventually the Tsai-Hill failure criterion.

As shown in tables 4.6 - 4.14, graphs of ν_{13} versus Tsai-Hill failure criterion are plotted for each stacking sequence. A parabolic graph is obtained in most cases. For instance, by taking into consideration ST1, i.e. table 4.6, the same value of ν_{13} =0.28 is achieved when $\theta=10^o$ and when $\theta=35^o$, whereas two different failure values are obtained using the Tsai-Hill failure criterion, i.e. 1.30 MPa for $\theta=10^o$ and 0.21 MPa for $\theta=35^o$. This shows that the fibre orientation not only affects the auxeticity of the laminate, but also its possible rupture strength. A similar parabolic graph was obtained for ST2, ST7, ST8, ST10, ST14 and ST15. On the other hand, as shown in tables 4.13 and 4.14, a linear graph was obtained for ST18 and ST19 where positive values of Poisson's ratio were achieved.

General Data	
Characteristics	**UM graphite/epoxy**
E_1 [Pa]	2.90E+11
E_2 [Pa]	6.21E+09
E_3 [Pa]	6.21E+09
G_{12} [Pa]	4.83E+09
G_{13} [Pa]	4.83E+09
G_{23} [Pa]	2.66E+09
ν_{12}	0.25
ν_{13}	0.25
ν_{23}	0.42

Table 4.4: Characteristics of UM graphite/ epoxy laminate

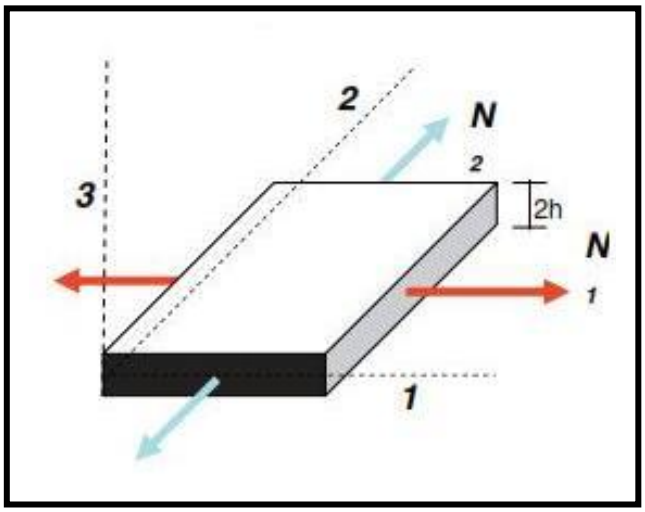

Figure 4.2: Laminate under axial loadings where *N* is the number of plies and 2*h* is the thickness of the laminate. (41:p.884)

Stacking Sequence Layouts					
ST1	$[\pm\theta_2]_s$	ST11	$[\pm33/\pm\theta]_s$	ST21	$[\pm10/\pm\theta]_s$
ST2	$[0_2/\pm\theta]_s$	ST12	$[\pm35/\pm\theta]_s$	ST22	$[\pm15/\pm\theta]_s$
ST3	$[90_2/\pm\theta]_s$	ST13	$[\pm37/\pm\theta]_s$	ST23	$[\pm16/\pm\theta]_s$
ST4	$[-\theta/+\theta/-\theta/+\theta]_s$	ST14	$[\pm40/\pm\theta]_s$	ST24	$[\pm17/\pm\theta]_s$
ST5	$[\pm\theta/0_2]_s$	ST15	$[\pm45/\pm\theta]_s$	ST25	$[\pm18/\pm\theta]_s$
ST6	$[\pm\theta/90_2]_s$	ST16	$[\pm50/\pm\theta]_s$	ST26	$[\pm19/\pm\theta]_s$
ST7	$[\pm20/\pm\theta]_s$	ST17	$[\pm60/\pm\theta]_s$	ST27	$[\pm21/\pm\theta]_s$
ST8	$[\pm25/\pm\theta]_s$	ST18	$[\pm70/\pm\theta]_s$	ST28	$[\pm22/\pm\theta]_s$
ST9	$[\pm27/\pm\theta]_s$	ST19	$[\pm80/\pm\theta]_s$	ST29	$[\pm23/\pm\theta]_s$
ST10	$[\pm30/\pm\theta]_s$	ST20	$[\pm5/\pm\theta]_s$	ST30	$[\pm24/\pm\theta]_s$

Table 4.5: Different stacking sequences tested.

ST1 - $[\pm\theta_2]_s$		
Angle (θ)	v_{13}	Tsai Hill (MPa)
10°	-0.275	1.300
15°	-0.6	1.010
20°	-0.74	0.672
25°	-0.65	0.436
30°	-0.45	0.294
35°	-0.28	0.212

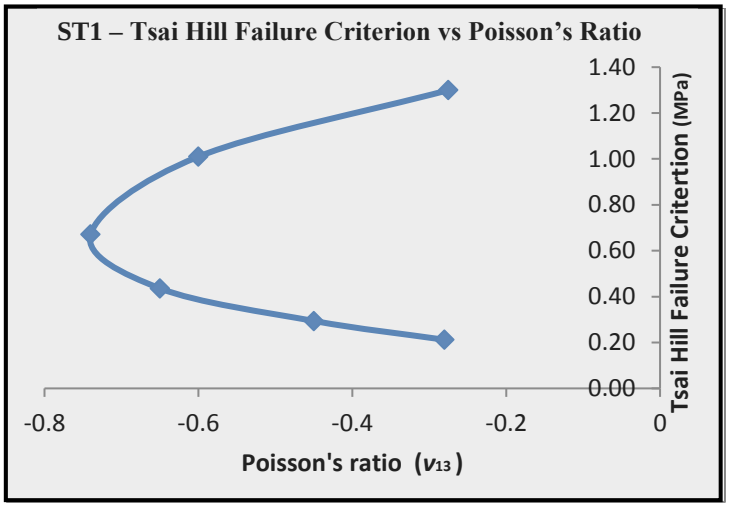

Table 4.6: Results of ST1 & Graph of Tsai-Hill Failure Criterion vs Poisson's ratio (v_{13})

ST2 - $[0_2/\pm\theta]_s$		
Angle (θ)	v_{13}	Tsai Hill (MPa)
10°	0	1.370
15°	-0.265	1.250
20°	-0.385	1.100
25°	-0.41	0.967
30°	-0.325	0.876
35°	-0.26	0.820

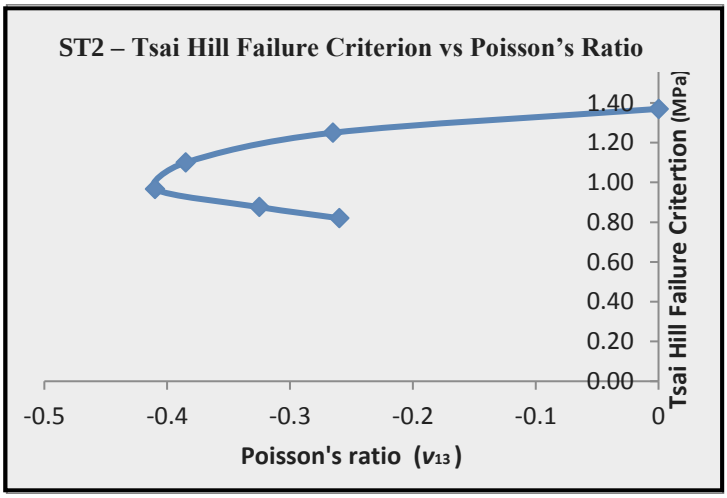

Table 4.7: Results of ST2 & Graph of Tsai-Hill Failure Criterion vs Poisson's ratio (v_{13})

ST7 - $[\pm20/\pm\theta]_s$		
Angle (θ)	v_{13}	Tsai Hill (MPa)
10°	-0.575	0.984
15°	-0.68	0.837
20°	-0.74	0.672
25°	-0.68	0.550
30°	-0.57	0.497
35°	-0.35	0.506

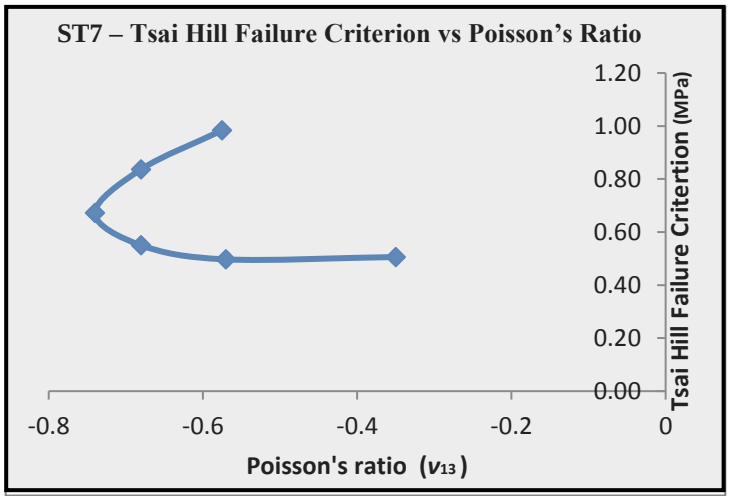

Table 4.8: Results of ST7 & Graph of Tsai-Hill Failure Criterion vs Poisson's ratio (v_{13})

ST8 - $[\pm 25/\pm\theta]_s$		
Angle (θ)	v_{13}	Tsai Hill (MPa)
10°	-0.55	0.856
15°	-0.64	0.712
20°	-0.7	0.550
25°	-0.66	0.436
30°	-0.52	0.370
35°	-0.38	0.363

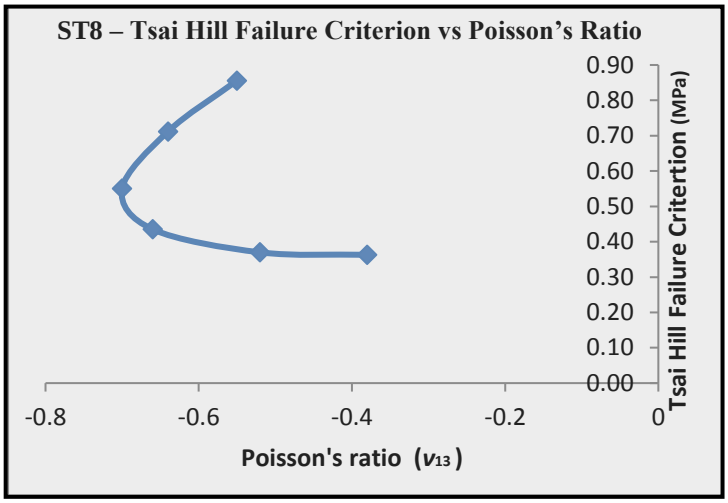

Table 4.9: Results of ST8 & Graph of Tsai-Hill Failure Criterion vs Poisson's ratio (v_{13})

ST10 - $[\pm 30/\pm\theta]_s$		
Angle (θ)	v_{13}	Tsai Hill (MPa)
10°	-0.41	0.779
15°	-0.5	0.659
20°	-0.57	0.497
25°	-0.55	0.370
30°	-0.45	0.294
35°	-0.33	0.264

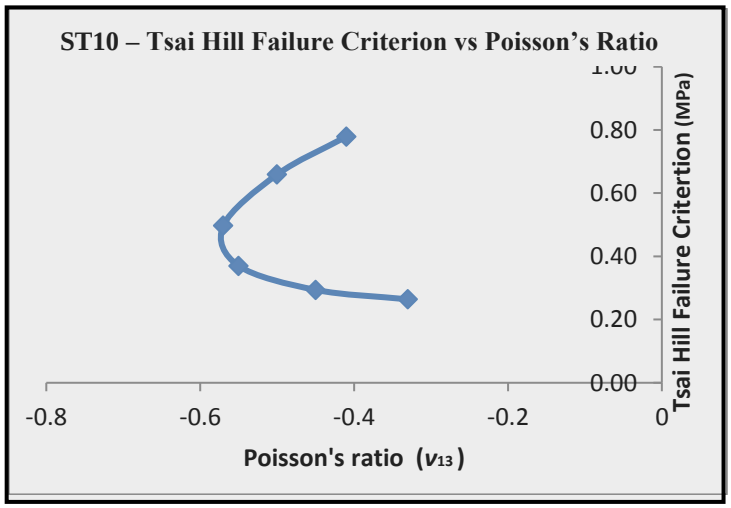

Table 4.10: Results of ST10 & Graph of Tsai-Hill Failure Criterion vs Poisson's ratio (v_{13})

ST14 - $[\pm 40/\pm\theta]_s$		
Angle (θ)	v_{13}	Tsai Hill (MPa)
10°	-0.14	0.721
15°	-0.18	0.636
20°	-0.23	0.522
25°	-0.26	0.395
30°	-0.24	0.279
35°	-0.15	0.200

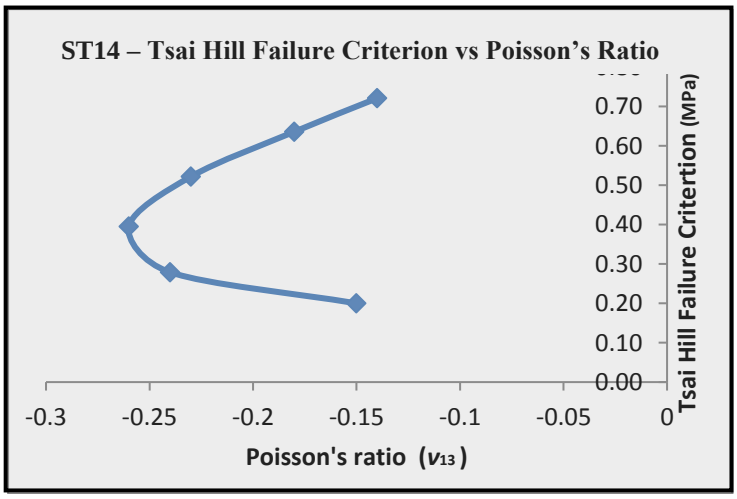

Table 4.11: Results of ST14 & Graph of Tsai-Hill Failure Criterion vs Poisson's ratio (v_{13})

ST15 - [±45/±θ]$_s$		
Angle (θ)	v_{13}	Tsai Hill (MPa)
10°	0	0.714
15°	-0.04	0.643
20°	-0.08	0.546
25°	-0.095	0.431
30°	-0.09	0.316
35°	-0.05	0.222

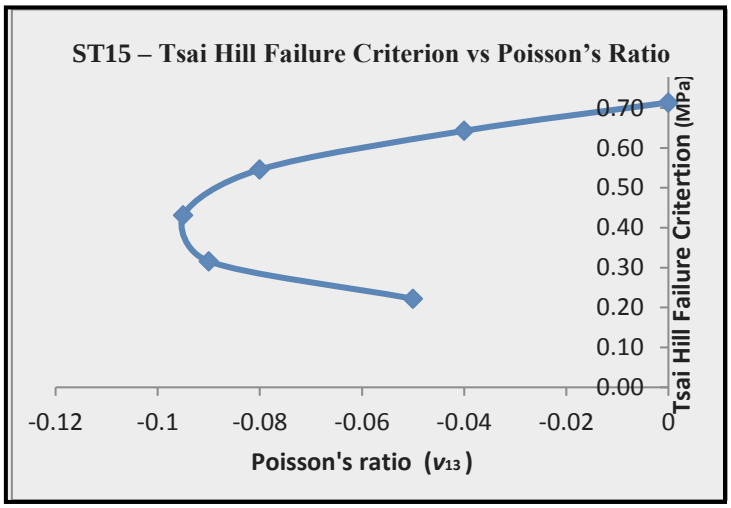

Table 4.12: Results of ST15 & Graph of Tsai-Hill Failure Criterion vs Poisson's ratio (v_{13})

ST18 - [±70/±θ]$_s$		
Angle (θ)	v_{13}	Tsai Hill (MPa)
10°	0.305	0.712
15°	0.3	0.675
20°	0.295	0.623
25°	0.29	0.557
30°	0.28	0.480
35°	0.27	0.395

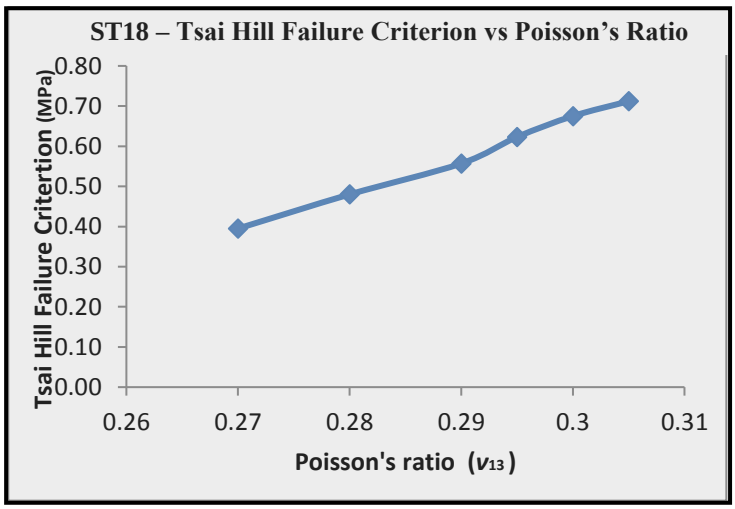

Table 4.13: Results of ST18 & Graph of Tsai-Hill Failure Criterion vs Poisson's ratio (v_{13})

ST19 - [±80/±θ]$_s$		
Angle (θ)	v_{13}	Tsai Hill (MPa)
10°	0.35	0.710
15°	0.34	0.676
20°	0.33	0.629
25°	0.32	0.570
30°	0.31	0.499
35°	0.305	0.421

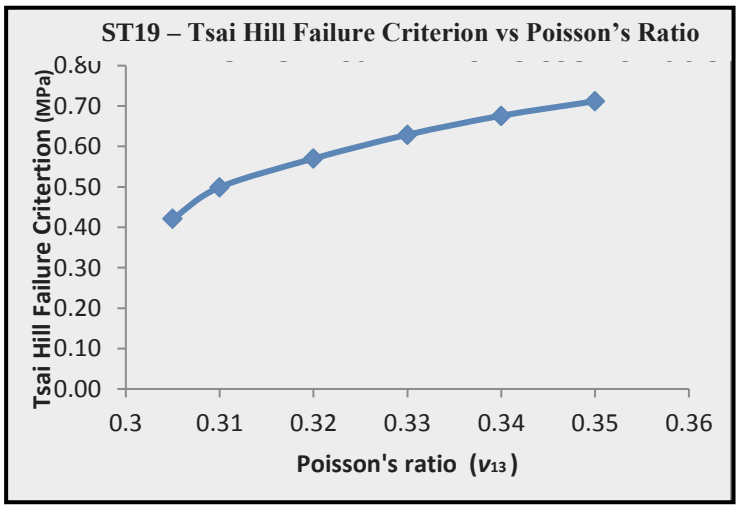

Table 4.14: Results of ST19 & Graph of Tsai-Hill Failure Criterion vs Poisson's ratio (v_{13})

The same procedure was repeated for the SE70 CFRP, where the symmetric balanced angle-ply laminates were considered, i.e. $[\pm\theta]_{2s}$. The negative values obtained for the stacking sequences shown in Table 4.2 were selected and a graphical representation was presented. As depicted in Table 4.15, a 'parabolic' graph was obtained with the peak occurring at v_{13} of -0.468. When comparing Table 4.6 with Table 4.15, it can be observed that the material properties forming the CFRP do have an impact on the behaviour of the laminate. As could be noted, the ranges of the negative values achieved together with the values of when the failure of the laminate occurs using the Tsai-Hill failure criterion vary substantially.

ST1 - $[\pm\theta_2]_s$		
Angle (θ)	v_{13}	Tsai Hill (Mpa)
15˚	-0.195	1.380
20˚	-0.403	0.908
25˚	-0.468	0.585
30˚	-0.392	0.394
35˚	-0.239	0.279
40˚	-0.072	0.177

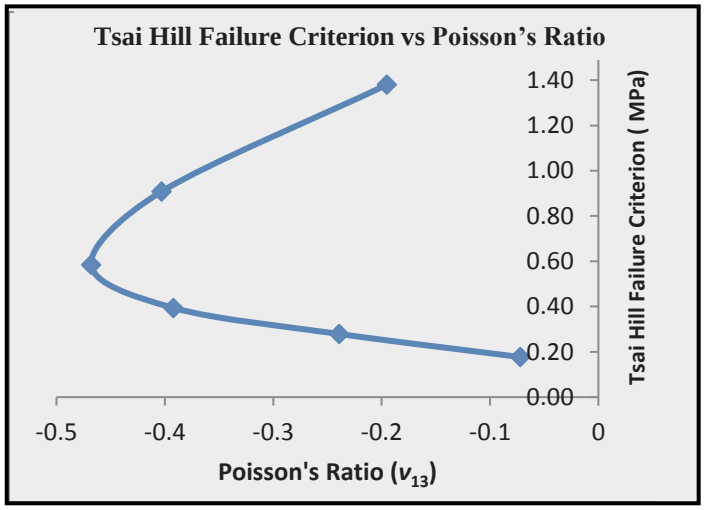

Table 4.15: Results of ST1 & Graph of Tsai Hill Failure Criterion vs Poisson's ratio (v_{13}) using SE70 CFRP prepreg properties

4.5 Design-Oriented Confinement Model

As discussed previously in Chapter 3, there are two main approaches for carrying out an initial study of the stresses for a confined concrete cylinder. These are namely the design-oriented and analysis-oriented models. Both types of models were studied extensively by various researchers, each proposing their own methodology, where they focus on particular aspects. Thus, as shown by Sutherland (191) some models may have some deficiencies when compared to others. The selection of the models chosen throughout this study was based on the methodology adopted and on the relevance of the work carried out by the researchers regarding this field. For instance, Lam et al. (19), Teng et al. (20) carried out extensive studies proposing

confinement models using both analysis (143) as well as design oriented models (19, 20), at times even proposing improvements to their original models. The design-oriented model proposed by these researchers was recognised and adopted for design guidance specifically for the strengthening of concrete structures using FRP issued by the Concrete Society (2004) in the UK (192) as well as by ACI-440.2r (2008) (116) with slight modifications. As a consequence, it was decided to use this model for this research study. The proposed design-oriented stress-strain model is suitable for concrete columns strengthened with an external FRP jacket in which the reinforcing fibres are predominantly oriented in the hoop directions (i.e. the jacket has little longitudinal stiffness). Their initial model (19) involved the use of a database containing experimental results available in open research literature. Analysis oriented-models proposed by other researchers, with particular reference to the work of Spoelstra and Monti (129), were also consulted and their findings were used for deriving closed form equations. In fact, Lam et al. (19) concluded that the criterion for insufficient confinement, adopted in Spoelstra and Monti's (129) analysis oriented-model, proved satisfactory. Thus, the FRP-confined concrete, having an actual confinement ratio (i.e. the ratio of the maximum confining pressure to the unconfined concrete strength) greater or equal to 0.07, is considered to be sufficiently-confined. In the refined version (20), using more data that was already available to the authors, the hoop tensile strain reached by the FRP jacket at rupture was subsequently revised.

The authors have also studied the mode of failure for FRP-confined concrete. It was shown that there is an evident difference between the FRP tensile strength or ultimate strain from material tests (i.e. tests done on the FRP alone) and the corresponding values reached in tests on FRP-confined concrete specimens. It appears that this difference is due to deformation localisation in cracked concrete that can lead to a non-uniform stress distribution in the FRP jacket, thereby causing premature rupture of the FRP and also due to the effect of curvature of an FRP jacket on the tensile strength of the FRP. It was stated that the specimens used in this model failed by rupture of the FRP jacket due to hoop tension. The stress-strain graphical representations of the experimental investigation were tested and it was noted that most specimens followed a monotonically ascending bi-linear shape, where both the compressive strength as well as the ultimate strain reach the same point. Eventually,

other types of stress-strain curves may result, but these too were taken into consideration.

By analysing the above-mentioned factors, Lam et al. (19) proposed their design-oriented stress strain model based on the following assumptions:

- 'the stress-strain curve consists of an initial parabolic portion followed by a straight line second portion;
- the slope of the parabola at zero axial strain (the initial slope) is the same as the elastic modulus of elasticity of the unconfined concrete, $E_{c;}$
- the non-linear part of the first portion is affected, to some degree, by the presence of an FRP jacket;
- the parabolic first portion meets the linear second portion smoothly (i.e. there is no change in slope between the two portions where they meet);
- the linear second portion terminates at a point, where both the compressive strength and the ultimate axial strain of confined concrete are reached;
- the linear second portion intercepts the axial stress axis at a stress equal to the unconfined concrete strength.' (19:p.480)

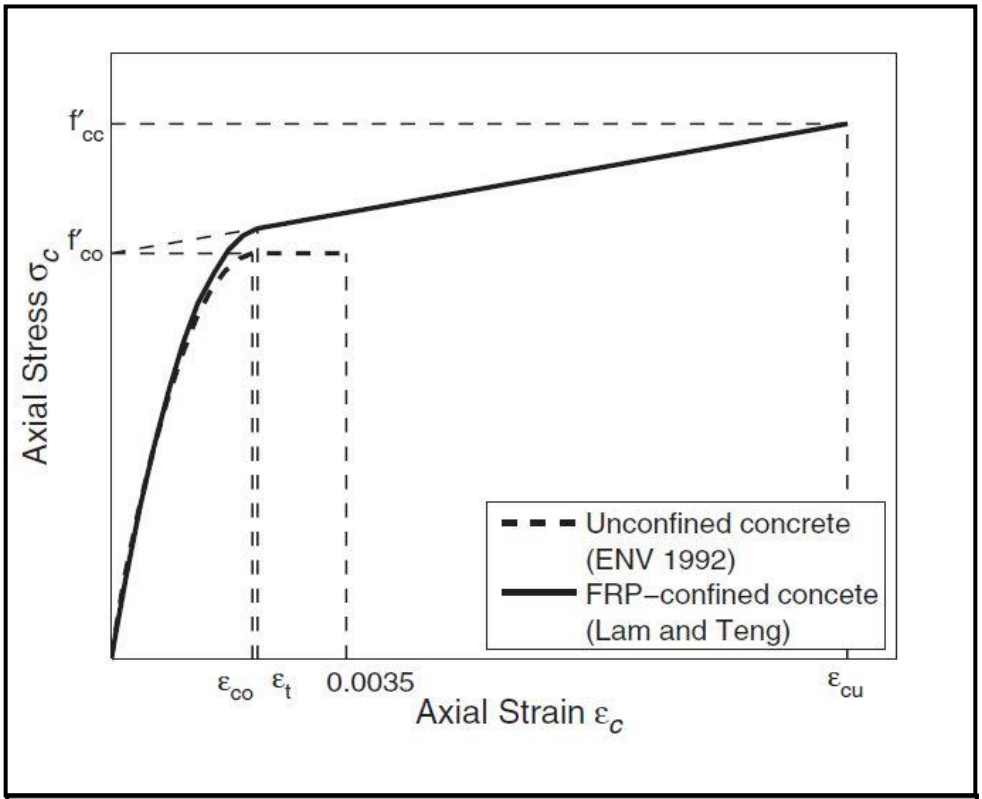

Figure 4.3: The graph is an illustration of Lam and Teng's design-oriented confinement model (20:p.272).

Based on these assumptions, the model is then followed by three basic ratios namely, the confinement ratio, the confinement stiffness ratio and the strain ratio. These are outlined by the following equations:

The confinement ratio f_l/f'_{co} (i.e. the ratio of the maximum confining pressure to the unconfined concrete strength):

$$\frac{f_l}{f'_{co}} = \frac{2E_{FRP}t\varepsilon_{h,rup}}{f'_{co}D} = \rho_K\rho_\varepsilon \qquad (4.22)$$

The confinement stiffness ratio, ρ_K (i.e. the stiffness of the FRP jacket relative to the unconfined concrete core stiffness):

$$\rho_K = \frac{2E_{FRP}t}{(f'_{co}/\varepsilon_{co})D} \qquad (4.23)$$

The strain ratio, ρ_ε (i.e. the ratio of the hoop rupture strain of the FRP jacket to the unconfined concrete axial strain):

$$\rho_\varepsilon = \frac{\varepsilon_{h,rup}}{\varepsilon_{co}} \qquad (4.24)$$

where, f_l: Confining pressure provided by the FRP jacket until it fails by rupture due to hoop tensile forces;

f'_{co}: Average value of unconfined concrete strength;

E_{FRP}: Elastic Modulus of elasticity of the CFRP in the hoop direction;

$\varepsilon_{h,rup}$: Hoop rupture strain of FRP jacket;

t: Thickness of FRP;

D: Diameter of the cylinder;

ε_{co}: Axial strain of unconfined concrete

Lam et al. (19), Teng et al. (20) stress-strain model can be developed using the following equations, where Equation 4.25 provides the stress-strain curve for the parabolic first portion of the graph, whereas Equation 4.26 estimates the linear second portion:

$$\sigma_c = E_C\varepsilon_C\frac{(E_C - E_2)^2}{4f'_{co}}\varepsilon_c^2 \qquad \text{for } 0 \le \varepsilon_c < \varepsilon_t \qquad (4.25)$$

$$\sigma_c = f'_{co} + E_2\varepsilon_C \qquad \text{for } \varepsilon_t \le \varepsilon_c \le \varepsilon_{cu} \qquad (4.26)$$

The slope of the second linear portion and the transition point are defined using the following equations:

$$E_2 = \frac{f'_{cc} - f'_{co}}{\varepsilon_{cu}} \qquad (4.27) \qquad \varepsilon_t = \frac{2 f'_{co}}{E_C - E_2} \qquad (4.28)$$

where, E_c: Elastic Modulus of elasticity of the unconfined concrete, defined as $4730\sqrt{f'_{co}}$;

E_2: The slope of the second linear portion;

ε_t: Transition point, i.e. where the parabolic first portion meets the linear second portion with a smooth transition;

σ_c: Axial stress;

f'_{cc}: Compressive strength at rupture;

ε_{cu}: Ultimate axial strain at failure;

f'_{cu} : Axial stress of FRP-confined concrete at ultimate axial strain.

The ultimate axial strain and the axial stress at the ultimate axial strain are found by using:

$$\frac{\varepsilon_{cu}}{\varepsilon_{co}} = 1.75 + 6.5\rho_K^{0.8}\rho_\varepsilon^{1.45} \qquad (4.29)$$

$$\frac{f'_{cu}}{f'_{co}} = 1 + (3.2\rho_K^{0.9} - 0.06)\rho_\varepsilon \qquad (4.30)$$

It is worth mentioning that the model provides a distinction between the values of f'_{cc} and f'_{cu}, where the former is the compressive strength of FRP confined concrete, whereas the latter predicts the ultimate axial stress at the ultimate axial strain. The difference is generally minimal and, in most situations, these values are taken to be equal in value, unless the stress-strain curve features a descending branch. Therefore, as proposed by Teng et al. (20), it can be stated that:

$$\frac{f'_{cc}}{f'_{co}} = 1 + 3.5(\rho_K - 0.01)\rho_\varepsilon \qquad \text{if } \rho_k \geq 0.01 \qquad (4.31)$$

$$\frac{f'_{cc}}{f'_{co}} = 1 \qquad \text{if } \rho_k < 0.01 \qquad (4.32)$$

Using the above methodology, a stress-strain diagram can be derived. By means of the concrete properties used for testing the cylinders, together with the Young's moduli of elasticity of the laminates provided in Table 4.3, for the SE70 prepreg CFRP confinement jackets tested in this study, it is possible to acquire an indication regarding the behaviour of the jackets.

The most common failure criterion is that the laminate is said to fail the moment one of the individual laminae fails. It is evident that this will occur on the weakest angle or lamina. On the other hand, the model of Lam et al. (19), refers to the ultimate rupture of the laminate, i.e. failure of all the layers. In fact, the only unknown parameter required is the ultimate hoop rupture strain, $\varepsilon_{h,rup}$. However, the model of Lam et al. (19), proposes that, for CFRP-wrapped concrete specimen, it can be assumed that the value of $\varepsilon_{h,rup}$ is 0.586 times the value of tensile strain ε_{frp} found from flat coupon tests. In addition, when referring to the studies of Spoelstra and Monti (129), it was assumed that the FRP hoop rupture strain of the jacket is equivalent to 60% of the value of the material's ultimate tensile strain achieved from coupon tests. Thus, using the failure loads obtained from the tensile tests carried out in the laboratory, it is possible to provide an initial understanding of the stress-strain behaviour using this design-oriented model.

In fact, tensile tests were carried out using the Instron 1342 tensile testing machine, for $[\pm 20]_{2s}$, $[\pm 25]_{2s}$, and $[0_8]$ configurations. Specimens with dimensions of 290mm in length and 20mm in width were tested to failure to investigate the through thickness behaviour. By assuming a linear-elastic behaviour and using the average failure loads obtained from the tensile tests, it is possible to evaluate the stresses and strains of these configurations. The stress-strain diagram (Figure 4.4) depicts a bi-linear curve as expected. The design-oriented model is, in fact, modelled in such a way as to provide a bi-linear curve. Using Equations 4.15 and 4.16, it is possible to plot a graphical representation of the actual values obtained versus the predicted ones. Therefore, it can be determined whether the ultimate axial strain and the ultimate compressive strength of the jackets give a better performance. These results are presented later on in Chapter 6.

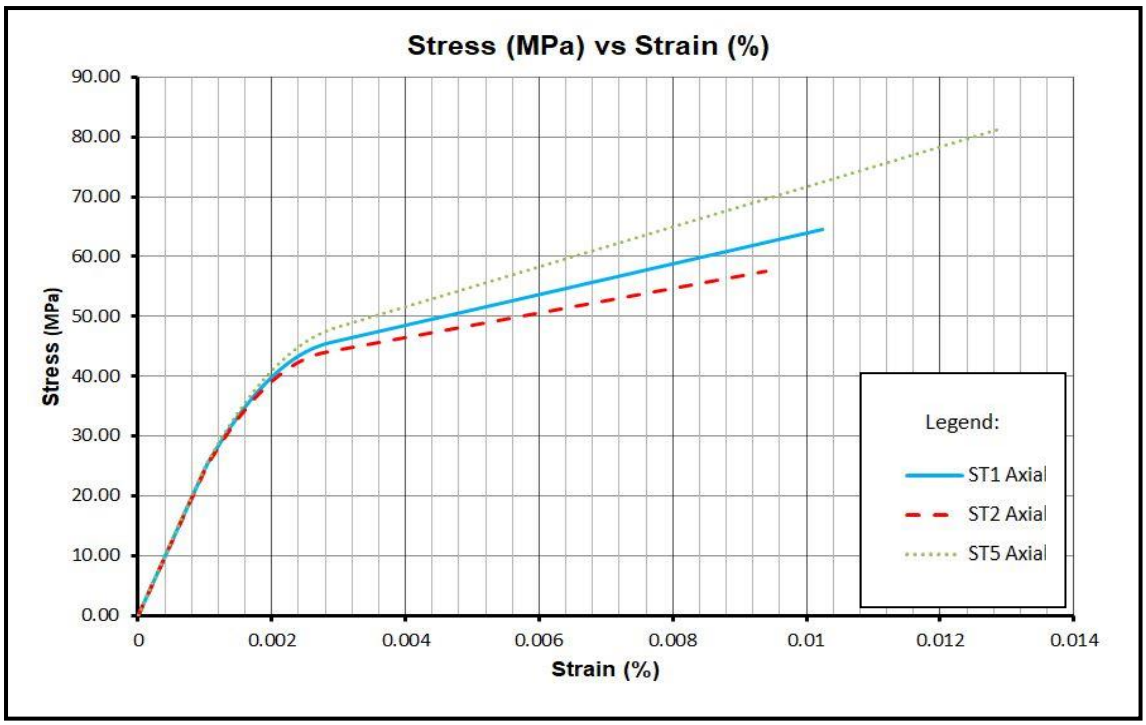

Figure 4.4: Stress (MPa) vs Strain (%) Graph showing a comparison of ST1, ST2 & ST5 using Lam and Teng's design-oriented confinement model (19, 20).

4.6 Analysis-Oriented Confinement Model

As discussed in Section 3.6.1, there are a number of confinement models that were developed over the years. Various methodologies and concepts were proposed, each offering a suitable approach for providing an initial estimate of the confinement stresses, and consequently the ultimate failure strength of the CFRP. An interesting concept was introduced in the iterative model formulated by Becque (17), Becque et al. (18). This analysis-oriented model is designed around Gerstle's (193, 194) octahedral theory and his equations for tri-axial state of stresses, where pressure has a significant influence on the deformation behaviour of the concrete. It reflects the passive confinement caused by an FRP jacket by adopting an incremental approach. The experimental results provided satisfactory results and were also approved by 'ISIS'.

The tri-axial state of stresses in concrete can be grouped into two equivalent 'octahedral' stresses: a hydrostatic stress σ_0 or octahedral normal stress that is related to the volume change of the material; and a deviatoric stress τ_0 or octahedral shear

stress that causes the distortional or shape change portion of the strains. These two stresses are subsets of any given stress tensor. Using the principal stresses in the concrete (i.e. σ_1, σ_2 and σ_3), the octahedral stresses are represented by the following equations:

Hydrostatic stress: $$\sigma_0 = \frac{1}{3}(\sigma_1 + \sigma_2 + \sigma_3) \quad (4.33)$$

Deviatoric stress: $$\tau_0 = \frac{1}{3}\sqrt{(\sigma_1 - \sigma_2)^2 + (\sigma_2 - \sigma_3)^2 + (\sigma_3 - \sigma_1)^2} \quad (4.34)$$

The confinement model presented by Becque (17) is based on the principles of strain compatibility and equilibrium occurring in the lateral direction between the CFRP laminate and the core, combined with the tri-axial constitutive relations for the concrete proposed by Gerstle (194). It is assumed that the compressive load is only applied to the concrete core and the CFRP laminate does not carry any load in the axial direction. The wrapped laminate around the concrete core is such that there is no transfer of stresses into the laminate at the interface and only provides confinement to the core. In his work, Becque (17), Becque et al. (18) takes into consideration the fact that the volumetric strain ε_0 varies with the hydrostatic stress σ_0, whereas both the deviatoric and volumetric strains vary with deviatoric stress.

The initial step is to determine the values of the principal stress increments. The value of σ_1 is dependent on the axial load applied to the concrete cylinder. This loading is applied in increments, $\Delta\sigma_1$. Assumed values of $\Delta\sigma_2$ are assigned. The concrete radial and circumferential stresses are equal in magnitude, i.e. $\Delta\sigma_2=\Delta\sigma_3$. The incremental hydrostatic stresses $\Delta\sigma_0$ and incremental deviatoric stresses $\Delta\tau_0$ can then be calculated using the equations below:

$$\Delta\sigma_0 = \frac{1}{3}(\Delta\sigma_1 + \Delta\sigma_2 + \Delta\sigma_3) \quad (4.35)$$

$$\Delta\tau_0 = \frac{1}{3}\sqrt{(\Delta\sigma_1 - \Delta\sigma_2)^2 + (\Delta\sigma_2 - \Delta\sigma_3)^2 + (\Delta\sigma_3 - \Delta\sigma_1)^2} \quad (4.36)$$

Stresses and strains are related to each other via their octahedral forms. Thus, the concrete radial and circumferential strain increments $\Delta\varepsilon_2$ and $\Delta\varepsilon_3$, that are equal in

magnitude, can be determined. Consequently, the octahedral volumetric strain increments $\Delta\varepsilon_0$ and the octahedral deviatoric strain increment $\Delta\gamma_0$ can be evaluated. These increments can be calculated using the equations as follows:

$$\Delta\varepsilon_0 = \frac{1}{3}(\Delta\varepsilon_1 + \Delta\varepsilon_2 + \Delta\varepsilon_3) \tag{4.37}$$

$$\Delta\gamma_0 = \frac{1}{3}\sqrt{(\Delta\varepsilon_1 - \Delta\varepsilon_2)^2 + (\Delta\varepsilon_2 - \Delta\varepsilon_3)^2 + (\Delta\varepsilon_3 - \Delta\varepsilon_1)^2} \tag{4.38}$$

The CFRP laminate wrapped around the cylinder is subjected to a bi-axial state of stress, i.e. longitudinal stresses in the loading direction and hoop stresses due to the lateral expansion of the core. The incremental stress state in the shell can be determined using:

$$\Delta\sigma_{long} = \frac{(\Delta\varepsilon_1 + \nu'_f\,\Delta\varepsilon_2)E_{long}}{1-\nu_f\nu'_f} \tag{4.39}$$

$$\Delta\sigma_{hoop} = \frac{(\Delta\varepsilon_2 + \nu'_f\,\Delta\varepsilon_1)E_{hoop}}{1-\nu_f\nu'_f} \tag{4.40}$$

where, $\Delta\sigma_{long}$: incremental longitudinal stress in the shell;

$\Delta\sigma_{hoop}$: incremental hoop stress in the shell;

E_{long} : Young's modulus of elasticity of the FRP shell material in the longitudinal direction;

E_{hoop} : Young's modulus of elasticity of the FRP shell material in the hoop direction;

ν'_f :minor Poisson's ratio of the FRP;

ν_f :major Poisson's ratio of the FRP;

$\Delta\varepsilon_1$ and $\Delta\varepsilon_2$:incremental principal strains in the concrete.

Referring to the available technical data of the laminate used together with classical laminate theory, it is possible to calculate the values of ν_f, ν'_f, E_{hoop} and E_{long} of the laminate having a particular stacking sequence configuration. The incremental confining pressure corresponding to the incremental hoop tensile stress in the shell is:

$$\Delta\sigma'_2 = \frac{\Delta\sigma_{hoop}t}{R} \tag{4.41}$$

where, $\Delta\sigma'_2$: incremental hoop tensile stress in the shell;

$\Delta\sigma_{hoop}$:incremental hoop stress in the shell;

t : thickness of the laminate;

R : radius of the concrete core.

The model assumes that the hoop stress increment is equal in value to the corresponding confining pressure increment. Thus, the initial values of σ_2 are changed and the above steps are repeated until the ratio of $\Delta\sigma'_2/\Delta\sigma_2$ is equivalent to 1. The complete methodology proposed by Becque (17), Becque et al. (18) was presented above, where all the necessary equations for evaluating the model have been outlined. The graph shown (Figure 4.5) depicts a comparison between the results obtained by Becque et al. (18) and the representation of Becque's model recreated for use in this research study. As can be noted, the graphs are quite similar and it can be concluded that Becque's reproduced model is optimal. Hence, it can be utilised as a comparison with the experimental investigations carried out.

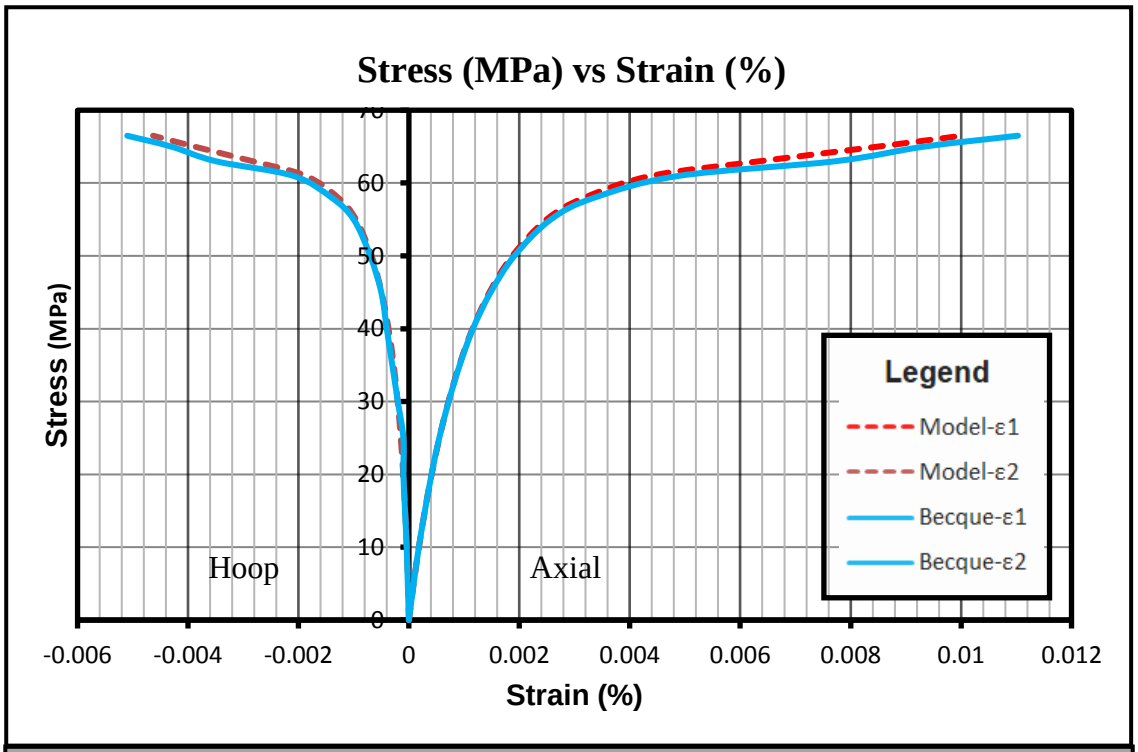

Figure 4.5: Stress (MPa) vs Strain (%) Graph showing a comparison between the results obtained by Becque (17), Becque et al. (18) and the reproduction of Becque's model to be used in this study.

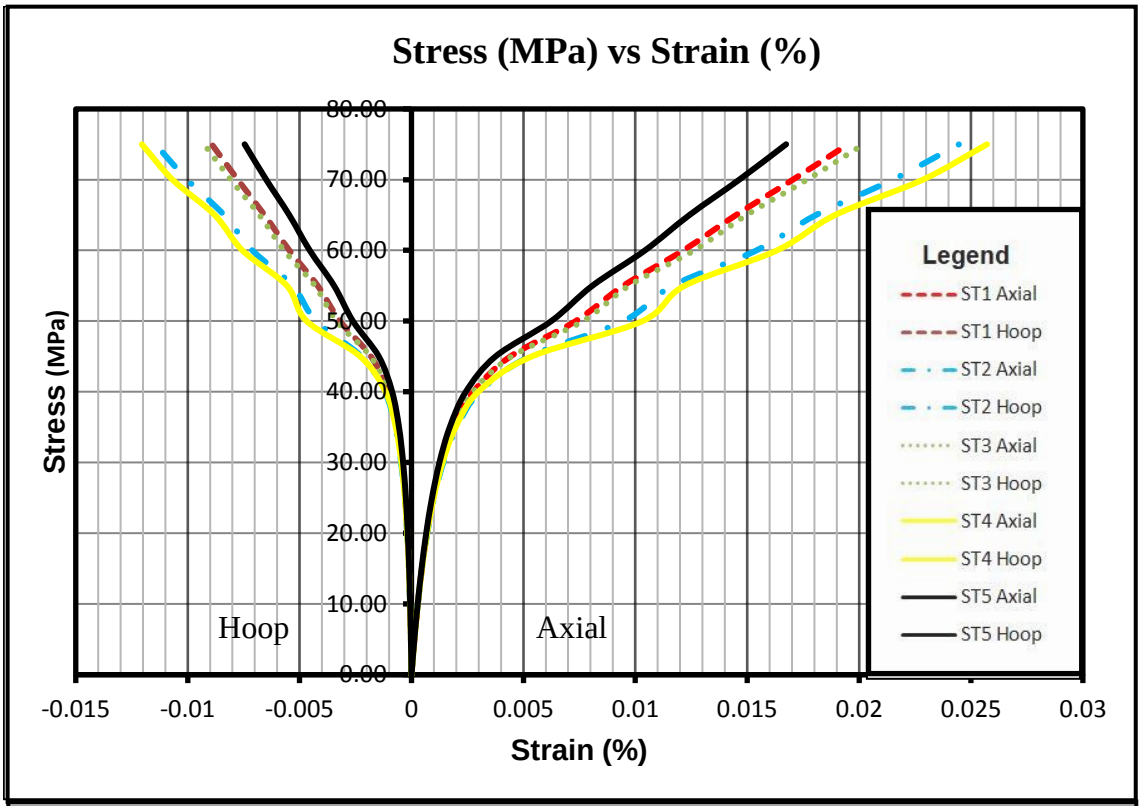

Figure 4.6 - Stress (MPa) vs Strain (%) Graph showing a comparison of the various jacket configurations studied.

The analysis-oriented model proposed by Becque will be implemented to examine the behaviour of the confinement jackets tested in this study. In this way, initial results can be achieved and it would be possible to examine the stresses and strains of the material. A graphic representation is shown in Chapter 6, where a comparison between the results obtained using the analytical model and the experimental results is shown.

Using classical laminated theory and the Tsai-Hill failure criterion, it is possible to achieve the required properties of the various laminates tested. The stress-strain diagram (Figure 4.6) groups together the different configurations, i.e. ST1-ST5. The graph indicates the strain values for stress values reaching a maximum of 80MPa. The model stops functioning the moment the iteration does not converge and the value of $\Delta\sigma'_2/\Delta\sigma_2$ is not equal to 1.

The graphs depict a bi-linear regime, where the initial slope is the same for all stacking sequences. This part of the graph is a concrete-dominated deformation and

so it is expected that all graphs follow the same path until the transition point is reached. The value of the transition point is dependent on the characteristic strength of the concrete. In this case, the unconfined compressive strength was assumed to be 38.35 MPa and this value was obtained from the experimental data available. As soon as the concrete fails, beyond the transition point, the stresses are taken by the jacket and this is depicted in the second part of the stress-strain diagram. The model reflects the strength and stiffness of the jacket. In fact, as shown in order of preference, ST5 (i.e. E_{xx} = 137GPa) has the highest Young's modulus of elasticity, followed by ST1 and ST3 (i.e. E_{xx} = 84GPa) whereas the graphs for ST2 and ST4 (i.e. E_{xx} = 58.4 GPa) have the least stiffness. ST6 was not plotted since the failure of the jacket is, more or less, equivalent to the failure of the concrete itself. Thus, it is worth mentioning that this model can provide a preliminary understanding of the stresses. It is important to note that, in auxetic laminates, the through thickness expansion should result in the improvement of strength. Yet, this might not be depicted in this model as the equations do not reflect this behaviour, i.e. the model can only be used to show the behaviour of the jacket when in hoop tension and give an indication of the possible strain within the given stresses (load). Therefore, experimental data is necessary to predict the actual behaviour.

4.7 Conclusion

This chapter outlined a set of preliminary analyses investigating the behaviour of auxetic jackets. An interesting aspect to be noted is that the value of failure using Tsai Hill criterion for the positive and negative Poisson's ratio does vary due to the fibre orientation, yet, it is evident, that actual material properties of the carbon fibre laminates have a greater impact on its value.

From the models presented in Sections 4.5 and 4.6, it is clear that both design and analysis oriented models have captured the dilation properties of the SE70 prepreg CFRP-confined concrete. Even though the results were achieved using different methodologies, both models provided the expected performance for both auxetic and non-auxetic stacking sequences, predicting the lateral-axial strain relationship and the ultimate condition.

Chapter 5.
Methodology of Experimental Investigation

5.1 Experimental Tests

This chapter outlines the experimental works that were carried out to examine the behaviour of auxetic prepreg CFRP laminates wrapped around concrete cylinders. A negative Poisson's ratio can lead to enhancements in properties that are unlikely to be obtained with materials having a positive Poisson's ratio (195). All experimental testing was done using SE70 prepreg CFRPs, where all laminates were cured in an oven at a temperature of 70°C for the duration of 16-20 hours. Tensile tests were carried out on rectangular specimens to evaluate and investigate the through thickness expansion that occurs when being pulled. Nevertheless, the constraints encountered in creating the confinement jackets for compression testing and the implementation of the vacuum bagging technique used for wrapping the concrete cylinder will be explained in detail. Although its application may be considered to be quite laborious, yet, it can be stated that this system is more efficient than the wet lay-up system. This is mainly due to the uniformity of the resin that occurs at curing stage between the individual layers. The approach adopted in rolling the layers around the concrete cylinder, in particular when applying the first layer to the concrete surface, was improved during the progression of the experiments until an effective system was established. The effects of these techniques are visible in the manner the laminate failed. The experimental programme carried out in this study includes:

- Tensile tests carried out using Instron 1342, using a total of 12 specimens having a stacking sequence configuration of $[\pm 20]_{2s}$, each with dimensions of 290mm in length and 20mm in width. Four of these specimens consist of four plies with a laminate thickness of 0.80mm, another four specimens consist of eight plies with a laminate thickness of 1.60mm and the remainder four specimens consist of sixteen plies with a laminate thickness of 3.2mm. A video gauge was used to examine the auxetic behaviour of the expansion through thickness when pulled and also measured the Poisson's ratio. The tests were carried out using a non-contact measurement system provided by

Imetrum (196) using the Video Gauge ™ software that are specialised in high resolution measurements with proprietary DIC algorithms that can detect strains smaller than 3 microstrain (point-point). Imtetrum (196) were the pioneers of point to point precision measurements using video. A telecentric lens was used for taking the readings**.** The reason for testing specimens with different thicknesses, i.e. 0.8mm, 1.6mm and 3.2mm respectively was to check whether the thickness of the laminate is directly proportional to the negative Poisson's ratio. The same procedure was created for another set of 12 specimens having a stacking sequence configuration of $[\pm 25]_{2s}$.

- Compression tests were carried out on a total of 66 cylinder samples, comprising both confined and unwrapped specimens, using Losenhousen 6,000 kN compression machine operating with Servocon software. These concrete cylinders were cast in 7 different sets, referred to as Groups A-G in this research study. Each set consists of 10 concrete cylinders bearing dimensions of 150mm in diameter and 300mm in height. Four of these cylinders were not tested. It is important to note that the experimental works mentioned in this study will be further divided into two groups, i.e. Cylinder Sets I for Groups A-D and Cylinder Sets II for Groups E-F. The aim for splitting these into two distinctive sets is mainly due to the application of a resin SA 70 between the concrete surface and the first CFRP prepreg layer that will be explained in detail at a later stage. The experimental results of these sets are to be compared and the effect of the presence of the resin will be delineated. In fact, it is important to clarify that Cylinder Set II was the first set of cylinders tested and the results are presented in Appendix B. However, these results will only be used as a means of comparison.

  These experiments were done so as to investigate the behaviour of auxetic laminates by compressing the wrapped concrete cylinder to failure, confirming whether the through thickness effect provides a better confinement and a higher failure strength. Every wrapped laminate used for confinement entailed eight SE70 prepreg CFRP layers having a global thickness of 1.60mm. As outlined in Section 4.5, it resulted that the symmetric balanced angle-ply

laminates of $[\pm 20]_{2s}$ and $[\pm 25]_{2s}$ have the highest NPR values and these were chosen as the chief auxetic jackets. In addition, stacking sequence configurations $[0_8]$, $[90_8]$, $[\pm 35,0_2]_s$, and $[\pm 16,\pm 45]_s$ were also tested. In this way, a fair comparison was obtained between configurations containing the same Young's moduli of elasticity as the auxetic laminates tested (i.e. $[\pm 35,0_2]_s$ and $[\pm 16,\pm 45]_s$), where it resulted that, $[\pm 35,0_2]_s$, had a negative NPR value of -0.1078. In addition, the auxetic jackets were compared with jackets having stacking configurations of $[0_8]$ and $[90_8]$, i.e. the maximum and minimum Young's modulus of elasticity respectively. It can be said that the most commonly used fibre orientations for retrofitting concrete columns are $[0_8]$ configuration. The $[90_8]$ is undoubtedly the weakest confinement jacket and this too was tested so as to examine the behaviour of the jacket.

In addition, a set of unwrapped concrete cylinders, which were placed in an oven and heated to a temperature of 70°C for 20 hours, i.e. the same curing time necessary to cure the resin of an SE70 prepreg, was also tested. In so doing, it was possible to conclude whether the heating of the specimen had an effect on the overall characteristic strength of the concrete. Table 5.1 groups together all the tested cylinders.

Tested Cylinders								
Stacking Sequence Configurations	ST1 $[\pm 20]_{2s}$	ST2 $[\pm 25]_{2s}$	ST3 $[\pm 35,0]_s$	ST4 $[\pm 16,\pm 45]_s$	ST5 $[0_8]$	ST6 $[90_8]$	Unheated & No Jacket	Heated & No Jacket
Cylinders Set I	4	4	5	5	3	3	8	8
Cylinders Set II	10	6	Nil	Nil	Nil	Nil	5	5
Total	14	10	5	5	3	3	13	13

Table 5.1: Total number of cylinders tested.

5.2 Experimental Procedures

5.2.1 Preparation of Specimen & Vacuum Bagging Technique

The experimental program includes tensile tests on SE70 CFRP specimens for investigating the through thickness negative Poisson's ratio. The specimens were manufactured using the vacuum bagging technique. This is a widely used system that creates mechanical pressure on a laminate during its curing cycle and it is generally recommended when using prepreg layers. This is mainly due to the fact that, when heat is applied to cure the resin and to accelerate the curing process, the use of vacuum bags is necessary to prevent bubbles from forming when trapped air expands. Vacuum bagging gives a better uniform spread of resin and prevents the shifting of fibre orientation throughout the curing process. It optimises the fibre-to-resin content throughout a part. In addition, it improves both the aesthetic and mechanical quality of parts, when compared to standard hand lay-ups. Moreover, this technique provides the manufacturing of complex shapes, exhibiting an efficient force-transmission amongst the fibre bundles.

Briefly, three different thicknesses were studied, mainly 0.80mm (4 layers), 1.60mm (8 layers) and 3.2mm (16 layers). Hence, rectangular specimens were cut in sizes of 290mm by 85mm x thickness from SE70 CFRP prepreg roll with fibre orientation angles of 20° and 25° to create specimens having stacking sequence configurations $[\pm 20]_{2s}$ and $[\pm 25]_{2s}$ respectively. When laying the individual layers, a roller was used for flattening and compacting prepreg layers. After the laying of every four layers, the specimens were covered with a breather and vacuumed for ten minutes. Once the stacking sequence layout was completed, the specimens were placed in a tray and bagged using tacky tape. The air was vacuumed out completely, monitoring the vacuum level, ensuring that all leaks were eliminated and no wrinkles were visible. All laminates were cured in an oven for 16 hours at a temperature of 70°C. A similar procedure was carried out for manufacturing GFRP laminates that were used as end tabs. The photographic representation shown in Figures 5.1-5.6 depicts the procedure used to create the specimens.

Once all laminates were cooled, a roller cutter was used to cut the CFRP prepreg laminates into rectangular specimens of 290mm x 20mm x thickness, whereas

Preparation of Specimen & Vacuum Bagging Technique

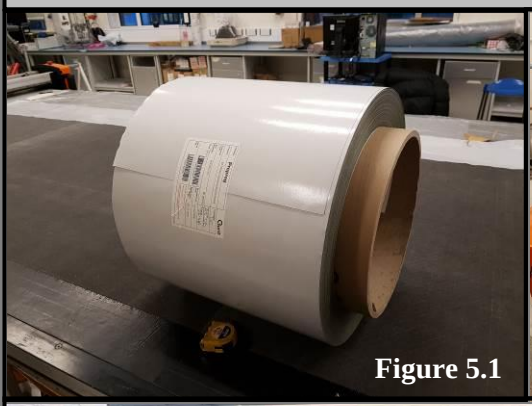
Figure 5.1

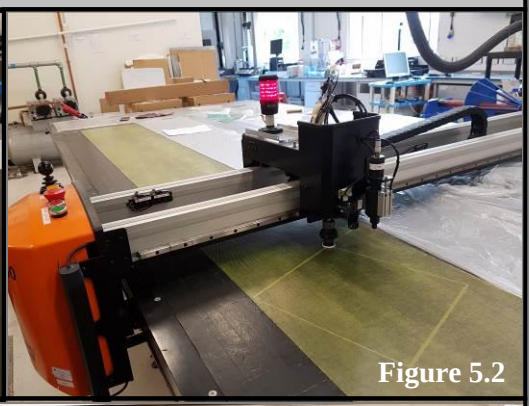
Figure 5.2


Figure 5.3

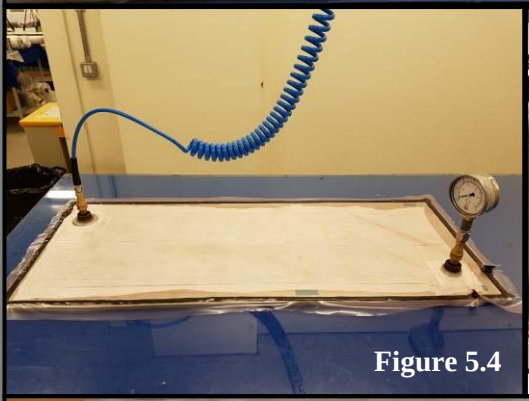
Figure 5.4


Figure 5.5


Figure 5.6

Figure 5.1 – SE70 Prepreg Roll provided by Gurit (See Appendix B)**.**
Figures 5.2 & 5.3 – Cutting & Preparation of $[\pm 20]_{2s}$ & $[\pm 25]_{2s}$ stacking sequences**.**
Figures 5.4 & 5.5 – Vacuum Bagging Technique & Curing of Prepreg**.**
Figure 5.6 – SE70 Prepreg Laminates.

the GFRP laminate required to form the end tabs were cut in 50mm x 20mm x 5mm. The dimensions of the end tabs were determined after measuring the grip ends of the machine**.** It is to be noted that the end tab sizes are as large as the grip ends of the testing machine being used so as to prevent any form of specimen slippage when tested. Using a shot/grit blast cabinet, a rough textured surface was also obtained on every end tab face. This too was necessary in order to provide a firm grip with the testing machine**.** The end tabs were bonded to the two surfaces of both ends of the specimen using a two component epoxy adhesive and were left to set for 24 hours. Tensile tests were carried out on a number of auxetic laminate specimens and the through thickness expansion was recorded. These tests were necessary to quantify and investigate whether the stacking sequences $[\pm 20]_{2s}$ and $[\pm 25]_{2s}$ have a negative Poisson's ratio. Three different thicknesses were studied, mainly 0.80mm (4 layers), 1.60mm (8 layers) and 3.2mm (16 layers). As shown in Figures 5.7 and 5.8, to investigate the through thickness expansion, the specimens' thicknesses were measured, using a vernier caliper, prior to testing whilst, for a few specimens, even prior to failure. This was made possible by stopping the tensile test once the elastic limit was exceeded. The Instron 1342 hydraulic testing machine was utilised for the tensile tests and each specimen was firmly gripped to the machine and pulled at an applied rate of 1mm/minute. These specimens were tested to failure so as to have an understanding of the mode of failure and the failure load.

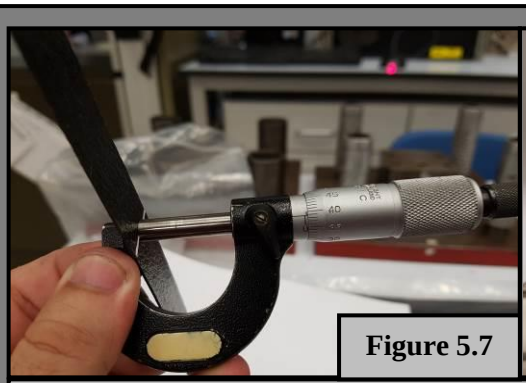

Figure 5.7

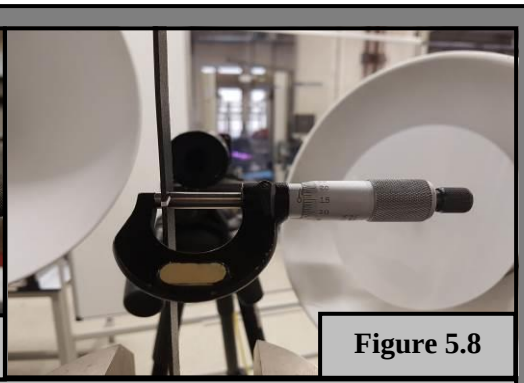

Figure 5.8

Figures 5.7 & 5.8 – Measurement of specimens using a vernier caliper prior to testing and prior to failure.

On the other hand, the negative Poisson's ratio was investigated using a contact free system. In the last decades, a number of interferometric and white-light optical methods were proposed and developed for experimentation purposes. With regards to this study, it was opted to make use of a video gauge that was positioned

facing the thickness of the specimen. This uses a non-contacting optical measurement system based on a digital camera and real time image processing to measure the Poisson's ratio. The equipment supplied by Imetrum (196) non-contact precision measurement was used for testing. This video gauge is suitable for measuring low strains and offers the possibility of multiple measurement points that can be monitored for measurements of axial and transverse strains. By a quick spray of paint and applying a speckle pattern to the specimen, the through thickness strains can be measured (See Figures 5.10 and 5.11). Through specialised algorithms and lenses, the system performs as a class 0.5 extensometer, allowing for accurate yield and modulus measurements. In addition, using tailored lenses, this range can be extended for strains up to 600%. Thus, using spray paint, a few white dots were scattered along the thickness of each specimen. The camera was placed very close to the specimen and the lens was used to focus until the white marks were clearly visible on the monitor. To enhance clear visibility of the white marks, light points were closely placed and directly pointed on the specimen. Eight points per sample were selected such that the negative Poisson's ratio can be investigated at two particular points along the specimen's thickness and it is possible to calculate an average value for every sample. As shown in Figure 5.16, two points with equal x co-ordinate values were selected to measure transverse strain, whereas the other two points with equal y co-ordinates values were selected to measure the axial strain.

Figure 5.9

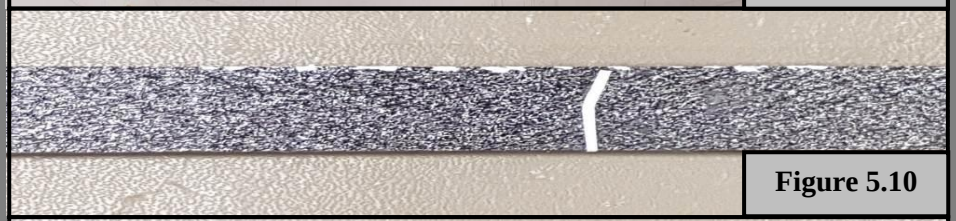

Figure 5.10

Figure 5.11

Figures 5.9 – 5.11 - Rectangular specimens have been marked with white dots along the thickness of the laminate.

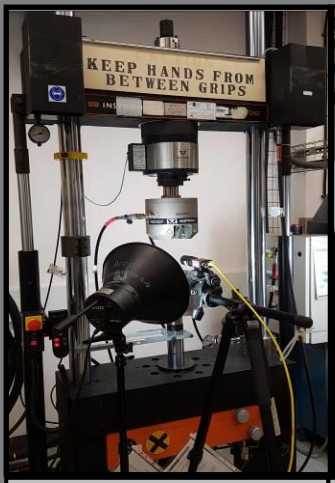

Figure 5.12

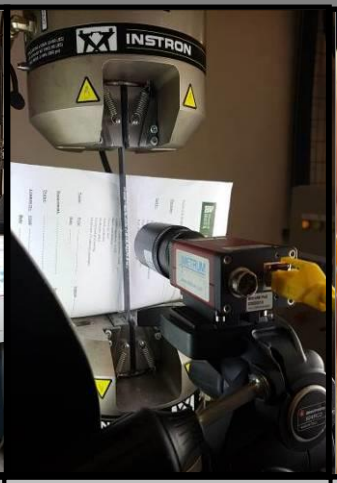

Figure 5.13

Figure 5.14

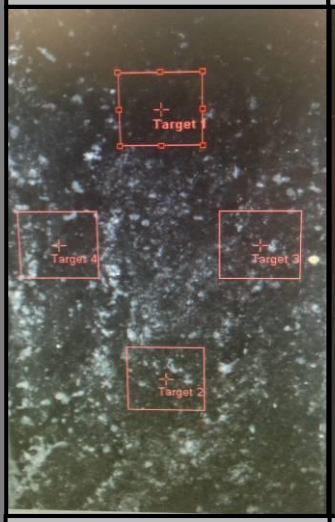

Figure 5.15

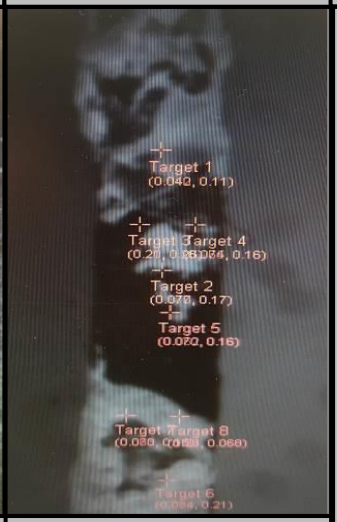

Figure 5.16

Figures 5.12 – 5.16 – These photos indicate the set up used to carry out the tensile tests where the Instron 1342 machine and video gauge have been used.

Figure 5.17

Figure 5.18

Figure 5.19

Figure 5.20

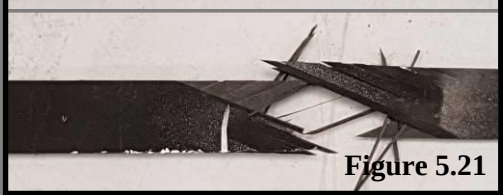

Figure 5.21

Figure 5.22

Figures 5.17 – 5.22 - The photos illustrate the failure of the tested tensile specimens.

5.2.2 Casting of Concrete Cylinders

The concrete cylinders used for testing were created in accordance with the BS EN 12390-1:2000 and BS EN 206:2013 (197, 198). The standard testing commonly used for measuring the concrete strength is carried out using either cubes with standard dimensions of 150mm x 150mm x 150mm or concrete cylinders with dimensions of 150mm (diameter) x 300mm (height) or 100mm (diameter) x 200mm (height). In addition, as specified in BS-EN 206-1 (198), it is worth noting that the characteristic strength of the cylinder specimen is approximated to be about 0.80-0.84 of the strength of a cube. The cylinder/cube strength ratios are presented in Table 7 of BS-EN 206-1 (198, 199).

Using standard construction materials, a total of 70 concrete cylinders with standard dimensions of 150mm in diameter and 300mm in height were cast. These cylindrical sizes have a height/diameter ratio that is equal to 2 and represent the sizes that are most commonly-used universally in construction research (200). It is also worth noting that the larger the diameter, the lower will be the strength (201). In general, there are many factors associated with the compressive strength of concrete, most of them being inter-dependent. In fact, there are a number of factors that affect the compressive strength of concrete and these were taken into account when creating the cylinders. For a given cement and acceptable aggregates, the strength that may be developed by a workable, well-placed mixture of cement, aggregate and water is influenced by the:

- water-cement ratio;
- ratio of cement to aggregate;
- grading, surface texture, shape, strength and stiffness of the aggregate particles;
- maximum size of aggregate; where it can be stated that ‘the compressive strength decreases with an increase in maximum coarse aggregate size especially for concrete with a low water-cement ratio’. (98, 202)

The casting was carried out in two sets, Cylinders Set I where a total of 40 cylinders were cast and Cylinders Set II, where 30 concrete cylinders were prepared

for testing. The same procedure was adopted for every group of cylinders A-F. Each mix was done manually and it is possible that this can cause differences in strength within the individual sets of 10 cylinders. During the mixing, attention was given to reduce, as much as possible, the incorporation of air bubbles in the concrete. This air entrainment can cause a reduction in compressive strength. In addition, to ensure a satisfactory development of strength, it is important that, during the reaction of water with cement, known as the hydration process, moisture loss is prevented.

The first set of concrete cylinders used in these experiments (i.e. Concrete Cylinders Set II), were designed with a Grade C30 concrete for a 28-day strength, using local gravels and Portland cement. This concrete grade is the most common grade used in the design of residential or commercial buildings. This means that the concrete will be designed to have a compression resistance of $30N/mm^2$ at 28 days. The concrete mix design for a Grade C30 concrete consists of 1:2:3 (i.e. cement:sand:aggregate/gravel). The procedure for each cast involved the mixing of 22kg of cement, 44kg of sand and 66kg of aggregate; where a third of the aggregate consisted of 6mm limestone chippings and the remaining two-thirds contained 14mm limestone chippings. The mix was done in open air using a shovel in an aluminium tray. An average water-cement ratio of 0.50 was kept throughout all mix designs. A slump test was carried out to determine the workability or consistency of the concrete mix. Attention was given during the mix to keep as much as possible a semi-liquid/semi-solid state. Once the mix was completed, the concrete was poured into cylindrical plastic moulds, that were internally-wiped with oil. While the concrete was poured, a steel bar was used to rod the concrete. The concrete cylinders were consequently vibrated with a poker and the top of the cylinders covered with a damp plastic sheet. These were left to set for a whole day. After 24 hours, the concrete cylinders were removed from the moulds, numbered and left to cure for a further 28 days in a tank full of water. The concrete cylinders were then measured in two locations at right angles to each other at mid-height of the specimen and their values were averaged to calculate the cross-sectional dimensions. The two measured locations of the cylinders did not differ by more than 2% and so the cylinders were deemed to be adequate for testing. A similar procedure was adopted when casting the second group of cylinders (i.e. Cylinders Set I).

A photographic representation is presented in Figures 5.23-5.33, showing the process involved in creating the concrete cylinders.


Figure 5.23


Figure 5.24


Figure 5.25


Figure 5.26


Figure 5.27


Figure 5.28


Figure 5.29


Figure 5.30


Figure 5.31

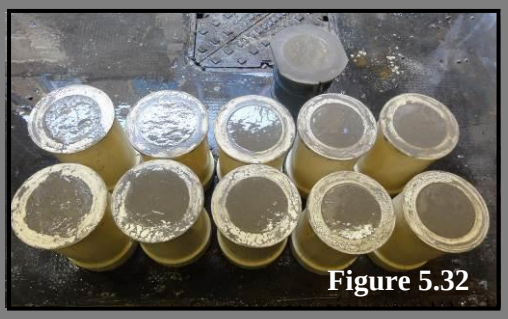
Figure 5.32


Figure 5.33

Figures 5.23 – 5.33 – The photos depict the process used to create the concrete cylinders. After mixing, the concrete mix is poured into the plastic moulds and vibrated. The concrete cylinders were left to cure for 28 days in a tank full of water.

5.2.3 Preparation of Wrapped Laminates

The parameters considered for investigating the confinement stresses caused by auxetic laminates include the number of (CFRP) composite layers and the fibre directions. Auxeticity is bound to occur through the thickness of the composite and the number of layers used must not have a major impact on the auxetic behaviour. In addition, it has been experimentally shown that the number of layers has an effect on the strength of the non-auxetic confined concrete cylinder, where additional layers improve the confinement stress. (203). The fibre orientations and the overlap length of each layer have an impact on the confined strength and failure of the laminate. According to the rules proposed in ASTM D7616/D7616M-11 (204), the finishing end of each sheet is to overlap the starting end of the next sheet by a minimum of 100mm. Each confinement jacket tested was composed, in total, of eight SE70 CFRP prepreg layers, having an overall thickness of 1.6mm. Using a cutting machine (See Figures 5.34 and 5.35), each layer was cut to a length of 597mm (i.e. the cylinder's circumference of 472mm and an additional 125mm lapping) and 300mm in height. The SE70 CFRP prepreg supplied by Gurit (See Appendix A) is available in rolls of 200m in length and approximately 0.40m in height. These roll dimensions created a constriction when the fibres were to be cut at particular angles, since it was not possible to have the layers cut in one full length. The angles used for the stacking sequences studied include: 0°, 16°, 20°, 25°, 35°, 45° and 90° (See Figures 5.36-5.40). All layers, except those where fibre orientations angles were 0°, had to be cut into two separate pieces. This might undoubtedly create a weak point. As could be noted in Figures 5.38-5.39, the triangular parts for the 20° and 25° layers can be considered to be quite small in size. So, it can be assumed that that this would cause minimal changes to the auxetic effect and the respective results, mainly because they are located at the ends/supports of the cylinder. The same cannot be said for layers having fibre orientation angles 35°, 45° and 90°. Yet, these angles were not used for the stacking sequences necessary to investigate the auxetic behaviour and, by carefully placing them at different positions along the composite; it is assumed that there is no effect on the strength of the confinement jacket.

To maintain the properties of the prepreg intact, it is vital to seal them tightly in a moisture proof bag and store them in a freezer at a continuous temperature of -18°C. The regular usage and thawing of the prepreg can cause minor deficiencies to

Figure 5.34

Figure 5.35

Figures 5.34 – 5.35 – The SE 70 prepreg layers are cut from a roll of 200m in length and approximately 0.40m in width.

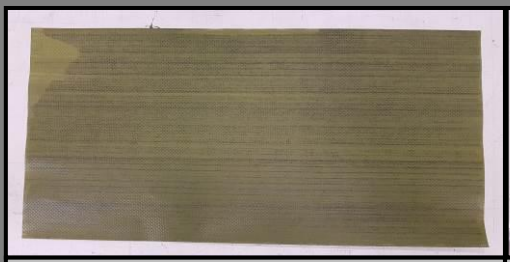

Figure 5.36 –Fibre orientation angle 0°.

Figure 5.37 –Fibre orientation angle 16°.

Figure 5.38 –Fibre orientation angle 20°.

Figure 5.39 –Fibre orientation angle 25°.

Figure 5.40 –Fibre orientation angle 35°.

Figure 5.41 –Fibre orientation angle 45°.

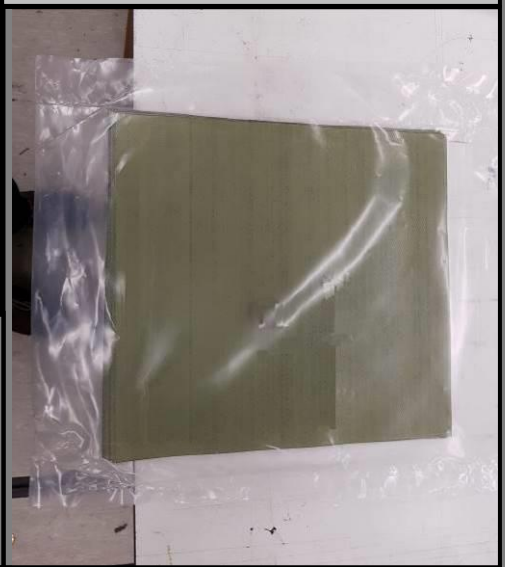

Figure 5.42 –Fibre orientation angle 90°.

the properties of the prepreg. The prepreg rolls used for manufacturing the confinement jackets were done using two separate rolls. Cylinders Set I was made using a fresh roll that had just been specifically bought for this study, whereas the jackets manufactured for Cylinders Set II were done using a roll that was previously used and which was close to its expiry date.

A technique was purposely devised to apply the layers around the cylinder. A simple approach was adopted, whereby the cylinder was rolled in a defined space, such that each layer was tightly fixed without any air entrapment. The layers were manually-applied and the use of the track was necessary to restrain the movement of the cylinder so as to minimise human errors. This consisted of two metal bars firmly clamped to a table, placed at a distance of 310 mm apart from each other (i.e. 10 mm greater than the actual height of the cylinders to allow better the handling of the cylinder). The confinement jacket was formed by rolling each layer onto a flat surface sheet of cardboard, above which the individual layers of CFRP were placed.

The same procedure was implemented for the creation of all confinement jackets i.e. stacking sequence configurations: $[\pm 20]_{2s}$, $[\pm 25]_{2s}$, $[0_8]$, $[90_8]$, $[\pm 35,0_2]_s$, and $[\pm 16,\pm 45]_s$. The Design guidance for strengthening concrete structures was followed (205, 206). Initially, the concrete cylinders were thoroughly cleaned from dust particles using compressed air. A wire brush was also utilised to clean and remove any pointed surfaces or bumps that were present around the cylinder's circumference. A smooth surface is most essential, otherwise the pointed surface might puncture the CFRP laminate causing its failure while being tested. In addition, any visible voids/holes present in the cylinder's surface were filled and left to set for a few hours. Yet, it can be stated that most of the cylinders achieved a smooth finish and only three cylinders needed to be filled. The following step was to divide the cylinder's surfaces into eight equal parts. These parts defined the starting positions of each individual layer of CFRP. In so doing, the starting and ending point of each layer was shifted from each individual layer. Thus, the lapping position of each individual layer was controlled by predetermining each lapping position along the circumference of the cylinder, reducing the possibility of weak seams. Each layer was placed in line with the metal bar and masking tape was used to keep the layer in place, whilst rolling the cylinder. This system was repeatedly used for each layer.

The main problem that was encountered was the adhesion of the first prepreg layer to the concrete cylinder. Although the surface of the concrete was thoroughly cleaned from dust, detachment of the first layer was, at times, observed. This was initially overcome by manually rubbing the prepregs to preheat its resin. The SE70 is said to cure at almost ambient temperature and this form of preheating creates the necessary adhesion between the concrete's surface and the prepreg. In addition, at times, after the placement of the first layer, the cylinder was vacuumed for 10 minutes. In so doing, better adhesion was achieved. Prior to applying the second layer of prepreg, the visible trapped air bubbles were flattened using a roller so as to prevent the possibility of creating any form of wrinkle along the laminate. Yet, after the testing was carried out on the first set of cylinders, it was noted that, although some of the results obtained were adequate, the failure of the laminate was not so convincing. As will be discussed in the next chapter, the laminates failed either along the wrinkles (i.e. a weak point), or at the centre of the cylinder along the circumference of the cylinder. The fibres do not break, but only tear in the weakest point. The only plausible reason for this mode of failure is probably due to the lack of adhesion between the concrete's surface and the wrapped laminate. In fact, it is important to clarify that Cylinder Set II, i.e. Groups E-G was the first set of cylinders to be tested and the results obtained will not be used in this study, but will be utilised solely as a means of comparison.

To overcome this problem and to improve the final results, an additional SA70 resin layer was placed between the concrete cylinder and the first prepreg layer. The SA70 is an adhesive film that is designed for secondary bonding, core-bonding and for co-curing with the range of Gurit prepregs. It can be cured at temperatures as low as 70°C or otherwise cured more rapidly at temperatures above 120°C. This resin was applied on the second set of cylinders tested, more specifically Cylinder Set I, i.e. Groups A-D. The SA70, which is available in rolls, was cut in sheets having dimensions of 472mm x 300mm (Figure 5.50). In this way, the resin could be applied around the whole circumference of each cylinder. The resin was manually applied on the cylinder's surface using an industrial high temperature blow dryer with a flat nozzle set at temperatures of 50°C-70°C. When the resin's back sheet was removed, the resin was heated and flattened manually until complete adhesion was visible between the surface and SA70 layer. The first prepreg CFRP layer was then applied.


Figure 5.43


Figure 5.44

Figures 5.43 – 5.44 – Concrete Cylinders (i.e. Cylinders Set I & II) used for testing


Figure 5.45


Figure 5.46

Figure 5.47

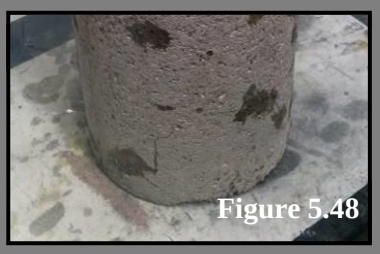
Figure 5.48

Figures 5.45 – 5.48 – Cleaning of concrete cylinders using compressed air & wire brush. Filling of voids using rapid hardener.

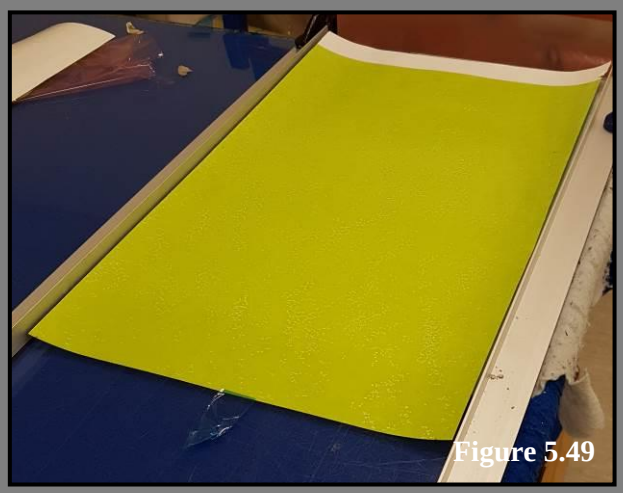
Figure 5.49

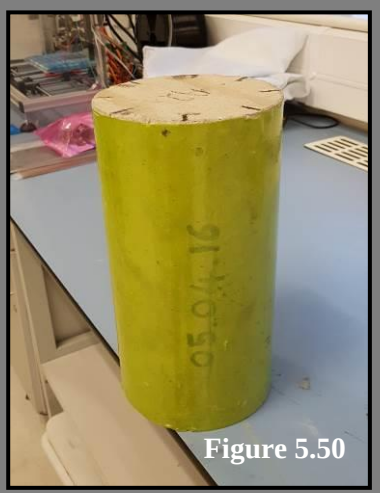
Figure 5.50

Figures 5.49 – 5.50 – SA 70 Resin sheets wrapped around the cylinders **.**

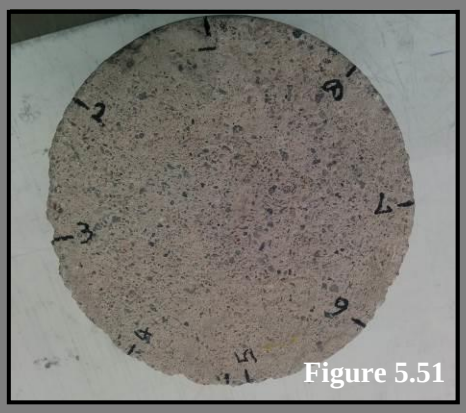

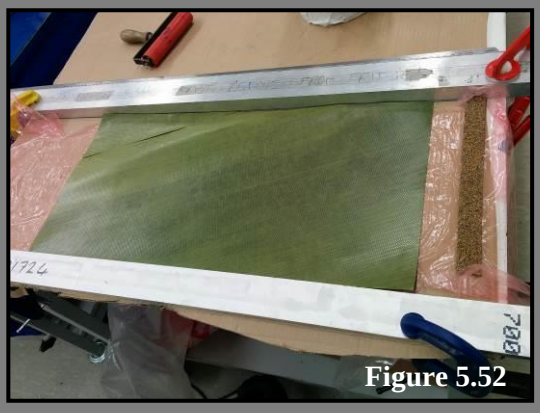

Figure 5.51 – Cylinder's surface divided in 8 sectors representing the position of each layer.
Fig 5.52 – Preparation of track to roll layers.

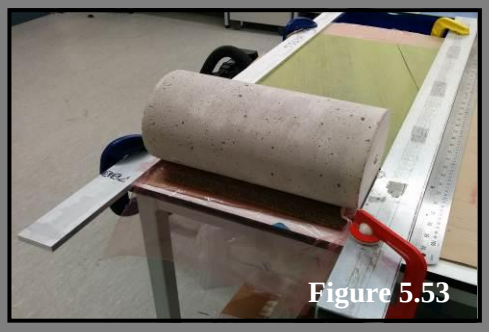

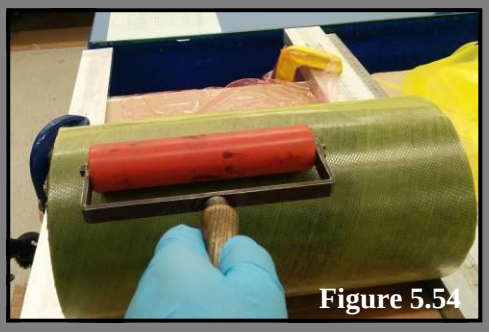

Figure 5.53 – Depicts the distance of the two metal bars firmly clamped to a table, placed at a distance of 310mm apart from each other.
Figure 5.54 – The smoothening of each layer using a roller.

Figure 5.55 – Removal of the film sheet.
Figure 5.56 – Vacuuming of prepregs after laying four layers.


Figure 5.57


Figure 5.58

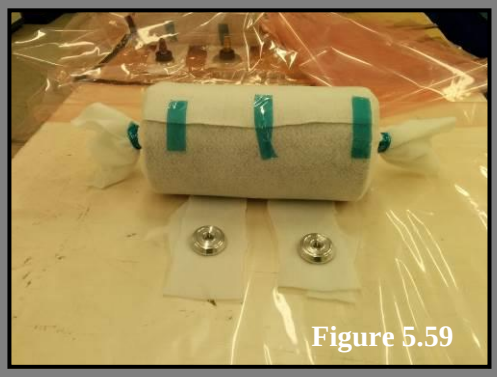
Figure 5.59

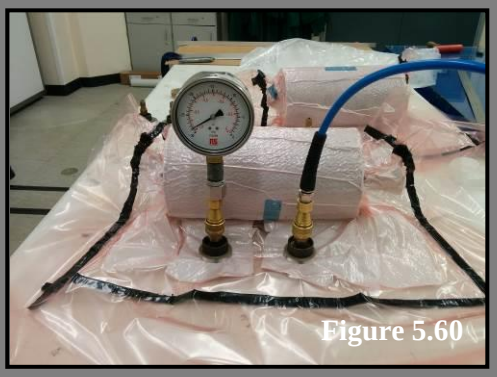
Figure 5.60


Figure 5.61


Figure 5.62

Figures 5.57 – 5.60 – Depict the process involved in bagging the cylinders.
Figures 5.61 & 5.62 – Three cylinders were cured in an oven and linked to each other by means of tubing connectors.

The use of prepregs indirectly imposed the methodology that had to be implemented for the manufacturing of the confinement jacket. In fact, the vacuum bagging system commonly used in the aerospace industry was adopted. When making use of prepregs, it is customary to vacuum air at regular intervals so as to remove the trapped air present between the layers and to compact the fibre layers providing efficient force transmission among fibre bundles. After the laying/rolling of four layers, the composite was covered with a breather, bagged and vacuumed for

ten minutes. This process was repeated for every four layers when rolled. At times, this process had to be carried out immediately after the wrapping of the first layer, so as to improve the adhesion of the composite when applied to the concrete cylinder.

Prepregs contain a pre-impregnated resin and need to be cured in an oven at a particular temperature. The vacuum bagging system (or vacuum bag laminating) uses atmospheric pressure to hold the adhesive or resin-coated components of a lamination in place until the adhesive cures. This system was adapted for curing confinement jackets. The bagging schedule (i.e. the sequence of materials) will be briefly described. The confined jacket was primarily covered with a release film, followed by a breather that is vital to provide a 'breather' path when transferred from the bag to the vacuum source, such that continuous pressure can be applied to the laminate. The bag film was consequently used to cover the cylinder in bagging material and this was firmly sealed at the edges using a rubberized sealant tape (i.e. black tacky tape). The bag film layer created was much larger than the cylinder in order to allow enough space for the positioning of two valves. A faultlessly vacuumed environment is essential during the curing stage. Hence, the air is vacuumed out completely from the bag until the atmospheric pressure of 28 bars is reached. Once completed, the confinement jacket has to be cured in the oven. Three cylinders were cured and linked to each other by means of tubing connectors that, in turn, were connected to a vacuum pump during the whole curing process. A photographic representation of the preparation process outlined above is presented in Figures 5.43-5.62.

The curing temperature recommended for an SE70 CFRP prepreg is equivalent to 70°C and the duration of completion is of 16 hours. An initial test was carried out on one cylinder to examine whether a constant temperature of 70°C was maintained throughout the curing time of 16 hours. A thermocouple was used to observe the temperature changes occurring on the surface of the composite while being heated. It resulted that the temperature rose gradually from 0°C – 57°C during the first two hours until the specified temperature of 72°C was reached within the next hour. A constant temperature of 72°C was subsequently recorded until completion. Hence, it was decided to increase the curing temperature of all the tested confinement jackets from 16 hours to 20 hours. A similar procedure was also carried out for an unwrapped concrete cylinder, where it was noted that a very small amount of water

was released from the cylinder and it was completely dry when removed from the oven.

When being used as a confinement jacket, the auxetic composite's remarkable feature must, to a certain extent, enhance confinement withstanding substantial axial forces. Unfortunately, it resulted that that it was not possible to show the effect that auxetic laminates provide whilst confining the cylinder. This is due mainly to the involvement of systems where placing gauges between the surface and laminate necessitate the puncturing through the laminate for its wiring. Uniformity was essential to provide the auxetic effect because any holes punctured within the jacket would break up the required uniformity.

5.2.4 **Positions of Strain Rosettes**

When all cylinders were cured, they were allowed to cool for 24 hours. To examine the confinement stresses, strain gauges were externally-applied to the jackets. Due to the CFRP's rough texture surface, it was recommended to make use of strain gauges having a grid resistance of 120.0±0.3% ohms. These are capable of measuring the extensional strain in the direction of where the gauge is oriented. The cylinders Set II (i.e. Groups E-G) were carried out using linear pattern strain gauges whilst strain rosettes were used for Cylinders Set I (i.e. Groups A-D).

The linear pattern strain gauges are one of the most common methods used. In the test specimen, the strain experienced was transferred directly to the strain gauge, which responded with a linear change in the electrical resistance. The carriers were attached to the CFRP's surface using M-Bond AE-10 Adhesive Kit and were left to set for 24 hours. The strain gauges adopted for measuring the strains of Cylinders Set II made use of the wheatstone bridge configuration. A total of six strain gauges were attached to each cylinder, three of which measured the axial strains whereas the remaining three measured the hoop strains. These strain gauges were strategically located such that it was possible to record the confinement stresses throughout the entire cylinder. As shown in Figure 5.63, a set of strain gauges, i.e. an axial and circumferential strain gauge, were placed at the centre of the cylinder, whereas another two sets of strain gauges were placed at both ends of the cylinder, 5cm away from the cylinder's surfaces. All gauges were wired and connected to a data logger to record the results.

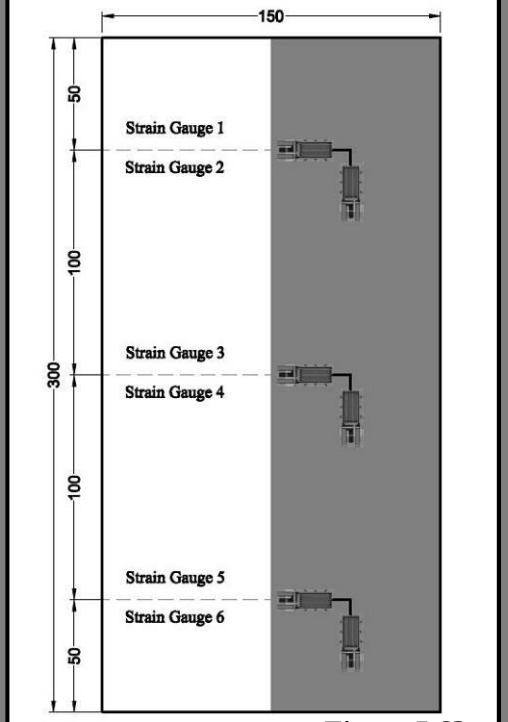

Figure 5.63

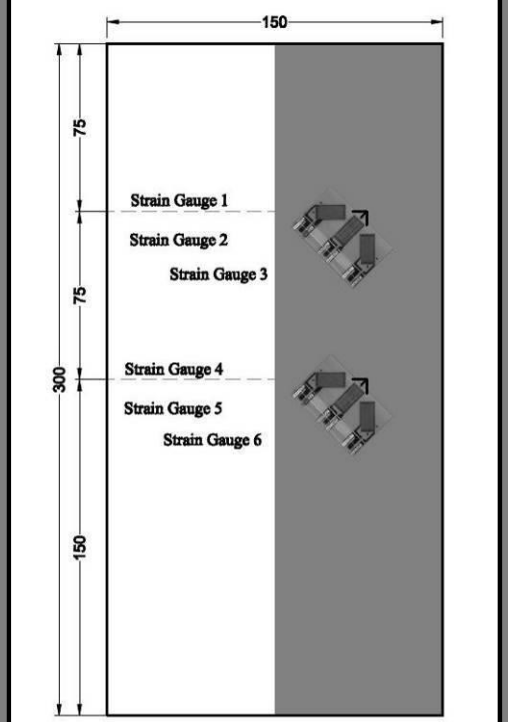

Figure 5.64

Figure 5.63 – Position of strain gauge for Cylinders Set II.
Figure 5.64 – Position of strain gauge rosettes for Cylinders Set I.

On the other hand, strain rosettes were used for measuring Cylinders Set I. When using these strain rosettes, it is possible to determine, the two extensional strains ε_x and ε_y as well as the shear strain γ_{xy} with respect to the xy axis system. The most common 3-gauge rosettes being used are the rectangular and delta rosettes. These strain gauge rosettes consist of three co-located strain gauges oriented at a fixed angle with respect to each other (i.e. with relative orientations of 30°, 45°, 60° or 90°) and positioned as close as possible so as to approximate a measurement at a point. The 125LR rectangular rosettes produced by VPG (207) were used for the second set of experiments, where two strain gauge rosettes to each cylinder were applied so as to study the behaviour of the SE70 CFRP composite laminates wrapped around the concrete cylinders. Before applying the strain rosettes, the cylinder was rubbed with a scratch paper. Acetone was applied and the strain rosette was glued to the laminate's surface. M- Bond 200 Adhesive kit was used for attaching the strain rosettes to the confinement jackets. To obtain optimal results, it was decided to place one of the strain rosettes in the middle of the cylinder. Moreover, the second strain rosette was

positioned 75mm away from the top of the cylinder, i.e. at ¼ the height of the cylinder specimen (See Figure 5.64). This location was chosen after taking into consideration Saint-Venant's principle. This principle states that, 'if a certain system of forces acting on a portion of the surface of a body is replaced by a different system of forces acting on the same portion of the body, then the effects of the two different systems at locations sufficiently far distant from the region of application of forces, are essentially the same, provided that the two systems of forces are statically-equivalent' (208:p.6). In other words, the stress state predicted by elementary theory does not hold in regions near loads or supports, and in fact, the strain rosette was positioned at a sufficient distance from these localised distortions.

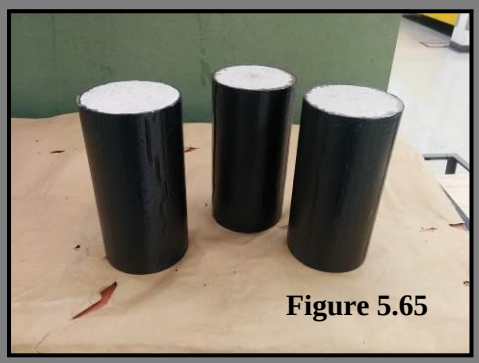

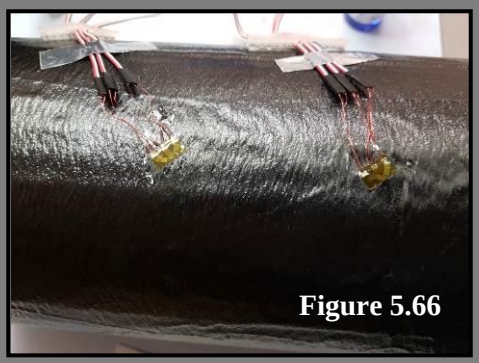

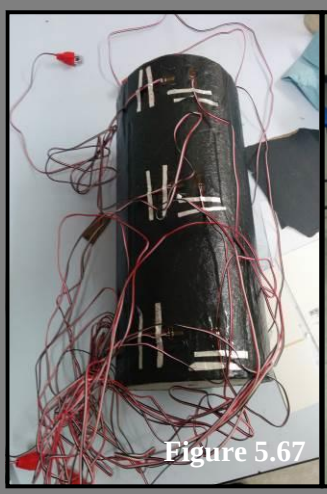

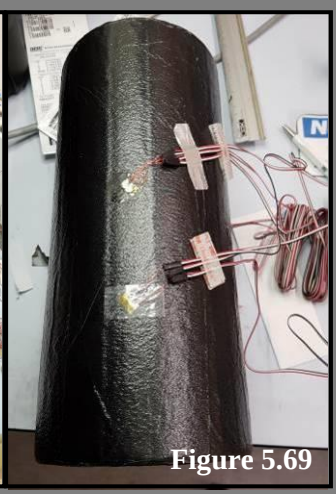

Figures 5.65-5.69: The process involved applying the strain gauges onto the cylinders prior to testing. Fig 5.67 depicts the linear strain gauges used for Cylinders Set II, whereas Fig 5.69 depicts the strain gauge rosettes that were used for testing Cylinders Set I.

Figures 5.65-5.69, depict the process involved applying the strain gauges onto the cylinders prior to testing. Figure 5.67 shows the linear strain gauges used for Cylinders Set II, whereas Figure 5.69 depicts the strain gauge rosettes that were used for testing Cylinders Set I.

The principal strains and their orientation with respect to the rectangular rosette gauge can be calculated using the strain measurement results obtained experimentally. It is also possible to calculate the state of strain at the gauge location with respect to any particular xy axis system using either the rosette readings or the principal strains and their axis orientations. The following equations can be used to compute the principal strains and the principal axis orientation directly from the rectangular rosette gauge readings:

$$\varepsilon_1 = \frac{\varepsilon_A + \varepsilon_C}{2} + \frac{1}{\sqrt{2}}\sqrt{(\varepsilon_A - \varepsilon_B)^2 + (\varepsilon_B - \varepsilon_C)^2} \qquad (5.1)$$

$$\varepsilon_2 = \frac{\varepsilon_A + \varepsilon_C}{2} - \frac{1}{\sqrt{2}}\sqrt{(\varepsilon_A - \varepsilon_B)^2 + (\varepsilon_B - \varepsilon_C)^2} \qquad (5.2)$$

$$\phi = \frac{1}{2}\tan^{-1}\left(\frac{\varepsilon_A - 2\varepsilon_B + \varepsilon_C}{\varepsilon_A - \varepsilon_C}\right) \qquad (5.3)$$

5.2.5 Capping of Concrete Cylinders

Prior to carrying out the compression testing of the cylinders, the ends of the concrete cylinders were checked to confirm whether they met the necessary requirements mentioned in ASTM C39/C39M (209) where it is recommended to have a smooth and flat surface. Irregular end surfaces or situations when the specimen axis is not perpendicular to the end faces will cause stress concentrations within the cylinder and reduce the measured strength. In fact, it is recommended to either cut the ends of the cylinders or use unbounded caps that correct the imperfections. In this way, it is feasible to achieve the planeness necessary for testing.

Capping of the cylindrical concrete specimens was done to ensure that all test cylinders had a smooth, parallel and uniform bearing surface perpendicular to the applied axial load during the compressive strength testing. When testing the unwrapped cylinders, the cylinders were capped with neoprene pad caps, which were


Figure 5.70


Figure 5.71


Figure 5.72


Figure 5.73

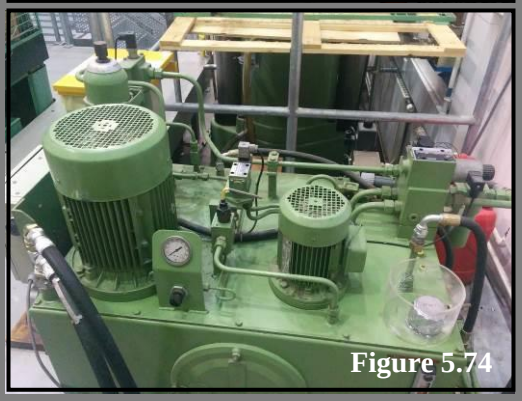
Figure 5.74


Figure 5.75

Figures 5.70-5.75 – The photos depict the Losenhousen 6,000kN compression machine operating with Servocon software used for testing the cylinders. As shown in Figure 5.71, a circular lead bearing was used as a capping material and this was placed at the top of the cylinder. In this way, the force was only applied onto the concrete cylinder.

in conformity with the strengths tested. For the testing of Cylinders Set I, a circular lead bearing, approximately 147mm in diameter, i.e.3 mm smaller than the cylinder's

diameter, was placed at the top surface of the concrete cylinders. In this way, the pressure exerted by the compression machine is only transmitted in the concrete cylinder and no form of load is transferred into the laminate. The failure of the confinement jacket will be solely due to the confinement pressure exerted by the compressed concrete cylinder onto the composite.

To measure the confinement stresses and examine better the influence that auxetics provide when used as a confined jacket, the wrapped cylinders were subjected to a uni-axial compressive loading until failure was reached. The two most common testing methods used for studying the confinement stresses are the load-control (i.e. stress-controlled) and displacement-control (i.e. strain-controlled) systems. Using a strain-controlled system, the compression test is conducted by increasing the displacement at a given rate obtaining a ductile failure, whereas, on the other hand, in a stress-controlled test, the force is increased at a given rate obtaining a brittle failure (i.e. abrupt failure).

The compression machine supplied by Losenhousen and operated using Servocon Systems, was suitable for carrying out these experiments, since it is capable of taking a maximum load of 6,000 kN (See Figures 5.70-5.75). Unfortunately, it seems that this machine was not regularly used and updates were rarely carried out. The only problem encountered when using this machine was that the testing had to take place within a maximum of 1,000 seconds. This unpleasant constraint did cause some limitations to the testing program. Yet, it was decided to proceed with the first set of experiments with the aim of solving this issue, when the second set of experiments was done. Initially, the compression machine gave the possibility of testing both the displacement-controlled system as well as the force-controlled system. In fact, as shown in Table 5.3, the first set of cylinders, i.e. Cylinders Set II was tested using both systems. Due to the constraints imposed by the equipment, the rates chosen were such that the failure of the wrapped concrete cylinders would occur within the stipulated time of 1,000 seconds. In fact, using a preliminary analysis, the tests conducted using the displacement-control system were set at a rate of 12mm in 1000 seconds (i.e. 0.012mm/sec), whereas, in the case of the force-control system, the rate was set to 2kN/sec. Using both test methods it is possible to compare and analyse any differences that may result in the behaviour of the cylinder.

Cylinders Set I				
Stacking Sequence Configuration	**Young's Modulus E_{xx} (N/mm^2)**	**Displacement or Force-Control**	**Cylinder Name**	**Concrete Set**
No Prepeg Not Heated	**N/A**	**Force-Control**	**1**	**A**
			2	**A**
			3	**B**
			4	**B**
			5	**C**
			6	**C**
			7	**D**
			8	**D**
No Prepeg Heated	**N/A**	**Force-Control**	**9**	**A**
			10	**A**
			11	**B**
			12	**B**
			13	**C**
			14	**C**
			15	**D**
			16	**D**
$[\pm 20]_{2s}$	**84,000**	**Force-Control**	**17**	**A**
			18	**A**
			19	**A**
			20	**A**
$[\pm 25]_{2s}$	**58,400**	**Force-Control**	**21**	**B**
			22	**B**
			23	**B**
			24	**B**
$[0_8]$	**137,000**	**Force-Control**	**25**	**C**
			26	**C**
			27	**C**
			28	**C**
			29	**C**
$[90_8]$	**7,810**	**Force-Control**	**30**	**D**
			31	**D**
			32	**D**
			33	**D**
			34	**D**
$[\pm 35, \pm 0_2]_s$	**83,800**	**Force-Control**	**35**	**A**
			36	**A**
			37	**D**
$[\pm 16, \pm 45]_s$	**58,200**	**Force-Control**	**38**	**B**
			39	**B**
			40	**C**

Table 5.2: Stacking Sequence Configurations to be tested for Cylinders Set I

Cylinders Set II				
Stacking Sequence Configuration	**Young's Modulus E_{xx} (N/mm^2)**	**Displacement or Force-Control**	**Cylinder Name**	**Concrete Set**
No Prepeg Not Heated	**N/A**	**Force-Control**	**41**	**F**
			42	**F**
		Displacement-Control	**43**	**G**
			44	**G**
			45	**G**
No Prepeg Heated	**N/A**	**Displacement-Control**	**46**	**E**
			47	**E**
			48	**E**
			49	**G**
			50	**G**
$[\pm 20]_{2s}$	**84,000**	**Force-Control**	**51**	**E**
			52	**E**
			53	**F**
			54	**E**
		Displacement-Control	**55**	**E**
			56	**E**
			57	**E**
			58	**E**
$[\pm 25]_{2s}$	**58,400**	**Force-Control**	**59**	**F**
			60	**F**
			61	**F**
			62	**F**
		Displacement - Control	**63**	**G**
			64	**F**

Table 5.3: Stacking Sequence Configurations to be tested for Cylinders Set II

For the second round of experiments, the machine was adjusted to remove the limitation of testing within a stipulated time frame and it gave the possibility of carrying out compression tests at any predetermined rate necessary. Yet, a different limitation was then encountered by the machine, where all compression tests could only be carried out using a load-control system as the displacement-control system had a malfunction that unfortunately could not be adjusted. Hence, due to logistical constraints, the experiments of Concrete Cylinders Set I were carried out using the force-control system. However, as shown in publications (155, 191), no particular difference was noticed in the behaviour of the material. The main difference between a force-control and a displacement-control system is with regards to the ability of the

latter system to describe the behaviour beyond the ultimate limit of the material. It is mainly for this reason that most of the confinement tests (19, 20) carried out by previous researchers were done using a displacement-control system. Yet, for this particular research study, either system may be considered as adequate, since the primary scope of the research is to test the behaviour of auxetic laminates and compare their ultimate strength with other stacking sequences as described in the initial part of this Chapter. The second set of experiments, i.e. Cylinders Set I were carried out using a force-control system. These cylinders were tested at a rate of 1kN/sec.

Two video cameras were set up on either end of the machine to record the mode of failure of the composite and capture, whenever possible, the actual position of rupture.

5.3 Force-Control System vs Displacement-Control System

A brief description of works carried out by other researchers is hereby given to obtain a better understanding of the distinction between a stress- controlled and strain-controlled system of experimental loading. Even though, a displacement-control system is most often chosen because it is considered to be the most conservative approach, researchers such as Bouchelaghem et al. (155) and Toutanji (210), have shown that load control tests give satisfactory results. Toutanji (210) proposed a confinement model based on specimens that were loaded with a constant stress. Likewise, Lam et al. (19), Teng et al. (20) confinement model was designed by grouping together a number of experimental results already tested using either force or displacement control-systems, with the aim of providing a suitable model capable of predicting the stress-strain response of confined concrete.

The main difference depicted when comparing a stress-strain graph derived from a force-control system to the one attained from a displacement-control system occurs in the region beyond the ultimate limit. In fact, it can be said that the initial shape of the graphs are very similar. When loading, using a force-control system, the stress-strain graph initially follows a ductile behaviour and then fails in a brittle

manner, whereas, the contrary is likely to occur for a displacement-control system. An interesting study presented by Sutherland (191), gives the possibility of understanding the differences that may arise between these two systems of experimental loading. The study consisted of comparing experimental results using both systems with unconfined and confined models designed by other researchers. It resulted that a few confinement models gave different stress-strain diagrams for cylinders tested using a displacement-control mechanism when compared to others tested using a load-control system. This is because the factors identified in most confinement models have an impact on the stress-strain diagrams. In most cases, particular parameters are specifically chosen to be evaluated depending on the scope of the model. For instance, Popovics (119) proposed a model for plain, unconfined concrete and lists a set of parameters that have an effect on the results, namely: testing conditions (i.e. duration of load, equipment used during testing, the rate of loading), physical parameters of the specimen (i.e size and shape), position of strain gauges, the age of the concrete and the actual mix constituents of the concrete. Popovics (119, 211) states that loading at a constant stress (i.e. load-control), as opposed to loading at a constant strain (i.e. displacement-control), results in a stress-strain curve that has a stiffer initial modulus of elasticity for specimens loaded at a constant stress. However, Sutherland (191) experimentally proves the contrary and shows that, when placing the strain gauges in the middle of the concrete cylinder, identical ascending branches of the stress-strain diagrams were achieved for the different loading patterns. In addition, it is evident that the initial ascending branch is nearly identical for confined and unconfined concrete. It is only once the peak unconfined stress is reached, that the behaviour of the graph varies. This depends on which model one follows. In certain situations, a few models started to deviate from the ascending branch of the unconfined concrete when the linear portion of the stress-strain diagram was passed. This was probably attributed to the fact that the FRP was getting engaged due to the cracking occurring within the concrete cylinder.

Sutherland (191) concludes by stating that most confinement models examined gave satisfactory results. Yet, this does not mean that there is general agreement between the models in all circumstances. Different models are designed using different parameters, where some models are more versatile than others. A

number of confinement models are developed from experimental data conducted under particular controlled laboratory environments. It is evident that the experimental results are strongly influenced by these environments and this will, in turn, be reflected in the confinement model. Such models have the tendency to fail in predicting accurate results, especially when specimens are tested under different laboratory conditions. While a number of improvements have been carried out to provide reasonable accuracy in the stress-strain predictions, it is recommended to include in these models more realistic parameters, such as the effect of sustained loading or the arrangement of reinforcement in the specimens, so as to provide the models with improved accuracy and a more realistic prediction.

Chapter 6
Discussion of Experimental Results

6.1 Introduction

The concrete cylinders tested in this study can be considered as almost concentrically loaded RC members with circular cross-sections that are laterally-confined with CFRP jackets. The column's circular geometrical configuration allows the fibres to be uniformly-stressed across the entire cross-section. In this way, the confinement jacket provides a highly-effective confinement, improving the strength and deformability of the RC column itself. All FRP confined cylinders were strain gauged and compressed until failure so as to examine their load capacity and ductility. Both auxetic and non auxetic jackets were tested to compare their behaviour and analyse their confinement results.

6.2 Sign Convention, Nomenclature & Loading Rate

The Concrete Cylinders Set I were compressed at a loading rate of 1kN/sec. This corresponds to a static rate of loading so as to exclude dynamic effects. It is also worth noting that the main difference between a force-control and a displacement-control system is with regards to the ability of the latter system to describe the behaviour beyond the ultimate limit of the material. In this research work, the main focus was to obtain the maximum failure loads of the jackets. In addition, the experimental results showed an explosive failure at the ultimate failure point. Therefore, due to the absence of post ultimate behaviour beyond ultimate failure point, a force-control system is considered to be adequate for the purposes of this study.

The sign convention adopted in this thesis assumes a negative sign for compressive stresses, and consequently a positive sign for tensile stresses. Nevertheless, the stress-strain diagrams shown in this section depict the axial stresses/strains on the –ve side of the x-axis, whereas the hoop stresses/strains are shown on the +ve side of the x-axis.

It is worth noting that the stress-strain curves that are curtailed short correspond to samples where, during the testing, the machine tripped and the sample was then re-tested to failure.

The schematic representation shown in Figure 6.1 outlines the terminology used in this chapter to describe the behaviour of the confined concrete cylinder during the different loading stages.

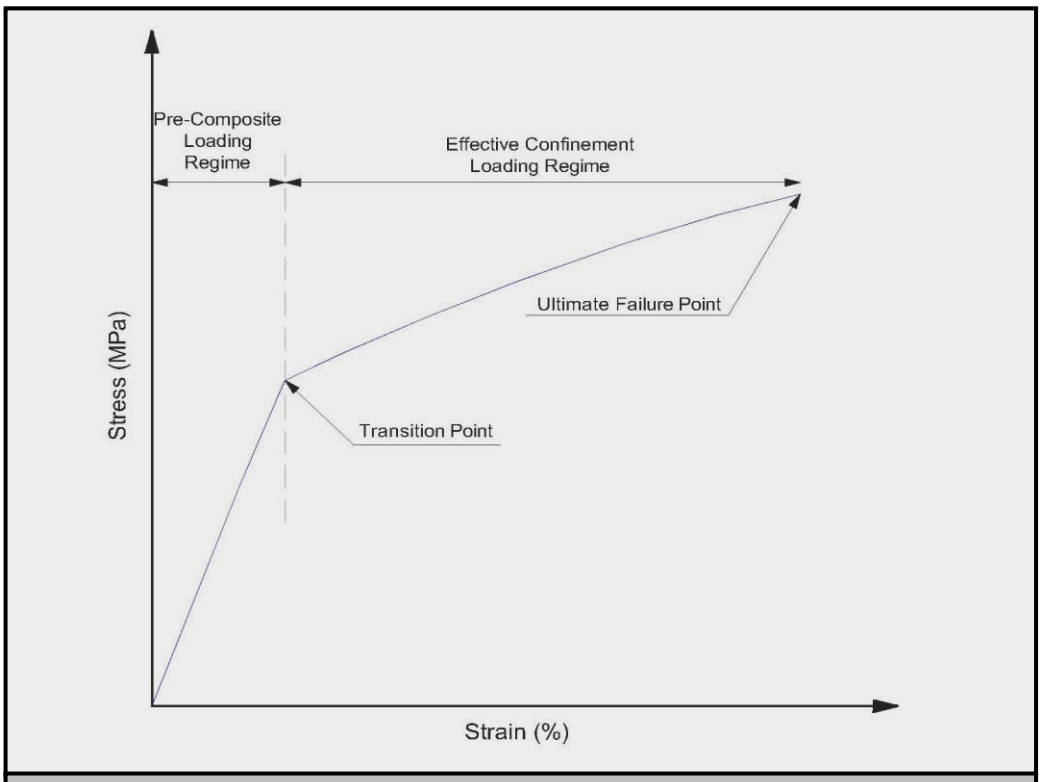

Figure 6.1 – Schematic representation to explain the terminology used to describe the behaviour of the confined concrete cylinder

The pre-composite loading regime is a ‘concrete-dominated deformation’ and mainly represents the deformation behaviour of the unconfined concrete cylinder.

The effective confinement loading regime is a ‘jacket-dominated deformation’ and mainly represents the behaviour of the confined jacketed concrete cylinder.

The transition point is the point at which the behaviour changes from a pre-composite loading regime to an effective confinement loading regime.

The ultimate failure point occurs when the jacket ruptures, which corresponds to the failure of all layers.

The abbreviations outlined in this section and shown in the legends are given below:

SR1 – Strain Rosette positioned 75mm away from the cylinder's surface;
SR2 – Strain Rosette positioned at the centre of the cylinder;
ST1 – Stacking sequence configuration - $[\pm 20]_{2s}$;
ST2 – Stacking sequence configuration - $[\pm 25]_{2s}$;
ST3 – Stacking sequence configuration - $[\pm 35°, 0_2]_s$;
ST4 – Stacking sequence configuration - $[\pm 16, \pm 45]_s$;
ST5 – Stacking sequence configuration - $[0_8]$;
ST6 – Stacking sequence configuration - $[90_8]$ configuration;
CM – Confinement Model;
S1-S40 – Individual Cylinders tested for compression.

6.3 Testing of Unconfined and Confined Concrete Cylinders

This section outlines the experiments that were carried out with a brief description related to the procedure adopted when testing both the unconfined and confined concrete cylinder samples. It is to be noted that the concrete Cylinders Set I were all manufactured and tested within a period of six weeks, where the manufacturing of the jackets were done within the first four weeks and their testing followed in the next two weeks. In other words, the jackets were manufactured using the same SE70 roll and by means of the procedures described in Chapter 5. Likewise, the Losenhousen 6,000 kN compression machine operating with Servocon software was prepared and set only once. During the two weeks of testing, the equipment was solely used for testing these cylinders and thus, no changes or differences took place in the settings during the course of the whole experiments. In this way, all cylinders were tested during the same period of time, under the same circumstances and with the use of the same techniques. In other words, the results achieved can provide a fair comparison between the auxetic laminates and other stacking sequences tested. It is assumed that some form of human error or slight misalignment might have occurred while rolling the layers. Yet, this too is a common aspect of all stacking sequences manufactured and it can be assumed that this should not cause any significant impact on the end results.

Referring to the concrete cylinders, these were cast using the same mix design and using the same standard procedures as described in Chapter 5. Four sets of cylinders, each consisting of ten cylinders were cast in a span of three weeks. However, it is not possible to produce cylinders having identical characteristic strengths, since many influencing factors are involved. In fact, it is common practice to experience differences in strength within the same batch of cylinders. The first sets of cylinders to be tested consisted of the unconfined concrete cylinders, where a total of four cylinders per batch were tested. These were further subdivided into two categories, namely heated and non-heated concrete cylinders. In all, a total of eight heated and eight non-heated cylinders were tested and the results are presented hereunder in Table 6.1.

Cylinders	Cylinder Name	Failure Load (kN)	Mean Failure Load (kN)	Compressed Distance (mm)	Failure Height (mm)	Mean Failure Height (mm)
Not Heated	Sample 1	686.93	751.67	3.52	296.48	296.25
	Sample 2	765.38		3.16	296.84	
	Sample 3	771.75		4.88	295.12	
	Sample 4	734.65		3.03	296.97	
	Sample 5	780.65		3.48	296.52	
	Sample 6	796.54		3.75	296.25	
	Sample 7	760.93		3.41	296.59	
	Sample 8	716.56		4.81	295.19	
Heated at 70° for 20 hours	Sample 9	759.87	678.09	3.21	296.79	297.13
	Sample 10	713.61		2.42	297.58	
	Sample 11	593.25		3.03	296.97	
	Sample 12	595.35		3.30	296.70	
	Sample 13	666.25		3.09	296.91	
	Sample 14	707.89		2.86	297.14	
	Sample 15	742.91		3.14	296.86	
	Sample 16	645.61		1.95	298.05	

Table 6.1 – Concrete Cylinders Set I: Failure Loads & Failure Cylinder Height of unwrapped cylinders

Moreover, to cure the resin, the SE70 CFRP prepreg needs to have a temperature of 70°C. Thus, the heating and testing of the cylinders was done so as to check whether there might be an effect on the overall strength of the concrete. It can be observed that, the failure loads of the heated and unheated cylinders varied, on

average, by 73.58 kN. Yet, when testing the individual heated samples, it can be noted, that Sample 11 and Sample 12 had the lowest failure load, whereas the remaining cylinders had failure loads and characteristic strengths similar in value to those of the non-heated samples.

The same procedure was retained to test the first set of cylinders and these results are shown in Table 6.2. Nevertheless, a similar pattern was observed between the heated and unheated cylinders, where a difference of 85.46kN was noticed. Thus, in both situations, a slight reduction in the characteristic strengths of the concrete was observed due to the heating of the cylinders. The mean characteristic stresses achieved are equivalent to 42.46 MPa for the unheated Cylinders Set I and 29.24 MPa for Cylinders Set II. Likewise, a mean value of 38.24 MPa was obtained for the heated Cylinders Set I and 24.41 MPa for Cylinders Set II. The concrete sets were cast at different periods and using different aggregates limestone chippings. All these factors, amongst others, might have caused the differences observed in the characteristic strengths. It is to be noted that the Cylinders Set II specimens were tested using a displacement-control system at a compressive rate of 12 mm/second. However, as stated earlier, due to a malfunction of the testing machine, this system was no longer an option and, therefore, all the Cylinder Set I samples were tested using a force-control system at a rate of 1 kN/second. It was observed that the graphs for these samples exhibited a different kind of behaviour, albeit with a similar shape.

Cylinders	Cylinder Name	Failure Load (kN)	Mean Failure Load (kN)	Mean Stress (MPa)
Not Heated	Sample 41	624.81	517.55	29.24
	Sample 42	494.72		
	Sample 43	520.73		
	Sample 44	431.53		
	Sample 45	515.96		
Heated at 70° for 20hours	Sample 46	475.42	432.09	24.41
	Sample 47	445.51		
	Sample 48	395.60		
	Sample 49	376.30		
	Sample 50	467.63		

Table 6.2 – Concrete Cylinders Set II: Failure Loads & Stresses of unwrapped cylinders

Last but not least, Table 6.3 summarises up the mean stresses, the standard deviations and the coefficients of variation of these tested cylinders, where satisfactory results were obtained.

Cylinder Set I	No. of Tested Cylinders	Mean Stress (MPa)	Standard Deviation	Coefficient of Variation
No Jacket & Unheated	8	42.46	2.07	0.05
No Jacket & Heated	8	38.24	3.79	0.10
Cylinder Set II	**No. of Tested Cylinders**	**Mean Stress (MPa)**	**Standard Deviation**	**Coefficient of Variation**
No Jacket & Unheated	5	29.24	3.94	0.13
No Jacket & Heated	5	24.41	2.49	0.10

Table 6.3 – Mean Stress, Standard Deviation & Coefficient of Variation for the heated and unheated concrete cylinder specimens of Cylinders Set I & Set II

Figures 6.2 and 6.3 show the graphs of stress versus time for the tested unheated and heated concrete specimen respectively.

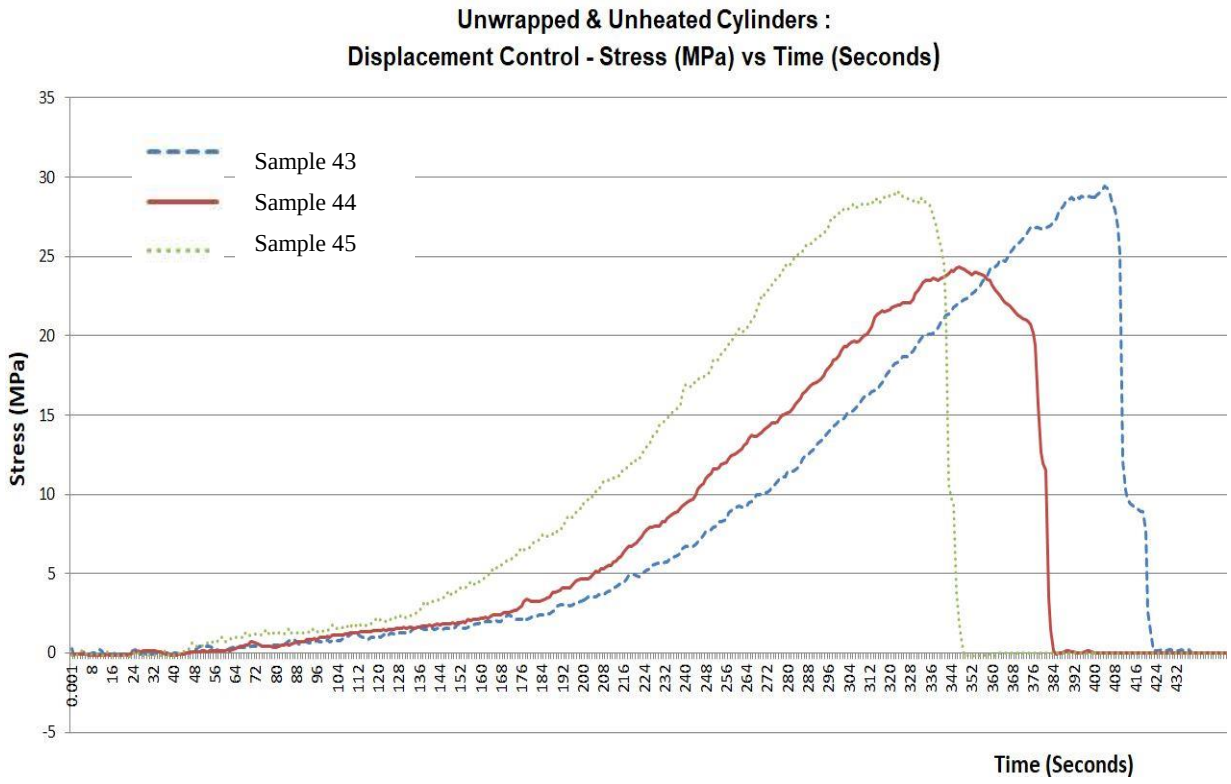

Figure 6.2 – Stress (MPa) vs Time (s) for cylinders tested using a displacement control system. Unwrapped and unheated Cylinder – Cylinders Set II

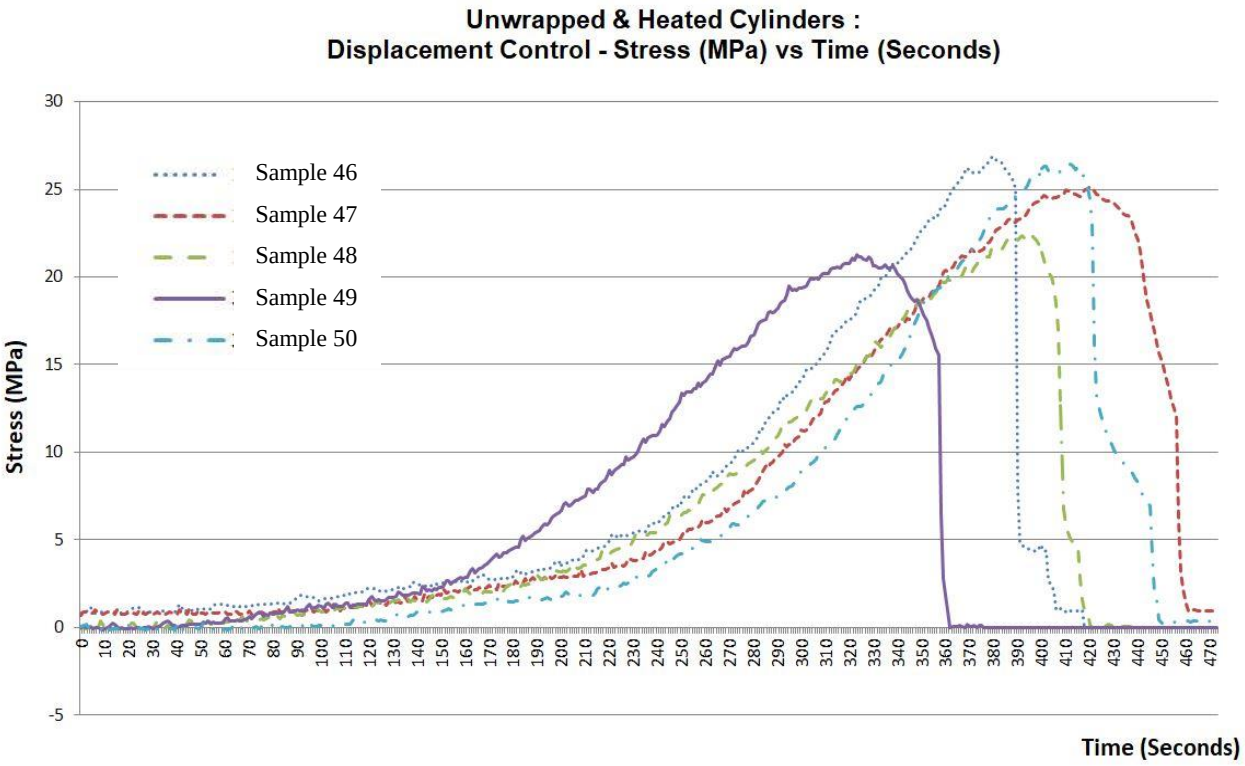

Figure 6.3 – Stress (MPa) vs Time (s) for cylinders tested using a displacement control system. Unwrapped and heated Cylinder – Cylinders Set II

6.4 Experimental Tests & Observations Noted During Testing

To obtain a better understanding of the failure mode, a brief description is given below regarding the behaviour of each confinement jacket during the testing. In this way, the pre-composite loading regime and the effective confinement loading regime noted during experimentation would shed some light upon the structural performance of the jackets. Whilst testing the auxetic confinement jackets ST1, it was noted that initially both strain rosettes gave similar readings. A similar process was kept for all ST1 specimens tested, where the initial fibre breakages were visible when the compressive force was in the region of 2,350 kN. A gradual fibre failure was seen along the jacket until a sudden and abrupt explosive failure was reached. In the case of Sample 17, the gauges were detached from the jacket a few seconds prior to failure and, thus, the strain rosettes stopped recorded strain readings. The actual

failure of this cylinder sample occurred when the compressive force reached 2,650kN. Unfortunately, due to a manufacturing error, cylinder Sample 18 experienced a premature failure and the corresponding failure load will not be used in the analysis of the test results. As shown in Figure C.45**,** the back paper sheet of the roll was erroneously left during the manufacturing process of Sample 18.

Likewise, while testing ST2 auxetic jackets, the strain readings of the two differently-positioned strain rosettes seemed to give very similar values, with only a 25με difference between the top and central strain rosette. Initially, a gradual increase was shown in the strain values until a rapid increase occurred when the force reached approximately 850kN. Most likely, at this stage, the concrete cylinder was not resisting any load, whilst the jacket was withstanding the compressive force. The initial fibre failures began when the force was in the region of 1,900 kN, followed by the failure of the laminate.

While testing confinement jackets with stacking sequence configuration of $[\pm 16,\pm 45]_s$, it was noticed that initially the strain values of both strain rosettes were relatively similar in value and increased gradually at a steady rate until the loading reached, on average, a force of 900 kN. From this point onwards, the strain values increased rapidly and, at a particular stage, a difference of approximately 1000 με was observed between the central rosette and the rosette located close to the cylinder's surface. The first fibre cracks or breakages occurred when the compressive force reached an average value of 1,350 kN. Most probably, the failure occurred within the first few layers of the confinement jacket, since no fibre cracks or detachments were visible externally. At an average load of 1,600 kN, the fibres of the confinement jacket began to detach from the cylinder until an explosive failure was reached.

A similar pattern was observed when testing confinement jackets with stacking sequence configuration of $[\pm 35,0_2]_s$. Initially, the strains increased gradually, where a difference of approximately 60 με was depicted between the two strain rosettes with the largest value noticed in the centrally-located strain rosette. When the compressive force reached 750 kN, the strain rosettes were almost equal in value. From this point onwards, a rapid increase in strain values was noted, particularly in

the top strain rosette. It is evident that when it reached this point, the concrete cylinder began to fail and the pressure exerted on the CFRP increased rapidly. The first minor fibre cracks appeared when the load was in the region of 1,025 kN. Yet, the actual laminate failure and the initial fibre detachment were noticed at a load of 1,675 kN. An explosive failure occurred at an average stress of 129.10 MPa.

The ST5 confinement jackets were the only laminates to be tested with individual layers consisting of full length sheets. As explained in the previous chapter, due to the SE70 roll limitations, it was not always possible to cut full-length laminae. This jacket possessed the highest maximum stiffness (i.e. highest Young's modulus of elasticity), and so it is expected that this stacking sequence configuration resists high stresses. When testing ST5 confinement jackets, minimal strain readings were noted for the central strain rosette, until the compressive load of 650 kN was reached. This value is almost equivalent to the compressive failure load of the heated concrete cylinders. For test Samples 25-27, it can be said that the first fibre cracks were heard when the compressive load reached the value of 1,450 kN. At 1,800 kN, the cracks and fibre detachment were visible in several parts of the cylinder, until an explosive failure occurred. Similar results were reached for test Samples 28 and 29, yet at slightly higher values. It is also worth mentioning that for test Samples 26 and 27, the central strain gauge restarted to take readings from scratch when the load was 1,650 kN.

On the other hand, it resulted that ST6 confinement jackets were the weakest ones tested. The SE70 fibres were in the same direction as the load application. Thus, the composite did not restrict the cylinder from bulging. On the contrary, the jacket accommodated the cylinder's shape, where bulges were visible prior to tearing and failing of the jacket. The initial fibre failure occurred at very low forces, more precisely in the region of 150 kN. The failure of the composite was very silent and consisted in the tearing up of the jacket. Most of the times, these jackets failed before the concrete, at times at a load in the region of 350 kN, whereas the concrete cylinder failed, on average, in the region of 600 kN. As shown, in Figure 6.14**,** the graphs depict a haphazard shape, where only a few readings were taken, since even the strain rosettes failed at an early stage. It is worth mentioning that the average compressive

failure stress of these concrete cylinders was lower when compared with the values obtained for the heated cylinder tests. The ST6 confinement jackets were tested using concrete Cylinders Set I-D, as shown in Table 6.1, where the failure stresses of the unheated samples (i.e. Samples 7 and 8) and the heated samples (i.e. Samples 15 and 16), failed at higher values. This difference can be attributed to the capping system adopted. As was previously explained, circular lead plates used when testing the confined jacket cylinders had a relatively smaller diameter than the concrete cylinder. This might have resulted in a non-uniform distribution of stresses that may have caused the ST6 cylinders to fail at a lower failure load than the non-jacketed heated concrete cylinders. On the other hand, rubber cappings covered both the top and bottom surfaces of the unwrapped concrete cylinders.

6.5 Discussion & Interpretation of Results.

The results obtained from the tested concrete cylinders are represented in terms of stress-strain curves, as shown in Figures 6.4-6.14, where each graph depicts the axial and hoop strains. At first glance, all jacketed cylinders show a similar bi-linear behaviour, where an initial curve slope is controlled by the deformation behaviour of the unconstrained concrete cylinder until the transition point is reached. Once the pre-composite loading regime is exceeded, an effective confinement loading regime follows until the ultimate failure of the confined jacket is reached. The extent and the level of the effective confinement loading regime is greatly dependent on the jacket's characteristics (i.e. number of layers, SE70 CFRP properties etc.) and the stacking sequence configuration of the composite. Thus, the external CFRP has little effect on the initial linear portion of the stress-strain curve, but it has a strong influence on the softening of the effective confinement loading region. Only stacking sequence configuration ST6 exhibited a different behaviour. As expected, this configuration was the weakest confinement jacket tested. The fibres were in the same direction as the applied load, i.e. dependent on the matrix and these jackets were tested so as to acquire a better understanding of the behaviour of laminates having the minimum possible Young's modulus of elasticity. As will be seen further on, the laminate's failure occurred before the actual failure of the concrete cylinder.

On the other hand, the observed failure mode of the CFRP-reinforced cylinders tested (i.e. ST1-ST5) can be considered to be a brittle type failure. When applying a load on the confined cylinders, the fibres stretch in tension in the hoop direction. It can be said that a uniform gradual failure of the jacket was not visible. On the contrary, the failure was quite abrupt and explosive. This occurred due to the high resistance of the carbon fibres together with the accumulated pressure occurring between the concrete and the jacket. Initially, the cracks of the first fibres emitted hushed sounds. Eventually, prior to failure, sudden and abrupt fibre detachments occurred, mainly in the central region of the cylinder. The failure mode was explosive and the confinement jacket ended up scattered around the machine's enclosure in two or three separate parts, particularly when testing ST1, ST2 and ST5. The concrete cylinders were completely crushed and pulverised. Only the top and bottom surface of the cylinder were observed to have remained intact. It is evident that the non-uniform deformations, together with significant loading on the cracked concrete, provoked significant stress concentrations on the FRP jacket, leading to the abrupt failure of the cylinder. A brittle but less explosive failure was noted when testing the ST3 and ST4 confinement jackets.

From the tabular results (See Table 6.4) and graphic representations (See Figures 6.4-6.14) presented in this section, it was observed that the auxetic jackets gave satisfactory results. When compared to the other stacking sequence configurations tested in this study, they provided better confinement, since the failure load obtained was the highest. ST1 and ST2 were chosen to be tested as they offered the highest negative Poisson's ratio amongst all the symmetric balanced angle-ply laminates. In addition, when selecting the stacking sequences that had the same Young's moduli of elasticity as ST1 and ST2, it resulted that ST3 too had a negative Poisson's ratio equivalent to -0.1078. An interesting observation is that, from the acquired results, these three auxetic jackets seem to have resisted the highest compressive loads. Thus, by assuming uniform resin distribution between the individual layers, the through thickness expansion caused by a negative Poisson's ratio did produce a better effect on the confined jacket behaviour providing, in turn, an improved stress confinement. It is worth pointing out that, in the available research literature, with particular reference to the confinement models discussed in

Chapter 3, the models do show that to a certain extent, the ultimate failure of the jacket is dependent on the strength of the material. Thus, it is expected that the jacket having the highest axial rigidity should be capable of resisting more load, which, in this case, is represented by the results of ST5.

Stacking Sequence	Cylinder Name	Failure Load (kN)	Mean Failure Load (kN)	Compressed Distance (mm)	Failure Height (mm)	Mean Failure Height (mm)
ST1 $[\pm 20]_{2s}$	Sample 17	2582.95	2619.11	19.05	280.95	282.09
	Sample 18	2082.66		11.74	288.26	
	Sample 19	2578.74		13.65	286.35	
	Sample 20	2695.63		21.03	278.97	
ST2 $[\pm 25]_{2s}$	Sample 21	2409.17	2371.65	16.22	283.78	284.68
	Sample 22	2420.60		14.50	285.50	
	Sample 23	2424.70		16.86	283.14	
	Sample 24	2232.14		13.72	286.28	
ST5 $[0_8]$	Sample 25	2031.59	2186.90	11.38	288.62	288.45
	Sample 26	1904.38		9.95	290.05	
	Sample 27	2102.26		11.12	288.88	
	Sample 28	2363.48		10.63	289.37	
	Sample 29	2532.80		14.66	285.34	
ST6 $[90_8]$	Sample 30	633.75	602.56	6.75	293.25	294.19
	Sample 31	680.01		4.91	295.09	
	Sample 32	650.37		7.12	292.88	
	Sample 33	621.85		5.20	294.80	
	Sample 34	426.81		5.08	294.92	
ST3 $[\pm 35,0_2]_s$	Sample 35	2311.77	2282.77	19.05	280.95	284.40
	Sample 36	2242.90		13.65	286.35	
	Sample 37	2293.65		14.10	285.9	
ST4 $[\pm 16,\pm 45]_s$	Sample 38	1680.60	1660.87	5.31	294.69	293.31
	Sample 39	1692.61		6.85	293.15	
	Sample 40	1609.42		7.92	292.08	

Table 6.4 – Results of the Confinement Jackets Tested

In this study, all confinement jackets consisted of 8 layers of SE70 CFRP prepregs, having a total thickness of 1.6mm, where all jackets were manufactured using the same vacuum bagging technique. It can be deduced that, although ST1 and ST3, as well as, ST2 and ST4 have the same Young's moduli of elasticity, a

considerable difference is visible in the failure stress of the respective confinement jackets. In fact, from the results presented in Table 6.4, it can be said that ST1 had an improved mean failure stress of 19.14 MPa when compared to the corresponding value for ST3. In this case, both jackets have a negative Poisson's ratio, with ST1 having the highest value. Likewise, the difference in mean failure stress between ST2 and ST4 was equivalent to 40.65 MPa. It is likely that the actual angles forming the confinement jackets have an effect on the ductility and strength of the jacket. In addition, the through thickness expansion, in particular the Poisson's ratio negative value, seems to provide better confinement.

Table 6.5 below summarises the mean stresses, the standard deviations and the coefficients of variation of these tested cylinders, where satisfactory results were obtained.

Cylinder Set I	No. of Tested Cylinders	Mean Stress (MPa)	Standard Deviation	Coefficient of Variation
ST1: $[\pm 20]_{2s}$	3	148.24	3.79	0.03
ST2: $[\pm 25]_{2s}$	4	134.15	5.23	0.04
ST5: $[0_8]$	5	124.16	14.34	0.12
ST6: $[90_8]$	5	32.69	5.18	0.16
ST3: $[\pm 35, 0_2]_s$	3	129.10	2.02	0.02
ST4: $[\pm 16, \pm 45]_s$	3	93.50	2.26	0.02

Table 6.5 – Mean Stress, Standard Deviation & Coefficient of Variation for the confined concrete specimen tested. (Cylinders Set I)

Sample 18, being one of the tested cylinders wrapped with an auxetic confinement jacket of stacking sequence $[\pm 20]_{2s}$ failed at an early stage due to the presence of the back paper that was erroneously not removed during the rolling of the lamina. This caused a premature failure of the cylinder that failed at a load of 2,082kN. Consequently, its failure load was not used for calculating the mean stress and standard deviation. Furthermore, no initial fibre breakage occurred.

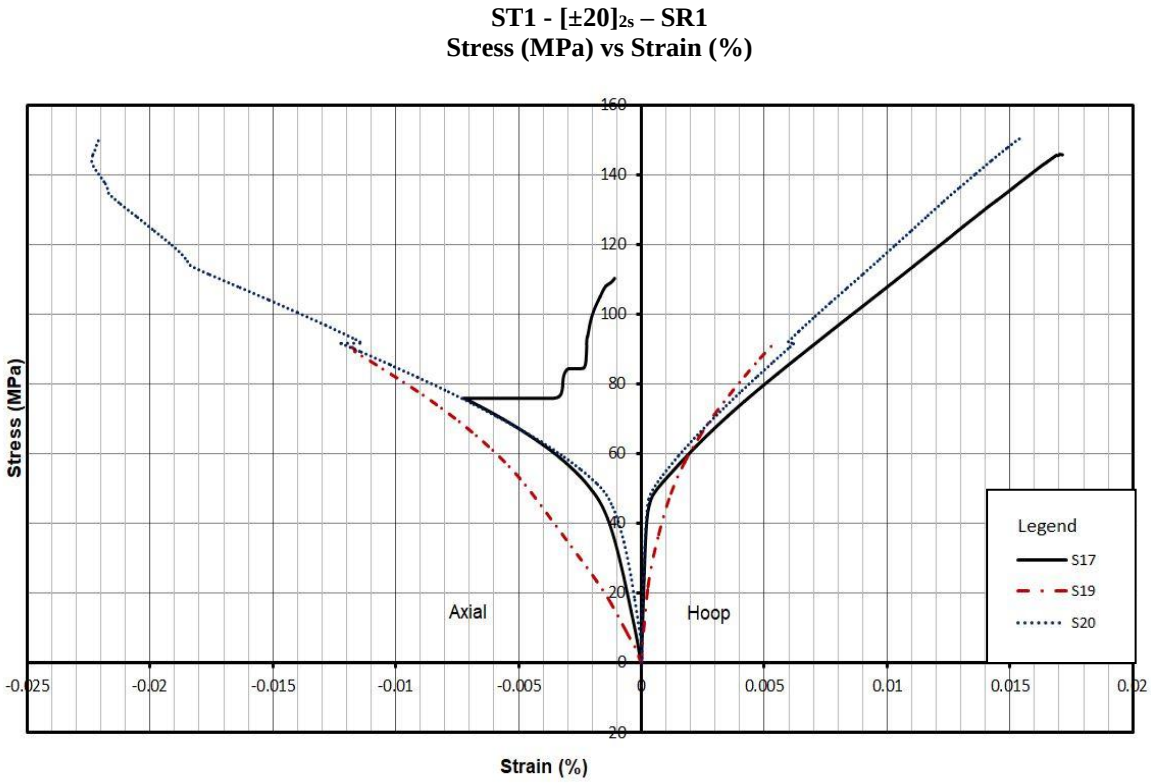

Figure 6.4 – Stress (MPa) vs Strain (%) – Stacking Sequence $[\pm 20]_{2s}$ for Strain Gauge Rosette I. Cylinders tested using a Force Control System**.**

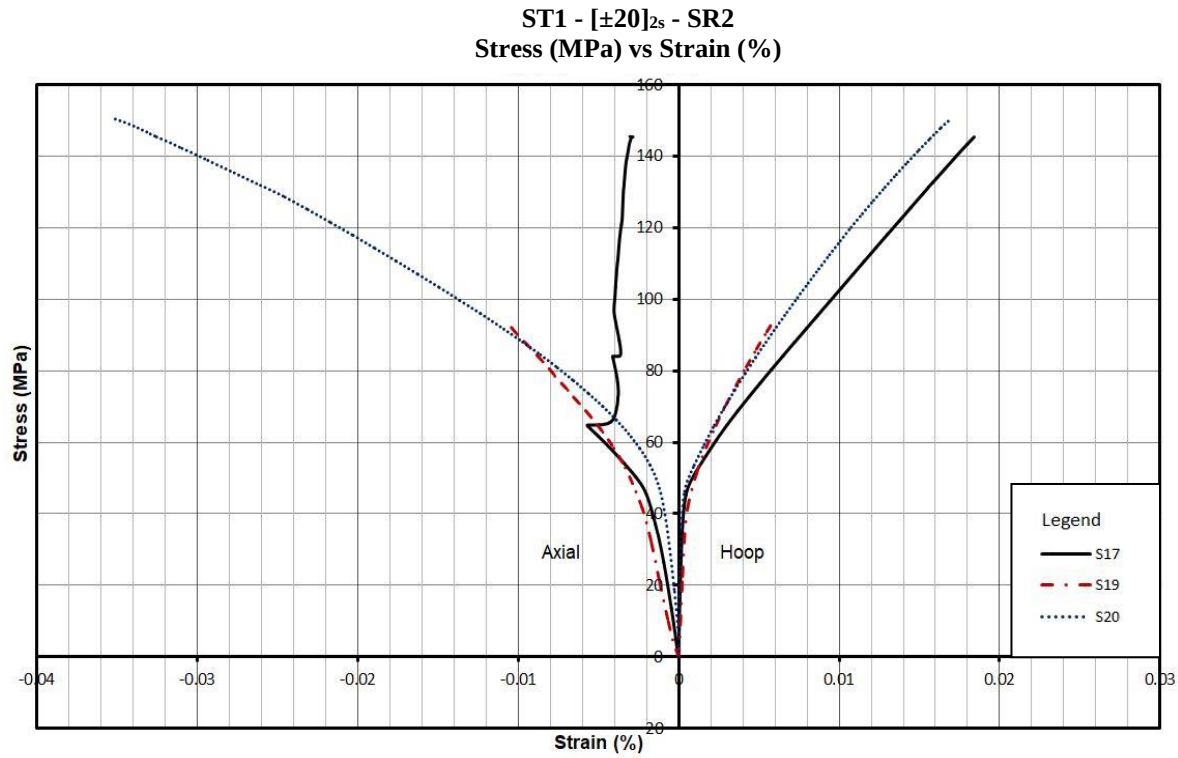

Figure 6.5 – Stress (MPa) vs Strain (%) – Stacking Sequence $[\pm 20]_{2s}$ for Strain Gauge Rosette II. Cylinders tested using a Force Control System**.**

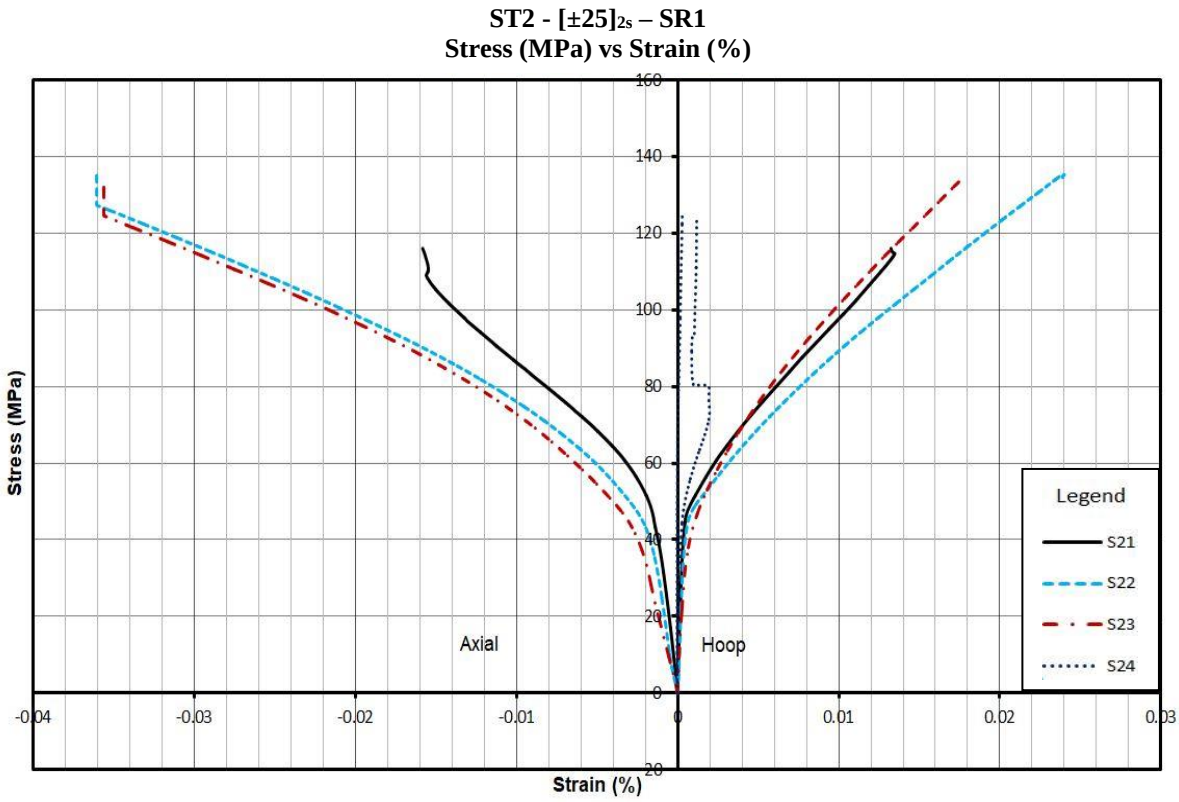

Figure 6.6 – Stress (MPa) vs Strain (%) – Stacking Sequence $[\pm 25]_{2s}$ for Strain Gauge Rosette I. Cylinders tested using a Force Control System**.**

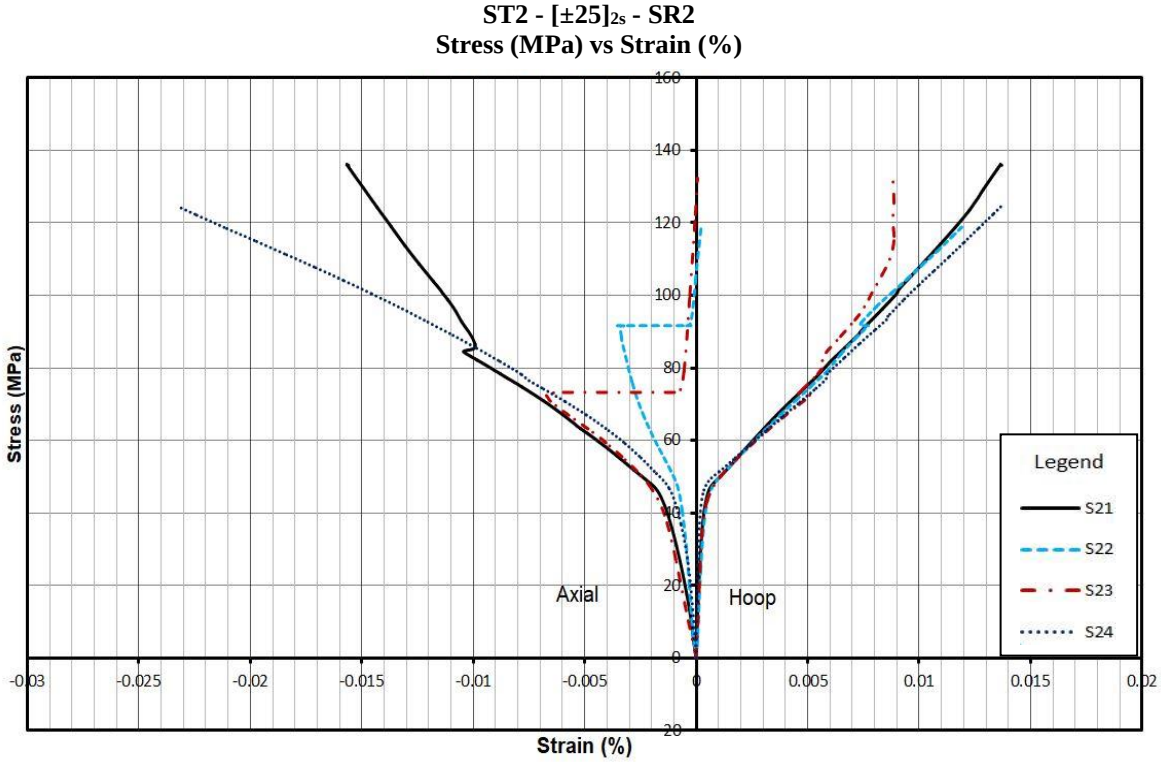

Figure 6.7 – Stress (MPa) vs Strain (%) – Stacking Sequence $[\pm 25]_{2s}$ for Strain Gauge Rosette II. Cylinders tested using a Force Control System**.**

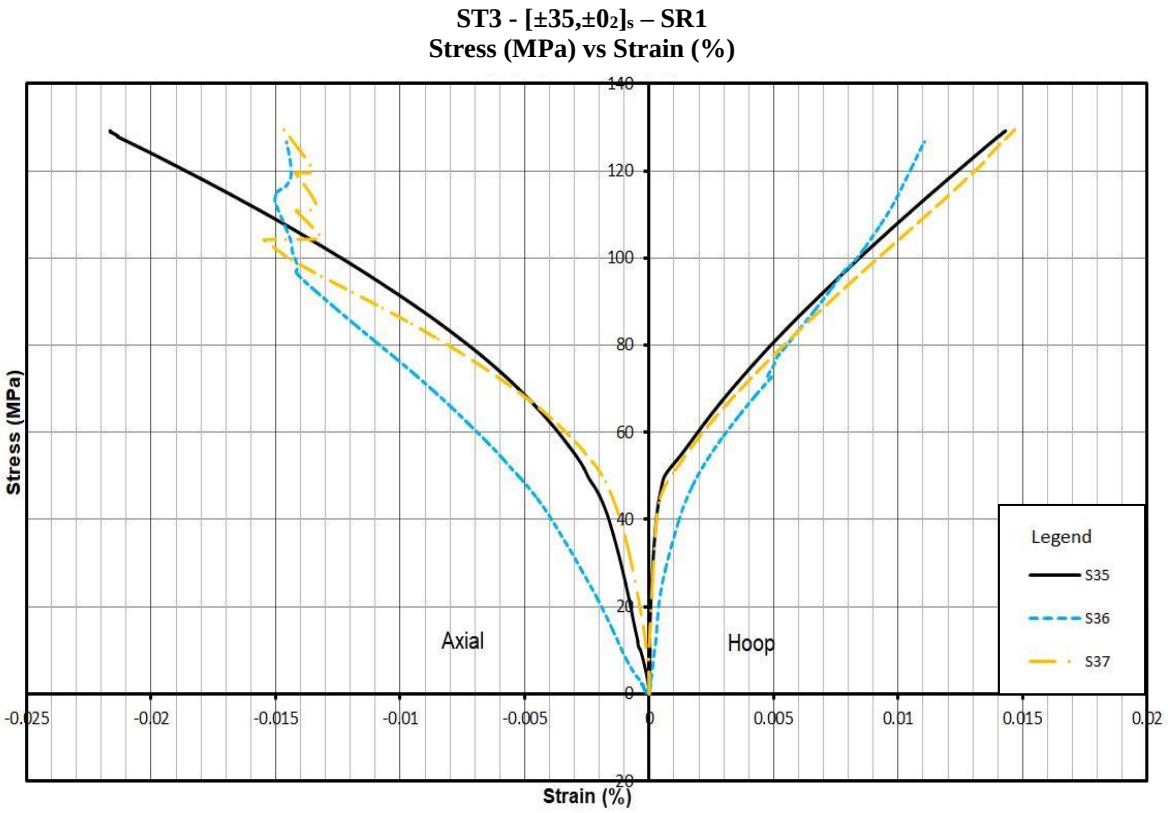

Figure 6.8 – Stress (MPa) vs Strain (%) – Stacking Sequence $[\pm 35,0_2]_s$ for Strain Gauge Rosette I. Cylinders tested using a Force Control System**.**

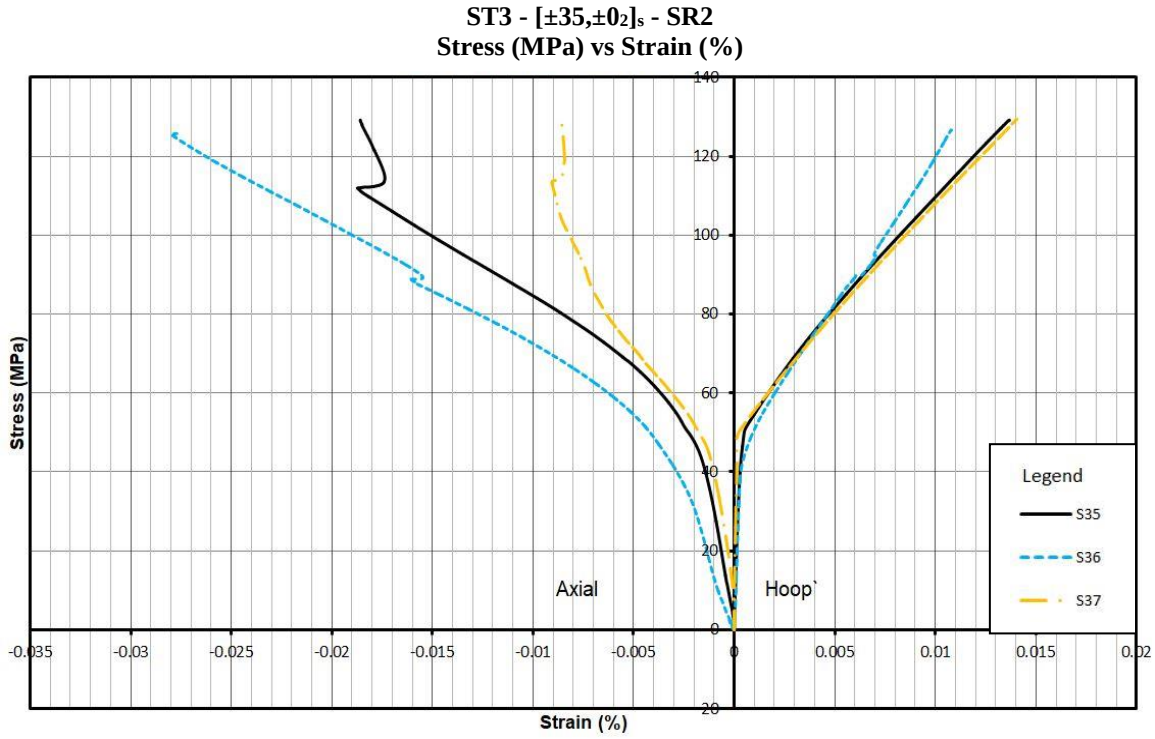

Figure 6.9 – Stress (MPa) vs Strain (%) – Stacking Sequence $[\pm 35,0_2]_s$ for Strain Gauge Rosette II. Cylinders tested using a Force Control System**.**

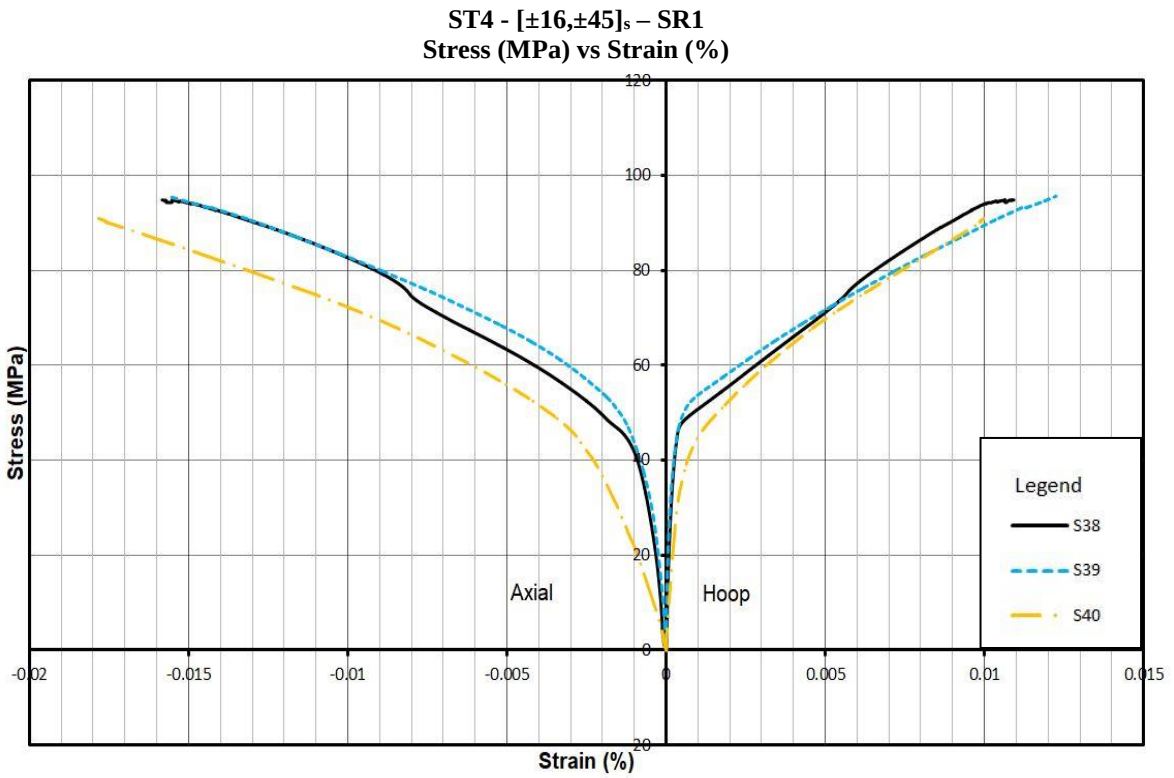

Figure 6.10 – Stress (MPa) vs Strain (%) – Stacking Sequence $[\pm 16,\pm 45]_s$ for Strain Gauge Rosette I. Cylinders tested using a Force Control System**.**

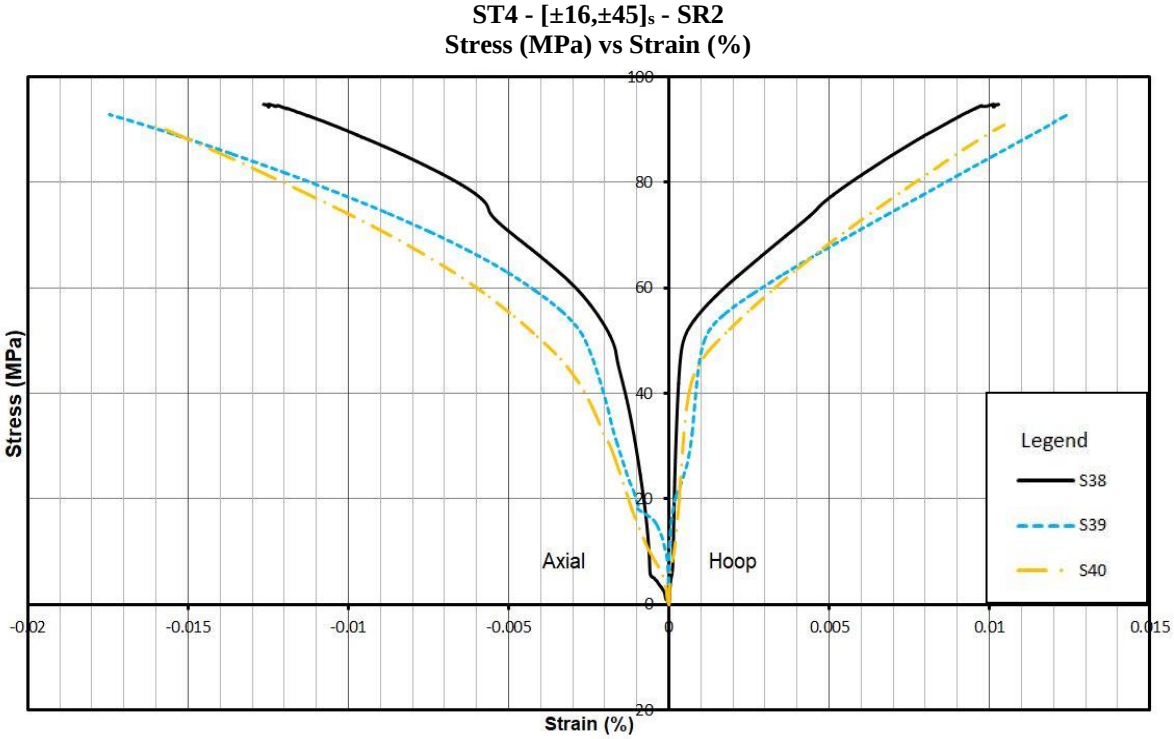

Figure 6.11– Stress (MPa) vs Strain (%) – Stacking Sequence $[\pm 16,\pm 45]_s$ for Strain Gauge Rosette II. Cylinders tested using a Force Control System**.**

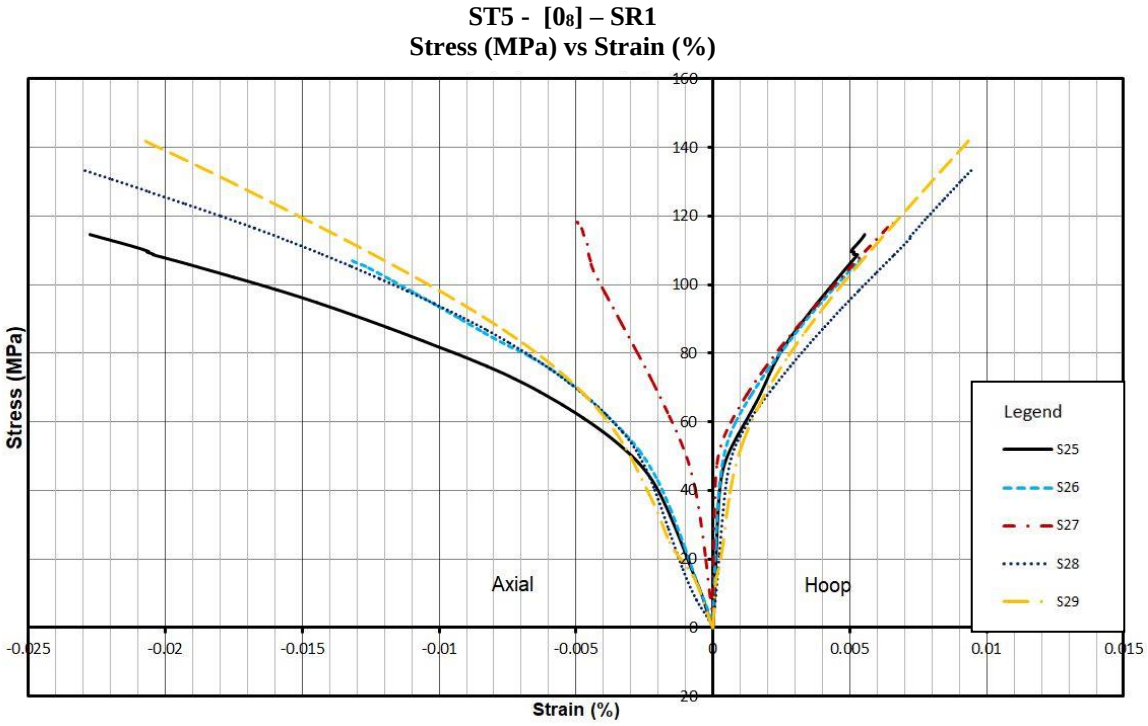

Figure 6.12 – Stress (MPa) vs Strain (%) – Stacking Sequence [0_8] for Strain Gauge Rosette I. Cylinders tested using a Force Control System**.**

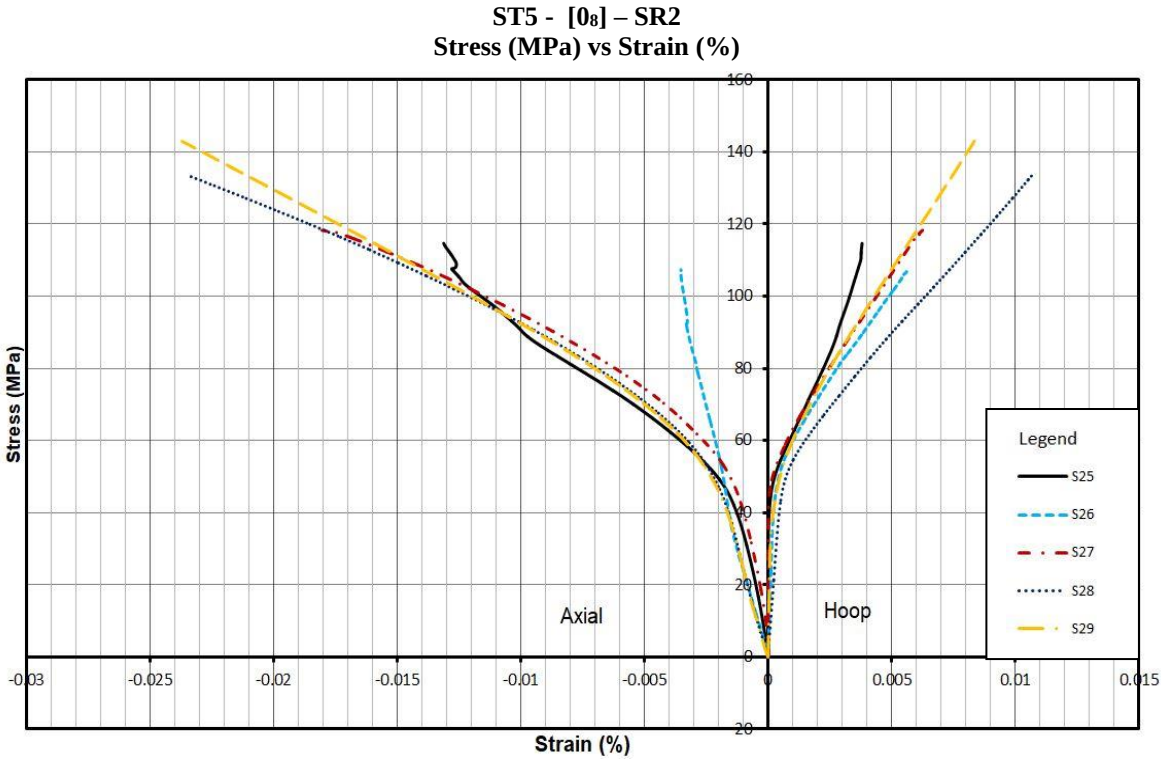

Figure 6.13– Stress (MPa) vs Strain (%) – Stacking Sequence [0_8] for Strain Gauge Rosette II. Cylinders tested using a Force Control System**.**

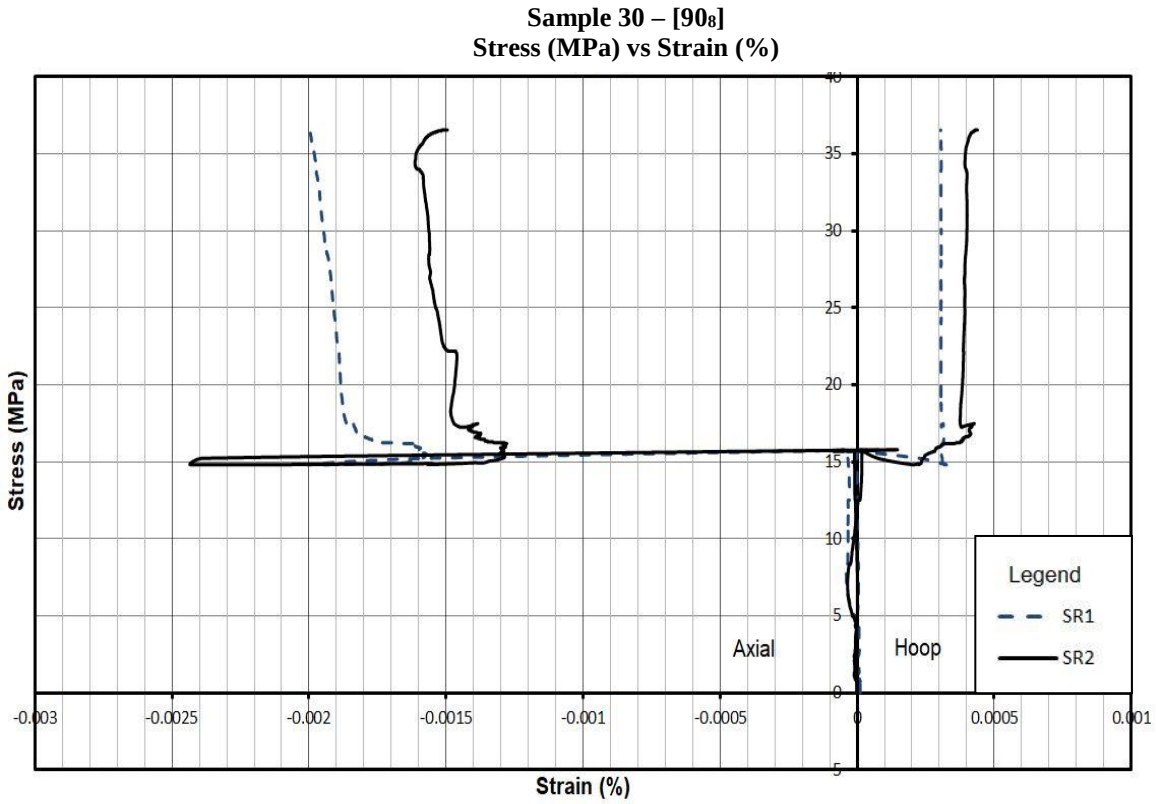

Figure 6.14 – Typical Example of a Stress (MPa) vs Strain (%) graph for ST6, i.e. stacking sequence [90_8]. The confined jacket failed prematurely, before the actual failure of the concrete cylinder and the strain gauge rosettes got detached from the jacket at an early stage. Graphs of this form were obtained. Cylinders tested using a Force Control System.

6.6 Auxetic Confinement

6.6.1 Tensile tests

It is not simple to quantify and analyse the behaviour of an auxetic jacket. As stated, in Chapter 5, appropriate measures were purposely taken so as to provide a uniform auxetic effect and no puncturing or holes were allowed that might have disrupted this uniformity. It is also worth mentioning that the scope of manufacturing the jackets using a prepreg system was to reduce human errors and improve this uniformity. The through thickness tensile tests and findings, with particular reference to the work carried out by Donoghue et al. (212), can help in describing the possible beneficial effects of the jacket when subjected to hoop tension.

Different sample thicknesses, i.e. 0.8mm, 1.6mm and 3.2mm thick laminates, were tested with the initial aim of checking whether the thickness of the sample had an effect on the actual value of the Poisson's ratio. The tests were performed in tension using an Instron 1342 hydraulic testing machine together with a video gauge positioned accurately to measure the through thickness dilation. They were pulled in tension at a crosshead speed of 2mm/min until ultimate failure occurred. Unfortunately, the first two thinnest specimens tested did not provide a consistent value and so it is not deemed prudent to make use of these test results for this study. Even though a powerful lens was used to focus on the through thickness expansion, minor movements, caused by the tensile machine while pulling the specimens, created an out-of-focus situation for layers with a 0.8mm and 1.6mm thickness. Typical results obtained for these two thicknesses are presented in Figures 6.21 and 6.22, where the scatter diagrams depict haphazard points without providing a stable value. On the contrary, as shown in Figures 6.15 - 6.20, the specimens that had an overall thickness laminate of 3.2mm (i.e. 16 layers) can be said to have given adequate results. When using the 3.2mm thick laminates, it was noted that, during the first part of the testing, the negative Poisson's ratios varied substantially until a constant value was consequently reached until failure. Thus, the two data points per specimen do confirm the presence of a negative Poisson's ratio, where both auxetic stacking sequences tested exhibited a negative value that varied approximately between -0.3 and -0.6. Even though it is difficult to derive a precise value from these tests, it can be said that they do follow a similar pattern to those estimated using the classical laminate theory. In addition, the values obtained when pulling the specimen, indicated that there is a through thickness expansion. A few samples were stopped, approximately in the region of the elastic limit, so as to tentatively take measurements of the though thickness expansion using a vernier caliper. However, the expansion was a minimal and, therefore, only minor differences were noted. Hence, the negative Poisson's ratios assumed in this study, for ST1 and ST2 are -0.403 and -0.468 respectively (see Table 4.2). Tensile tests were also carried out for ST5 laminates. A similar scattered diagram was obtained, yet, with a positive Poisson's ratio.

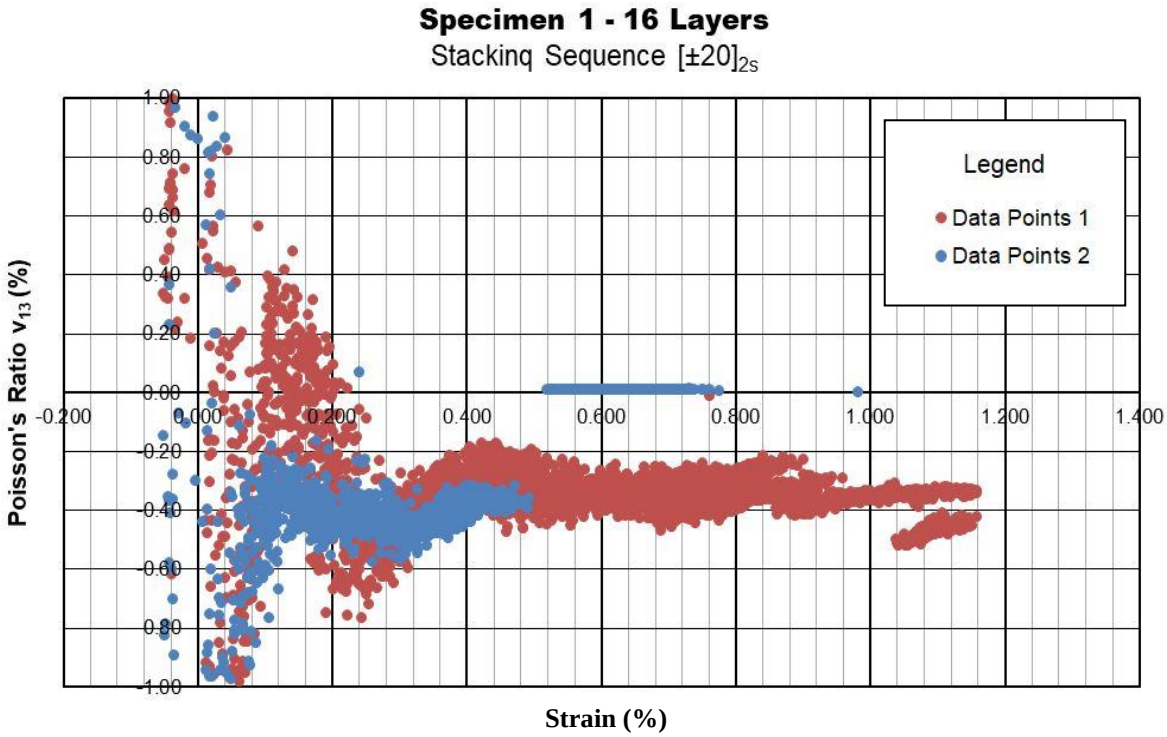

Figure 6.15– Poisson's Ratio ν_{13} (%) vs strain (%) – Specimen 1 -Stacking Sequence $[\pm 20]_{2s}$

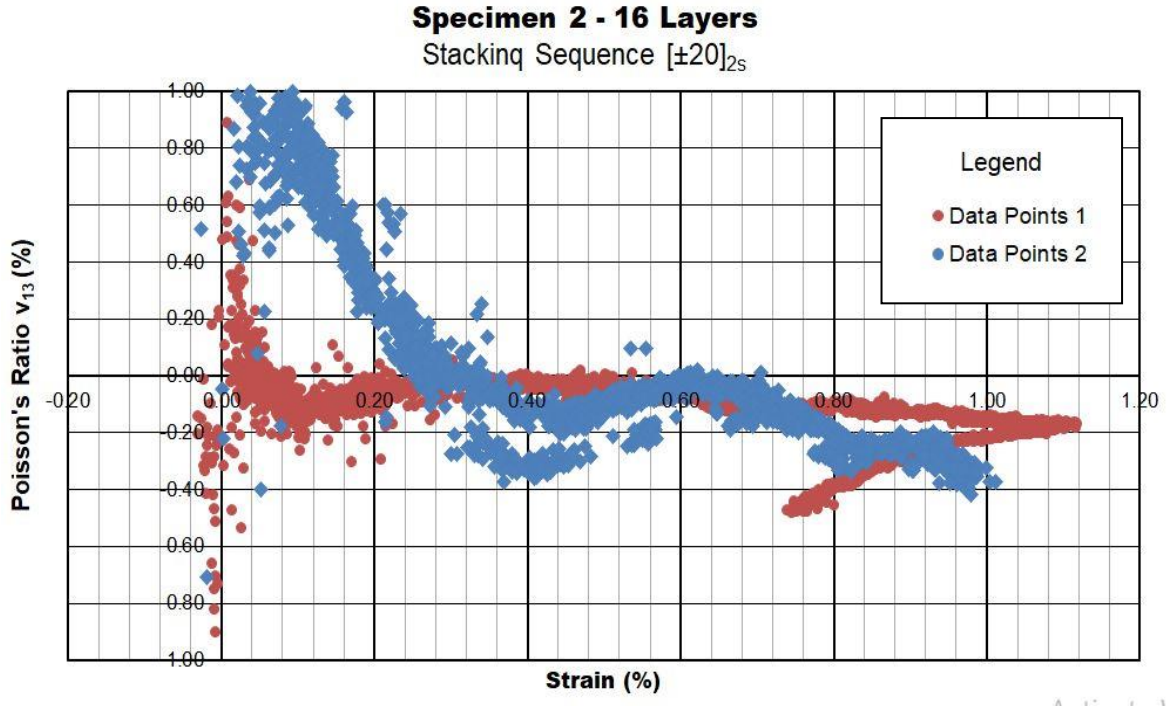

Figure 6.16– Poisson's Ratio ν_{13} (%) vs strain (%) – Specimen 2 - Stacking Sequence $[\pm 20]_{2s}$

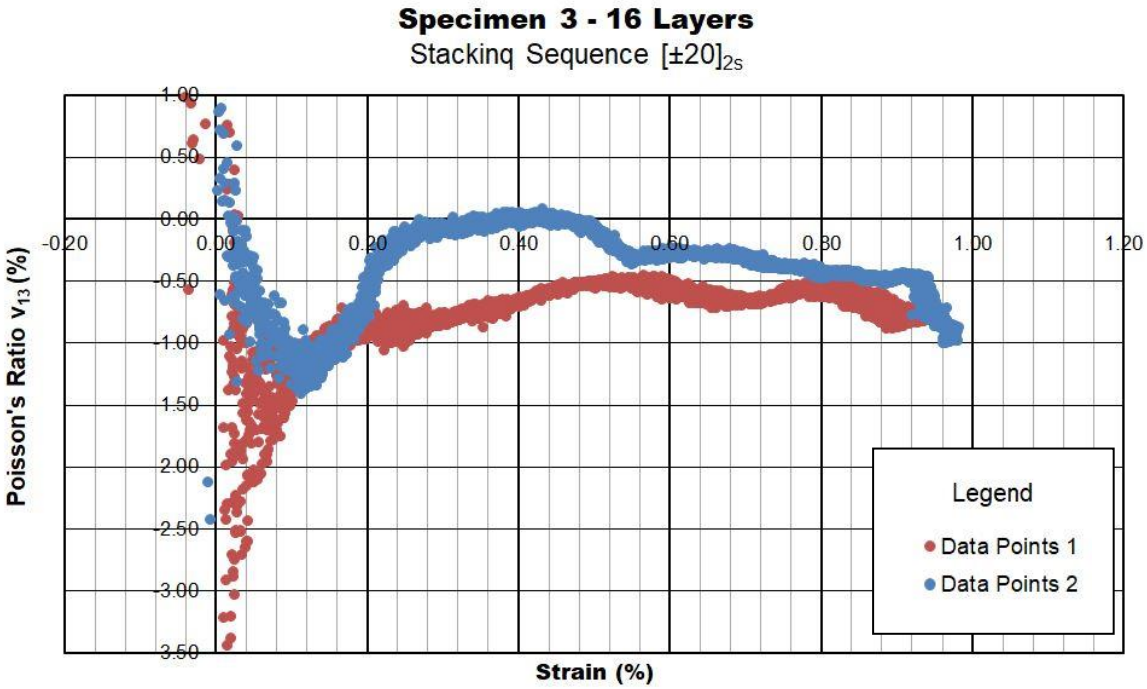

Figure 6.17– Poisson's Ratio ν_{13} (%) vs strain (%) – Specimen 3 -Stacking Sequence $[\pm 20]_{2s}$

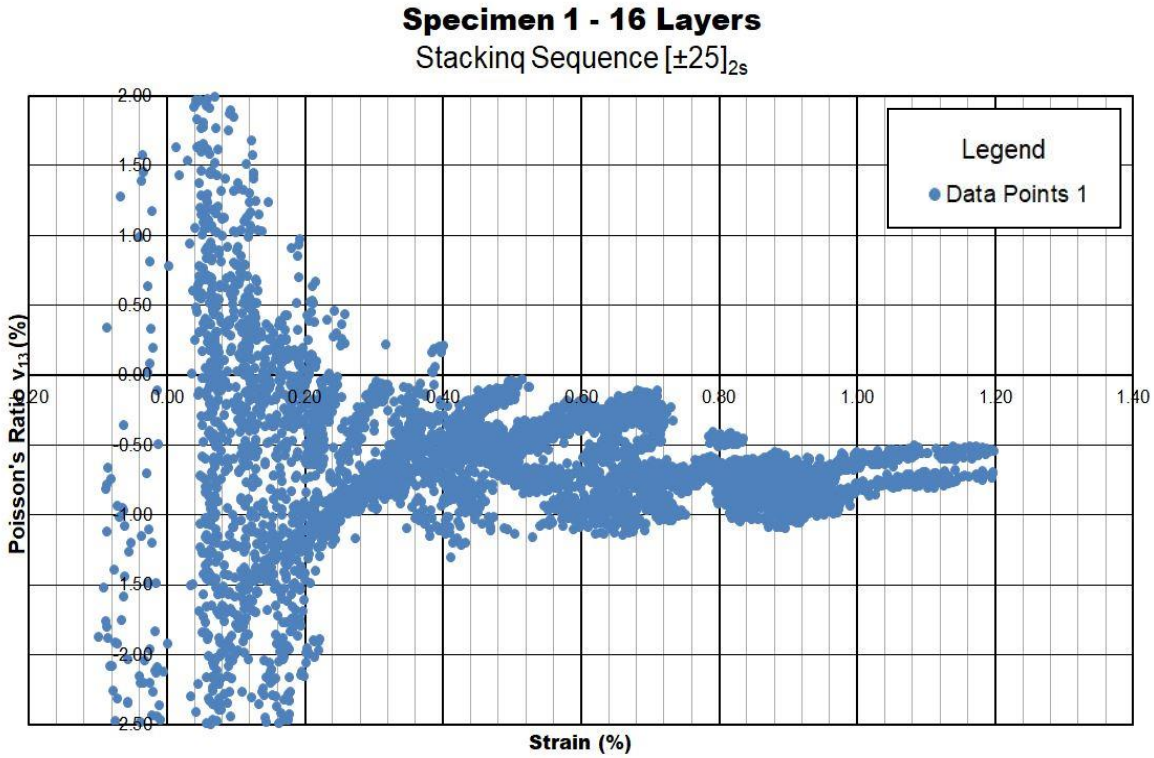

Figure 6.18– Poisson's Ratio ν_{13} (%) vs strain (%) – Specimen 1 - Stacking Sequence $[\pm 25]_{2s}$

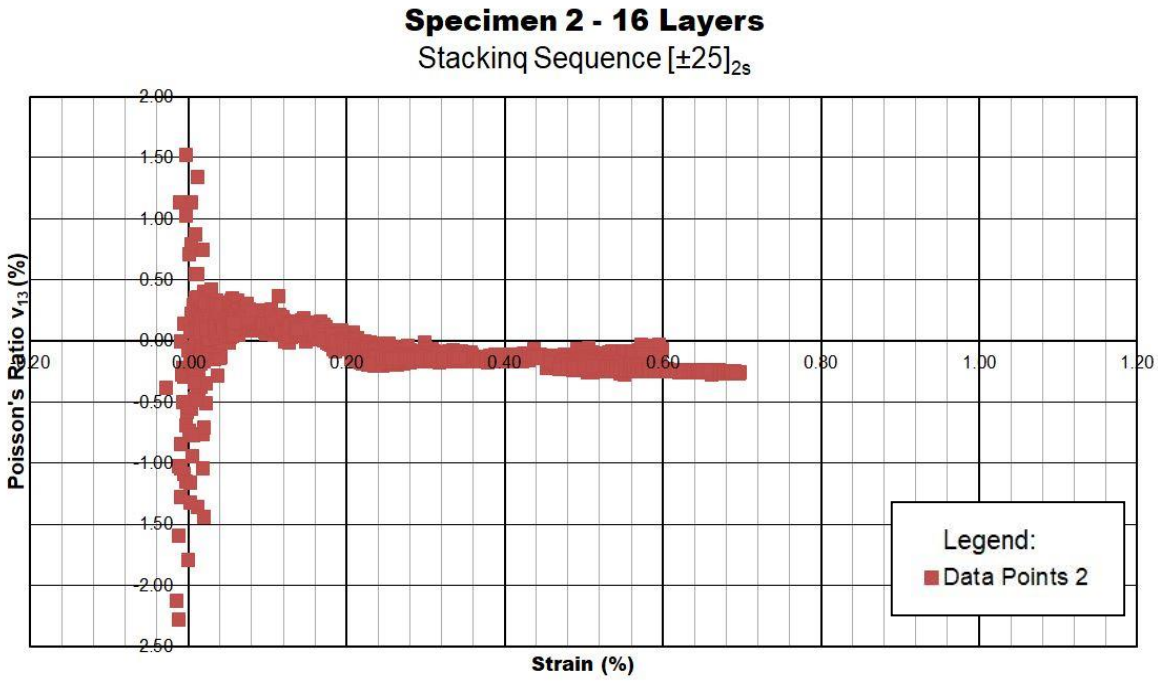

Figure 6.19– Poisson's Ratio v_{13} (%) vs strain (%) – Specimen 2 -Stacking Sequence $[\pm 25]_{2s}$

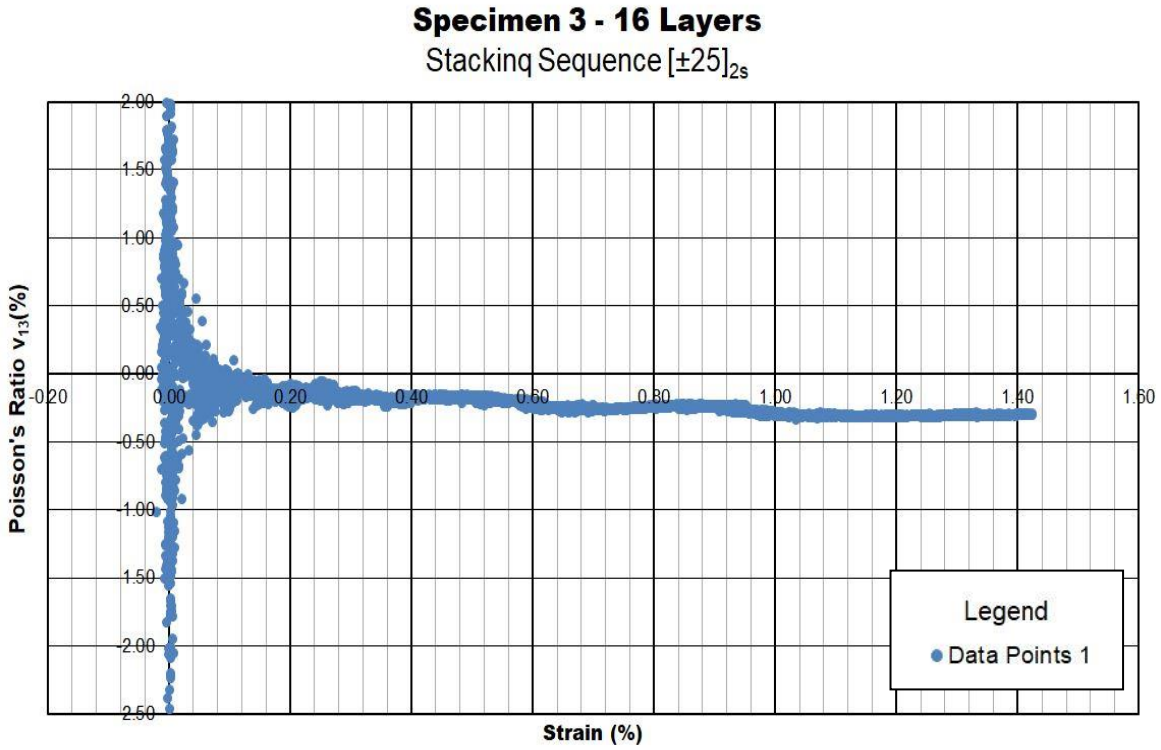

Figure 6.20– Poisson's Ratio v_{13} (%) vs strain (%) – Specimen 3 - Stacking Sequence $[\pm 25]_{2s}$

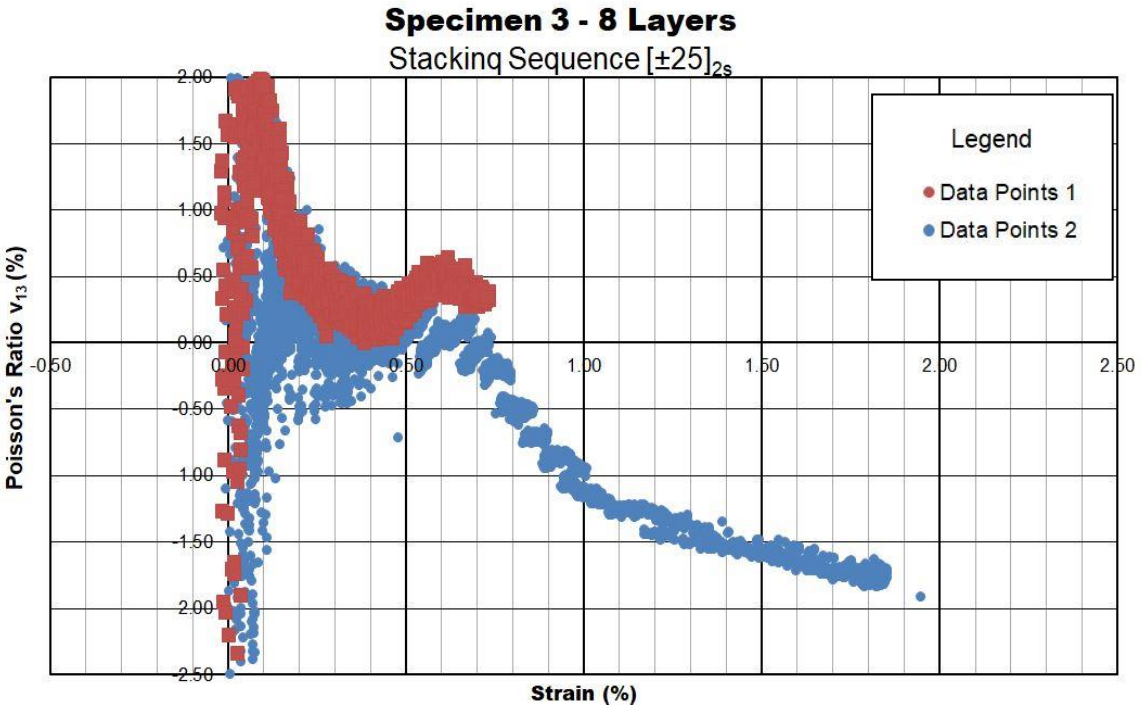

Figure 6.21– Typical example of the Poisson's Ratio ν_{13} (%) vs strain (%) obtained when testing a specimen consisting of 8 layers. The data obtained could not be considered as adequate even though signs of a negative Poisson's ratio are noted.

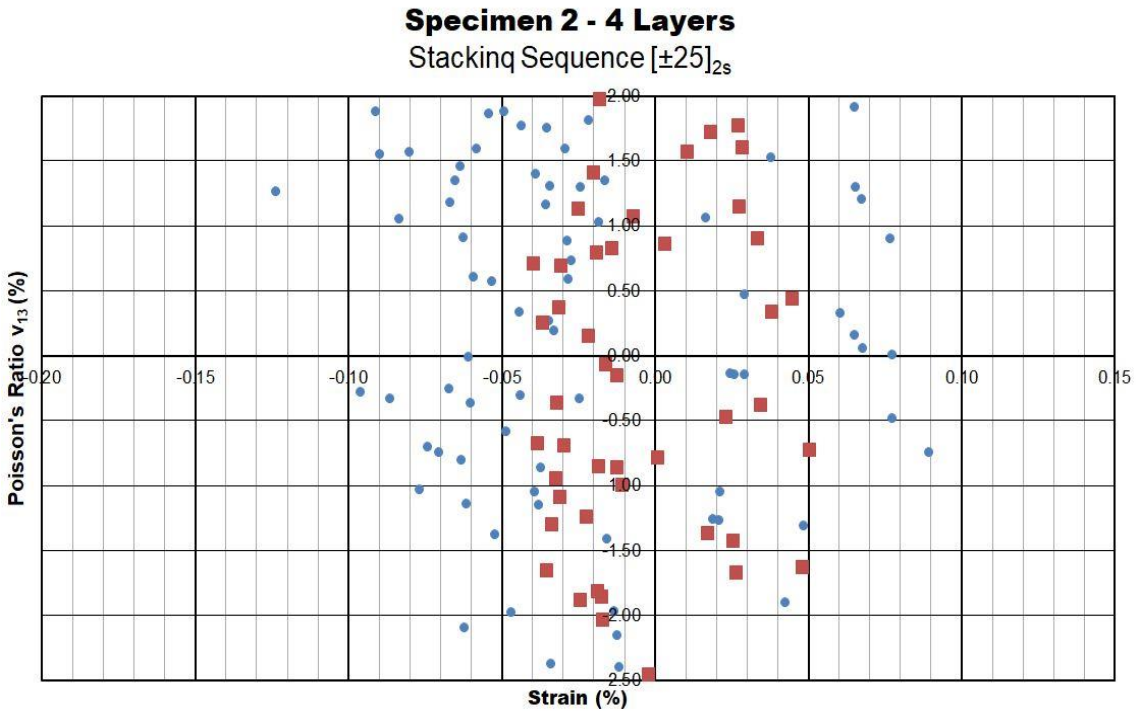

Figure 6.22– Typical example of the Poisson's Ratio ν_{13} (%) vs strain (%) obtained when testing a specimen consisting of 4 layers. Scattered points were obtained. The laminated was too thin to take proper readings using a video gauge.

6.6.2 Improved Fracture Toughness

The results obtained through experiments do give an indication that auxetic jackets give a better performance and are capable of resisting more stresses. The through thickness expansion, even though minimal, is probably extending or prolonging the lifespan of the jacket due to particular characteristics that are affecting the behaviour of the material. One of these characteristics relates to the improved fracture toughness of auxetic laminates. This property describes the ability of a material resisting fracture, where high fracture toughness can lead to a ductile fracture. Tests were carried out on AS4/3501-6 carbon fibre/epoxy prepreg (212)**,** to investigate the behaviour of fracture toughness of auxetic laminates having a $[\pm 30]_{6s}$ configuration when compared to laminates with matched Young's moduli of elasticity having a positive through thickness Poisson's ratio using stacking sequence configurations of $[35/-20/25/40/-85/40/25/-45/35/15/35/40]_s$ and $([-10/40/-40/40]_2)_3$. The ν_{13} value for the auxetic laminate was equivalent to -0.156, whereas values of 0.187 and 0.017 respectively were achieved for the other tested laminates. The in-plane elastic constants were derived by applying double T strain gauge rosettes bonded on both the front and back surfaces. The specimens were then tested in tension and readings of both transverse and longitudinal strains were taken. It resulted that the $[\pm 30]_{6s}$ configuration had the largest strain energy release rate (i.e. the energy dissipated during fracture per unit of newly created fractured surface area) as well as the largest value of fracture toughness. Researchers (212) attribute this behaviour to the fact that, when the laminate is in tension, it is expanding through its thickness and reducing in its width. In so doing, it increases the fracture toughness by spreading the stress concentration at the crack tip over a wider area. Consequently, this reduces the effective stress concentration and the likelihood of a crack onset. On the contrary, in the case of a positive ν_{12} and positive ν_{13}, the contraction occurs in both the thickness and width resulting in an increase in the effective stress concentration at the crack tip.

It can be said that this concept can be applied to the confinement jackets, where-in this situation, when the jacket is in hoop tension, it too expands through its thickness and reduces in its width. Thus, it is likely that there is an increase in fracture toughness that could be helping in spreading the stress concentration at the

crack tip. This, in turn, diminishes the crack propagation and enhances the strength. In other words, the auxetic jacket is capable of absorbing more energy, it diminishes the possibility of cracks or prolongs the initiation of a crack, and as a result, extends the load-carrying capacity of a jacket until a sudden explosive failure occurs. Consequently, the hoop stresses exerted on the jacket would spread further, since it would be capable of withstanding more strain energy, resulting in better confinement. In fact, when comparing the jackets of equal Young's moduli of elasticity, i.e. ST1 with ST3, and ST2 with ST4, it results that they exhibit the same pattern. The values with the maximum negative Poisson's ratio resisted the most stress. It is also evident, that, when comparing ST1 and ST2, other factors come into play and these affect the failure strength of the jacket. In fact, in this case, the Young's moduli of elasticity (E_{xx}) vary, where ST1 is stiffer than ST2 by approximately 25.6 GPa. Both configurations are auxetic and the difference in their negative Poisson's ratio is minimal. So, it is likely that both stacking sequence configurations have a similar rate of expansion when placed in tension. Thus, in this situation, it appears that, even though ST2 has a higher negative Poisson's ratio, the stiffest configuration prevails. Otherwise, if one were to compare ST2 and ST3 stacking sequences, a different scenario is noted. As shown, ST1 and ST3 have the same Young's modulus of elasticity, where ST3 is stiffer than ST2 by approximately 25.6 GPa. Moreover, the value of the negative Poisson's ratio varies by 0.35. Thus, it follows that the ST2 has a higher fracture toughness and a higher strain energy release rate that result in better confinement. Yet, due to a number of variations between these two configurations, other factors might prevail in improving confinement. Nevertheless, it is interesting to point out, that ST1, ST2 and ST3 are auxetic configurations and they all performed better than the other jackets.

One of the main contributory factors that affects the failure of a confined concrete cylinder in compression is undoubtedly the stiffness of the laminate and this is dependent on the Young's modulus of elasticity E_{xx} (i.e. axial rigidity of the jacket). It is probable that the maximum value occurs in the direction of the fibres (i.e. 0°), whereas the weakest value occurs in the direction of the matrix (i.e. 90°). Hence, these two angles define the bounds of behaviour of any fibre or laminate. All other laminae or laminates, that contain different angles other than 0° and 90°, will result in

a Young's modulus of elasticity that fluctuates between the maximum and minimum values provided by the 0° and 90° angles respectively. At first glance, it can be expected that ST5 bearing the highest Young's modulus of elasticity, equivalent to 137 GPa, should withstand the greatest load. In fact, it should be noted that there is a difference in stiffness equivalent to 53 GPa between this configuration, ST1 and ST3, whereas a larger difference of 78.6 GPa lies between ST5, ST2 and ST4. Yet, it resulted that the auxetic jackets tested performed better than the jacket bearing the highest Young's modulus of elasticity. So, it can be deduced that, the ultimate cause of failure of the jacket is due to both the material's quality and strength as well as to the high fracture toughness caused by the through thickness expansion.

Another aspect that is worth mentioning is that the confinement models, being presented and discussed in the previous chapters, give an indication that the largest hoop stresses can be resisted by the strongest CFRP jackets. Most of these models, besides considering the characteristics of concrete, also focus mainly on the properties of the lamina and the stacking sequence configurations used. The models do not take into account the possibility of improved fracture toughness or possible expansion of the laminate when in tension. In this respect, further research is required in order to obtain a closer approximation to the final test results.

6.7 Retardation & Experimental Defects

All the stress-strain graphs presented in this chapter have been drawn using the actual data obtained during testing. The axial and hoop strains were achieved from two strain gauge rosettes attached externally on every cylinder, whereas the load and crushed distance of the cylinder (See Table 6.4) were taken from load transfer using the Losenhousen 6,000kN compression machine. From the stress-strain graphs, it can be noted, that there is some form of instability. During testing, there are a number of factors or defects that could have an effect on the results, particularly during the initial stages of loading. For instance, the lead plate capping that was used on the confinement jacket was smaller than the actual diameter of the cylinder. Even though this was centrally-placed, there might have been some slight movement the moment the machine made contact with the plate. So, it is possible that the first set of readings might be incorrect, since the load might not have been uniformly-distributed, but

instead it could have been applied in certain parts of the cylinder's surface, leading to errors in the results. This issue only happened at the initial stages of loading until a uniform compressive load was then being transferred into the cylinder.

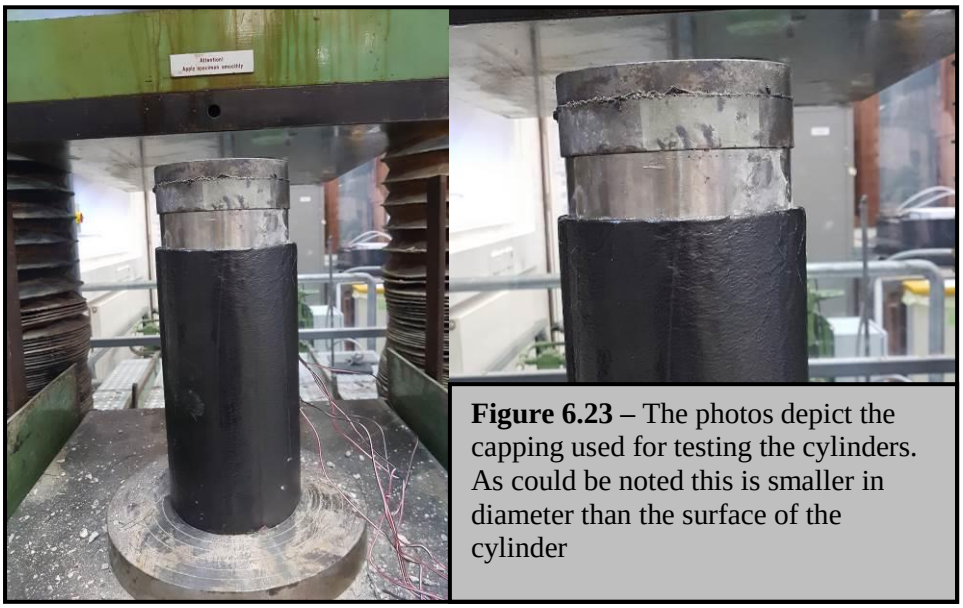

Figure 6.23 – The photos depict the capping used for testing the cylinders. As could be noted this is smaller in diameter than the surface of the cylinder

As discussed in the previous chapter, the compressive tests of concrete Cylinders Set I had to be carried out using a force-control system due to the limitations imposed by the testing machine. As a conservative approach, it is generally recommended to carry out the testing using a displacement-control system. Yet, both approaches are recognised to provide similar results. From research works carried out (191), it can be said that no significant differences between the two loading systems are noted in the initial part until the transition point is reached. In fact, it can be said that the pre-composite loading regime of the stress-strain curves are very similar in shape. On the other hand, a different behaviour occurs in the effective confinement loading regime. When loading, using a force-control system, the stress-strain diagram initially follows a ductile behaviour and then fails in a brittle manner, whereas, with a displacement-control system, it is the opposite. The confinement models used in this study were designed from data used in previous experiments, where most of the testing was carried out using a displacement-control system. The proposed model by Lam et al. (19), Teng et al. (20), contains incorporated data extracted from experiments using both a force-control and a displacement-control system. Yet, the force-control experimental data included only a minor batch of test data and this was reflected in the results obtained from the model. In fact, when comparing these models with the experimental data, the

differences are noticeable in the effective confinement loading regime. The pre-composite loading regime follows, more or less, the same trajectory with the transition point occurring nearly at the same stress. The stress-strain graphs indicate that the jackets tested were stiffer than expected and were capable of withstanding high stresses. Both the design-oriented and analysis-oriented models used throughout this study gave an indication of what is expected with the behaviour of the jackets. In addition, as already mentioned, the through thickness expansion that seemed to be contributing to provide better confinement is not included in these models. As a result, this too can affect the outcome of the stress-strain curve.

When using the equations provided in Teng et. al model (20), it was also possible to compare the actual results with the predicted results obtained for the ultimate axial strain and compressive strength of all the samples tested. In fact, the graphs depicted in Figures 6.24 and 6.25 compare the ultimate compressive strength and ultimate axial strains achieved by the tested specimen and the predicted values obtained using Teng et. al model (20).

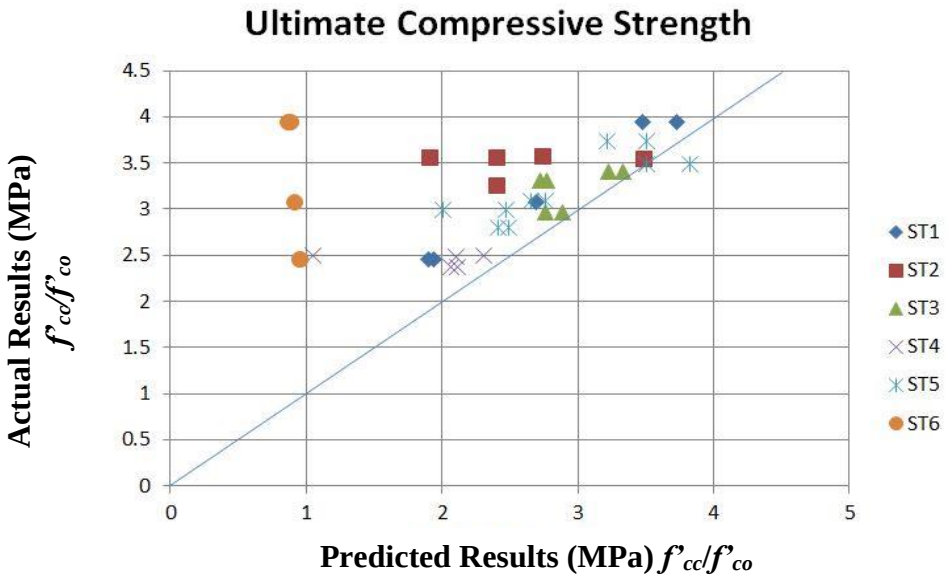

Figure 6.24 – The graph depicts the actual results vs the predicted results for the ultimate compressive strength for all the cylinders tested.

In an ideal situation, the values obtained for the actual and tested ultimate compression strength or ultimate axial strain should have equal values. In fact, the straight line shown in Figures 6.24 and 6.25 is an indicative line portraying this

situation. Any plot points falling within the inner part of the graph show that the laboratory results obtained are higher than the predicted results using Teng et. al model (20). On the other hand, the predicted results are higher when the plot points are situated on the outer part of the straight line. As visible in Figure 6.24, the tested specimen performed better in terms of ultimate compressive strength, whereas scattered plot points were obtained for the ulimate axial strains. In fact, as shown in Figure 6.25, it can be said that higher values were achieved for the tested ultimate axial strains for ST5 and ST6, whereas the predicted values were higher for ST1, ST2, ST3 and ST4.

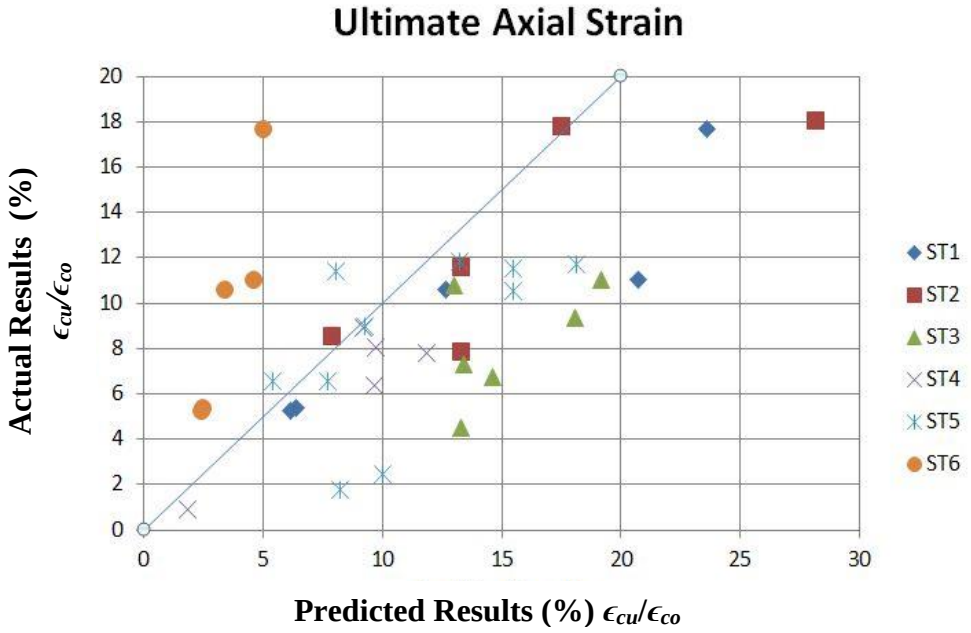

Figure 6.25 – The graph depicts the actual results vs the predicted results for the ultimate axial strain for all the cylinders tested.

6.8 Failure of Confined Jackets

6.8.1 Experimental Failure of Confined Concrete Cylinders

As shown in Figures 6.26 – 6.30, an axial failure is the predominant failure of all confinement jackets except the ones with a ST6 configuration (Figure 6.31). This is particularly noticeable at the ends of the jackets in Figures 6.27 – 6.29, where a clear cut is visible indicating that the fibres could not stretch any further because the jackets are no longer capable of resisting the tensile forces exerted in the hoop direction. Other forms of failure such as debonding and fibre delamination are also seen in various parts of the jackets.

A detailed photographic representation showing the failure modes of each tested cylinder is presented in Appendix C. (Refer to Figures C.1 – C.170). The photographic representation shows the condition of the confinement jackets prior to testing and the failure after testing was completed. It is evident that the manufacturing process of the jackets has a great effect on the failure of the jacket. When manufacturing the first set of cylinders, no extra resin was placed between the surface of the concrete and the first layer, as it was assumed that the pre-impregnated resin present within the CFRP was adequate to provide the bond. Concrete, being dusty in nature, did provide some issues at the beginning of the testing program. Yet, when pre-heating the CFRP manually, adequate bond was achieved. As depicted in the photos, a complete smooth jacket was not always achieved, and areas with creases or air bubbles were visible. At times, the concrete itself was not completely smooth and minor crevices were spotted, creating defects in the jacket. It occurred that the jackets, when tested, failed in these areas. It is likely that, due to the presence of air at these points, the bond between the concrete and the jacket was not adequately achieved. This, in turn, meant that the stresses transferred into the jacket were not being uniformly-distributed. As shown, most of these cylinders failed by tearing up in these creases or in locations where air bubbles were present, leading to premature failure. At times, actual fibre breakages were also noted. However, due to these deficiencies, the test results obtained for these cylinders were discarded.

Another factor worth mentioning is the major difference that lies between the failure strength of the Cylinder Set I and Cylinder Set II when tested. Even though the SA70 resin was added to improve the bond and the difference in the characteristic strengths of the concrete between the two sets was approximately 10 MPa, the difference in the failure was quite substantial. Two different SE70 rolls were used for manufacturing the jackets. The first set of experiments (i.e. those having a premature failure) were produced using a roll that was already used and, hence, mishandling during storage might have been an issue. On the other hand, the second set of experiments was carried out using a new roll, where improvements were noted in the packaging of the prepreg. Even though the SE70 rolls used in both sets of experiments had the same material properties, it seems that the new roll was slightly stiffer. Dr. Tim Coope, who, at the time, made use of the same SE70 roll to carry out

his tests, confirmed that he too noticed some improvements in his results. In an email, Coope (213), stated that no difference was noted for the composite applications, but a 10% improvement in load-carrying capacity was noted when joining metals to composites. This was partly due to void filling for laminates containing cut plies. All experiments tested were manufactured using the same roll, and so a fair comparison was made. Yet, this improvement could have contributed to obtaining stiffer stress-strain graphs.

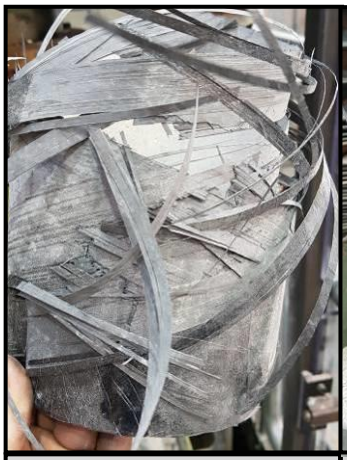

Figure 6.26: Typical failure of jacket for ST1

Figure 6.27: Typical failure of jacket for ST2

Figure 6.28: Typical failure of jacket for ST3

Figure 6.29: Typical failure of jacket for ST4

Figure 6.30: Typical failure of jacket for ST5

Figure 6.31: Typical failure of jacket for ST6

Figures 6.26 – 6.31: depict the failure mode of the confinement jackets for the different stacking sequence configurations tested. In general for ST1 – ST5 confinement jackets, it can be said that a vertical (i.e. axial failure) as well as fibre delamination was noted. On the other hand the failure mode of ST6 confinement jackets consisted in a vertical failure in the direction of the fibre. Failure occurred before the actual failure of the concrete.

6.8.2 Auxetic Failure of Jackets

When examining the failure modes of the jackets tested, (i.e. Cylinders Set I) the auxetic jackets, particularly ST1 and ST2, had an explosive failure and the remains of the cylinder were scattered all over the place. This sudden explosive failure might have been the result of a sudden release of energy**.** Auxetic laminates seem to provide improved properties in strength as they are capable of resisting more energy. Alderson and Coenen (51) carried out tests on auxetic composites, using hydraulic testing equipment. Samples were loaded in compression and equipped with a 12.7mm diameter hemispherical indentator, with the load applied directly at the centre of the specimen at a speed of 2mm / min up to a depth of 5 mm. In these tests, it resulted that, at failure, the auxetic laminate did not present delaminations and the breakage of the fibres was localised in the region near the point of contact with the indentator. Following this, when compared to laminates with a positive Poisson's ratio, the size of the damaged area, displayed by means of 2MHz C-SCAN technology, appeared to be more contained. In the stress-strain curve proposed, it was shown that, at the time of failure, the auxetic laminate had a greater load when compared to that of the other two non-auxetic laminates, highlighting the fact that it is able to absorb a greater amount of energy. So, it can be stated that the through thickness expansion of the jackets ST1, ST2 and ST3 increases the strength of the CFRP, storing large amounts of energy until the fibres are stretched to their limit, resulting in a sudden release of energy generating an explosive failure. The higher the negative Poisson's ratio, the more energy is stored and the larger the explosive failure.

Designing laminates that have improved toughness (212), or provide better resistance to indentation (51) and impact (214) was always considered to be an important aspect with respect to this research study. Nevertheless, it is also worth mentioning that it can be expected that a negative v_{13} might result in an inter-laminar tension that effects the through thickness strength. Research carried out by Alderson et al. (215) show that, contrary to what usually happens, the delamination growth for a negative v_{13} under low velocity impact and indentation testing is reduced when compared with the laminates having the same Young's modulus of elasticity with a positive Poisson's ratio.

Similar to all jackets when tested, ST4 and ST5 had a brittle failure. As depicted in the photos, the jackets fail in a similar way. An axial failure is noted, i.e. the failure occurs perpendicular to the hoop tension. In fact, most of the times, a vertical line is visible in the fibres. Fibre detachments were noticed until sudden rupture occurred. Debonding between the concrete surface and the jackets was not visible and the failure of the jacket did not always occur in the same position. Yet, most of the times the failure of all jackets except ST6, occurred either at the centre or towards the lower third of the specimen. When compressed, the concrete deforms non-uniformly causing more stress concentrations in particular parts of the jacket, which is exhibited in the failure of the jacket. As discussed previously, ST6, failed by tearing of the jacket. The fibres are in the same direction as the applied force, where the jacket fails before the actual failure of the concrete.

6.8.3 Graphic Representation using Stress-Strain Diagrams

The stress-strain curves of the confined concrete cylinders, i.e. ST1-ST5, follow a similar behaviour (Figures 6.32-6.37). The graphs depict a bi-linear regime, where the initial slope is almost the same for all the stacking sequences. This part of the graph is a concrete-dominated deformation. In fact, the transition point of most graphs occurs in the region of 40 MPa. The mean average strength obtained for the non-jacketed concrete cylinders tested was equivalent to 38.5MPa. Thus, as was expected, the transition point of these graphs occurred when the concrete failed. The moment the concrete failed, beyond the transition point, the stresses are taken by the jacket and this is depicted in the second part of the stress-strain diagram, i.e. effective confinement loading regime, until rupture occurs. The stress-strain diagram of the ST6 configuration depicts only the pre-composite loading regime, as the jacket failed before the actual failure of the concrete. In most cases, the strain gauges were detached from the jacket at the early stages, and so, the readings that were recorded were not so precise.

Moreover, most of the results, that were attained from the two strain gauge rosettes that were placed on each cylinder, were quite similar. It is evident that, when compressed, the concrete did not bulge or deform in a uniform manner, and so differences in strain values were expected. On the whole, however, satisfactory

results were obtained. To achieve a better understanding regarding the behaviour of the separate configurations tested, the median of each set of test results was drawn. The mean curve represented the average of all the individual strains for the same stress. With reference to the stress-strain diagrams, there were situations where the strain gauge rosettes malfunctioned and acted bizarrely beyond a particular point of loading. The graphic representation shows clearly this pattern and consequently, these values were not used to draw the mean graph. Samples 17, 22 and 23 are typical examples. Yet, it is evident that the strain gauge rosette positioned in the middle of the cylinder recorded accurate readings up to a particular point. The cause of this could be that, while the cylinder was being compressed, an abrupt bulge or push created by the concrete occurred close to the strain gauge rosette, thus causing it to record erroneous readings. Therefore, the mean of the graphs obtained using the data available from specimens exhibiting the correct values. It is important to compare the behaviour of each configuration reaching the maximum failure load. From the graphical representation, it is evident, that the Young's modulus of elasticity obtained is highest for ST5, followed by ST1, ST3, and eventually ST2 and ST4. Yet, the ultimate failure strength occurred when the jackets, having a negative Poisson's ratio, reached the highest stresses.

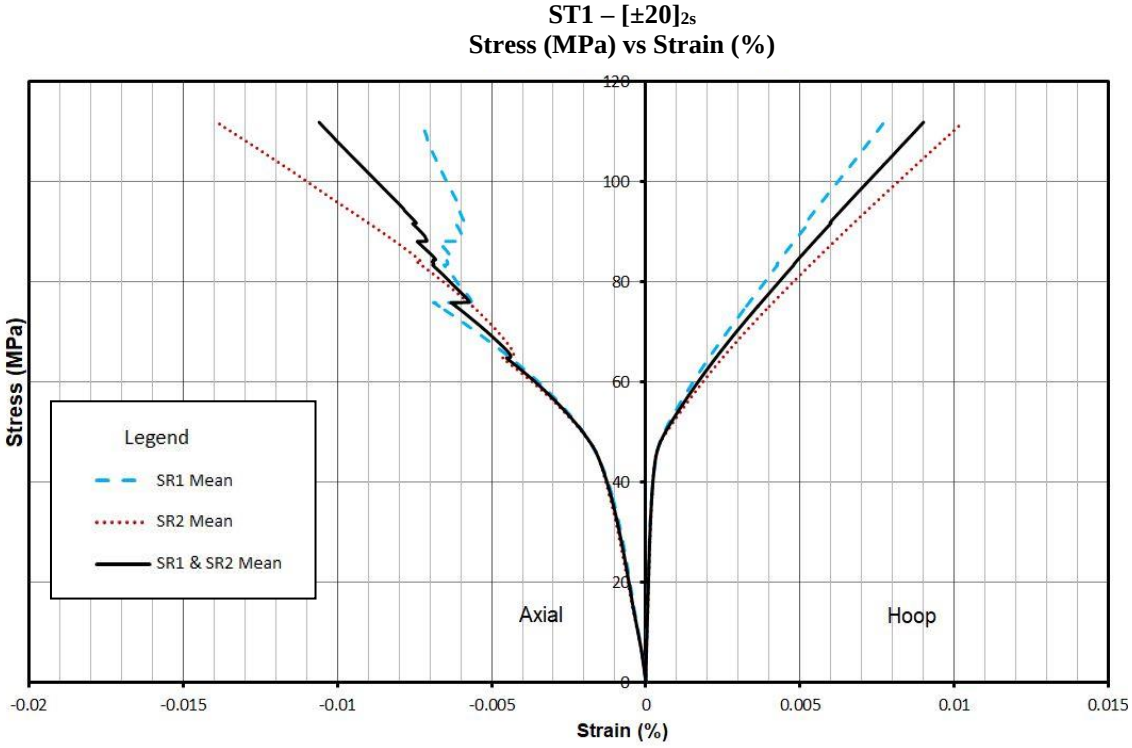

Figure 6.32 – Stress (MPa) vs Strain (%) – representing the Mean of the tested cylinders for Stacking Sequence $[\pm 20]_{2s}$.

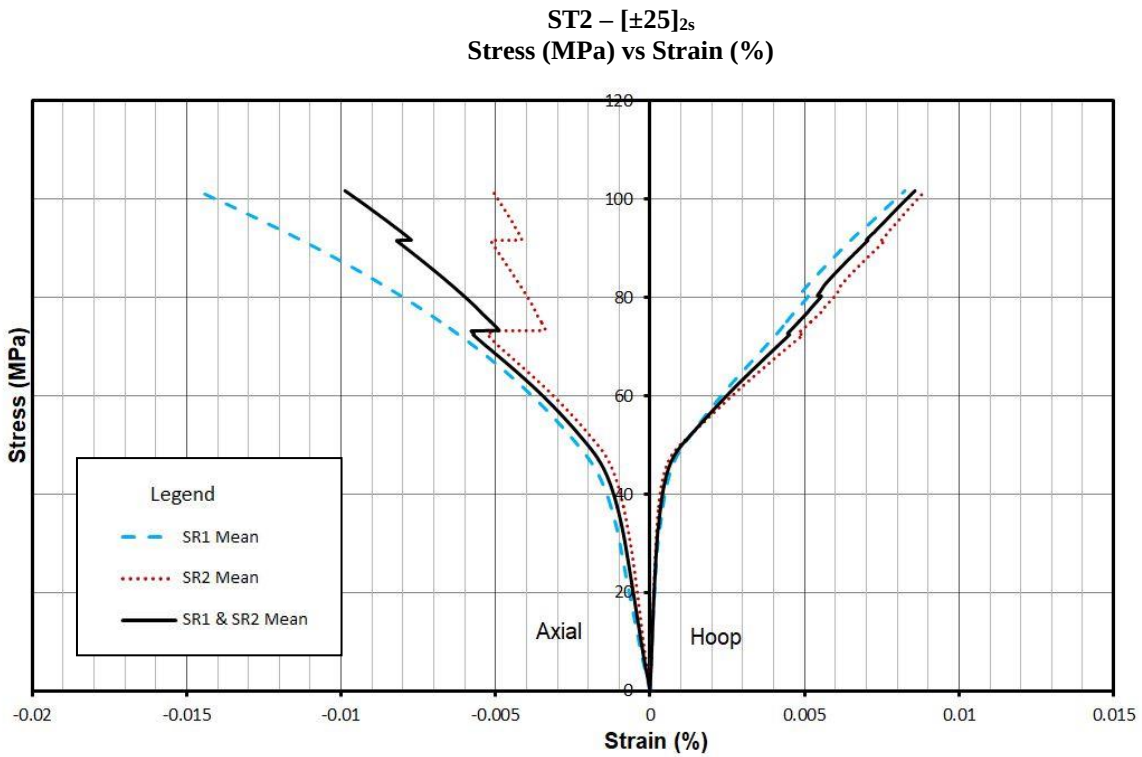

Figure 6.33 – Stress (MPa) vs Strain (%) – representing the Mean of the tested cylinders for Stacking Sequence $[\pm 25]_{2s}$.

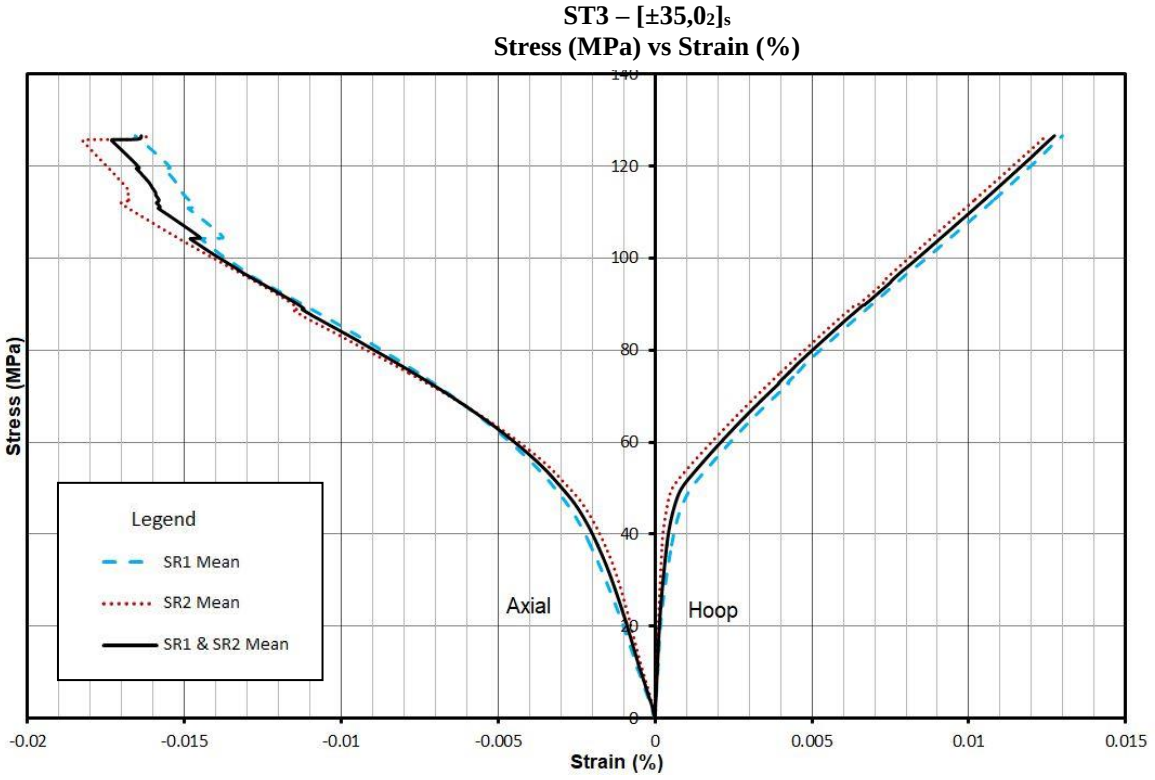

Figure 6.34 – Stress (MPa) vs Strain (%) – representing the Mean of the tested cylinders for Stacking Sequence $[\pm 35,0_2]_s$.

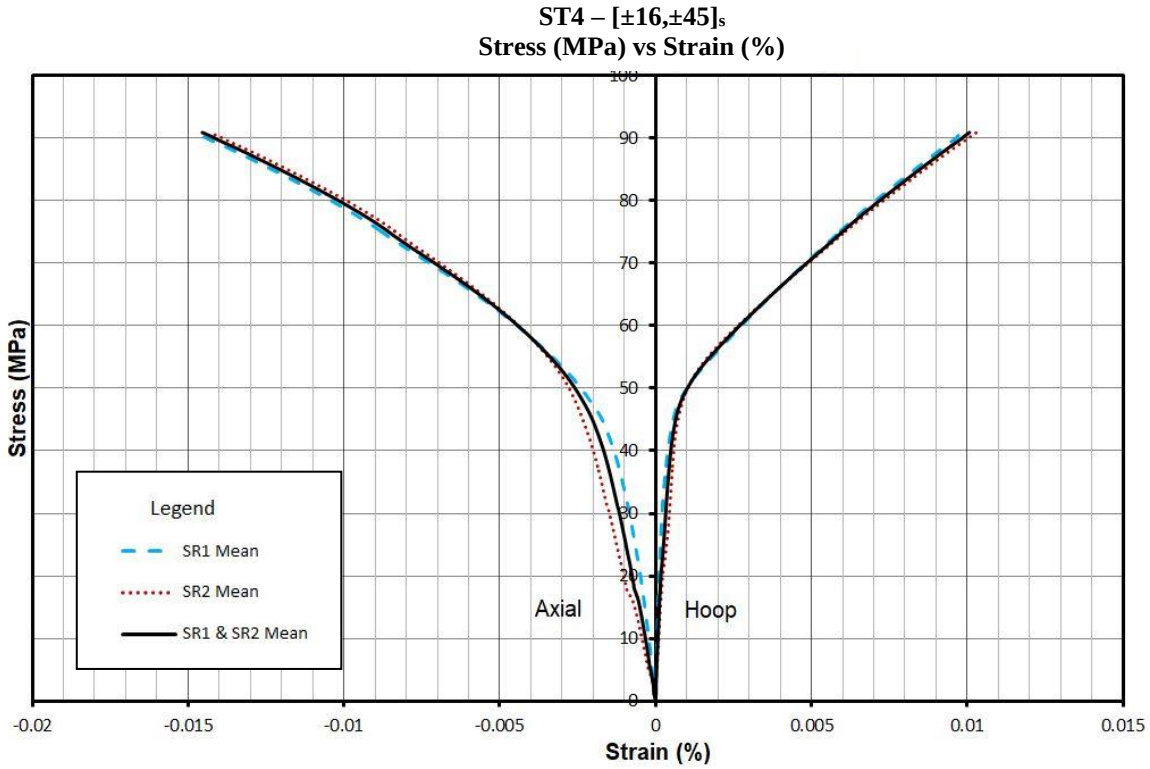

Figure 6.35 – Stress (MPa) vs Strain (%) – representing the Mean of the tested cylinders for Stacking Sequence $[\pm16,\pm45]_s$.

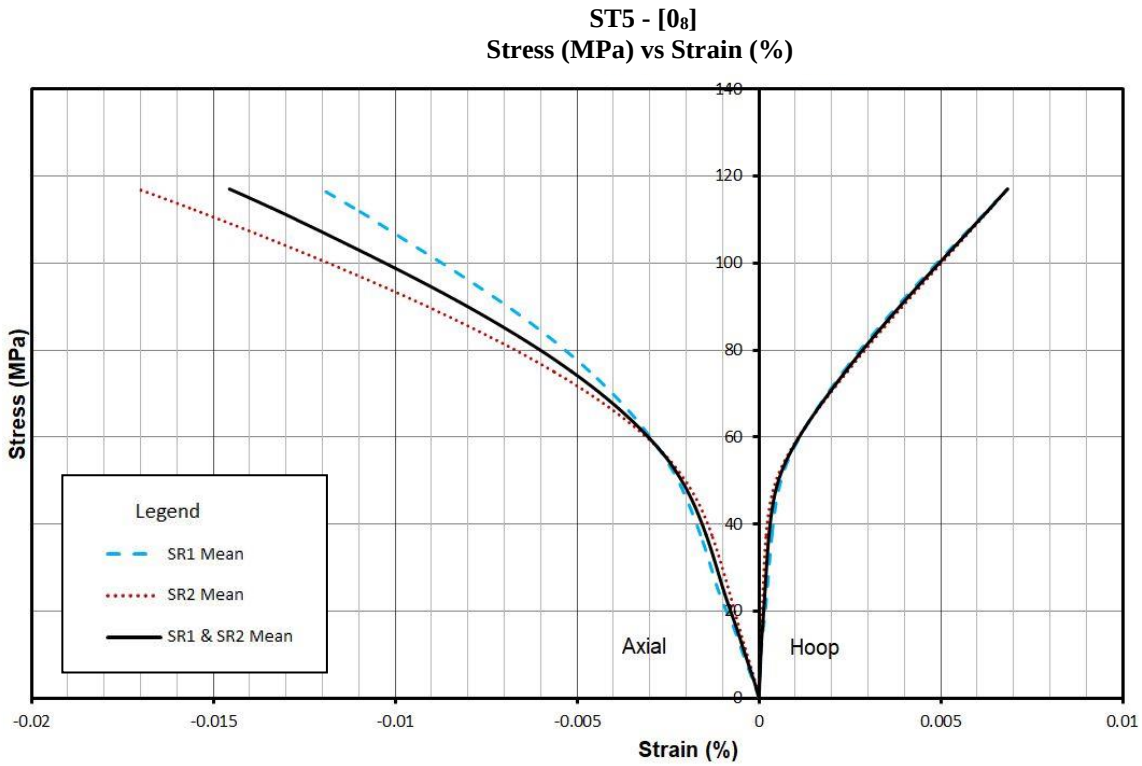

Figure 6.36 – Stress (MPa) vs Strain (%) – representing the Mean of the tested cylinders for Stacking Sequence $[0_8]$

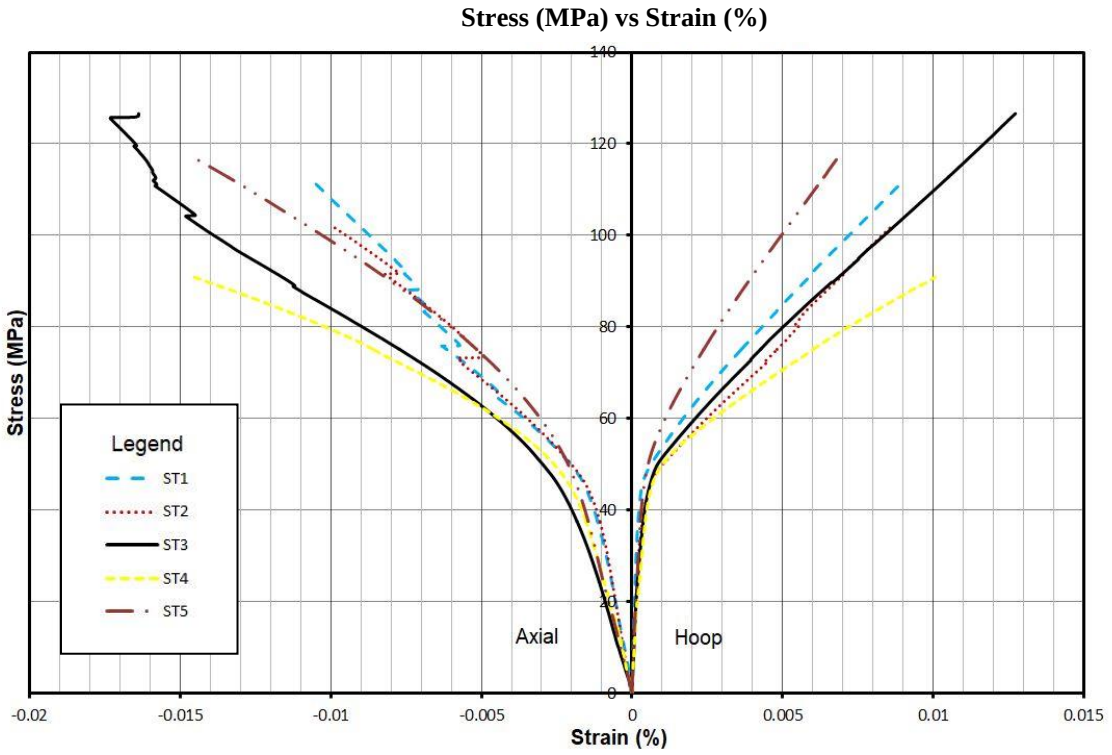

Figure 6.37 – Stress (MPa) vs Strain (%) – representing the Mean of all the tested cylinders.

The standard deviation is used to check and quantify the dispersion of the set of values achieved during experimentation. It measures how concentrated the data are around the mean. The standard deviations obtained had small values. Therefore, the strains recorded by the strain gauges are small and their variations are minimal. In fact, Figure 6.38, depicts the standard deviation for the axial stresses and-strains of all stacking sequences tested. As could be seen, a similar trend was noted for these stacking sequences. The maximum values of standard deviations obtained for the axial stress-strain curve are equivalent to 0.0088, 0.0111, 0.0058, 0.0027 and 0.0045 for ST1, ST2, ST3, ST4 and ST5 respectively. An analysis of the standard deviation on either side of the mean, creating the upper and lower bound, was also drawn for the tested jackets. By analysing the standard deviation graph obtained for ST2 and localising a small part of the graph as shown in Figure 6.40, it can be said that a consistent variation was noted on either side of the mean graph (i.e. upper and lower bound). . Similar patterns were obtained for all other stacking sequence configurations.

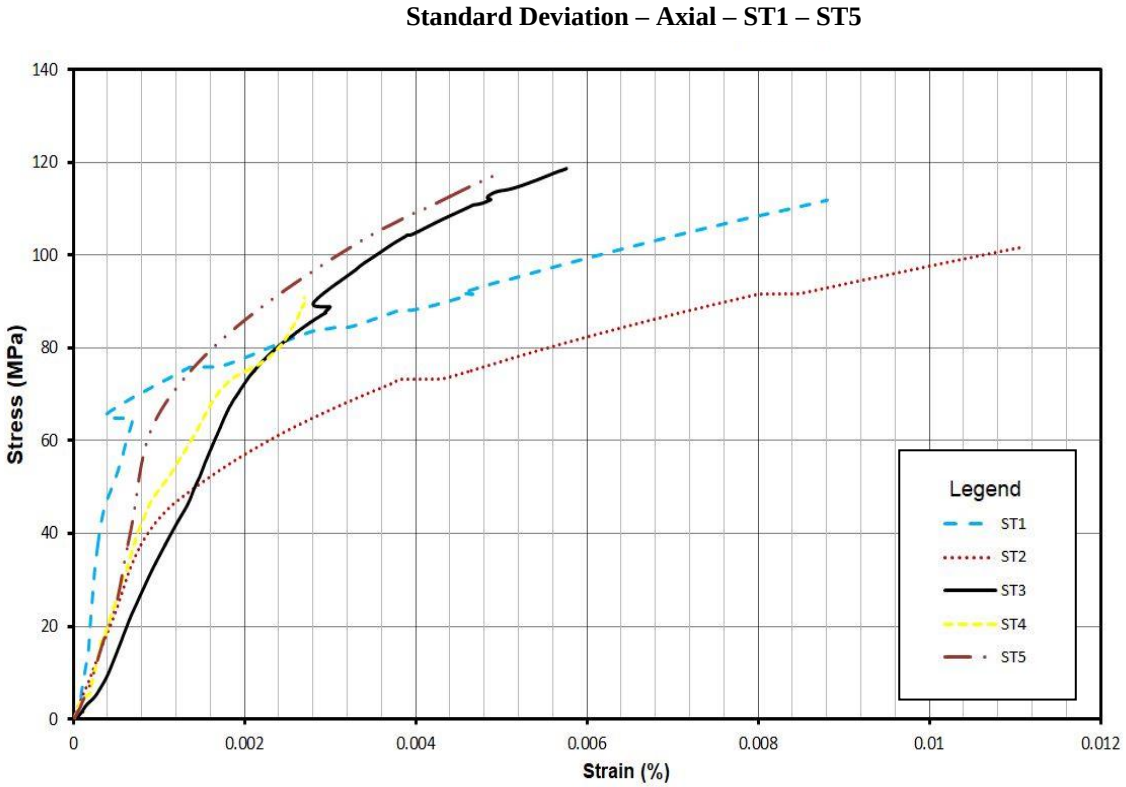

Figure 6.38– Stress (MPa) vs Strain (%) – representing the Standard Deviation (Axial) of all the tested cylinders.

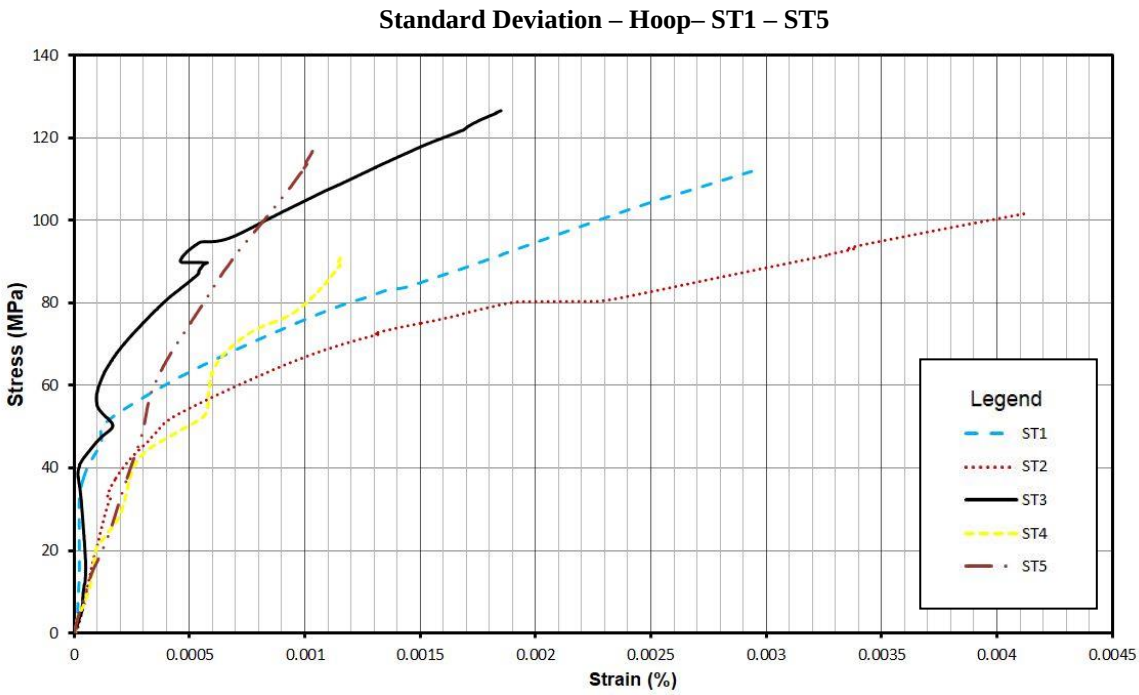

Figure 6.39– Stress (MPa) vs Strain (%) – representing the Standard Deviation (Hoop) of all the tested cylinders.

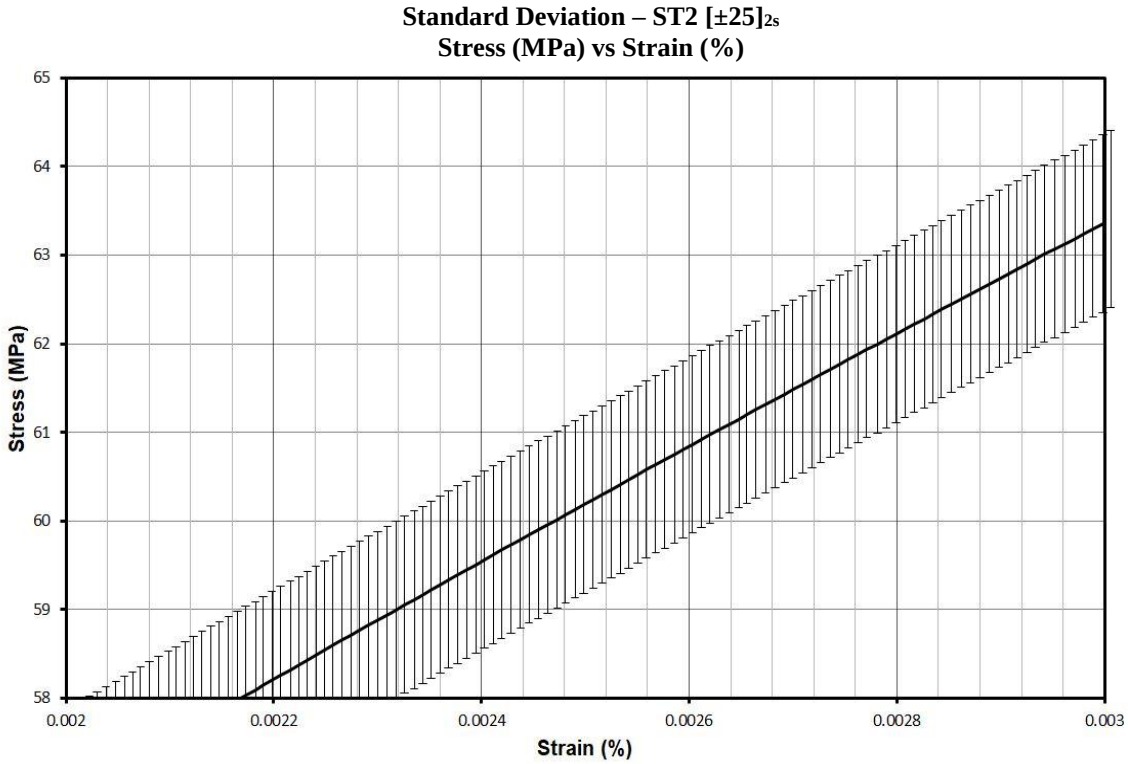

Figure 6.40 – Localisation of a small part of the Standard Deviation from the Mean for ST2. A consistent variation was noted on either side of the mean curve.

6.9 Structural Efficiency of FRP Jackets

From the results presented in Table 6.6, it can be observed that all stacking sequences, except ST6, have resisted a substantial amount of load when compared to the heated and unconfined concrete cylinder. ST6 is the configuration having least stiffness and, in turn, resisted the least load. On the contrary, the experiments have shown, that on average, these cylinders had a lower compressive strength than the control concrete cylinder. As previously discussed, this can be attributed to the capping system used and to the slight variations in the mix.

In terms of compressive strength, the concrete samples, each wrapped with eight layers of SE70 CFRP, show gains of 387%, 351% and 338% for ST1, ST2 and ST3 respectively when compared with the control concrete cylinder. These auxetic laminates resulted to be the most efficient when compared to the other stacking

Stacking Sequence	Cylinder Name	Failure Load (kN)	Mean Failure Load (kN)	f'_c (MPa)	f'_{cc} (MPa)	f'_{cc}/f'_{co}	v_{13}	E_{xx} (GPa)
ST1 $[\pm 20]_{2s}$	Sample 17	2582.95	2619.11	38.24	148.15	3.87	-0.403	84.00
	Sample 19	2578.74						
	Sample 20	2695.63						
ST2 $[\pm 25]_{2s}$	Sample 21	2409.17	2371.65		134.15	3.51	-0.468	58.40
	Sample 22	2420.60						
	Sample 23	2424.70						
	Sample 24	2232.14						
ST5 $[0_8]$	Sample 25	2031.59	2186.90		123.70	3.23	0.560	137.00
	Sample 26	1904.38						
	Sample 27	2102.26						
	Sample 28	2363.48						
	Sample 29	2532.80						
ST6 $[90_8]$	Sample 30	633.75	602.56		34.08	0.89	0.324	7.81
	Sample 31	680.01						
	Sample 32	650.37						
	Sample 33	621.85						
	Sample 34	426.81						
ST3 $[\pm 35,0_2]_s$	Sample 35	2311.77	2282.77		129.13	3.38	-0.108	84.00
	Sample 36	2242.90						
	Sample 37	2293.65						
ST4 $[\pm 16,\pm 45]_s$	Sample 38	1680.60	1660.87		93.95	2.46	0.007	58.40
	Sample 39	1692.61						
	Sample 40	1609.42						

Table 6.6 – Comparison of the improved strength of each jacket, except ST6, is provided. The increased efficiency is a result of both the through thickness expansion and the stiffness of the jacket.

sequences tested. In fact, ST4 and ST5 have shown lower gains in confinement strength equivalent to 246 % and 323% respectively. It is evident that the stiffness of the material does have a major impact on the strength outcome. The maximum Young's modulus of elasticity for the assumed layers is provided by ST5. Thus, a reduction in the Young's modulus of elasticity of 38.6% for ST1 (i.e. 137.0 GPa to 84.0 GPa) and of 57.4% for ST2 (i.e. 137.0 GPa to 58.4 GPa) showed an increase in strength of 19% and 8% for ST1 and ST2 respectively. When considering the through thickness expansion, it can be stated that, by utilising symmetric balanced angle-ply

laminates, such as angles of 20° and 25°, or other configurations that exhibit a negative Poisson's ratio, an increase in confinement strength is obtained. In other words, it can be concluded that, when using the same material and the same amount of layers, a better performance is achieved for auxetic jackets. Hence, by proposing an adequate system for confining in-situ concrete columns using these angles, it is possible to improve the confinement strength without any increase in cost by using the standard methodologies available. The bar chart in Figure 6.41 shows the increase in compression resistance of each individual sample tested.

UnJacketed Heated Cylinders				Jacketed Cylinders			
Cylinder Name	Failure Stress (MPa)	Cylinder Name	Failure Stress (MPa)	Cylinder Name ST1	Stress at Transition Point (MPa)	Cylinder Name ST2	Stress at Transition Point (MPa)
Sample 9	42	Sample 13	37	Sample 17	43	Sample 21	43
Sample 10	40	Sample 14	40	Sample 18	43	Sample 22	40
Sample 11	33	Sample 15	42	Sample 19	Not clear	Sample 23	42
Sample 12	33	Sample 16	35	Sample 20	45	Sample 24	43
Jacketed Cylinders							
Cylinder Name ST3	Stress at Transition Point (MPa)	Cylinder Name ST4	Stress at Transition Point (MPa)	Cylinder Name ST5	Stress at Transition Point (MPa)	Cylinder Name ST5	Stress at Transition Point (MPa)
Sample 35	43	Sample 38	40	Sample 25	42	Sample 28	42
Sample 36	Not clear	Sample 39	43	Sample 26	Not clear	Sample 29	42
Sample 37	43	Sample 40	Not clear	Sample 27	42		

Table 6.7 – Comparison of failure stresses obtained from the unjacketed heated cylinder specimens with the stresses corresponding with the transition points obtained from the stress-strain curves of all jacketed cylinders tested.

Table 6.7, compares the failure stresses obtained from the unjacketed heated cylinder specimens with the stresses corresponding with the transition points obtained from the stress-strain curves of all jacketed cylinders tested. (Refer to Appendix B).

Most graphs give an indication that the transition point (i.e. the stress or load where the first loading regime changes to the second loading regime) is in the region of 42 or 43 MPa, which corresponds approximately to the failure stress of the unjacketed heated cylinder. Thus, it can be assumed that the initial slope obtained in the pre-confinement loading regime follows the same behaviour as the unjacketed heated cylinder specimens.

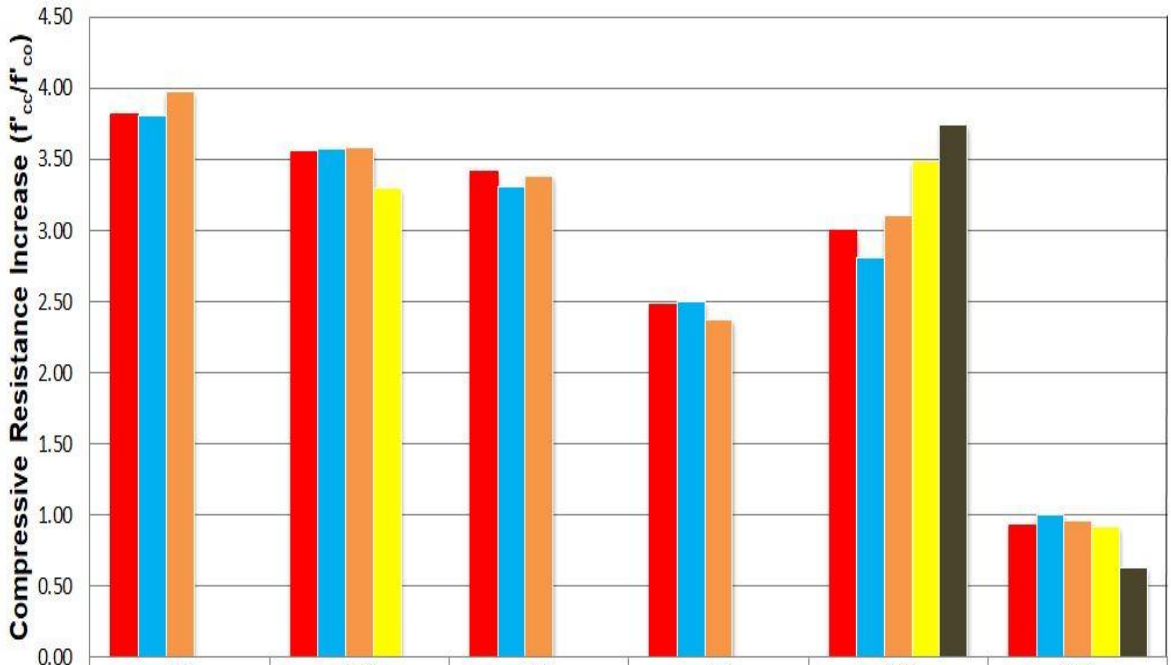

	ST1	ST2	ST3	ST4	ST5	ST6
Test 1	3.82	3.56	3.42	2.49	3.00	0.94
Test 2	3.81	3.58	3.32	2.50	2.82	1.01
Test 3	3.99	3.59	3.39	2.38	3.11	0.96
Test 4		3.30			3.50	0.92
Test 5					3.75	0.63

Figure 6.41 – The bar chart illustrates the increase in compressive resistance obtained for the jacket configurations tested.

A bar chart illustrating the ultimate axial and hoop strains for the various stacking sequences tested is shown in Figure 6.42. Only the readings of the strain gauge rosettes, that gave accurate readings until the end of the compression tests, were selected for calculating the mean ultimate and hoop strains. It can be observed that the maximum axial strain was achieved for ST1, whereas the maximum hoop strain was obtained for ST4. Comparing the values achieved with the stacking sequence 5, i.e. the configuration that has maximum Young's modulus of elasticity of

137 GPa, it can be noted that increases in axial strain of 63.10%, 60.50%, and 5.72% were achieved for the auxetic configurations ST1, ST2 and ST3 respectively, whereas a reduction in axial strain of 21.45% was noted for ST4.

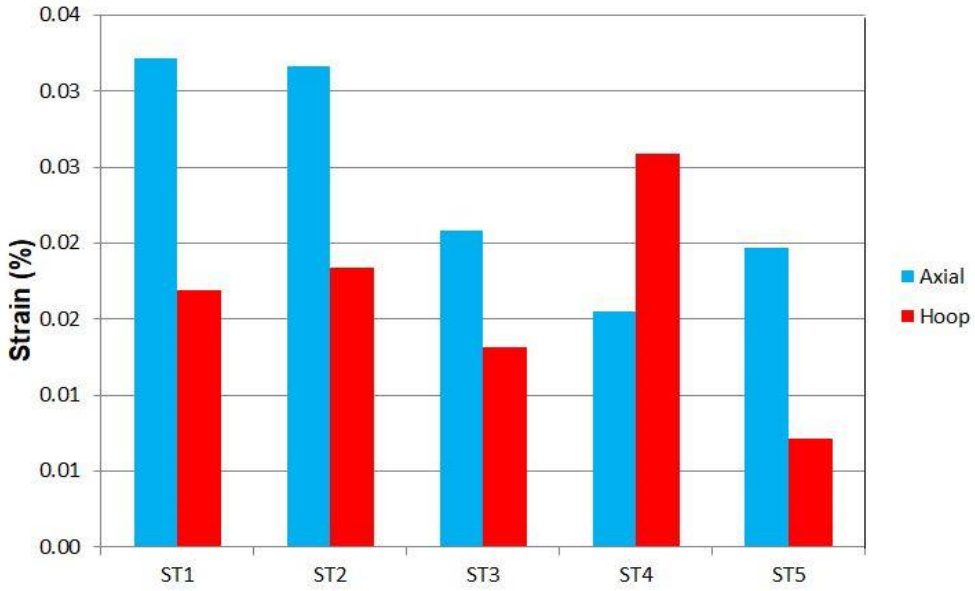

Figure 6.42 – The bar chart illustrates the maximum mean axial and hoop strains achieved for the jacket configurations tested.

6.10 Parametric Analysis & Confinement Models

A parametric analysis was carried on the confinement model to understand further the validity of the results obtained when comparing the experimental data with the analysis-oriented model proposed in this study. By carrying out a sensitivity analysis using the test results, it would be possible to determine the robustness of the model results and to increase the understanding of the relationship between the input and the output variables. The materials used in this research study can have statistical variabilities that can affect the behaviour of the stress-strain diagrams. Generally, the uncertainties associated with the concrete strength are rather high and difficult to control, whilst the ones related to the manufacturing of the jacket using a prepreg system can be controlled within certain limits. Thus, it is interesting to conduct a parametric analysis by varying the Young's modulus of elasticity of the concrete and study the effect of this parameter on the behaviour of the jacketed samples.

The Young's modulus of elasticity of concrete proposed in the model is a function of the characteristic strength, where it varies linearly with the compressive

strength. In fact, the model uses the following equation: $E_0 = 2f'_c/0.002$ (where, f'_c is the characteristic strength of the concrete). It is to be noted that the value of the concrete strain was assumed to be 0.002, which would correspond to a 0.2% proof stress. Thus, the model shows that, on the concrete stress-strain curve in compression, the maximum stress in the concrete is reached at a strain of 0.02. This, in turn, is an assumption that affects the transition point of the stress-strain graph.

The stress-strain diagrams in Figures 6.43 – 6.44 show the differences obtained when varying the Young's modulus of elasticity. It is noted that the graphs follow the same trend in behaviour, where the transition point of the graph is dependent on the characteristic strength of the concrete and occurs when the strain is in the region of 0.002. Yet, beyond the transition point, i.e. in the effective confinement loading regime, it is noted that a small change from the unconfined compressive strength of concrete from 45 MPa to 38.5 MPa has a much stronger effect on the behaviour towards failure. In fact, when considering the strain values at a stress of 75 MPa, it can be deduced from the graph, that a reduction in the unconfined compressive strength of approximately 16.88% (i.e. a difference in Young's modulus of

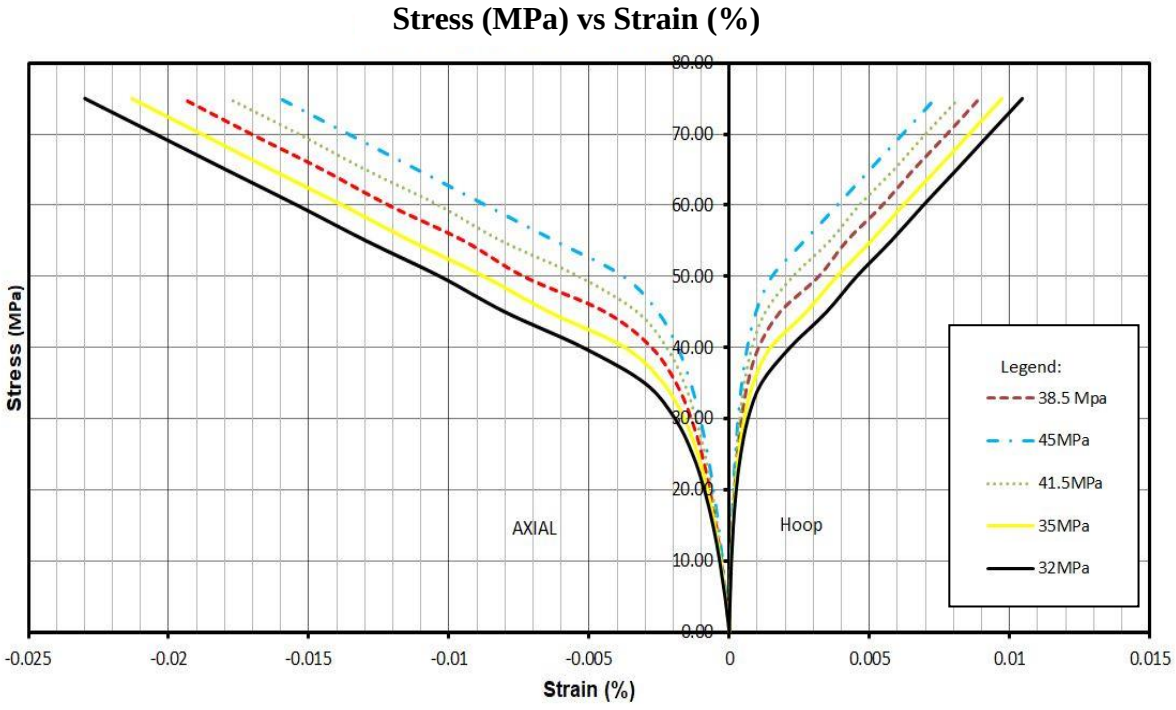

Figure 6.43 – Stress (MPa) vs Strain (%) – for different compressive strength values using the confinement model proposed by Becque (17,18).

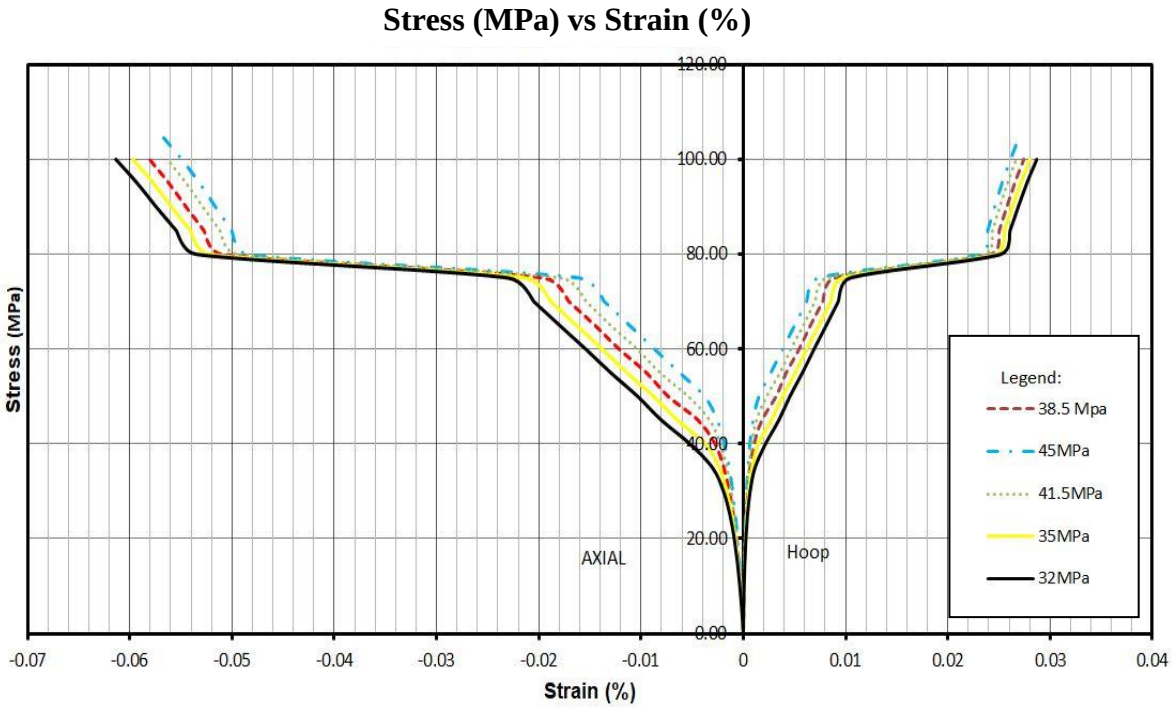

Figure 6.44 – Stress (MPa) vs Strain (%) – for different compressive strength values using the confinement model proposed by Becque (17,18).

elasticity from 45.0 GPa to 38.5 GPa leads to an increase in strain of approximately 19.50% (i.e. a difference in strain from 0.01550 to 0.01925). A similar approach is obtained when comparing the reduction in compressive strength from 38.5MPa to 32.0 MPa (i.e. approximately a 20% reduction in the Young's modulus of elasticity of concrete), followed by an increase in strain of 16.30% (i.e. a difference in strain from 0.01925 to 0.02300). Likewise, a small change from 45.0MPa to 41.5 MPa (i.e. a reduction of 8.45%) and a change from 35.0 MPa to 32.0MPa (i.e.a reduction of 9.37%) lead to an increase in strain of 13.90% and 7.85% respectively. In the effective confinement loading regime, the concrete appears to have failed and the ultimate failure load depends upon the properties of the jacket. In this parametric analysis, the properties of the jacket were kept constant, i.e. the analysis was carried out using the properties for a $[\pm 20]_{2s}$ configuration using SE70 prepreg CFRP. When considering the axial strains beyond the transition point, it can be deduced that the stresses and strains increased in a proportional manner until they reached the strain value of 0.002. It can be noted that all graphs follow the same trend and converge to a strain value of 0.002.

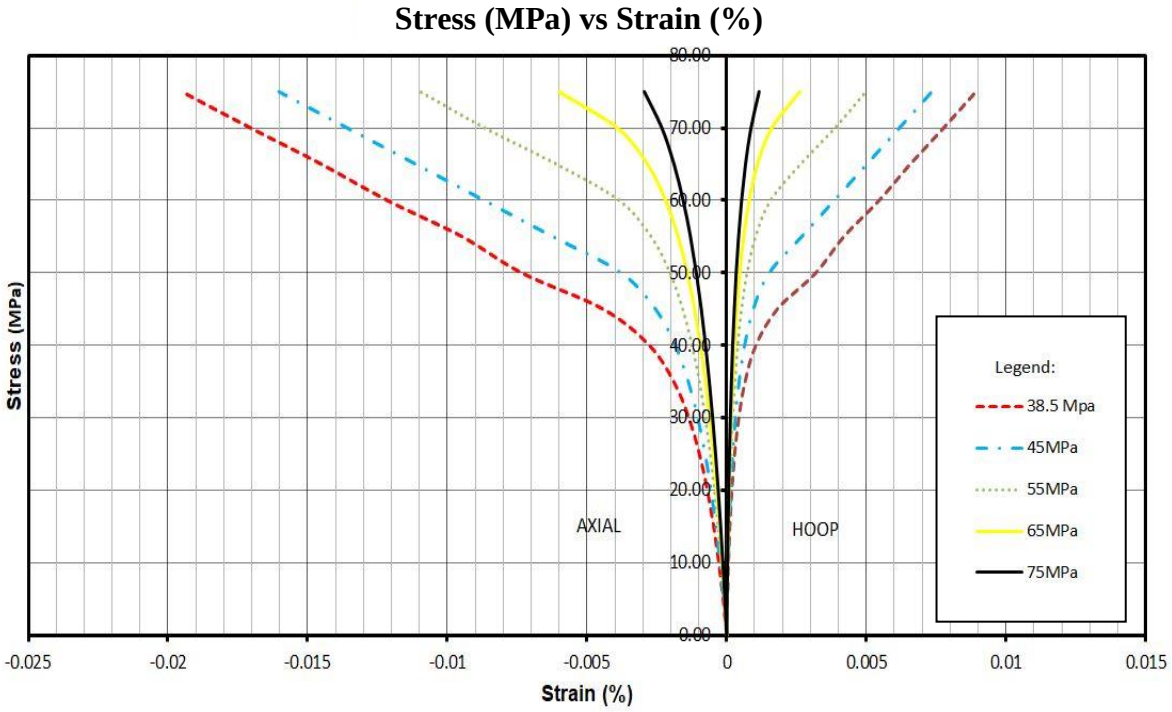

Figure 6.45 – Stress (MPa) vs Strain (%) – for different compressive strength values using the confinement model proposed by Becque (17, 18).

Figure 6.45 shows a stress-strain diagram depicting the behaviour of the confined concrete having higher values for Young's modulus of elasticity of concrete varying from 38.5 GPa to 75.0 GPa. Once again, this followed the same trend, where the sensitivity of the model seems to be shifted along the strain axis. From these graphs, it can be noted that the ultimate strengths of the individual materials, i.e. concrete and CFRP jacket, have an effect on the behaviour of the confined jacket. As indicated, in the elastic part, all graphs gave a linear increase until they reached a strain value of 0.002. In the effective confinement loading regime, the graphs are mainly dependent on the properties of the CFRP jacket, until they reach the ultimate rupture strength. In this case, it occurred when the stress reached approximately 75.0MPa.

In this parametric analysis, the variable that changed was the Young's modulus of elasticity of the concrete, whereas the properties of the jacket were kept constant. The jacket itself has a particular resistance to the applied load. Thus, irrespective of the strength of the concrete, the jacket will fail at its ultimate load-

carrying capacity. In fact, this behaviour is depicted in the graphs, where, for lower values of concrete Young's modulus of elasticity, a longer stress-strain curve is visible in the effective confinement loading regime. As a structural material, concrete has a number of uncontrolled variables during the mixing and casting process that can affect the characteristic strength of the concrete. Yet, from the test results carried out on the heated and unheated cylinders, it resulted that the variation from the mean value of the failure load of the unheated cylinders is equivalent to 8.60% for values less than the mean and 5.97% for values higher than the mean. Likewise, the variation from the mean value of the heated cylinders is equivalent to 12.51% for the values less than the mean and 12.06% for values higher than the mean. Thus, from these test samples, taken from each set of cast cylinders, it can be noted that average variability in the results achieved when testing the confined concrete cylinders is of the order of 12.50% (i.e. for higher and lower values than the mean), that is due to the variabilities in the concrete mix. Hence, due to this variation in the concrete characteristics, the mean failure load for ST1 is equivalent to 2,619.11kN ±12.50%. The same applies for the failure loads of other stacking sequences.

A similar reasoning could also be adapted for the jackets. However, in the absence of test data for the individual stacking sequences, it is not possible to quantify these variations. Yet, it can be argued that, when using a prepreg CFRP, the variations in the results can be controlled. Ultimately, the predominant variable occurs during the manufacture of a prepreg jacket. This is due to human error, which occurs when rolling the individual layers to form the required stacking sequence configuration. Other minor deficiencies, that might arise whilst manufacturing the jacket, are related to the bagging system used to cure the resin. Vacuum bagging is a technique that was used in the production of the samples in this research study in order to create mechanical pressure on the jacket during its curing cycle. The mechanical pressure eliminated excess air and resin within the lamination, and thus helped to maximise the physical properties of the finished composite part. An air-tight environment was achieved for each bag and no leakages were noted. In addition, the hose assemblies, that were used to connect the cylinders when placed in the oven, were checked and no air leakages seemed to have been present. Nonetheless, some variabilities could still occur in the final results, albeit these variabilities are much less than those present in the concrete.

In the experiments carried out, an additional variability was added to the concrete tests. As previously discussed, the confined concrete cylinders were heated for 20 hours at 70°C, which was the temperature required to cure the resin of the SE70 CFRP prepreg. The mean value of the failure load of the heated cylinders showed a reduction in strength by 10% when compared to the corresponding value for the unheated cylinders. In fact, to evaluate better the variations that may arise due to the heating of the concrete cylinders, a comparison of results was held between each batch. The bar chart (Figure 6.46) shows the failure loads of the heated and unheated cylinders per group. As can be noted, the pattern of the individual cylinders varies extensively. When comparing the failure loads of the unheated cylinders to the heated samples, it is noted that Batch 1 shows an increase in strength of about 1%. In other words, no significant difference in strength occurred, even though the cylinders were heated. On the contrary, Batch 2, Batch 3 and Batch 4 were associated with a reduction in strength of 20%, 13% and 8% respectively. Nevertheless, when referring to Batch 2, the reduction in strength is not solely due to the temperature but is also a result of other factors that affect the mix of the concrete contributing to a change in strength, such as the water cement ratio.

The bar chart (Figure 6.47) incorporates the maximum compressed distance of the cylinders while tested. The cylinders used for testing all had an initial overall height of 300mm. The maximum reduction in height of 5.97% was obtained for stacking sequence ST1, followed by ST2 and ST3, the latter two having a reduction in height of 5.20%, whereas ST5, ST4 and ST6 had a reduction of 3.85%, 2.23% and 1.94% respectively. It is also interesting to note that the unheated cylinders and heated cylinders had a minimal reduction in height of 1.25% and 0.96% respectively. It is evident that greater compressed distances are achieved for higher ultimate loads.

A comparison between the analysis-oriented model and the experimental data is shown in Figure 6.48. Needless to say, ST6, was not represented in the graph as, most of the times, the strain gauges used in ST6 were detached from the jacket at the initial stages of testing, and so all the data recorded from these strain gauges was dubious. However, as previously explained, the jackets failed prior to the actual failure of the concrete, and so their stress-strain diagram should be equivalent to

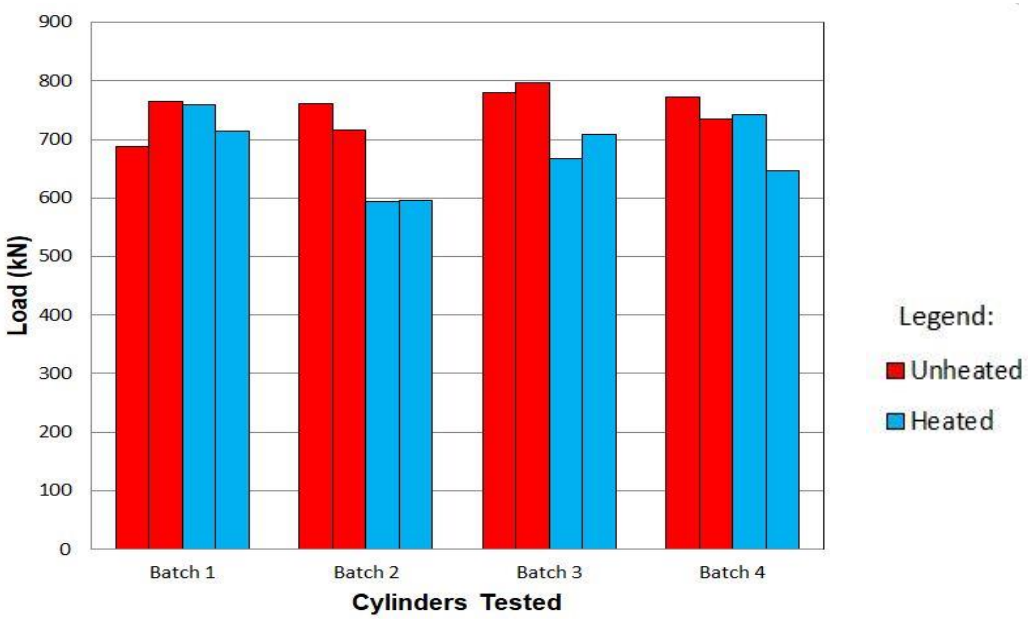

Figure 6.46 – The bar chart shows the failure loads of the heated and unheated tested cylinders.

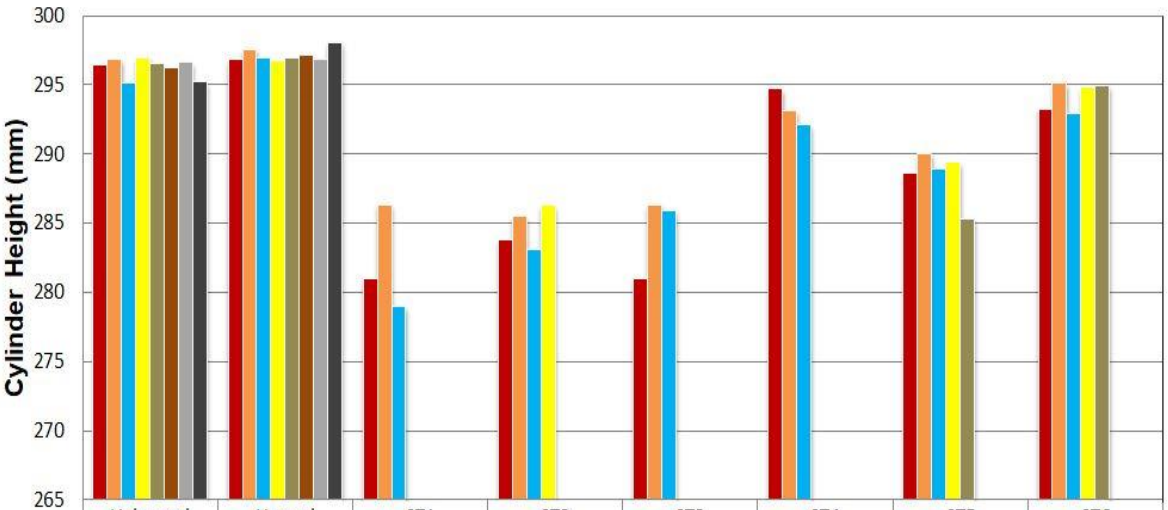

	Unheated	Heated	ST1	ST2	ST3	ST4	ST5	ST6
Test 1	296.48	296.79	280.95	283.78	280.95	294.69	288.62	293.25
Test 2	296.84	297.58	286.35	285.5	286.35	293.15	290.05	295.09
Test 3	295.12	296.97	278.97	283.14	285.9	292.08	288.88	292.88
Test 4	296.97	296.7		286.28			289.37	294.8
Test 5	296.52	296.91					285.34	294.92
Test 6	296.25	297.14						
Test 7	296.59	296.86						
Test 8	295.19	298.05						

Figure 6.47 – The bar chart shows the final cylinder height of all tested cylinders after completion of the compressive tests.

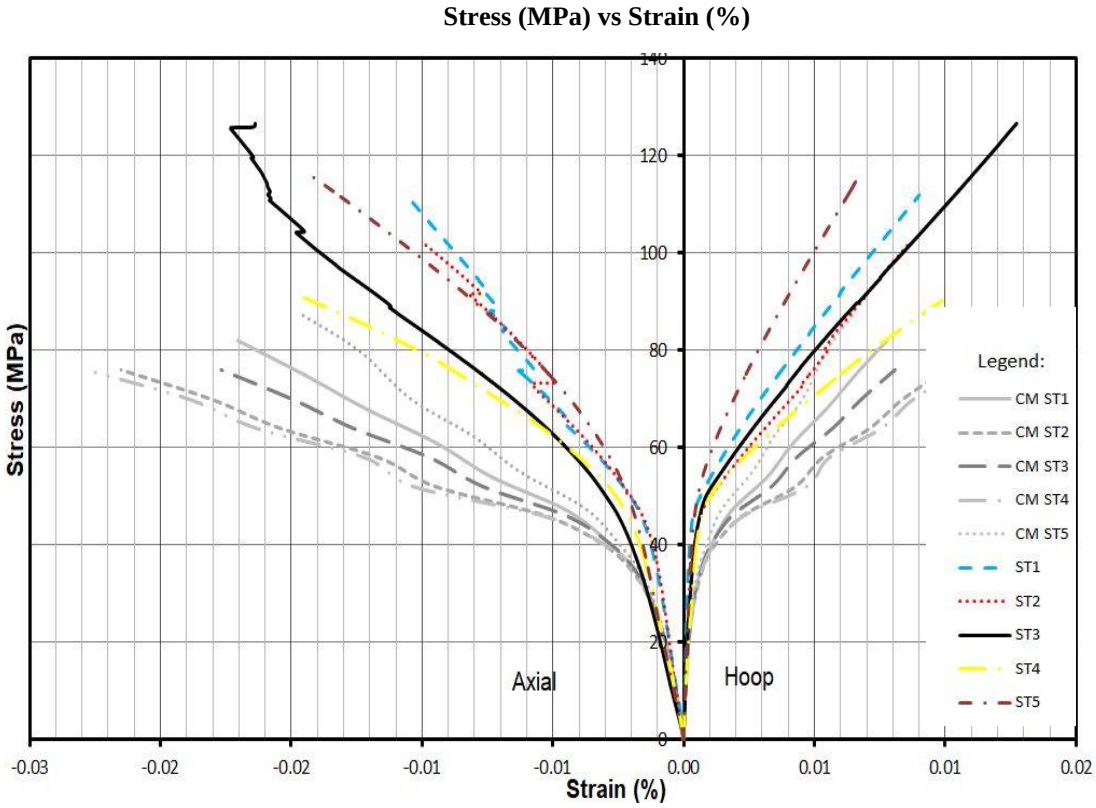

Figure 6.48 – Stress (MPa) vs Strain (%) – Comparison of experimental results with the confinement model studied**.**

that of the unwrapped cylinders. As outlined earlier, a number of variables can affect this behaviour and can have an influence on the test results. From the stress-strain diagram, the Young's modulus of elasticity of the confined cylinder can be interpreted. In simplified terms, the Young's modulus of elasticity of the composite can be considered to be equivalent to the summation of the Young's moduli of elasticity of the concrete cylinder and of the jacket. The graphs depict the performance of the compressed confined cylinder. In the first stages of the experiments, the load was primarily taken by the concrete itself and very little load was taken by the jacket. Once the characteristic strength of the concrete is reached, the jacket then starts to take more load. Thus, until the transition point is reached, it can be assumed that the Young's modulus of elasticity of the concrete cylinder governs behaviour, whereas, beyond the transition point, the jacket's Young's Modulus of elasticity takes over. The characteristic strength of the mean heated concrete is equivalent to approximately 38.5 MPa. It was noted that at a stress of 40.0 MPa (i.e. approximately at the transition point), the values of the experimental axial strains and the ones obtained using the confinement model vary considerably. The

confinement model predicts much higher strain values than the experimental data. For instance, from the experimental results obtained, ST1 shows a 55.40% strain reduction (i.e. 0.002770 to 0.001235). Likewise, ST2, ST3, ST4 and ST5 show strain reductions of 62.05% (i.e. from 0.001157 to 0.003050), 28.6% (i.e. 0.002750 to 0.001963), 45% (i.e. 0.002980 to 0.0016382) and 36.56% (i.e. from 0.002430 to 0.001540) respectively. As previously discussed, the confinement model proposed in this study assumes a value of 0.002 for the axial strain of concrete.

Theoretically, it is expected that the strain values of the concrete should be quite similar and that the elastic part of the graph should be almost identical. However, in the absence of data, it is not possible to compare the axial strain of the unwrapped concrete cylinders tested. Yet, it can be assumed that the difference in value of the axial strain at transition point for the tested cylinders is one of the causes affecting the shape of the bi-linear curve. In fact, the experimental graphs tend to be stiffer than those corresponding to the confinement model proposed. A similar but greater difference is noted at the ultimate failure point. As discussed earlier, there are a number of variables that have an effect on the experimental data. These include the capping system adopted, the improvement strength of the SE70 CFRP prepreg, the variability in the concrete mix as well other factors. In addition, the fact that the second set of experiments was carried out using a force-control system could have had an impact on the test results. At this stage, these considerations are all plausible yet arbitrary assumptions, and it is recommended that further experimentational research needs to be carried out so as to investigate these issues in greater depth.

6.11 Conclusion

The experimental results achieved were discussed and analysed. The stacking sequences examined provided a fair comparison for studying the behaviour of auxetic confined jackets. From the statistical data achieved and through the experimental graphical representation, it can be said that auxetic laminates do provide better confinement and better strength. The auxetic behaviour was compared to the predicted graphical representation achieved using confinement models proposed (17-20), where some differences were noted. In fact, it is recommended that future works or improvements are to be carried out as outlined in Chapter 7.

Chapter 7.
Conclusion & Further Research Work

7.1 Summary of Findings

The research carried out within this thesis provided positive results for the confinement stresses and ultimate rupture strength of composite jackets with a negative Poisson's ratio. Auxetic jackets tend to expand in the through thickness direction when subjected to tension. This behaviour results in storing more energy and improves the fracture resistance of the laminate by reducing the possibility of crack formation. In so doing, it increases the load-carrying capacity of the jacket. In fact, it was shown that these jackets enhanced the strengthening capacity of the concrete columns, confirming that the through thickness effect provided by the jacket contributes in improving further the strength of structural members.

Most research work carried out on auxetic laminates have been restricted to the use of coupons. Thus, this research study took a step further by exploiting the beneficial strengthening properties of auxetic laminates in the construction industry. The use of auxetic jackets gives the possibility of improving the ultimate strength capacity of a column by using the standard procedure and methodologies that are already available in the construction market. However, by applying particular stacking sequences that exhibit a negative Poisson's ratio, it is possible to achieve higher strengths. From an economical point of view, this too is satisfactory, since, by making use of the same number of layers (i.e. same material quantity and material cost), a better performance is acquired.

Both analytical and experimental work was carried out so as to obtain a better understanding of the behaviour of these jackets. However, the majority of this thesis was based on experimental research work, because it was considered to provide a better phenomenological understanding of the structural behaviour of jacketed concrete columns. Concrete is bulky in nature, and when compressed, its failure does not follow a standard path. In addition, it is possible that the pressure exerted on the jacket might not have been transferred uniformly and, in turn, this might not have exerted uniformity through thickness expansion of the concrete cylinder. In this

respect, therefore, this research study was focused on understanding better the practical problems associated with achieving effective jacket confinement using available equipment as well as simulating actual site conditions.

From the research work carried out in this thesis, the following salient results were obtained:

1. **Manufacturing of Jackets**: An adequate bond needs to be achieved between the concrete column surface and the CFRP jacket so as to fully obtain efficient stress transfer between the structural components. It was shown that when using prepegs, an additional layer of resin was required to create a perfect bond. The pre-impregnated resin present in the CFRP was not enough to overcome the dust particles of the concrete surface. In fact the absence of the SA 70 resin between the concrete and the jacket did result in creating problems in the experiments. In addition, it is recommended that smooth concrete surfaces are maintained throughout, otherwise, the presence of air bubbles or minor cracks in the jacket would disrupt the transfer of loads and, in certain situations, could also be the cause of premature failure. Consequently, these structural deficiencies could reduce the possibility of an efficient auxetic effect.

2. **Prepreg CFRP:** Throughout this study, prepregs were used to manufacture the jackets. So, the vacuum bagging technique was implemented. It resulted that this system actually performed efficiently. This was noted from the failure modes of the tested jackets and the ultimate strengths reached. A prepreg was primarily utilised to obtain a uniform distribution of the resin and provide a sustainable auxetic system. From the tested experimental samples, satisfactory results were obtained for the auxetic configurations. Therefore, it follows that the jackets performed satisfactorily. The CFRP prepreg system used can be adapted for actual retrofitting of existing structures. The SE70 prepreg was actually chosen due to its low curing temperature. Thus, concrete cylinders were tested to confirm whether the constant heating of 70°C for

20 consecutive hours could have had any adverse effects on the failure load. From the experiments carried out, it resulted that this issue only had a minor effect on the strength of the jacketed concrete specimen. In addition, minimal differences were noticed in the characteristic strength of the concrete. Nevertheless, with the application of flexible silicon heater pads and electronic controllers available from suppliers, it is possible to control the required curing temperature and to simulate the procedure carried out in the laboratory on site. In this way, human errors would be minimised and the through thickness expansion would be effective. Further studies are required to investigate whether similar results would be obtained when using a wet lay up method.

3. **Negative Poisson's Ratio**: A series of mathematical tools based on Classical Laminate Theory (CLT) were used in order to predict the material properties of the layouts. It resulted that SE70 symmetric balanced angle-ply laminates with angles varying between 15° and 40° exhibited a negative through thickness Poisson's ratio, with a maximum value of -0.468 reached in the region of 25°. It was deduced that the value is dependent on the properties of the CFRP material. The tensile tests completed did give an indication of the presence of a negative Poisson's ratio for $[\pm 20]_{2s}$ and $[\pm 25]_{2s}$ configurations. The values achieved indicate that some form of through thickness expansion of the laminates in the CFRP specimen, though not visible with the naked eye, actually occurs when the material is stretched.

4. **Auxetic Confinement:** The results achieved from the compression tests give an indication that auxetic laminates provide better confinement and better strength. To verify their valuable properties, the $[\pm 20]_{2s}$ and $[\pm 25]_{2s}$ configurations, each having a negative Poisson's ratio of -0.403 and-0.468 respectively, were tested and compared with configurations of equal Young's moduli of elasticity, but with different Poisson ratios. In addition, these were then compared to stacking sequences having the maximum and minimum Young's moduli of elasticity. It resulted that, by

ranking the results accordingly, the maximum ultimate rupture strength was reached primarily by the auxetic configurations ST1, ST2, ST3, followed by jackets ST5, ST4 and ST6, the latter three configurations having a positive Poisson's ratio. Every confinement jacket consisted of eight layers of CFRP, where gains of 387%, 351% and 338% were recorded for ST1, ST2 and ST3 auxetic configurations in terms of compressive strength when compared to the average compressive strength obtained from the heated non-jacketed concrete cylinders. Thus, from the stress-strain diagrams and test results discussed in detail in Chapter 6, it can be concluded that the stiffness of the material as well as the improved fracture toughness and the increase in energy storage instigated by the through thickness expansion were achieved due to the presence of a negative Poisson's ratio, which contributed to enhancing the strength of a confined concrete column.

7.2 Future Research Work

The main findings and contributions described in this thesis have addressed the objective of this research project. However, this research work can lead to other interesting opportunities related to the construction industry.

Analytical confinement models are useful tools used to help in providing an initial understanding of the behaviour of confinement jackets. These models are designed using various criteria. Yet, none of them envisage the possibility of increased strength that can result from a through thickness expansion of the CFRP jacket. Methodologies to quantify the values of a negative Poisson's ratio were discussed and implemented throughout this research study. It was shown that an auxetic laminate has the potential of storing more energy. Thus, it is recommended to investigate further whether this increased energy can be quantified and also to check whether this energy increases proportionally with the negative Poisson's ratio. In so doing, an improved confinement model can possibly be achieved. Nevertheless, by means of a negative Poisson's ratio, an additional improved strength, or rather, an

additional factor resulting from the increase in energy is to be inserted explicitly in the confinement model so as to improve its accuracy.

The use of auxetic laminates as a confined jacket can be considered as an introductory application of these auxetic properties in the construction field. In fact, it would be interesting to investigate the behaviour of these laminates when applied on other structural members. For instance, studies have been carried out on confinement of brick masonry columns with CFRP materials. (216) Theoretically, being a compression member, an auxetic jacket helps in improving further confinement in a similar way as the tested concrete cylinders. FRP retrofitting techniques were also used on concrete slabs and beams. Thus, it would be rather beneficial to find a way of exploiting the valuable properties of auxetics also in these structural members.

As previously discussed in this thesis, the confinement jackets studied were manufactured using prepreg layers. The most common method used for wrapping concrete cylinders on site is probably the wet lay up system. Further checking is essential to see whether an auxetic effect can still be achieved. A comparison between both systems should preferably be carried out to check whether substantial differences exist between both systems.

The auxetic confinement jackets were created using conventional methods. Studies have depicted the presence of a negative Poisson's ratio when creating helical auxetic yarns. These consist of two fibrous components spun together, using commercial fibres, into a helix. Research work (217) has shown that, when using mono-filament fibres, with Poisson's ratios ranging from 0.35 to 1.95, an auxetic effect equivalent to -2.7 is reached. In addition, the starting angle of the wrap fibre dominates the magnitude of the auxetic behaviour (217, 218). The auxetic values that are obtained using this system are substantially higher when compared to the ones that were achieved by laying up stacking sequences using CFRP layers in this research study. Thus, theoretically, this substantial increase in the auxetic value should indirectly imply improved auxetic properties. Hence, it is recommended to further study the use of helical auxetic yarns wound around concrete columns and to test whether they are capable of providing further compressive strength to the columns. It

is considered that its application on site should not be of a laborious nature, which would imply that such a strengthening technique could possibly become economically-feasible.

References:

(1) Liu Y., Hu H. A review on auxetic Structures and polymeric materials. *Scientific Research and Essays.* 2010; 5(10):1052-1063.

(2) Brinson H.F,, Brinson L.C. Stress and Strain Analysis and Measurement, In: *Polymer Engineering Science and Viscoelasticity An Introduction*. Springer Science+Business Media New York; 2015. p.15.

(3) The Physics Hypertextbook. *Elasticity.* Available from: https://physics.info/elasticity/ [Accessed 9th July 2018]

(4) Engineers Edge. *Poisson's Ratio Definition Equation.* Available from: https://www.engineersedge.com/material_science/poissons_ratio_definition_equation_13159.htm [Accessed 14th July 2018]

(5) Fuller J.D., Wisnom M.R. Ductility and pseudo-ductility of thin angle-ply CFRP laminates under quasi-static cyclic loading. *Composites:Part A.* 2018; 107:31-38.

(6) NPTEL courses. *Module 5: Laminate Theory – Lecture 17: Laminate Constitutive Relations.* Available from: http://nptel.ac.in/courses/101104010/lecture17/17_4.htm [Accessed 11th July 2018]

(7) Gooch J.W. Encyclopedic Dictionary of Polymers. Springer, New York, NY; 2011. Available from: https://link.springer.com/referenceworkentry/10.1007%2F978-1-4419-6247-8_1287#howtocite [Accessed 26th June 2018]

(8) Indian Institute of Technology, Kharagpur. *Macromechanical Behaviour.* Available from: http://www.ae.iitkgp.ac.in/ebooks/chapter6.html [Accessed 11th July 2018]

(9) Subhash G., *Dynamic Indentation Testing – ASM International.* Available from: https://www.asminternational.org/ [Accessed 9th July 2018]

(10) Hu. H. Auxetic Materials and Their Potential Applications in Textiles. *Textile Research Journal.* 2014; Vol. 85(15):1600-1611.

(11) Collins. *Definition of Pyrolysis.* Available from: https://www.collinsdictionary.com/dictionary/english/pyrolysis [Accessed 14th July 2018]

(12) Petrozzo R.A., Singer S.W. Telecentric lenses simplify non contact metrology. *Test & Measurement World.* 2001: 4-9.

(13) Halpin J.C.,(1992), *Primer on Composite Materials Analysis – Second Edition, Revised,* Tehcnomic Publication. Available from:

https://books.google.com.mt/books?id=bv34XH5-g6AC&pg=PA81&lpg=PA81&dq=stacking+sequence+notation&source=bl&ots=VBo_q6GyX3&sig=KWRLAlie-5gY-zrCtMtV7UNNa5Y&hl=en&sa=X&ved=2ahUKEwj3v5fAr8ffAhULiCwKHRrfDgs4ChDoATAGegQIAhAB#v=onepage&q=stacking%20sequence%20notation&f=false [Accessed 7th January 2019].

(14) NPTEL courses. *Module 5: Laminate Theory – Lecture 16: Introduction to Classical Plate Theory,* Available from: https://nptel.ac.in/courses/101104010/downloads/Lecture16.pdf [Accessed 7th January 2019].

(15) Evans K.E. Auxetic polymers: a new range of materials. *Endeavour*. 1991; 15 (4):170-174.

(16) Jayanty S. Negative Poisson's ratio composites: finite element modeling and experiments. [Masters thesis]. University of Toledo; 2010 [cited 2018 Jan 12] Available from: http://utdr.utoledo.edu/cgi/viewcontent.cgi?article=1890&context=theses-dissertations

(17) Becque J. Analytical Modeling of Concrete Columns Confined by FRP. [Masters thesis]. University of Manitoba, Canada; 2000.

(18) Becque J., Patnaik A.K., Rizkalla H. Analytical Models for Concrete Confined with FRP Tubes. *Journal of Composite Construction.* 2003; 7 (1): 31-38.

(19) Lam L., Teng J.G. Design-oriented stress-strain model of FRP confined concrete. *Construction and Building Materials*. 2003; 17:471-489.

(20) Teng J.G., Jiang T., Lam L., Luo Y.Z. Refinement of a Design-Oriented Stress-Strain Model for FRP-Confined Concrete. *Journal of Composites For Construction.* 2009; 13:269-278.

(21) Artem L. Applying Carbon Fiber in Building Structures. [Bachelor's thesis] - Saimaa University of Applied Sciences Faculty of Technology, Lappeenranta; 2010 [cited 2018 Feb 15] Available from: https://www.theseus.fi/bitstream/handle/10024/17402/Litvinov_Artem.pdf

(22) Sheikh S.A. Performance of concrete structures retrofitted with fibre reinforced polymers. *Engineering Structures*. 2002; 24(7): 869-879.

(23) Alkhrdaji T. Strengthening of Concrete Structures Using FRP Composites. *Structure magazine.* 2015; 18-20. Available from: http://www.structuremag.org/?p=8643 [Accessed 28th June 2017].

(24) Knedall D. Development in FRP bridge design. *Reinforced plastics.* 2010; 38-42. Available from: https://www.materialstoday.com/composite-industry/features/developments-in-frp-bridge-design/ [Accessed 28th June 2017].

(25) Stock M., Schilling B. *Carbon Fiber vs. Steel – What's the Best Structural Foundation Repair?* Available from: https://www.uswaterproofing.com/learning-center/carbon-fiber-vs.-steel-whats-the-best-structural-foundation-repair [Accessed 28th June 2017].

(26) Correia L., Sena-Cruz J., Michels J., França P., Pereira E., Escusa G. Durability of RC slabs strengthened with prestressed CFRP laminate strips under different environmental and loading conditions. *Composites Part B: Engineering*. (2017); 125:71-88.

(27) Machida A., Maruyama K. Design Code development for fibre-reinforced polymer structures and repairs. *Progress in Structural Engineering and Materials* (2002); 4 (2), 149-160.

(28) Jiangtao Y., Yichao W., Kexu H., Kequan Y., Jianzhuang X. The performance of near-surface mounted CFRP strengthened RC beam in fire. *Fire Safety Journal.* 2017; 90:86-94.

(29) British Standards Institution. BS EN 1992-1-1: 2004, Eurocode 2. *Design of concrete structures – Part 1-1: General rules and rules for building.* London: BSI; 2004.

(30) Buchan PA, Chen J. Blast resistance of FRP composites and polymer strengthened concrete and masonry structures- A state-of-the-art review. *Composites Part B: Engineering*. 2007; 38(5-6):509-522.

(31) Pham T.M., Hao H. Review of Concrete Structures Strengthened with FRP Against Impact Loading. *Structures* 7:59-70.

(32) Colledge J.J., Warlow B. *Ships of the Royal Navy: The Complete Record of all Fighting Ships of the Royal Navy*, Greenhill; 2003.

(33) Bakis C.E., Bank L.C., Brown V.L., Cosenza E., Davalos J.F., Lesko J.J., Machida A., Rizkalla S.H., Triantafillou T.C. Fiber-Reinforced Polymer Composites for Construction – State-of-the-Art Review. *Journal of Composites for Construction*. 2002; 6 (2):73-87.

(34) Pora J., Composite Materials in the Airbus A380 – From History to Future – Available from:http://www.iccm-

central.org/Proceedings/ICCM13proceedings/SITE/PAPERS/paper-1695.pdf [Accessed March 16 2018]

(35) Atwater M. Boeing, Carbon Fiber and Engineering the Future of Aviation. Available from:https://www.engineering.com/DesignerEdge/DesignerEdgeArticles/ArticleID/6810/Boeing-Carbon-Fiber-and-Engineering-the-Future-of-Aviation.aspx [Accessed March 16 2018]

(36) Alderton M. Could Carbon Fibre Bethe Superhero of Building Materials? 2017; Available from: https://www.autodesk.com/redshift/carbon-fiber-building/ [Accessed March 16 2018]

(37) Gite B.E., Margaj S.R. Carbon Fibre as a recent material in Construction. Available from:https://www.engineeringcivil.com/carbon-fibre-as-a-recent-material-use-in-construction.html [Accessed April 7 2018]

(38) GuruRaja M.N., HariRao A.N. Influence of Angle Ply Orientation on Tensile Properties of Carbon/Glass Hybrid Composite. *Journal of Minerals and Materials Characterization and Engineering*. 2013; 1:231-235.

(39) Zoltek Toray Group. *Zoltek Applications.* Available from: http://zoltek.com/applications/. [Accessed December 20 2018].

(40) Sadeghian P., Rahai A.R., Ehsani M.R. Effect of Fiber Orientation on Nonlinear Behavior of CFRP Composites. *Journal of Reinforced Plastics and Composites*. 2008; 28 (18):1-28.

(41) Lima Mehdi M., Doh Jeung-Hwan, Hadi Muahmmad N.S., Miller Dane. The effects of CFRP orientation on the strengthening of reinforced concrete structures. *Structural Design of Tall and Special Buildings.* 2016; 25:759-784.

(42) Huang Z.M., Zhou Y.X. *Strength of Fibrous Composites* . Advanced Topics in Science and Technology in China. 1st Edition. Springer, Berlin, Heidelberg; 2012.

(43) Fuller J.D., Wisnom M.R. Pseudo ductility and damage suppression in thin ply CFRP angle ply laminates. *Composites Part A: Applied Science and Manufacturing.* 2015; 69: 64-71.

(44) Fuller J.D., Wisnom M.R. Exploration of the potential for pseudo-ductility in thin ply CFRP angle-ply laminates via an analytical method. *Composites Science & Technology*. 2015; 112:8-15.

(45) Harkati E.H., Bezazi A., Scarpa F., Alderson K. & Alderson A. Modelling the influence of the orientation and fibre reinforcement on the Negative Poisson's ratio in composite laminates. *Physica Status Solidi (b)*. 2007; 244(3):883-892.

(46) Clarke J.F., Duckett R.A., Hine P.J., Hutchinson I.J. & Ward I.M. Negative Poisson's ratios in angle-ply laminates: theory and experiment. - *Composites.* 1994; 25(9):863 – 868.

(47) Herakovich. C.T. Influence of Layer Thickness on the Strength of Angle Ply Laminates. *Journal of Composite Materials*. 1982;16:216-227.

(48) Fuller J.D., Wisnom M.R., Jalavand M. Combining fibre orientation and fragmentation to achieve pseudo-ductile CFRP laminates. *Composite Structures*. 2016;142:155-166.

(49) Alderson K.L., Simkins V.R., Coenen V.L., Davies P.J., Alderson A., Evans K.E. How to make auxetic fibre reinforced composites. *Physica Status Solidi (b).* 2005; 242(3):509-518.

(50) Evans K.E., Donoghue J.P., Alderson K.L. The Design, Matching and Manufacture of Auxetic Carbon Fibre Laminates. *Journal of Composite Material*. 2003; 38(2):95-106.

(51) Alderson K.L., Coenen V.L. The low velocity impact response of auxetic carbon fibre laminates, *Physica Status Solidi (b).* 2008; 245(3):489-496.

(52) Alderson K.L., Coenen V.L. Mechanisms of Failure in the Static Indentation Resistance of Auxetic Carbon Fibre Laminates - *Physica Status Solidi B.* 2011; 248(1): 66-72.

(53) Bezazi A., Boukharouba W. & Scarpa F. Mechanical properties of auxetic carbon/epoxy composites: static and cyclic fatigue behaviour. *Physica Status Solidi (b),* 2009; 246 (9): 2102-2110.

(54) Matsuda T., Goto K., Kubota N. , Ohno N. Negative through-the-thickness Poisson's ratio of elastic-viscoplastic angle-ply carbon fiber-reinforced plastic laminates – Homogenization analysis. *International Journal of Plasticity*. 2014;63: 152-169.

(55) Alderson A. A triumph of lateral thought. *Chemistry & Industry*. 1999; 17:384-391.

(56) Wang, Z. & Hu, H. Auxetic Materials and Their Potential Applications in Textiles. *Textile Research Journal*. 2014; 85 (15):1600-1611.

(57) Saxena K.K., Das R., Calius E.P. Three Decades of Auxetics Research – Materials with Negative Poisson's Ratio: A Review - *Advanced Engineering Material.* 2016; 18(11): 1847-1870.

(58) Alderson K.L., Alderson A. Auxetic Materials. *Proceedings of the Institution of Mechanical Engineers, Part G, Journal of Aerospace Engineering*. 2007; 221: 565-575.

(59) Alderson A., Rasburn J., Evans K.E. Mass transport properties of auxetic (negative Poisson's ratio) foams. *Physica Status Solidi B.* 2007; 244 (3):817-827.

(60) Bianchi M., Frontoni S., Scarpa F., Smith C.W. Density change during the manufacturing process of PU-PE open cell auxetic foams. *Physica Status Solidi B.* 2011; 248 (1):30-38.

(61) Bianchi M., Scarpa F., Banse M., Smith C.W. Novel generation of auxetic open cell foams for curved and arbitrary shapes. *Acta Materialia*. 2011; 59 (2):686-691.

(62) Bianchi M., Scarpa F, Smith C.W. Shape memory behaviour in auxetic foams: Mechanical Properties. *Acta Materiala.* 2010; 58 (3):858-865.

(63) Bianchi M., Scarpa F., Smith C.W., Whittell G.R. Physical and thermal effects on the shape memory behaviour of auxetic cell foams. *Journal of Materials Science*. 2010; 45:341-347.

(64) Bezazi A., Scarpa F. Mechanical behaviour of conventional and negative Poisson's ratio thermoplastic polyurethane foams under compressive cyclic loading. *International Journal of Fatigue*. 2007; 29 (5):922-930.

(65) Webber R.S., Alderson K.L., Evans K.E. Novel Variations in the Microstructure of the Auxetic Microporous Ultra-High Molecular Weight Polyethylene Part 1: Processing and Microstructure. *Polymer Engineering and Science.* 2000; 40 (8):1894-1905.

(66) Webber R.S., Alderson K.L., Evans K.E. Novel Variations in the Microstructure of Auxetic Ultra-High Molecular Weight Polyethylene Part 2: Mechanical Properties. *Polymer Engineering and Science.* 2000; 40 (8):1906-1914.

(67) Alderson K.L., Webber R.S, Evans K.E. A Novel Fabrication Route for Auxetic Polyethylene. Part 2. Mechanical Properties. *Polymer Engineering and Science.* 2008; 48 (7):1351-1358.

(68) Alderson K.L., Webber R.S., Kettle A.P., Evans K.E. Novel Fabrication Route for Auxetic Polyethylene. Part 1. Processing and Microstructure. *Polymer Engineering and Science.* 2005; 45 (4):568-578.

(69) Ravirala N., Alderson A., Alderson K.L., Davies P.J. Expanding the range of auxetic polymeric products using a novel melt-spinning route. *Physica Status Solidi (b).* 2005; 242 (3):653-664.

(70) Chan N., Evans K.E. Fabrication methods for auxetic foams. *Journal of Materials Science.* 1997; 32 (22): 5945-5953.

(71) Create your cosmos. Building toward Posthuman Enlightenment. Available from: http://createyourcosmos.blogspot.com/2010/11/new-materials-for-industrial-designers.html [Accessed 12th August 2017]

(72) Snynasia. Technology will create future. Available from: http://www.synasia.com.cn/en/page.asp?id=370 [Accessed 12th August 2017]

(73) Times of Malta. *Maltese researchers develop life-saving foam.* 2009; Available from: https://www.timesofmalta.com/articles/view/20090731/local/maltese-researchers-develop-life-saving-foam.267518 [Accessed 14th August 2017]

(74) Times of Malta. *Maltese researchers foam that 'can save lives'.* 2009; Available from: https://www.timesofmalta.com/articles/view/20090802/education/maltese-researchers- develop-foam-that-can-save-lives.267756 [Accessed 14th August 2017]

(75) Nike News - The New Dimensions of Nike Free. Available from: https://news.nike.com/news/nike-free-2016-running-training [Accessed 14th August 2017]

(76) Yang L., Harrysson O., West H., Cormier D. A Comparison of Bending Properties for Cellular Core Sandwich Panels. *Materials Sciences and Applications.* 2013; 4: 471-477.

(77) Diaz J. Zetix Blast-Proof Fabric Resists Multiple Car Bombs, Makes Our Heads Explode. (2007) Available from: https://gizmodo.com/330343/zetix-blast-proof-fabric-resists-multiple-car-bombs-makes-our-heads-explode [Accessed 14th August 2017]

(78) Mirante L. Auxetic Structures – Towards Bending-Active Architectural Applications – [Master Thesis] Faculy of Architecture, Politecnico di Milano. 2015 [cited 2018 Feb 10] Available from: https://www.politesi.polimi.it/bitstream/10589/116372/1/2015_12_Mirante.pdf

(79) Moyers R.E. Dilator For Opening the Lumen of a Tubular Organ. *United States Patent* Patent no. 5,108,413. 1992

(80) Friis E.A. Surgical Implants Incorporating Re-entrant Material. *United States Patent*. Patent no. 5,035,713. 1991

(81) Rodie, J.B. . The auxetic effect: Zetix™ helical-auxetic technology offers 'game-changing' solutions for blast mitigation and numerous other textile applications. 2010; Available from: https://www.researchgate.net/publication/294376121_The_auxetic_effect_Zetix_helical-auxetic_technology_offers_'game-changing'_solutions_for_blast_mitigation_and_numerous_other_textile_applications [Accessed 31st March 2017]

(82) Das B.R. & Hati S. Auxetic Textiles: Advantage of Being Negative-fibre2fashion, 2010 Available from: http://www.fibre2fashion.com/industry-article/4675/auxetic-textiles [Accessed 31st March 2017]

(83) Auxetix Expanding Technology. Commercial Uses for Helical-Auxetic Materials. Available from: from www.auxetix.com. [Accessed 27th July 2016]

(84) Critchley R., Corni I., Wharton J.A., Walsh F.C., Wood J.K., Stokes K.R. A review of the manufacture, mechanical properties and potential applications of auxetic foams. *Physical Status Solidi B.* 2013; 250 (10):1963-1982.

(85) Bhullar S.K., Mawanane Hewage A.T., Alderson A., Alderson K., Jun M.B.G. Influence of negative Poisson's ratio on stent applications. *Advances in Materials.* 2013; 2 (3): 42-47.

(86) Bhullar S.K., Lala N.L., Ramkrishna S., (2015) - Smart Biomaterials – A review. *Reviews on Advanced Materials Science*. 2015; 40:303-314.

(87) Ko.J., Bhullar S., Cho Y., Lee P.C., Jun M.B.G. Design and Fabrication of auxetic stretchable force sensor for hand rehabilitation. *Smart Material Structures.* 2015; 24:1-8.

(88) Airoldi A., Bettini P., Panichelli P., Oktem M.F., Sala G. Chiral topologies for composite morphing structure – Part 1: Development of a chiral rib for deformable airfoils. *Physica Status Solidi B.* 2015; 252 (7): 1435-1445.

(89) Allen T., Martinello N., Zampieri D., Hewage T., Senior T., Foster L, Alderson A. Auxetic Foams for Sport Safety Applications. *Procedia Engineering.* 2015; 112:104-109.

(90) Agnese F., Remillat C, Scarpa F. & Payne C. Composite chiral shear vibration damper. *Composite Structures.* 2015; 132: 215-225.

(91) Borg Bonnici, S.L. The Application of Auxetics to Structural Engineering. [Bachelor's Thesis] Architecture and Civil Engineering, University of Malta. 2005.

(92) Lord. Magneto Rheological Fluid. Available from: https://www.lord.com/products-and-solutions/active-vibration-control/industrial-suspension-systems/magneto-rheological-%28mr%29-fluid [Accessed 7th April 2018]

(93) MalekzadehFard K., Gholami M., Reshadi F., Livani M. Free vibration and buckling analyses of cylindrical sandwich panel with magneto rheological fluid layer. *Journal of Sandwich Structure and Materials.* 2017; 19 (4):347-423.

(94) Ungureanu B., Achaoui Y., Enoch S., Brûlé S., Guenneau S. Auxetic– like metamaterials as novel earthquake protections – *EPJ Applied Metamaterials*. 2015; 2 (17):1-8.

(95) Zmuda C. Design of Structural Composite with Auxetic Behaviour [Bachelors Thesis] Faculty of Worcester Polytechnic Institute. 2017. [cited 14th January 2018] Accessed from:https://web.wpi.edu/Pubs/E-project/Available/E-project-042717-143007/unrestricted/Auxetic-Composite.pdf

(96) Fichant S, La Borderie C., Pijaudier-Cabot G. Isotropic and anisotropic descriptions of damage in concrete structures. *Mechanics of Cohesive-frictional Materials*. 1999; 4 (4):339-359.

(97) Miki M. & Murotsu Y. The Peculiar Behaviour of the Poisson's Ratio of Laminated Fibrous Composites. *JSME International Journal: Series 1*. 1999; 32 (1):67-72.

(98) Neville, A.M. *Properties of Concrete.* 5th Edition. Prentice Hall, United Kingdom: Pearson Education; 2013.

(99) Naus D.J. The Effect of Elevated Temperature on Concrete Materials and Structures – A Literature Review - *Manuscript prepared for the U.S. Nuclear Regulatory Commission, Office of Nuclear Regulatory Research.* 2005. Accessed from: https://info.ornl.gov/sites/publications/Files/Pub1043.pdf

(100) Suk Wong Kang, Sung-Gul Hong. Behavior of Concrete Members at Elevated Temperatures Considering Inelastic Deformation. *Fire Technology*. 2003;39(1): 9-22.

(101) Fédération Internationale du Béton (*fib*). *Externally Bonded FRP Reinforcement for RC Structures –Technical Report – Bulletin 14*. International Federation for Structural Concrete (fib). Switzerland; 2001.

(102) Xiao Y. Applications of FRP Composites in Concrete Columns. *Advances in Structural Engineering*. 2004; 7 (4):335-343.

(103) Setunge S., Kumar A., Nezamian A., De Silva S., Carse A., Spathonis J., Chandler L., Gilbert D., Johnson B., Jeary A. & Pham L., *Review of Strengthening Techniques using Externally Bonded Fibre Reinforced Polymer Composites*. CRC Construction Innovation Building and Future. Report number: 2002-005-C-01, 2002.

(104) Taranu N., Oprisan G., Isopescu D., Entuc I., Munteanu V., Banu C. Fibre Reinforced Polymer Composites as Internal and External Reinforcements for Building Elements - *Article in Bulletin of the Polytechnic Institute of Jassy, Constructions Architecture Section*. 2008. Accessed from: http://www.bipcons.ce.tuiasi.ro/Content/ArticleInformation.php?ArticleID=105

(105) Fédération Internationale du Béton (*fib*). *Retrofitting of concrete structures by externally bonded FRPs, with emphasis on seismic applications – Bulletin.35*. International Federation for Structural Concrete (fib), Switzerland; 2006.

(106) Karbhari V.M. Materials Consideration in FRP Rehabilitation of Concrete Structures. *Journal of Materials in Civil Engineering*. 2001; 13 (2):90-97.

(107) Ghanem S.Y. Circular Columns Partially Confined with CFRP. [PhD Thesis] University of Kentucky. 2016. [cited 7th April 2018] Accessed from: https://uknowledge.uky.edu/cgi/viewcontent.cgi?article=1040&context=ce_etds

(108) Paepegem W.V. *Mechanics of Composite Materials – Vacuum Infusion – The Equipment and Process of Resin Infusion.* Available from: http://www.composites.ugent.be/home_made_composites/documentation/FibreGlast_Vacuum_infusion_process.pdf [Accessed 18th August 2017].

(109) JR Technology Limited. *Flexible Rubber Heater Mats*. Available from: http://www.jrtech.co.uk/products/heater-mats [Accessed 18th May 2018].

(110) JR Technology Limited. *Portable Hot Bonding Controllers.* Available from: http://www.jrtech.co.uk/products/hot-bonding-controllers [Accessed 18th May 2018].

(111) Arabshahi A., Moghaddam N.G., Tavakkolizadeh M. A New Strength Model for FRP Confined Circular Columns. In: *SMAR 2015: Third Conference on Smart Monitoring Assessment and Rehabilitation of Civil Structures*. 2015, 7-9 September 2015, Antalya, Turkey; 2015. p. 1-8.

(112) Campione G., Miraglia N., Papia M. Strength and Strain Enhancements of concrete columns confined with FRP sheets. *Structural Engineering and Mechanics*. 2004;18 (6): 1-22.

(113) Lam L., Teng J.G. Behavior and Modeling of Fiber Reinforced Polymer Confined Concrete. *Journal of Structural Engineering*. 2004; 130:1713-1723.

(114) Mirmiran A., Shahawy M. Dilation characteristics of confined concrete. *Mechanics of Cohesive-Frictional Materials*. 1997; 2:237-249.

(115) Moran D.A., Pantelides C.P. *FRP Confined Concrete Stress-Strain Model utilizing a variable Strain Ductility Ratio.* 2002.

(116) American Concrete Institute (ACI). Guide for the design and construction of externally bonded FRP systems for strengthening concrete structures. ACI-440 2R, Farmington Hills, Mich. 2008.

(117) Guler S., Ashour A. Review of Current Design Guidelines for Circular FRP-Wrapped Plain Concrete Cylinders. *Journal of Composites for Construction*. 2016; 20 (2):1-15.

(118) Honegstad E. Study of combined bending and axial load in reinforced concrete members. 1951.

(119) Popovics S. A numerical approach to the complete stress-strain curve of concrete. *Cement and Concrete Research*. 1973; 3:583-599.

(120) Sargin M. Stress-strain relationships for concrete and the analysis of structural concrete sections: Solid mechanics division, University of Waterloo. 1971.

(121) Sargin M., Ghosho S., Handa. V. Effects of lateral reinforcement upon the strength and deformation properties of concrete. *Magazine of Concrete Research*. 1972; 23:99-110.

(122) Wang P., Shah S., Namman A. Stress-strain curves of normal and lightweight concrete in compression. ACI. 1978

(123) Kent D., Park R. Flexural members with confined concrete. *Journal of Structural Division.* 1971,97:1964-1990.

(124) Sheikh S., Uzumeri S. Analytical model for concrete confinement in tied columns. *Journal of Structural Division.* 1982; 108:2703-2722.

(125) Saatcioglu M., Ravzi S. Strength and ductility of confined concrete. *Journal of Structural Engineering*. 1992; 188 (6):1590-1607.

(126) Mander M., Priestley M.J.N., Park R. Theoretical stress strain model for confined concrete. *Journal of Structural Engineering.* 1988; 114 (8):1804-1826.

(127) Mander M., Priestley M.J.N., Park R. Observed Stress Strain Behaviour of confined concrete. *Journal of Structural Engineering.* 1988; 114 (8): 1827-1849.

(128) Al-Alaily H.M. Retrofit of Reinforced Concrete Columns By Composite Jacketing [Masters thesis] Arab Academy For Science and Technology and Maritime Transport. 2011. [Cited 5th April 2018] Accessed from: http://www.aast.edu/en/openfiles/opencmsfiles/pdf_retreive_cms.php?disp_unit=350/alaily1.pdf

(129) Marijn R., Spoelstra R., Monti G. FRP Confined Concrete Model. *Journal of Composites for Construction.* 1999; 3:143-150.

(130) Nistico N., Monti G. - RC square sections confined by FRP: Analytical prediction of peak strength. *Composites: Part B* 2013; 45:127-137.

(131) Monti G. - Confining Reinforced Concrete with FRP: Behaviour and Modeling, In: *Workshop 'Composites in Construction: A reality*', Capri, Italy; 2001. p. 1-12.

(132) Campione G. Influence of FRP wrapping techniques on the compressive behaviour of concrete prisms. *Cement & Concrete Composites.* 2006; 28 (5):497-505.

(133) Campione G., Miraglia N., Scibilia N. Comportamento in compressione di elementi in calcestruzzo armato a sezione circolare e quadrata rinforzati con FRP *Ingegneria Sismica* 2002; 2:5-12.

(134) Campione G., Miraglia N. Strength and strain capacities of concrete compression members reinforced with FRP. *Cement & Concrete Composites*. 2003; 25(1):31-41.

(135) Lam L., Teng J.G. Compressive Behavior of Carbon Fiber Reinforced Polymer Confined Concrete in Elliptical Columns. *Journal of Structural Engineering.* 2002; 128:1535-1543.

(136) Lam L., Teng J.G. Strength Models for Fiber-Reinforced Plastic-confined Concrete. *Journal of Structural Engineering*, 2002; 128 (5)612-623.

(137) Ozbakkaloglu T., Lim J.C. Confinement Model for FRP-Confined High Strength Concrete. *Journal of Composites for Construction*, 2014; 18 (4): 1-19.

(138) Ozbakkaloglu T., Lim J.C. Hoop strains in FRP-confined concrete columns experimental observations. *Materials and Structures* 2015; 48: 2839-2854.

(139) Ozbakkaloglu T., Lim J.C., Vincent T. FRP-confined concrete in circular sections: Review and assessment of stress-strain models. *Engineering Structures* 2013; 49: 1068-1088.

(140) Ozbakkaloglu T., Lim J.C., Vincent T. Investigation of the Influence of the Application Path of Confining Pressure: Tests on Actively Confined and FRP Confined Concretes. *Journal of Structural Engineering*. 2014; 141(8):1-12.

(141) De Lorenzis L., Tepfers R. Comparative Study of Models on Confinement of concrete Cylinder with Fiber-Reinforced Polymer Composites, *Journal of Composites for Construction.* 2003; 7(3): 219-237.

(142) Samani A.K., Attard M. A stress strain model for uniaxial and confined concrete under compression. *Engineering Structures*. 2012; 41: 335-349.

(143) Jiang T., Teng J.G. Analysis oriented stress strain models for FRP confined concrete. *Engineering Structures.* 2007; 29: 2968-2986.

(144) Huang L., Gao C., Yan L., Kasal B., Ma G. Reliability assessment of confinement models of carbon fiber reinforced polymer-confined concrete. *Journal of Reinforced Plastics and Composites.* 2016; 35(12): 996-1026.

(145) Samaan M., Mirmiran A., Shahawy M. Model of concrete confined by fiber composites, *Journal of Structural Engineering*. 1998; 124 (9):1025-1031.

(146) Xiao Y., Wu H. Compressive behaviour of concrete confined by carbon fiber composite jackets. *Journal of Materials in Civil Engineering.* 2000; 12(2):139-146.

(147) Mirmiran A., Shahawy M. A new concrete filled hollow FRP composite column. *Composites Part B-Engineering*. 1996; 27(3-4): 263-268.

(148) Fam A.Z., Rizkalla S.H. Confinement model for axially loaded concrete confined by circular fiber reinforced polymer tubes. *ACI Structural Journal*. 2001; 98 (4):451-461.

(149) Harkati E.H., Bezazi A., Boukharouba W., Scarpa F. Influence of carbon fibre on the through-the-thickness NPR behaviour of composite laminates. *Physica Status Solidi B.* 2009; 246(9): 2111-2117.

(150) Steeves C.A., Fleck N.A. In-Plane Properties of CFRP Laminates containing through-thickness reinforcing rods (Z-Pins*). International Journal of Solids and Structures.* 2006; 43: 3197-3212.

(151) Pipes R.B., Daniel I.M. Moiré Analysis of the Interlaminar Shear Edge Effect in Laminated Composites. *Journal of Composite Materials*. 1971; 5: 255-259.

(152) Thompson L.F. Through-Thickness Compression Testing and Theory of Carbon Fibre Composite Materials [PhD thesis] Faculty of Engineering and Physical Sciences, University of Manchester; 2011. [Cited 108 April 7] Available from: https://www.escholar.manchester.ac.uk/jrul/item/?pid=uk-ac-man-scw:128551

(153) Guo Y., Post D., Han B. Thick Composites in Compression: An Experimental Study of Micromechanical Behaviour and Smeared Engineering Properties. *Journal of Composite Materials*. 1992; 26(13):1930-1944.

(154) Yoneyama S., Ifju P.G., Rohde S.E. Identifying through-thickness material properties of carbon fiber reinforced plastics using the virtual fields method combined with moiré interferometry. *Advanced Composite Materials*. 2018; 27(1): 1-17.

(155) Bouchelaghem H., Bezazi A., Scarpa F. Compressive behaviour of concrete cylindrical FRP confined columns subjected to a new sequential loading technique. *Composites: Part B.* 2011; 42: 1987-1993.

(156) Richardson M.O.W., Wisheart M.J. Review of low velocity impact properties of composite materials. *Composites Part A.* 1996; 27: 1123-1131.

(157) Rahai. A.R., Sadeghian P., Ehsani M.R. Experimental Behaviour of concrete Cylinders Confined with CFRP Composites In: *14th World Conference on Earthquake Engineering, 2008, 12-17 October 2018, Beijing China.* 2018. Available from: http://www.iitk.ac.in/nicee/wcee/article/14_05-03-0147.pdf

(158) Karabinis A.I., Rousakis T.C. Carbon FRP confined concrete elements under axial load, In: *Proceedings of the International Conference on FRP Composites in Civil Engineering*, 2001. Volume 1. 309-313.

(159) Liu D. Impact Induced Delamination – A view of Bending Stiffness Mismatching, *Journal of Composite Materials*. 1988; 22: 674-692.

(160) Chen J.F., Morozov E.V., Shankar K. Simulating progressive failure of composite laminates including in-ply and delamination damage effects. *Composites: Part A.* 2014; 61: 185-200.

(161) Chen H. Damage Detection of Carbon Fiber Reinforced Polymer using Electrical Measurement and Analysis of Acoustic Emission Signals. [Masters thesis] University of Akron, 2013. [Cited 25th March 2018] Accessed from: https://etd.ohiolink.edu/rws_etd/document/get/akron1383455687/inline

(162) Yuan Y., Yao X., Liu B., Yang H., Imtiaz H. Failure modes and strength prediction of thin ply CFRP angle-ply laminates. *Composite Structures.* 2017; 176: 729-735.

(163) Katsumata H., Kimura K., Kobtake Y. Seismic Retrofitting Technique using Carbon Fibres for Reinforced Concrete Building. In: *Fracture Mechanic of Concrete Structure, Proceedings FRAMCOS-3*. AEDIFACTIO Publishers, 1998. p. 1727-1728. Available from:http://framcos.org/FraMCoS-3/3-14-3.pdf

(164) Khorramian K., Sadeghian P. Strengthening Short Concrete Column using Longitudinally Bonded CFRP Laminates. In: *APFIS 2017 – 6th Asia Pacific Conference on FRP in Structures*. 2017. Accessed from: https://www.iifc.org/proceedings/APFIS_2017/Conference%20Proceedings/All%20papers/P74.pdf

(165) Dandapat R., Deb A. Bhattacharyya S.K. Failure modes for FRP wrapped cylindrical concrete columns. *Journal of Reinforced Plastics and Composites.* 2011; 30(7):561-579.

(166) Jalalvand M., Czél G., Wisnom R. Damage analysis of pseudo-ductile thin-ply UD hybrid composites – A new analytical method. *Composites: Part A.* 2015; 69:83-93.

(167) Jalalvand M., Czél G., Wisnom R. Parametric study of failure mechanisms and optimal configurations of pseudo-ductile thin-ply UD hybrid composites. *Composites: Part A* 2015; 74: 123-131.

(168) Altenbach H., Altenbach J., Kissing W. *Mechanics of Composite Structural Elements.* 1st edition. Springer-Verlag Berlin Heidelberg; 2004.

(169) Tsai S.W., Wu E.W. A General Theory of Strength for Anisotropic Materials. *Journal of Composite Materials.* 1971; 5:58-80.

(170) Matthews F.L., Rawlings R.D. *Composite Materials: Engineering and Science.* 1st edition. Woodhead Publishing Limited Cambridge, England; 1993.

(171) Camanho P.P. *Failure Criteria For Fibre-Reinforced Polymer Composites*. Available from: https://web.fe.up.pt/~stpinho/teaching/feup/y0506/fcriteria.pdf [Accessed 31st March 2018]

(172) Li S., Sitnikova E., Liang Y., Kaddour A.S. The Tsai-Wu failure criterion rationalised in the context of UD composites. *Composites: Part A.* 2017; 102:207-217.

(173) Franklin H.G. Classic Theories of Failure of Anisotropic Materials. *Fibre Science and Technology*. 1968: 137-150.

(174) Hoffman O. The Brittle Strength of Orthotropic Materials. *Journal of Composite Materials*. 1967; 1:200-206.

(175) Chamis. C. Failure Criteria For Filamentary Composites – NASA Technical Note National Aeronautics and Space Administration – 1969.

(176) Puck A., Schurmann H. Failure Analysis of FRP Laminates by means of Physically based phenomenological models. *Composites Science and Technology*. 1998; 58: 1045-1067.

(177) Lee C.S., Kim J.H., Kim S.K., Ryu D.M., Lee J.M. Initial and progressive failure analyse for composite laminates using Puck failure criterion and damage coupled finite element method - *Composite Structures*. 2015;12: 406-419.

(178) Meng. M. Effects of marine environment exposure on the static and fatigue mechanical properties of carbon fibre epoxy composite [PhD thesis] - University of Plymouth, 2016. [Cited 2018 May 18] Available from: https://pearl.plymouth.ac.uk/handle/10026.1/5341

(179) Koruche U.S., Patil S.F. Application of Classical Lamination Theory and Analytical Modeling of Laminates. *International Research Journal of Engineering and Technology (IRJET)*. 2015; 2(2):pp. 958-965.

(180) Nettles A.T., Basic Mechanics of Laminated Composite Plates, NASA Reference Publication 1351; 1994.

(181) Jones R.M., (1998) Mechanics of Composite Materials – Second Edition, *Taylor & Francis Ltd.*

(182) Chapter 2 Laminate Theory. Available from: http://bibing.us.es/proyectos/abreproy/70301/fichero/5_Laminate+Theory.pdf [Accessed 8th January 2019]

(183) Tessari M. Studio del Comportamento Auxetico di Materiali Compositi Laminati – Study on the Auxetic Behaviour of Laminates. [Bachelors Thesis] Aerospace Engineering Department, University of Padova. 2013. [Cited 2018 May 18] Available from: http://tesi.cab.unipd.it/44547/1/TESI_TESSARI_MARCO_1012858.pdf

(184) Herakovich C.T. *Mechanics of fibrous composites*. John Wiley and Sons, 1998.

(185) Herakovich C.T. Composite laminates with negative through-the-thickness Poisson's ratio. *Journal of Composite Materials.* 1984; 18:447-455.

(186) McCartney L.N., Kelly. A. Effective thermal and elastic properties of [θ/-θ]s laminates. *Composites Science and Technology*. 2007; 67:646-661.

(187) Gibson A.G. Through-thickness elastic constants of composite laminates. *Journal of Composite Materials.* 2012; 47(28):3487-3499.

(188) Clarke J.F., Duckett R.A., Hine P.J., Hutchinson I.J. & Ward I.M. Negative Poisson's ratios in angle-ply laminates: theory and experiment. *Composites* 1994;25 (9):863-868.

(189) Bower A.F. – Applied Mechanics of Solids – Constitutive Models – Relations between Stress and Strain – Available from: http://solidmechanics.org/text/Chapter3_2/Chapter3_2.htm [Accessed 24th April 2017]

(190) Blackman B.R.K., Pavan A., Williams J.G. *Fracture of Polymers, Composites & Adhesives II* – Volume 32, 1st edition. Elsevier; 2003 Available from: https://books.google.fr/books?id=-DO_gQMIEyUC&pg=PA375&lpg=PA375&dq=v23+carbon+prepreg&source=bl&ots=Bn60ex7e4h&sig=fc_6Ekw0pEleYgT7C8CymR7nddE&hl=en&sa=X&ved=0ahUKEwibxceMgN7bAhUkCcAKHQFiAKo4ChDoAQg6MAM#v=onepage&q=v23%20carbon%20prepreg&f=false [Accessed 18th August 2017]

(191) Sutherland B. Experimental and Analytical Analysis of the Stress-Strain Diagram of FRP Confined Concrete with Different Loading Rates [Masters thesis] Kansas State University, 2007. [Cited 2018 June 7] Available from: https://core.ac.uk/download/pdf/5164514.pdf

(192) Concrete Society. Design guidance for strengthening concrete structures with fibre composite materials. Technical Report. No.55, 2nd edition, Crowthorne, Berkshire, U.K. 2004.

(193) Gerstle K.H. Simple formulation of biaxial concrete behaviour. *ACI Journal.* 1981; 78(1): 62-68.

(194) Gerstle K.H. Simple formulation of triaxial conocrete behaviour. *ACI Journal.* 1981; 78 (5): 382-387.

(195) Azo Materials – An Introduction to Auxetic Materials: an Interview with Professor Andrew Alderson. Available from: https://www.azom.com/article.aspx?ArticleID=11450 [Accessed 24th March 2018]

(196) Imetrum Non Contact Precision Measurement - Tensile Testing – Available from: https://www.imetrum.com/material-testing/tensile-testing/ [Accessed July 11, 2015]

(197) British Standards Institution. BS EN 12390-1:2012. *Testing hardened concrete. Shape, dimensions and other requirements for specimens and moulds.* London: BSI; 2012.

(198) British Standard Institution. BS EN 206: 2013. *Concrete – Specification, performance, production and conformity.* London: BSI; 2013.

(199) British Standard Institution. BS EN 206:2013+A1:2016. *Concrete. Specification, performance, production and conformity.* London: BSI: 2016.

(200) Hamad A.J. Size and shape effect of specimen on the compressive strength of HPLWFC reinforced with glass fibres. *Journal of King Saud University-Engineering Sciences*. 2017; 29:373-380.

(201) Kim J.K., Seong Tae Y. Application of size effect to compressive strength of concrete members, Sadhana – *Academy Proceeding in Engineering Sciences*. 2002; 27(4): 467-484.

(202) Gilkey, H.J. Water-cement Ratio versus Strength-Another Look. *Journal of the American Concrete Institute Part 2*. 1961; 58:1851-1878.

(203) Seffo M., Hamcho M. Strength of Concrete Cylinder Confined by Composite Materials (CFRP) *Energy Procedia.* 2012; 19: 276-285

(204) ASTM International. ASTM D7616/D7616M-11(2017) *Standard Test Method for Determining Apparent Overlap Splice Shear Strength Properties of Wet Lay-Up Fiber-Reinforced Polymer Matrix Composites Used for Strengthening Civil Structures.* ASTM International, West Conshohocken, PA, 2017.

(205) Concrete Society. *Design guidance for strengthening concrete structures using fibre composite materials - 3rd edition (includes amendment No.1 dated October 2013)* The Concrete Society, Wiltshire UK. Technical Report number: 55, 2013.

(206) Arya C., Clarke J.L., Kay E.A., O'Regan P.D. TR55: Design guidance for strengthening concrete structures using fibre composite materials: A review. *Engineering Structures*. 2002; 24:889-900.

(207) Vishay Precision Group. *Micro-Measurements*. Available from: http://www.vishaypg.com/micro-measurements/ [Accessed 12th March 2015].

(208) Sitharam T.G., GvindaRaju L. Module 4: Stress-Strain Reltaions, In: *Applied elasticity for Engineers.* Available from: https://nptel.ac.in/courses/105108070/module4/lecture8.pdf [Accessed 24th April 2018]

(209) ASTM International. ASTM C39/C39M-18 *Standard test method for compressive strength of cylindrical concrete specimens.* ASTM International, West Conshohocken, PA, 2018.

(210) Toutanji H.A. Stress-strain characteristics of concrete columns externally confined with advanced fiber composite sheets. *ACI Materials Journal.* 1999;96(3): 397-404.

(211) Popovics S. Review of Stress-Strain Relationships of Concrete. *Journal of the American Concrete Institute.* 1970; 67(3):243-248

(212) Donoghue J.P., Alderson K.L., Evans K.E. The fracture toughness of composite laminates with a negative Poisson's ratio, *Phys. Status Solidi B.* 2009; 246 (9): 2011-2017.

(213) Attard S. Email sent to: Tim Coope. 5th April 2018

(214) Argatvo I., Guinovart-Diaz R., Sabina F.J. On local indentation and impact compliance of isotropic auxetic materials from the continuum mechanics viewpoint. *International Journal of Engineering Sceince.* 2012; 54:42-57.

(215) Alderson K.L., Alderson A., Smart G., Simkins VR., Davies P.J. Auxetic polypropylene fibres, Part 1. Manufacture and characterisation. *Plastics. Rubber and Composites.* 2002; 31: 344-349.

(216) Corradi M., Grazini A., Borri A. Confinement of brick masonry columns with CFRP materials. *Composites Science and Technology*. 2007; 67:1772-1783.

(217) Sloan M.R., Wright J.R., Evans K.E. The helical auxetic yarn – A novel structure for composites and textiles; geometry, manufacture and mechanical properties. *Mechanics of Materials*. 2011; 43:476-486.

(218) Zhang G., Ghita O., Lin C., Evans K.E. Varying the performance of helical auxetic yarns by altering component properties and geometry. *Composite Structures.* 2016; 140: 369-377.

APPENDIX A

DATA SHEETS

PROVIDED BY GURIT

SA 70

Epoxy Adhesive Film

- Low temperature cure
- Designed for bonding prepreg skins to honeycomb and certain foam cores
- Compatible with SE 70 prepregs
- Toughened for impact resistance and peel strength
- Controlled flow for maximum bond integrity

Introduction

SA 70 adhesive film is a toughened epoxy film on a glass carrier with excellent tack and drape characteristics. It offers many advantages over traditional wet lay-up techniques for bonding of composite skins to cores, including: consistent bond-line thickness and weight, high strain to failure, high toughness, handling convenience, controlled flow and a 4 week outlife at ambient temperature (21°C).

Properties

Uncured Resin Properties			
Adhesive Film Weight (standard products)	150gm^2	250gm^2	400gm^2
Glass Carrier Weight	25gm^2	25gm^2	25gm^2
Total Film Weight	175gm^2	275gm^2	425gm^2
Resin Colour	Turquoise blue		
Stability @ 21°C	4 weeks		
Stability @ -18°C	1 year		

Curing Schedule

Cure Cycles	
at 85% vacuum pressure (650mm hg) throughout	
Minimum cure time at 70ºC	16 hours
Minimum cure time at 80ºC	8 hours
Minimum cure time at 100ºC	2 hours
Minimum cure time at 120ºC	30 minutes

Mechanical Properties

Cure	1 hour @ 120°C	16 hours @ 70°C
Shear Strength on Steel (MPa)	36	35.5
Cleavage Strength on Steel (kN)	9.5	9.25
Tg1 (DMA)	108.3	95.2

SE 70

LOW TEMPERATURE CURE HIGH TOUGHNESS EPOXY PREPREG SYSTEM

- **Low temperature 70°C (158°F) curing**
  - Faster cycle times at elevated temperature
  - Excellent balance of mechanical properties and toughness
  - Long out-life – up to 4 weeks @ 18-22°C (64-72°F)
  - Range of compatible adhesive films and ancillary products
  - Excellent surface finish
  - Good Tg
- **Suitable for vacuum bag, press or autoclave consolidation**
  - Germanischer Lloyd Certified

INTRODUCTION

SE70 is part of the range of prepreg products. This unique product range provides technically and commercially competitive engineering materials, ideal for use either solely, or in conjunction with other products from within the product range along with other Gurit products.

SE70 is a hot melt epoxy prepreg ideally suited to the manufacture of thick sections. It can be cured at temperatures as low as 70ºC (158ºF), but can also be used for the rapid manufacture of components through its 25-minute cure at 120ºC (248ºF). All of this can be achieved together with out-life of 28 days at 21ºC (70ºF).

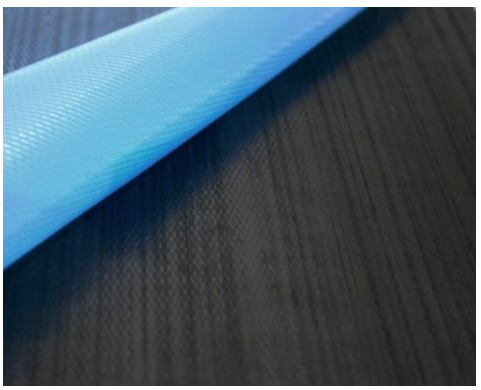

SE70 is designed for vacuum bag pressing and offers excellent mechanical performance on glass fibre reinforcements. Currently SE70 is manufactured into a prepreg structure with E-glass and Carbon fibres, which are manufactured into biax or woven materials. This data sheet is concerned with carbon reinforcements.

DNV·GL

MINIMUM CURE TIME & TEMPERATURE

Recommended minimum cure is 16 hours at 70°C (158°F) using vacuum bag processing.

PROPERTY	OVEN / VAC BAG				TEST STANDARD
Typical Laminate	8 plies of 200g/m^2 HEC UD carbon 37% resin content				-
Typical Ramp Rate	1 – 2°C (2 – 4°F) per minute				-
Cure Temperature	70°C (158°F)	80°C (176°F)	95°C (203°F)	110°C (230°F)	-
Cure Dwell Time	16 hours	8 hours	4 hours	50 minutes	-
Cure Pressure	-1bar (14.5Psi)				-
De-mould Temperature	< 60ºC / 140ºF				-
Dry Tg_1 (DMA)	89ºC / 192ºF	101ºC / 214ºF	110ºC / 230ºF	126 ºC / 259ºF	ISO 6721 (DMA)

*suitable for use in conjunction with hot-in / hot-out rapid component manufacture is possible using appropriate press tooling

LAMINATE PROPERTIES

CURED RESIN PROPERTIES

Oven cured using standard processing techniques and a minimum cure time of 16 hours at 70°C (158°F).

PROPERTY	SYMBOL	SE 70 RESIN CAST		TEST STANDARD
Tensile Strength	σ_T	54 MPa	7.83 ksi	ISO 527-2
Tensile Modulus	E_T	3.61 GPa	0.52 Msi	ISO 527-2
Flexural Strength	σ_F	80 MPa	11.6 Ksi	ISO 178
Flexural Modulus	E_F	3.45 GPa	0.50 Msi	ISO 178
Compressive Strength	σ_C	142 MPa	20.6 Ksi	ISO 604
Compressive Modulus	E_C	3.81 GPa	0.55 Msi	ISO 604

UNIDIRECTIONAL LAMINATE PROPERTIES

Cured using standard processing techniques at the standard cure cycle of 16 hours at 70ºC (ºF).

PROPERTY	SYMBOL	HEC 200		TEST STANDARD
Resin Content	-	37 %		-
Cure Method	-	Vacuum bag cured at -1 bar		-
Cure Schedule	-	16 hours at 70°C (158°F)		-
Glass Transition Temperature	Tg_1	89ºC	192ºF	ISO 6721 (DMA)
Cured Ply Thickness	t_{ply}	0.20 mm	0.008 in	ASTM D 3171 Method II
0° Tensile Cured Fibre Volume*	V_f	54.7 %		ASTM D 3171 Method II
0° Tensile Strength (Normalised to 60%)	X_T	2524 MPa	366 ksi	ISO 527-4
0° Tensile Modulus (Normalised to 60%)	E_t	137 GPa	19.9 Msi	ISO 527-4
0° Compressive Str. Fibre Volume*	V_f	55.2 %		ASTM D 3171 Method II
0° Compressive Strength (Normalised to 60%)	X_C	1490 MPa	216 ksi	SACMA SRM1-94
0° Compressive Mod. Fibre Volume*	V_f	56.0 %		ASTM D 3171 Method II
0° Compressive Modulus (Normalised to 60%)	E_{C11}	126 GPa	18.3 Msi	SACMA SRM1-94
90° Tensile Cured Fibre Volume*	V_f	54.0 %		ASTM D 3171 Method II
90° Tensile Strength	Y_T	42 MPa	6.1 ksi	ISO 527-4
90° Tensile Modulus	E_{T22}	7.81 GPa	1.13 Msi	ISO 527-4
0° Flexural Fibre Volume*		55.9 %		ASTM D 3171 Method II
0° Flexural Strength	X_F	1406 MPa	204 ksi	ISO 14125
0° Flexural Modulus	E_{F11}	99 GPa	14.4 Msi	ISO 14125
0° ILSS Fibre Volume*	V_f	50.8 %		ASTM D 3171 Method II
0° ILSS	X_{ILSS}	86 MPa	12.5 ksi	ISO 14130

* original laminate fibre volme fraction

APPENDIX B

CYLINDER SETS I & II:
STRESS STRAIN DIAGRAMS
OF TESTED CYLINDERS

Sample 17 – $[\pm 20]_{2s}$
Stress (MPa) vs Strain (%)

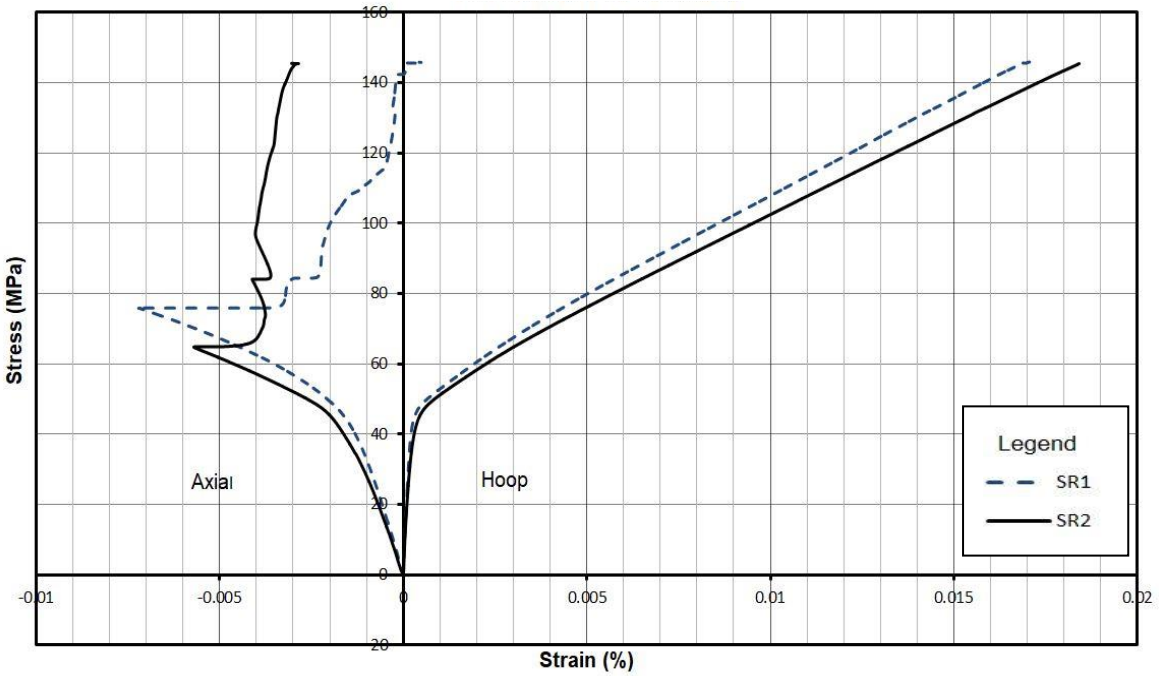

Figure B.1 – Stress (MPa) vs Strain (%)–Stacking Sequence $[\pm 20]_{2s}$ representing readings of Strain Gauge Rosette I & II for Sample 17. Cylinders tested using a Force Control System.

Sample 18 – $[\pm 20]_{2s}$
Stress (MPa) vs Strain (%)

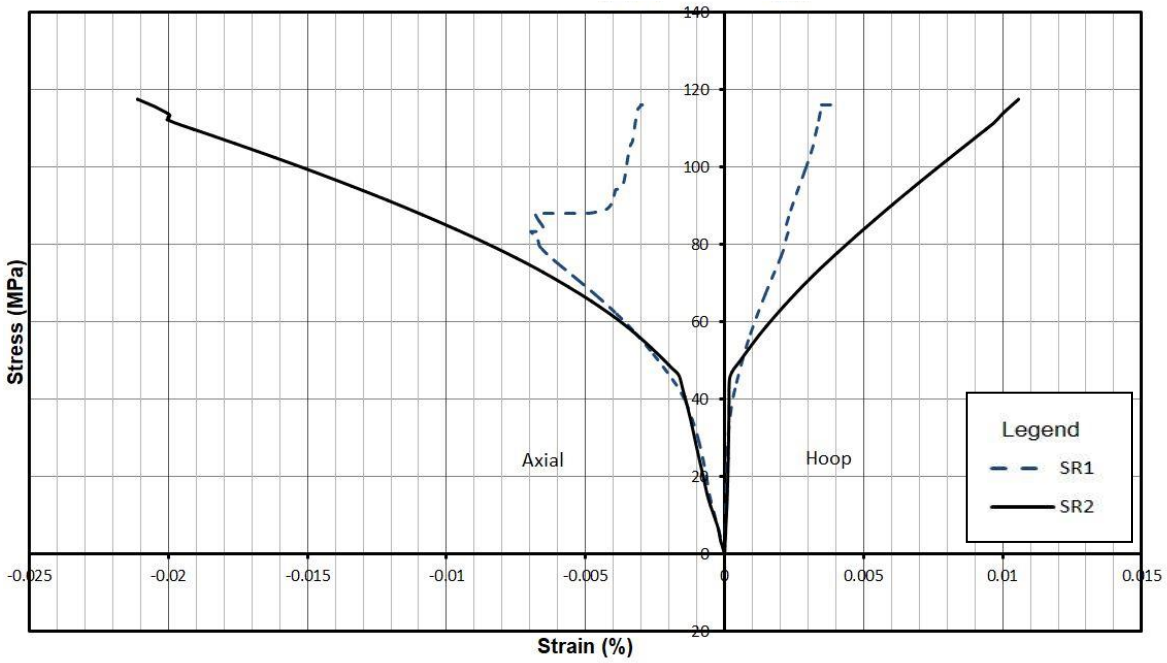

Figure B.2 – Stress (MPa) vs Strain (%)–Stacking Sequence $[\pm 20]_{2s}$ representing readings of Strain Gauge Rosette I & II for Sample 18. Cylinders tested using a Force Control System.

Sample 19 – $[\pm 20]_{2s}$
Stress (MPa) vs Strain (%)

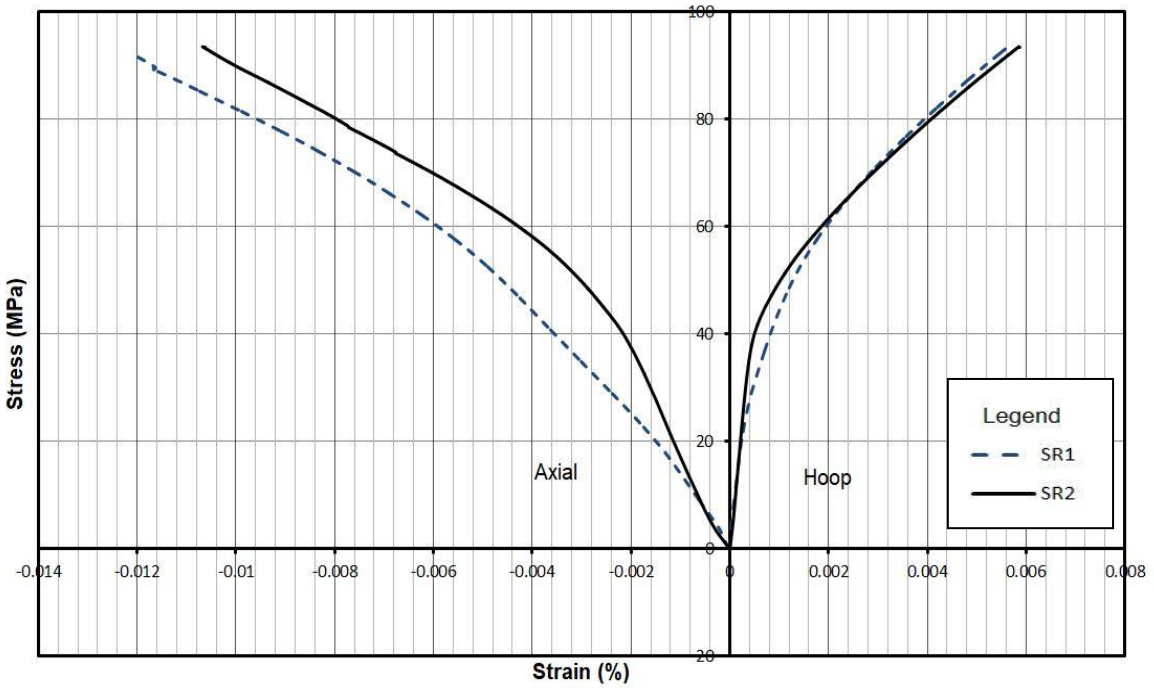

Figure B.3 – Stress (MPa) vs Strain (%)–Stacking Sequence $[\pm 20]_{2s}$ representing readings of Strain Gauge Rosette I & II for Sample 19. Cylinders tested using a Force Control System.

Sample 20 – $[\pm 20]_{2s}$
Stress (MPa) vs Strain (%)

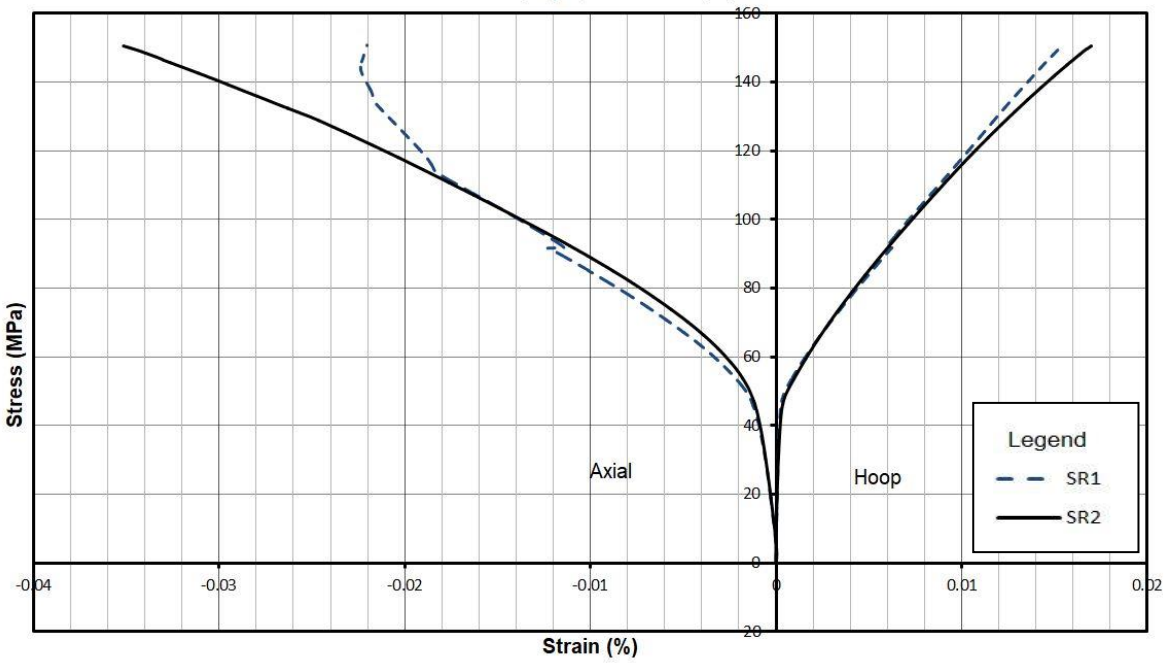

Figure B.4 Stress (MPa) vs Strain (%)–Stacking Sequence $[\pm 20]_{2s}$ representing readings of Strain Gauge Rosette I & II for Sample 20. Cylinders tested using a Force Control System.

Sample 21 – $[\pm 25]_{2s}$
Stress (MPa) vs Strain (%)

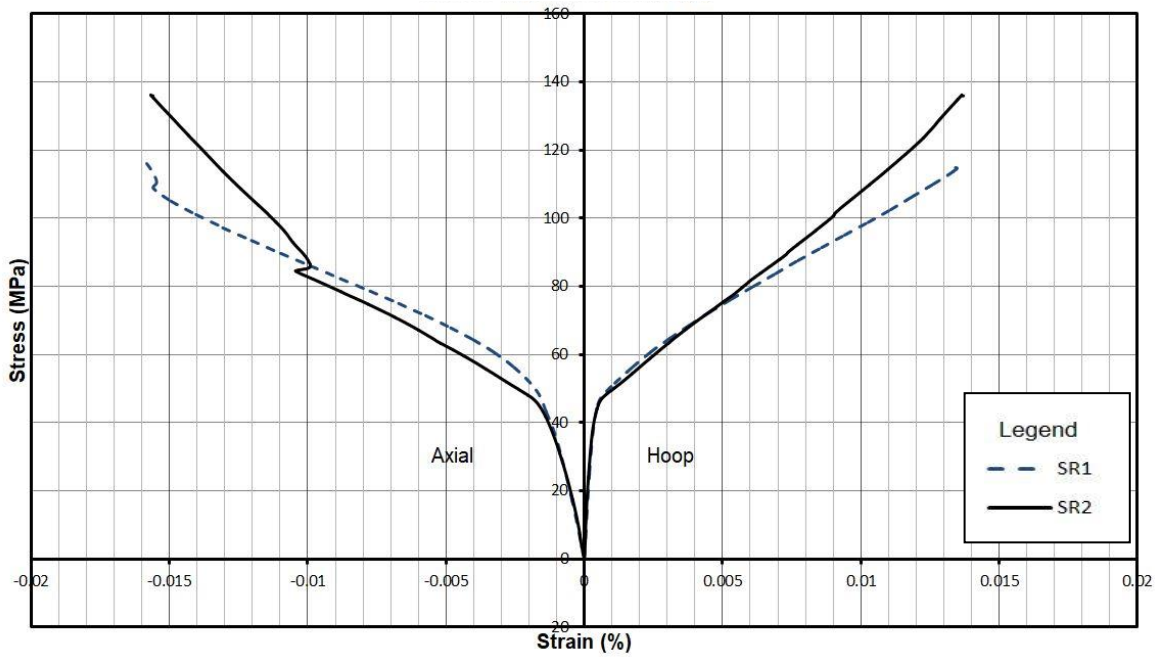

Figure B.5 – Stress (MPa) vs Strain (%)–Stacking Sequence $[\pm 25]_{2s}$ representing readings of Strain Gauge Rosette I & II for Sample 21. Cylinders tested using a Force Control System.

Sample 22 – $[\pm 25]_{2s}$
Stress (MPa) vs Strain (%)

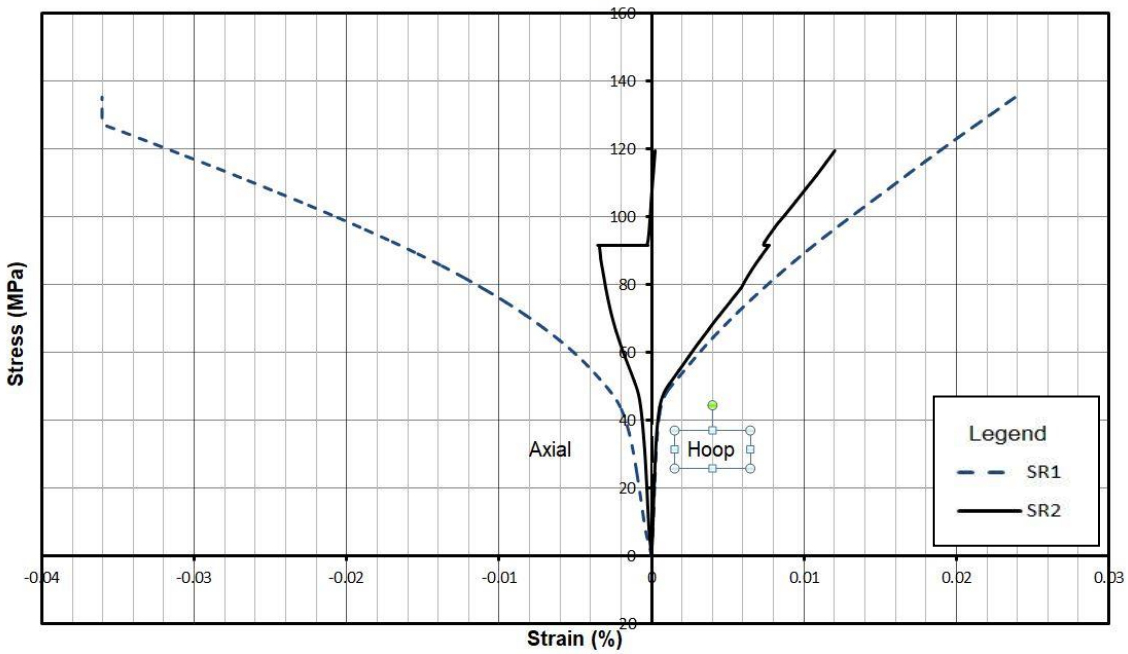

Figure B.6 – Stress (MPa) vs Strain (%)–Stacking Sequence $[\pm 25]_{2s}$ representing readings of Strain Gauge Rosette I & II for Sample 22. Cylinders tested using a Force Control System.

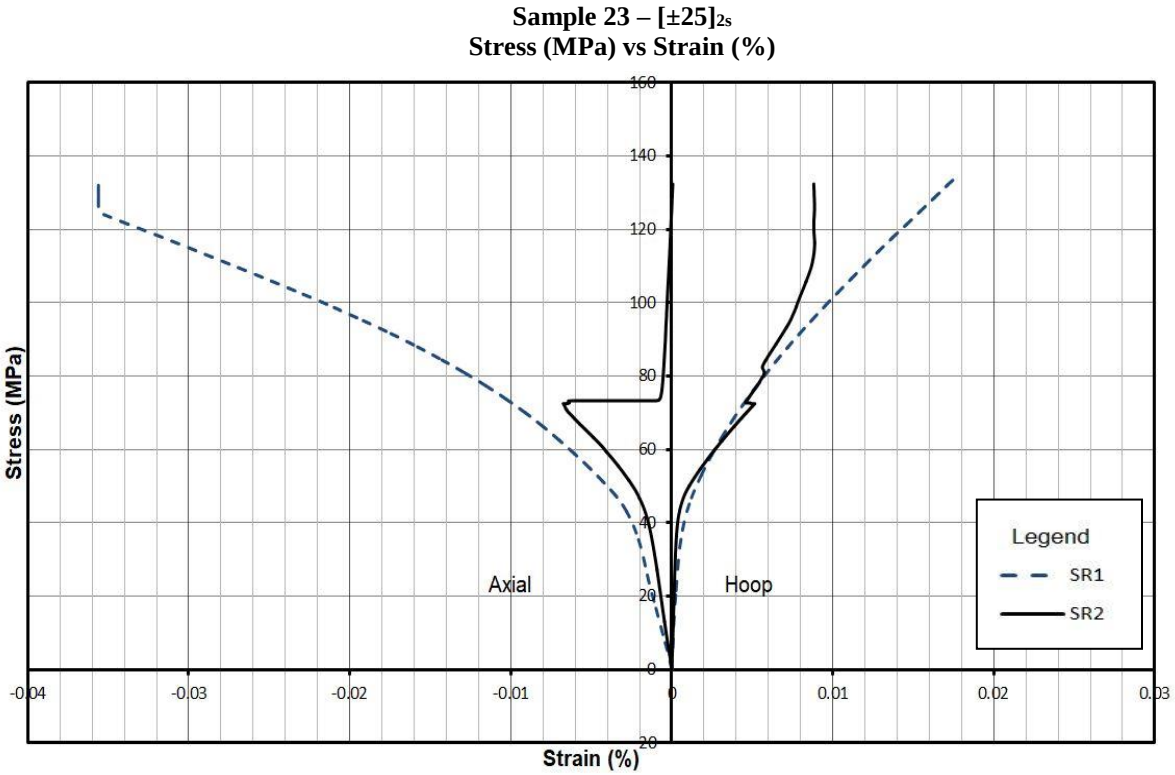

Figure B.7 – Stress (MPa) vs Strain (%)–Stacking Sequence $[\pm 25]_{2s}$ representing readings of Strain Gauge Rosette I & II for Sample 23. Cylinders tested using a Force Control System.

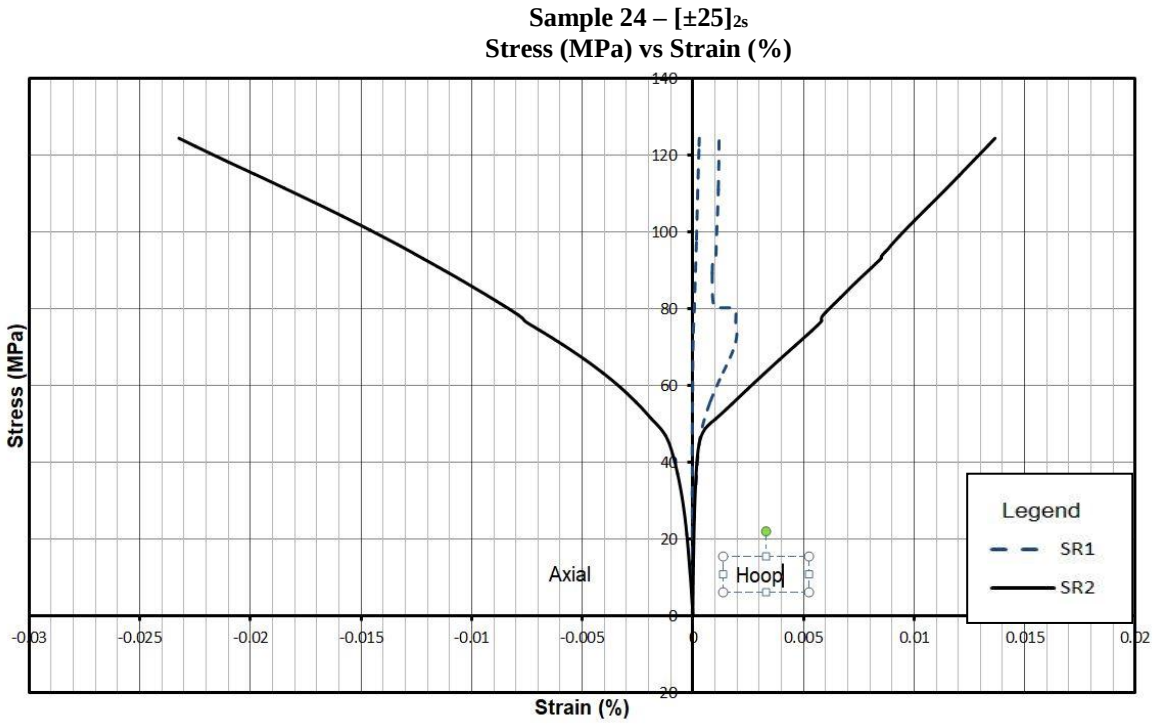

Figure B.8 – Stress (MPa) vs Strain (%)–Stacking Sequence $[\pm 25]_{2s}$ representing readings of Strain Gauge Rosette I & II for Sample 24. Cylinders tested using a Force Control System.

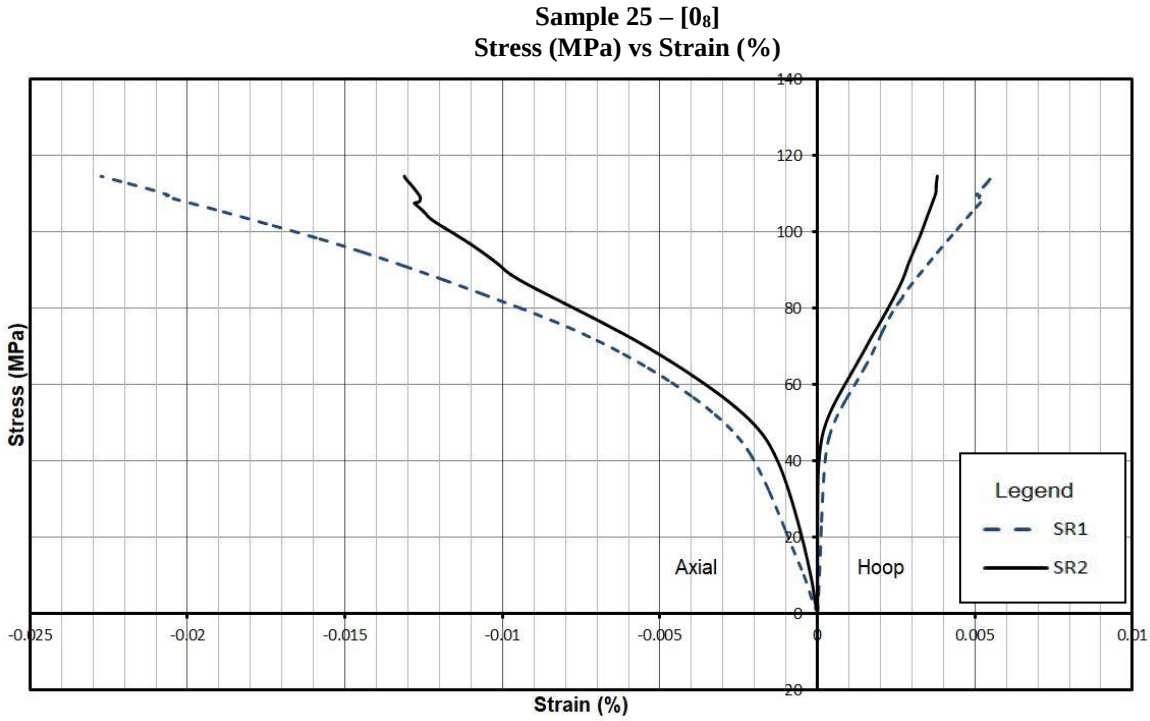

Figure B.9 – Stress (MPa) vs Strain (%)–Stacking Sequence [0_8] representing readings of Strain Gauge Rosette I & II for Sample 25. Cylinders tested using a Force Control System.

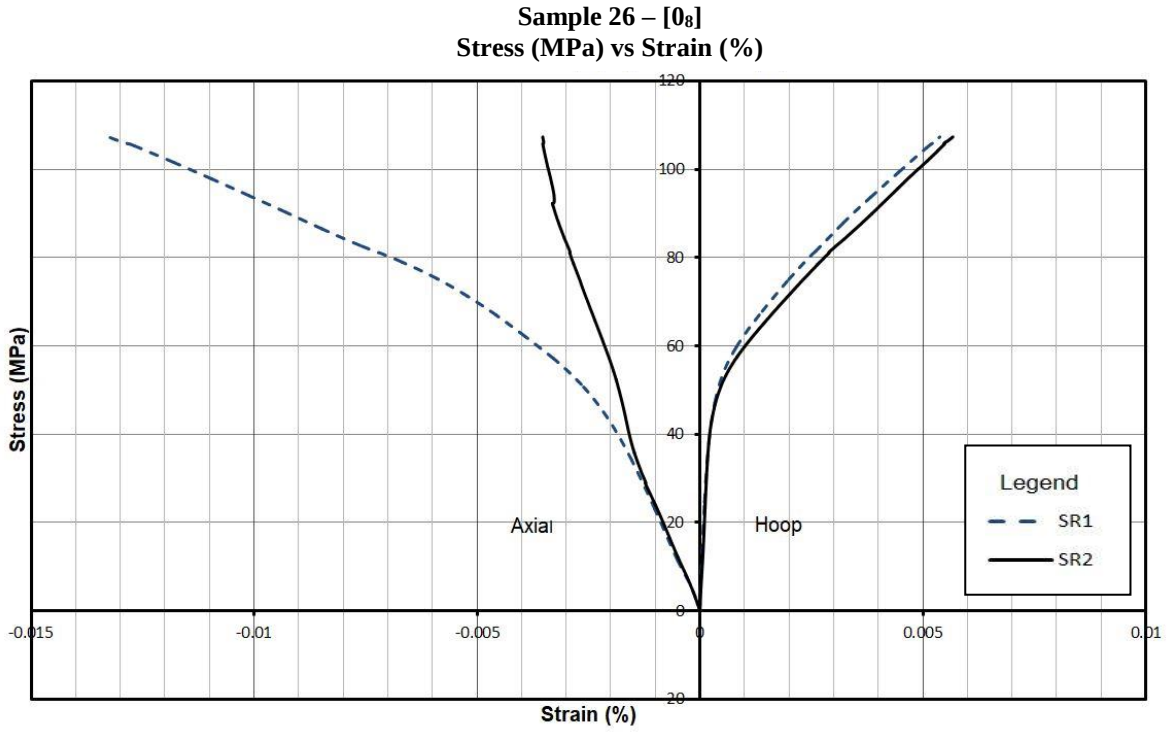

Figure B.10 – Stress (MPa) vs Strain (%)–Stacking Sequence [0_8] representing readings of Strain Gauge Rosette I & II for Sample 26. Cylinders tested using a Force Control System.

Sample 27 – [0_8]
Stress (MPa) vs Strain (%)

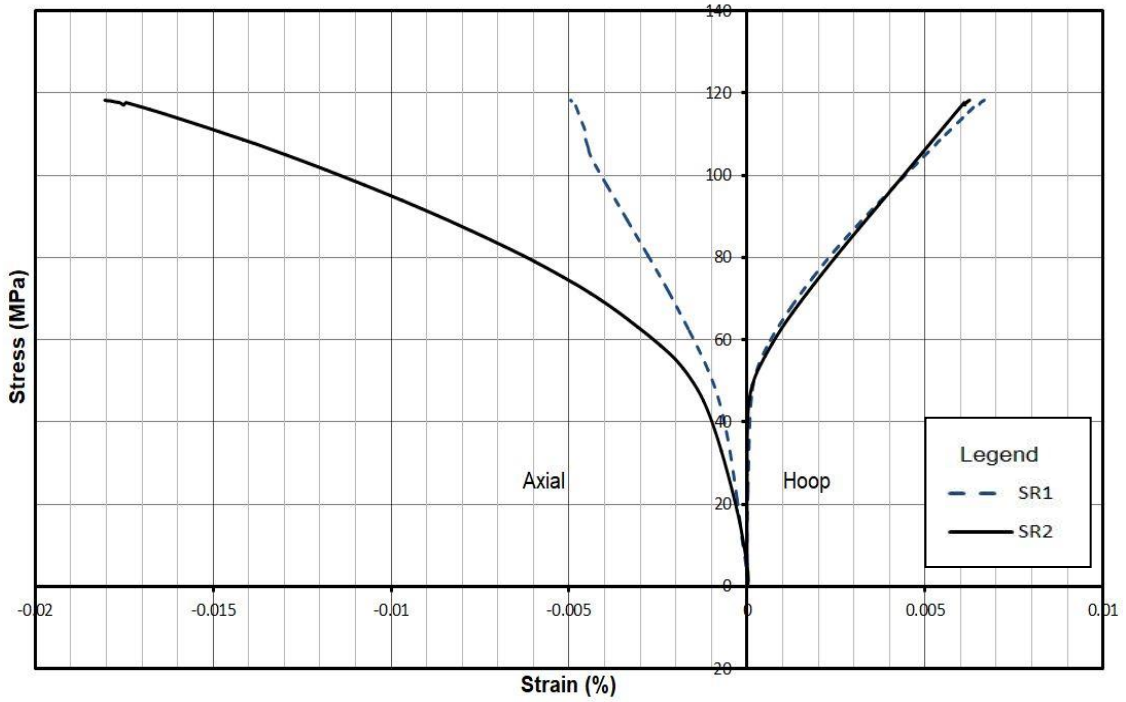

Figure B.11 – Stress (MPa) vs Strain (%)–Stacking Sequence [0_8] representing readings of Strain Gauge Rosette I & II for Sample 27. Cylinders tested using a Force Control System.

Sample 28 – [0_8]
Stress (MPa) vs Strain (%)

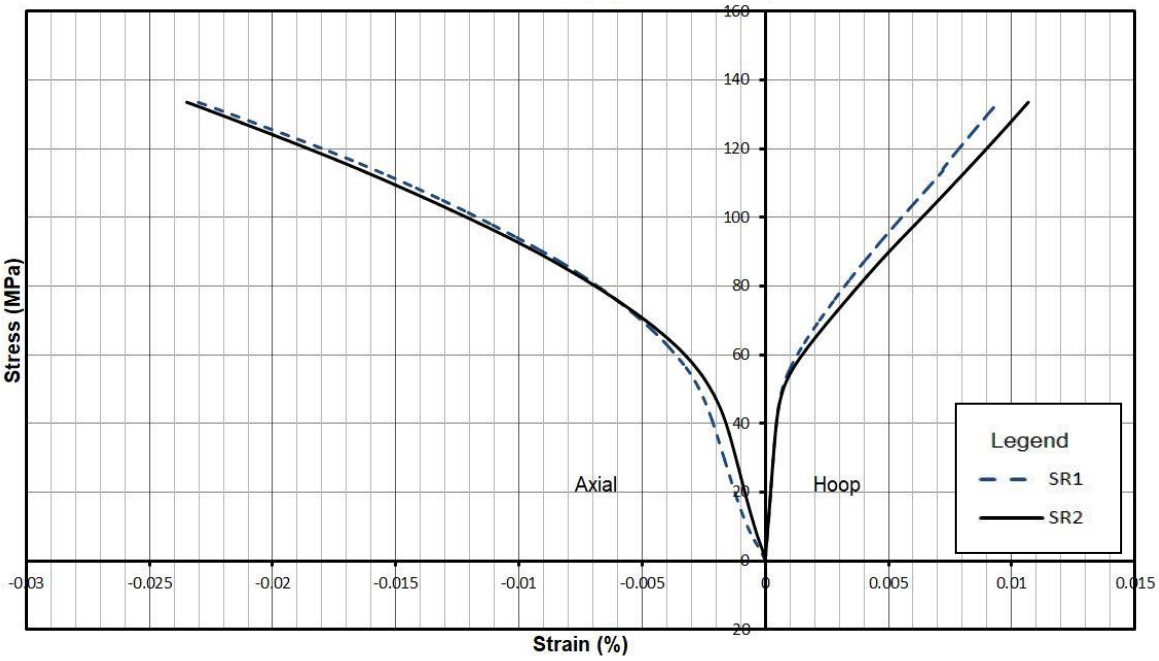

Figure B.12 – Stress (MPa) vs Strain (%)–Stacking Sequence [0_8] representing readings of Strain Gauge Rosette I & II for Sample 28. Cylinders tested using a Force Control System.

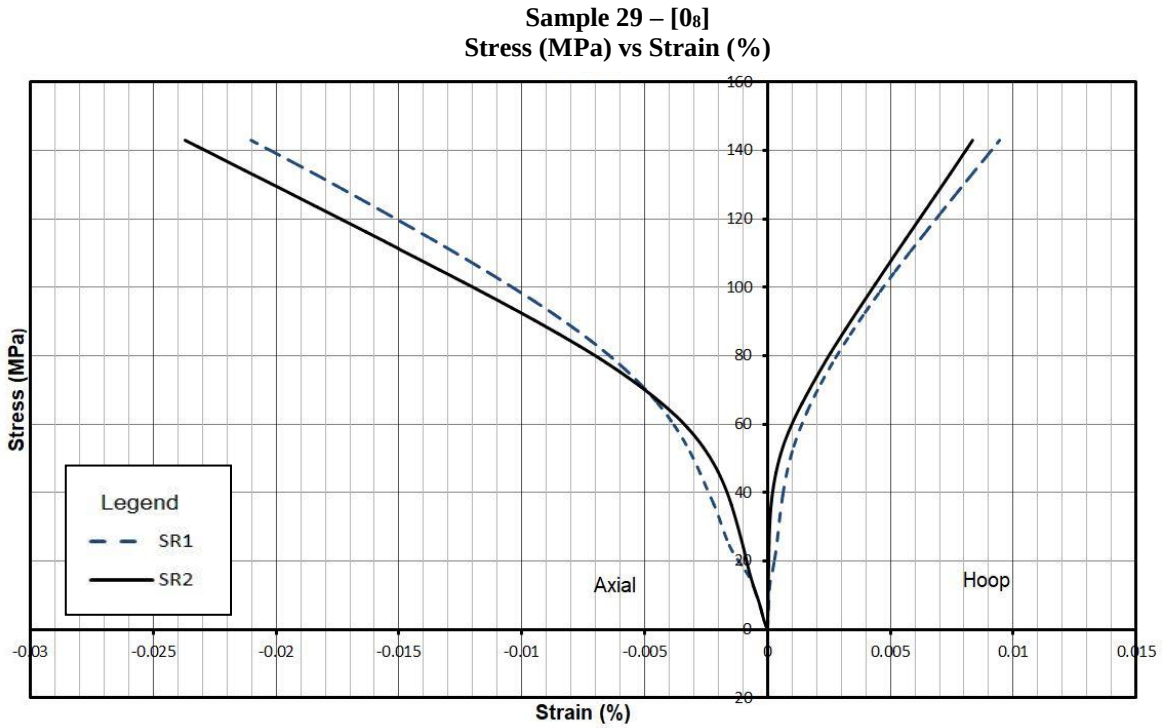

Figure B.13 – Stress (MPa) vs Strain (%)–Stacking Sequence [0_8] representing readings of Strain Gauge Rosette I & II for Sample 29. Cylinders tested using a Force Control System.

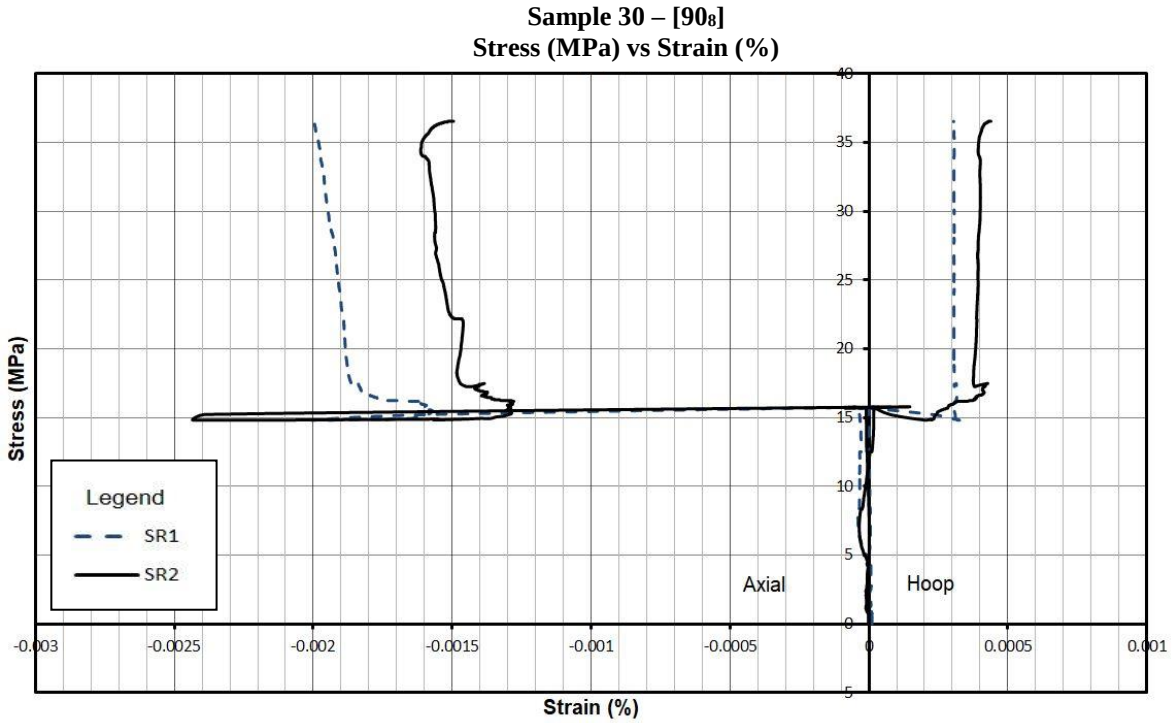

Figure B.14 – Stress (MPa) vs Strain (%)–Stacking Sequence [90_8] representing readings of Strain Gauge Rosette I & II for Sample 30. Cylinders tested using a Force Control System.

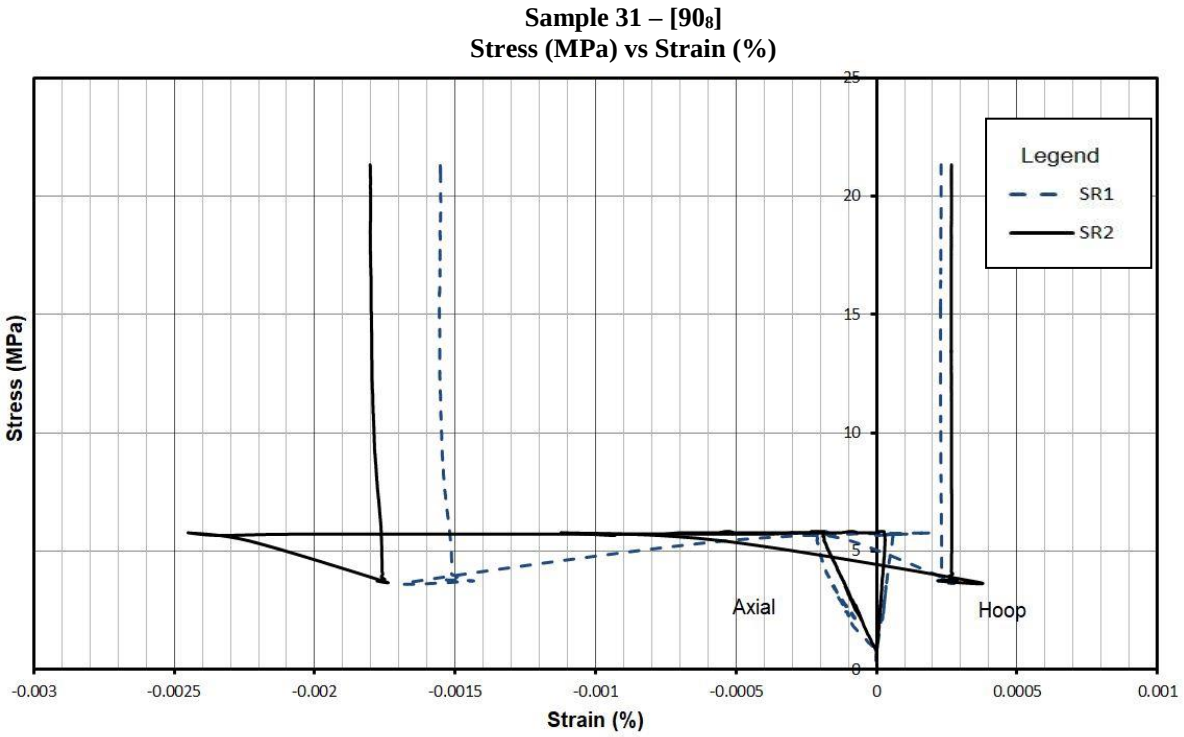

Figure B.15 – Stress (MPa) vs Strain (%)–Stacking Sequence [90_8] representing readings of Strain Gauge Rosette I & II for Sample 31. Cylinders tested using a Force Control System.

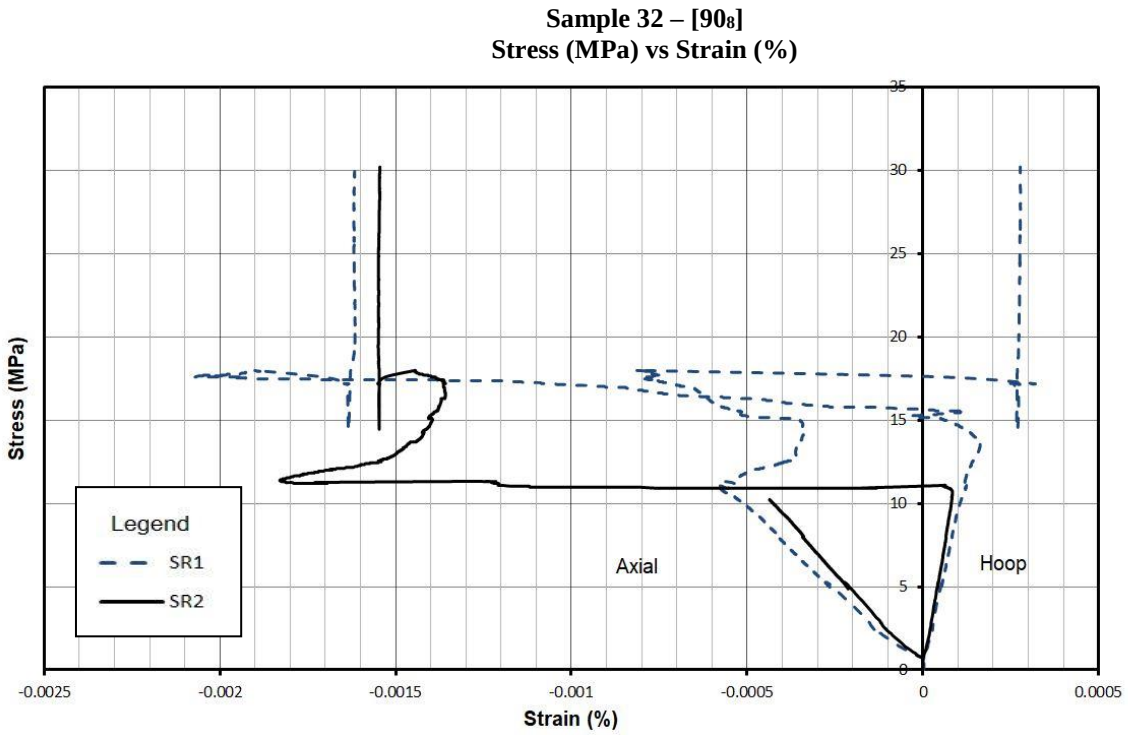

Figure B.16 – Stress (MPa) vs Strain (%)–Stacking Sequence [90_8] representing readings of Strain Gauge Rosette I & II for Sample 32. Cylinders tested using a Force Control System.

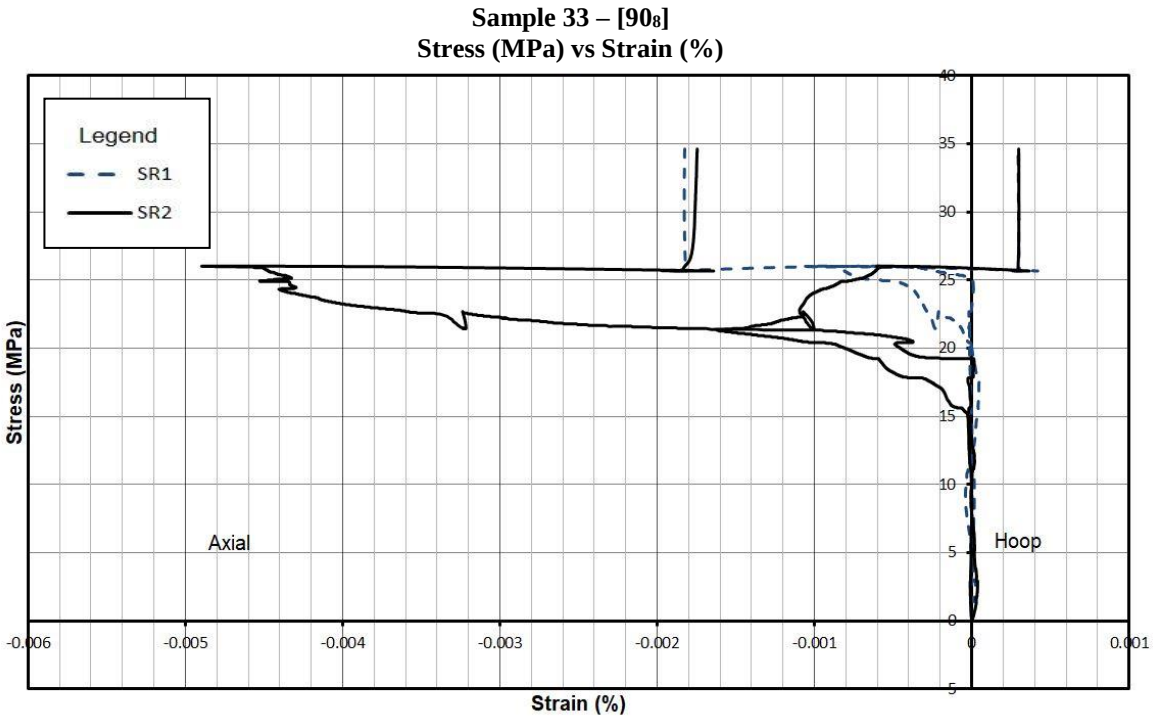

Figure B.17 – Stress (MPa) vs Strain (%)–Stacking Sequence [90_8] representing readings of Strain Gauge Rosette I & II for Sample 33. Cylinders tested using a Force Control System.

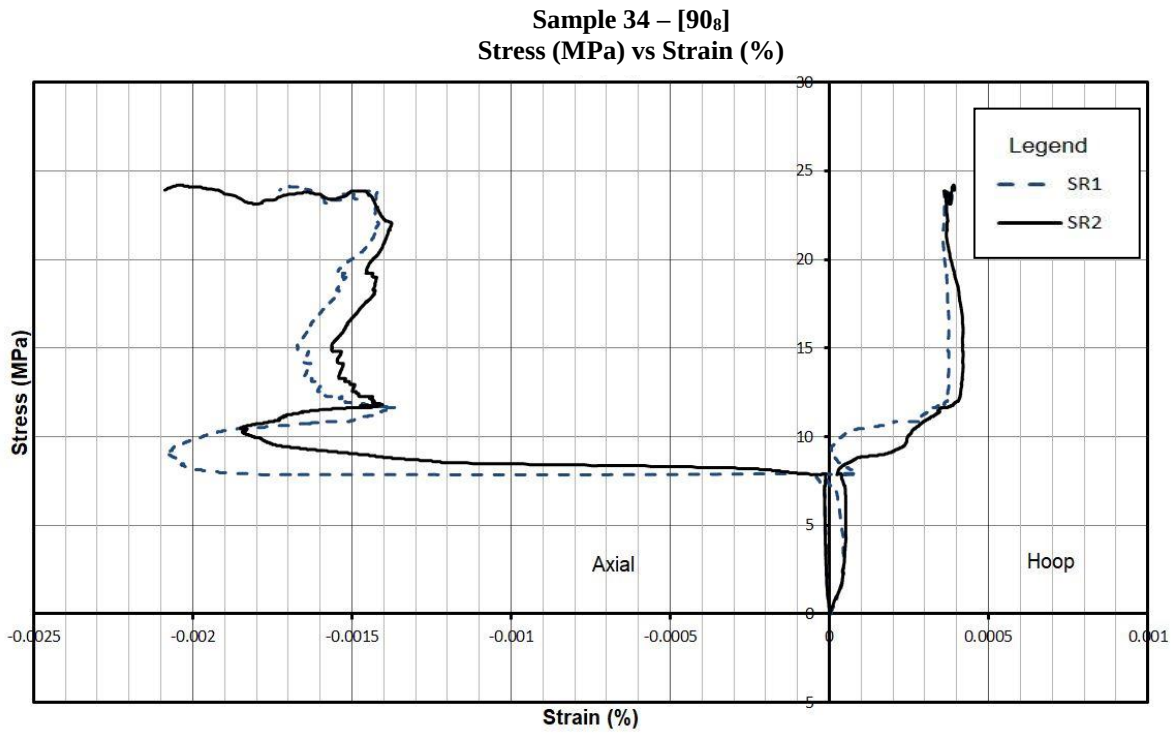

Figure B.18 Stress (MPa) vs Strain (%)–Stacking Sequence [90_8] representing readings of Strain Gauge Rosette I & II for Sample 34. Cylinders tested using a Force Control System.

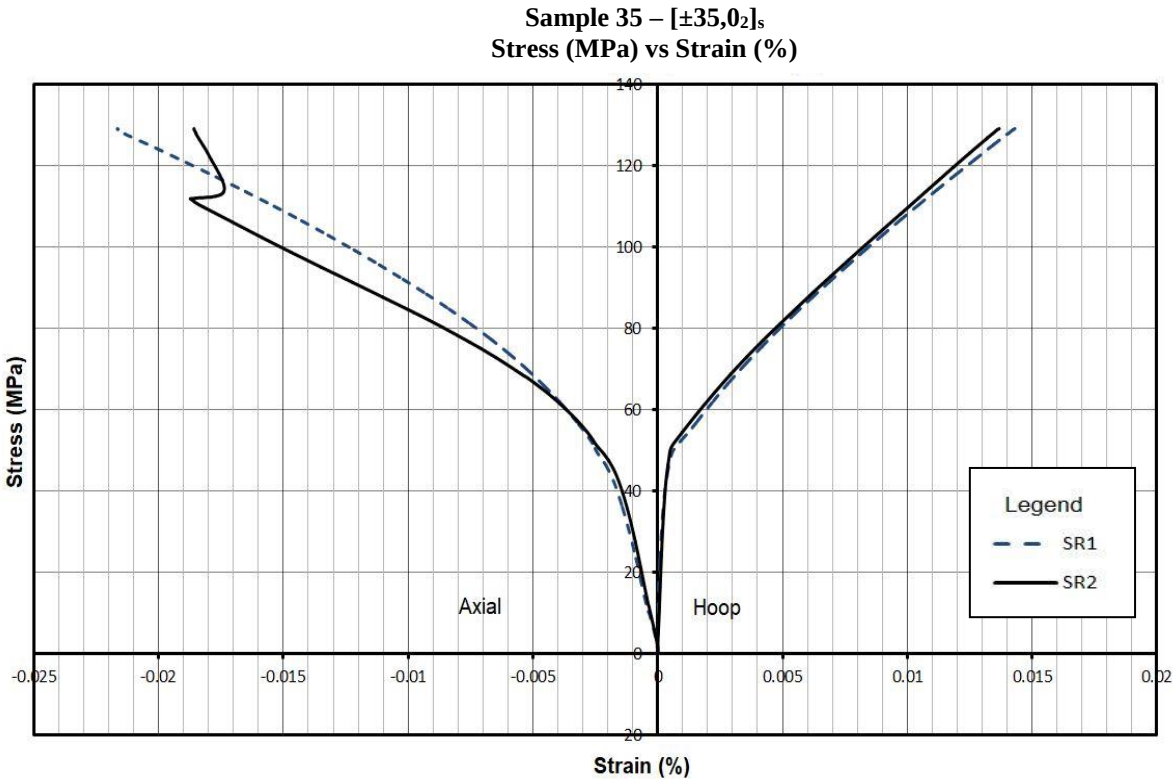

Figure B.19– Stress (MPa) vs Strain (%)–Stacking Sequence $[\pm 35,0_2]_s$ representing readings of Strain Gauge Rosette I & II for Sample 35. Cylinders tested using a Force Control System.

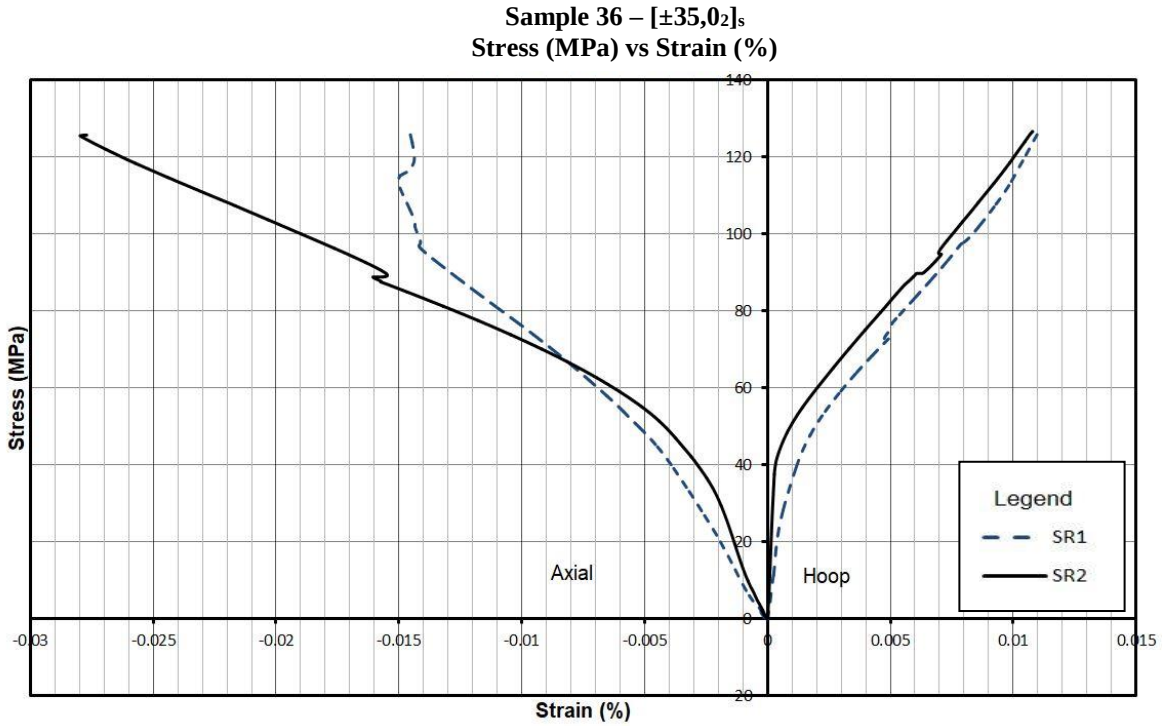

Figure B.20– Stress (MPa) vs Strain (%)–Stacking Sequence $[\pm 35,0_2]_s$ representing readings of Strain Gauge Rosette I & II for Sample 36. Cylinders tested using a Force Control System.

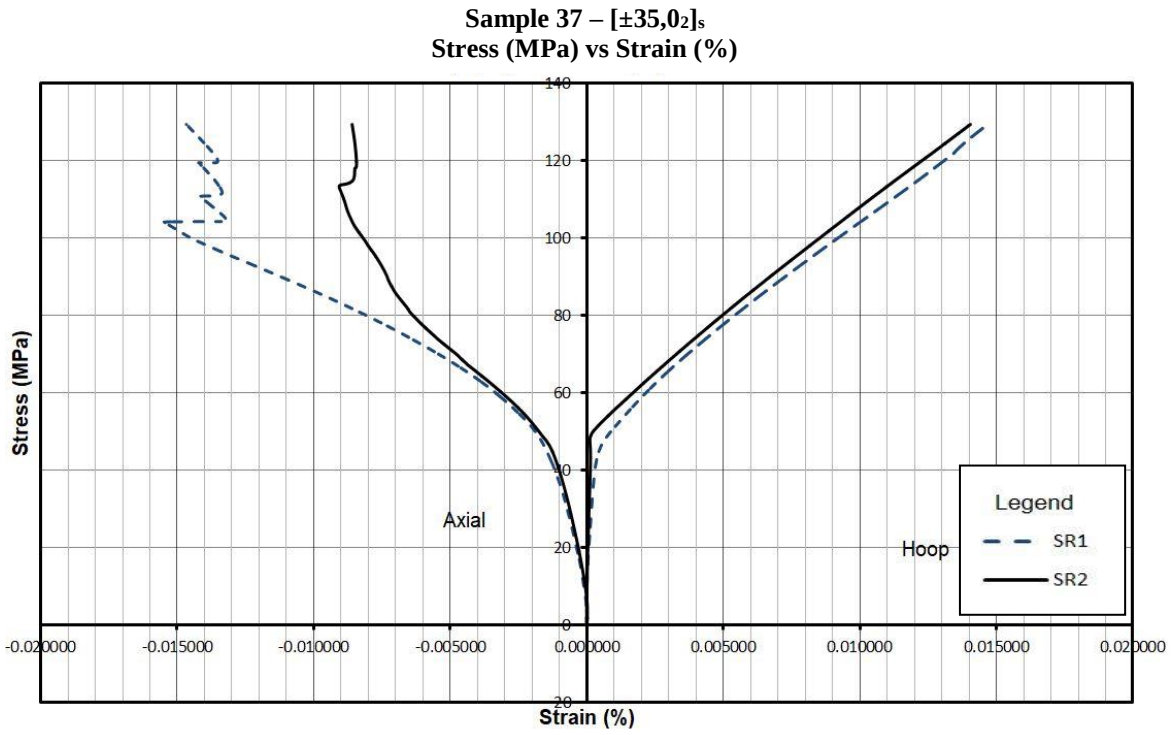

Figure B.21– Stress (MPa) vs Strain (%)–Stacking Sequence $[\pm 35,0_2]_s$ representing readings of Strain Gauge Rosette I & II for Sample 37. Cylinders tested using a Force Control System.

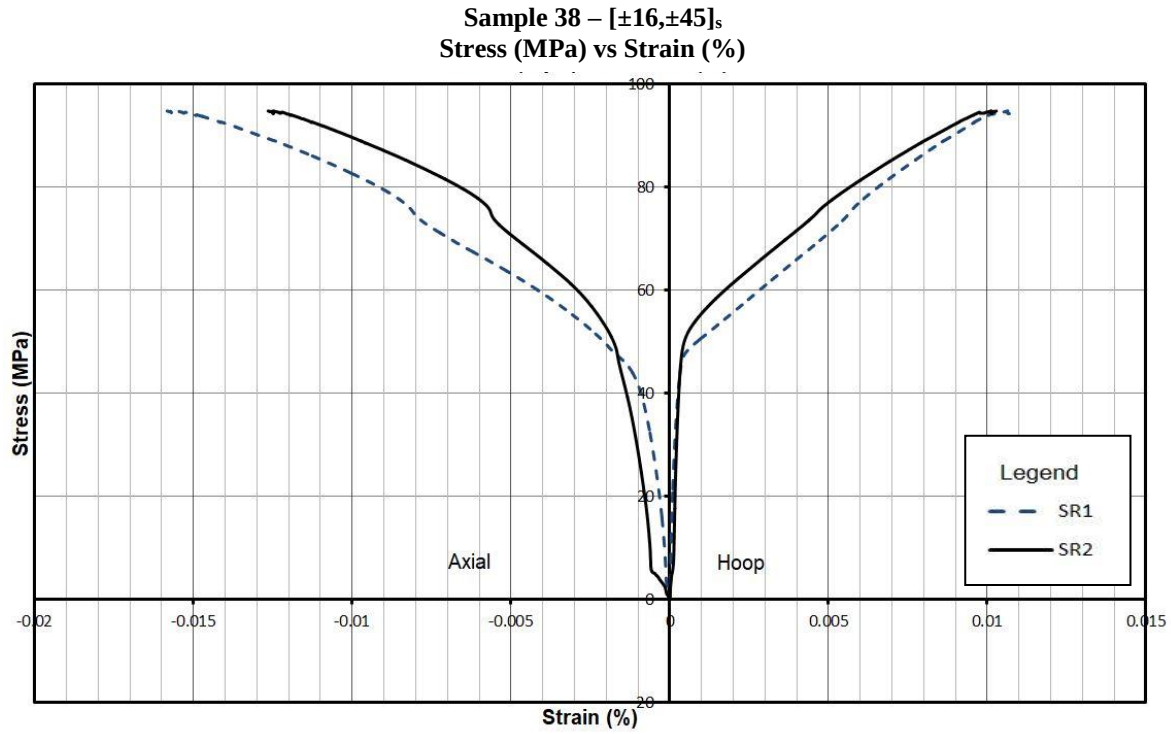

Figure B.22– Stress (MPa) vs Strain (%)–Stacking Sequence $[\pm 16,\pm 45]_s$ representing readings of Strain Gauge Rosette I & II for Sample 38. Cylinders tested using a Force Control System.

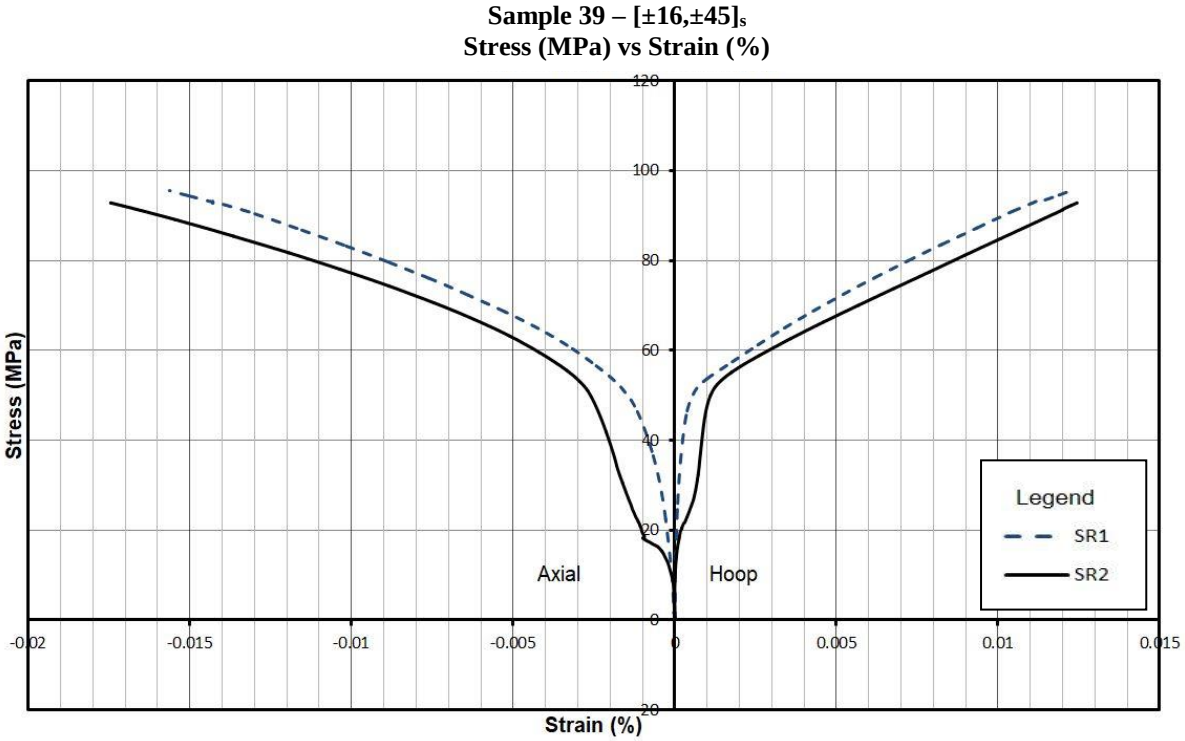

Figure B.23– Stress (MPa) vs Strain (%)–Stacking Sequence $[\pm 16,\pm 45]_s$ representing readings of Strain Gauge Rosette I & II for Sample 39. Cylinders tested using a Force Control System.

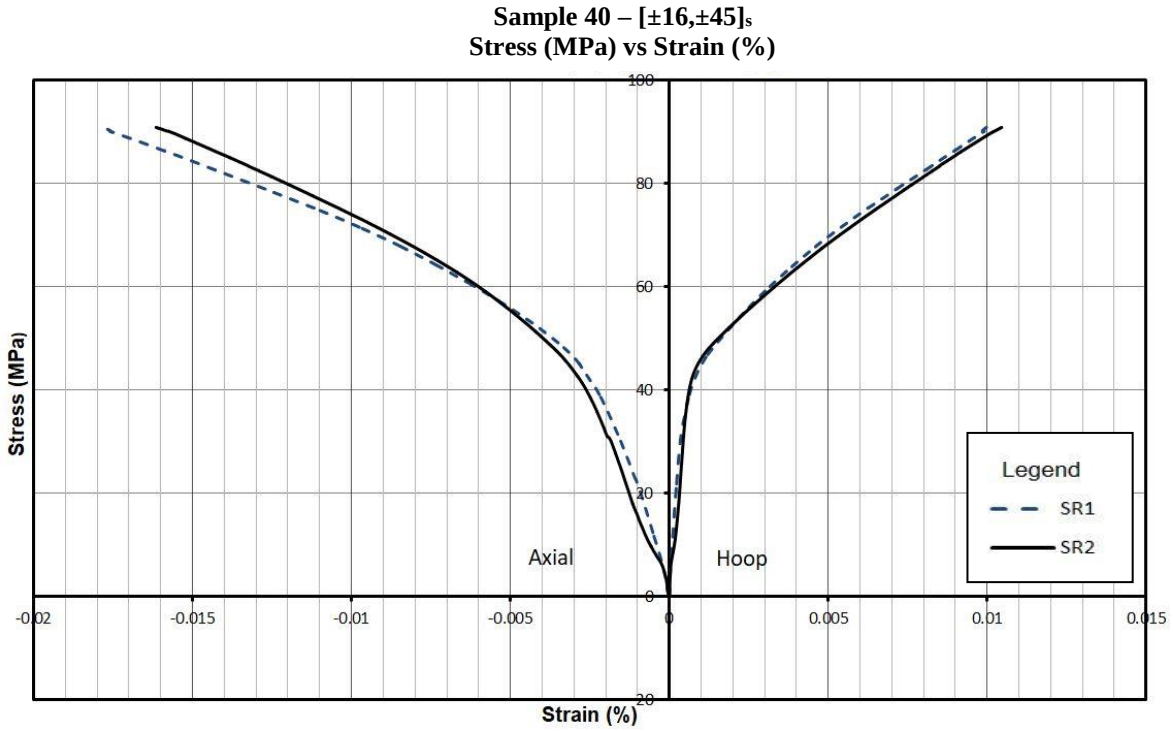

Figure B.24–Stress (MPa) vs Strain (%)–Stacking Sequence $[\pm 16,\pm 45]_s$ representing readings of Strain Gauge Rosette I & II for Sample 40. Cylinders tested using a Force Control System.

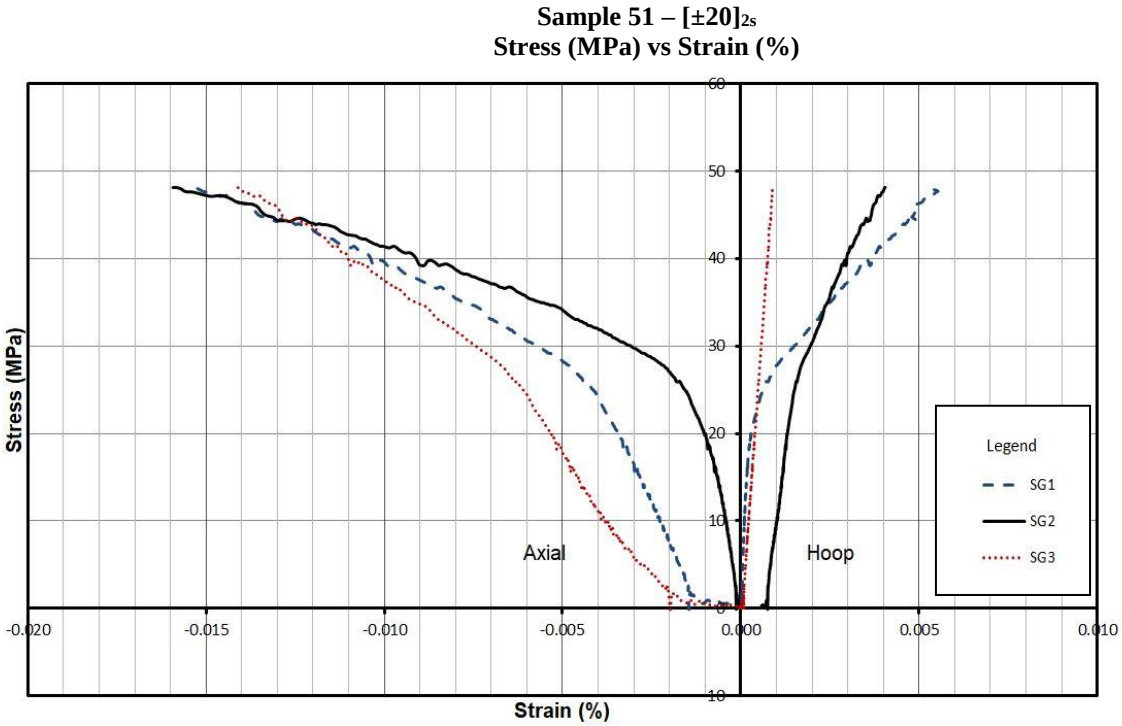

Figure B.25 – Stress (MPa) vs Strain (%) – Stacking Sequence $[\pm 20]_{2s}$ representing readings of Strain Gauges I, II & III for Sample 51.

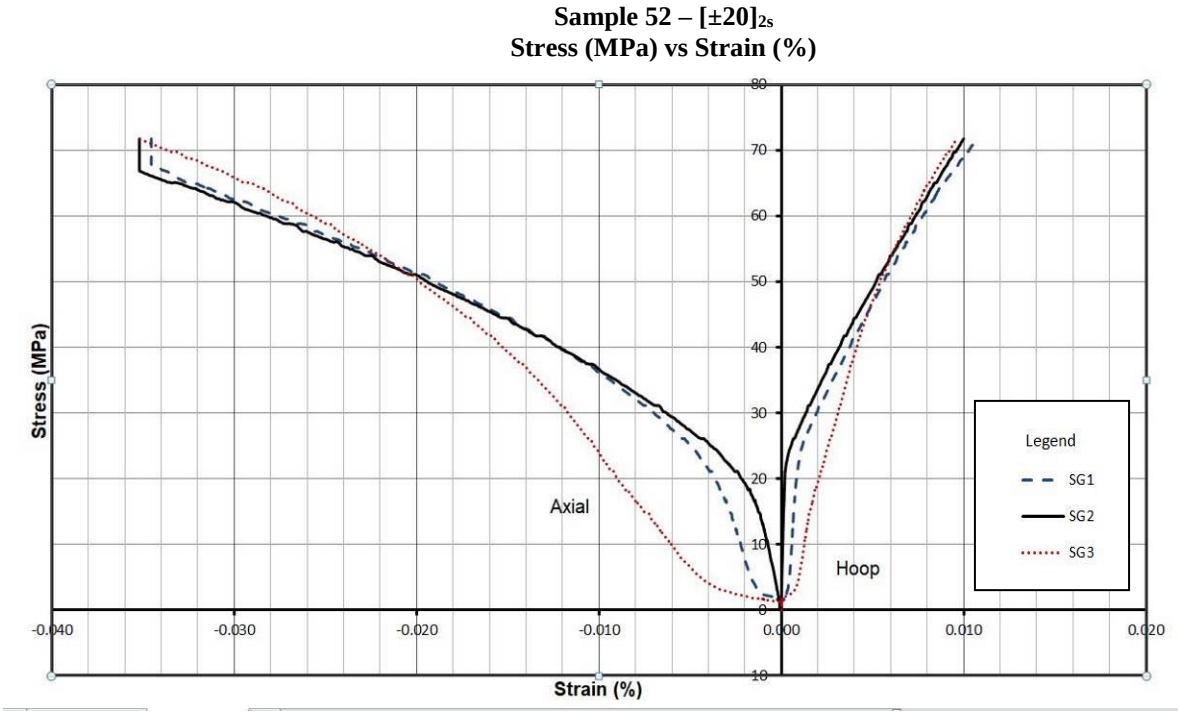

Figure B.26 – Stress (MPa) vs Strain (%) – Stacking Sequence $[\pm 20]_{2s}$ representing readings of Strain Gauges I, II & III for Sample 52.

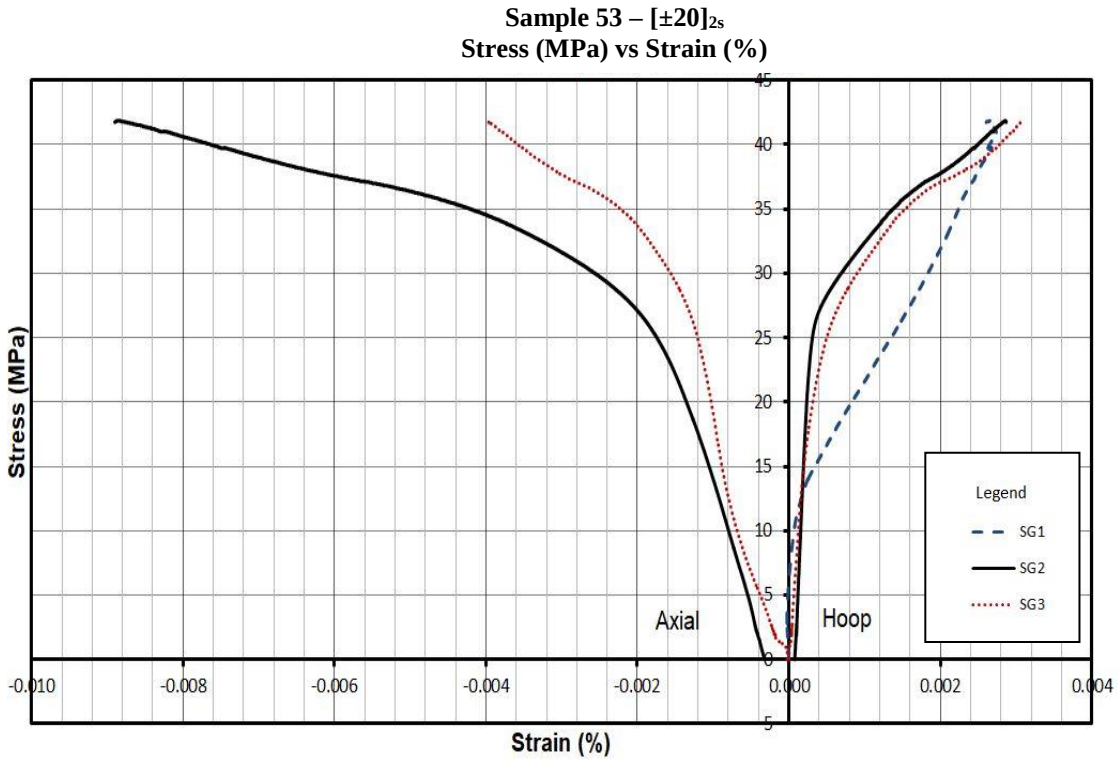

Figure B.27 – Stress (MPa) vs Strain (%) – Stacking Sequence $[\pm 20]_{2s}$ representing readings of Strain Gauges I, II & III for Sample 53.

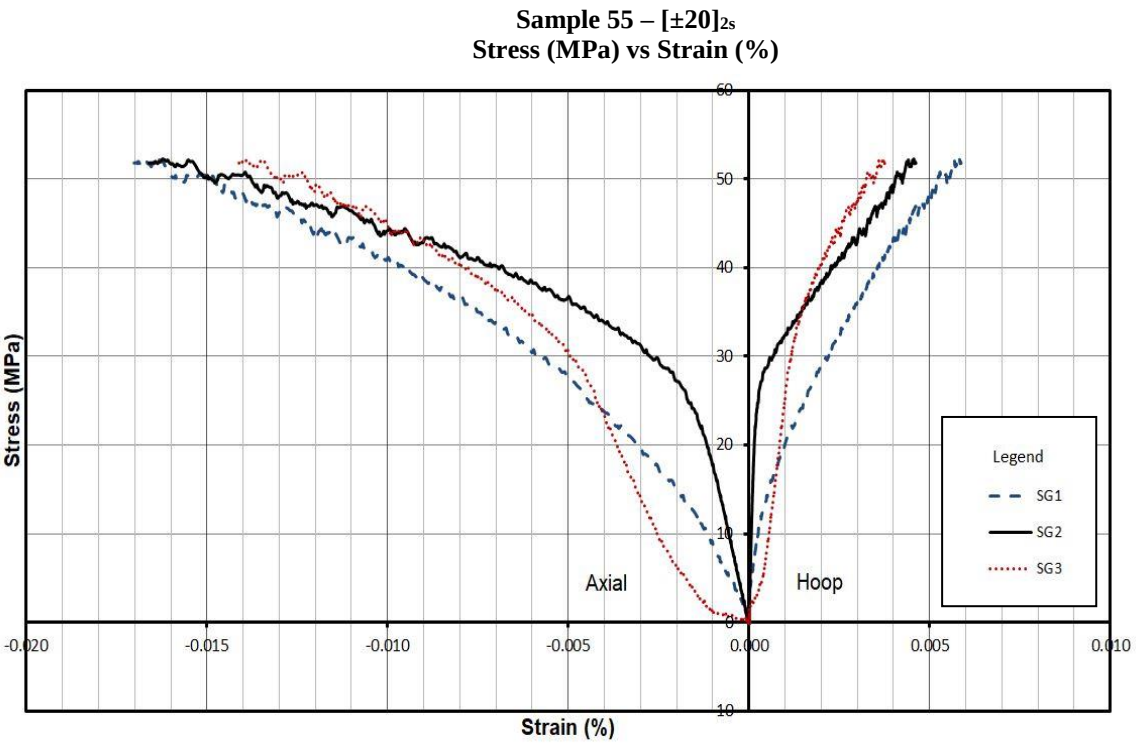

Figure B.28 – Stress (MPa) vs Strain (%) – Stacking Sequence $[\pm 20]_{2s}$ representing readings of Strain Gauges I, II & III for Sample 55.

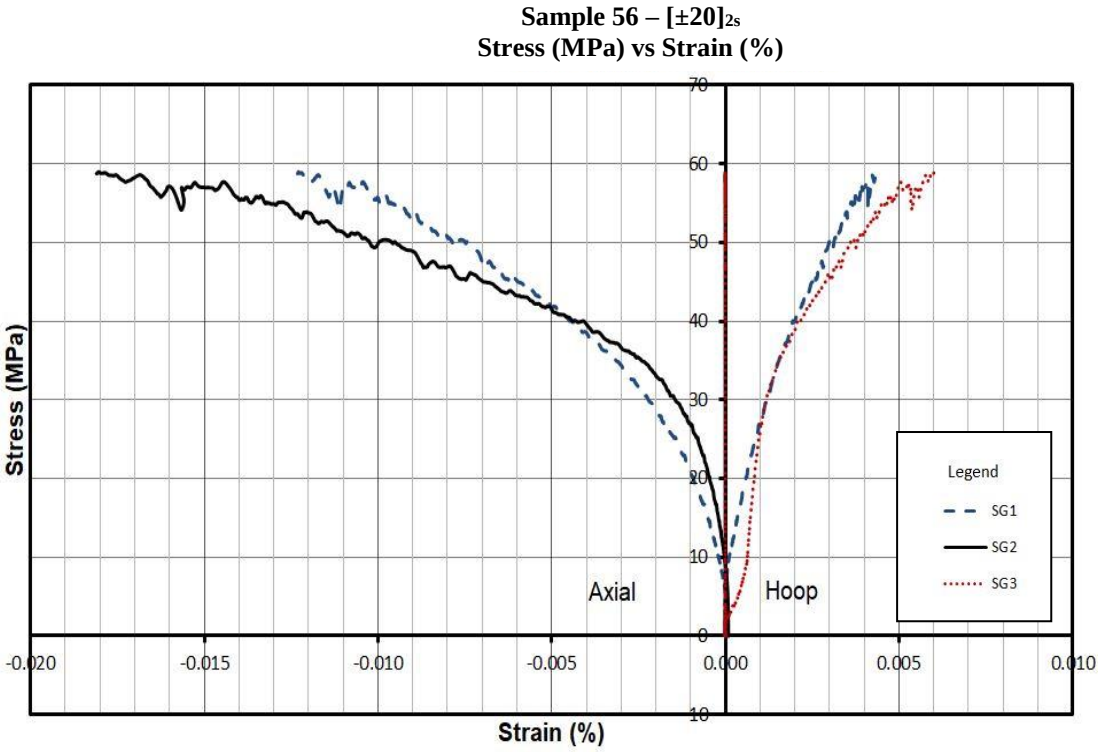

Figure B.29 – Stress (MPa) vs Strain (%) – Stacking Sequence $[\pm 20]_{2s}$ representing readings of Strain Gauges I, II & III for Sample 56.

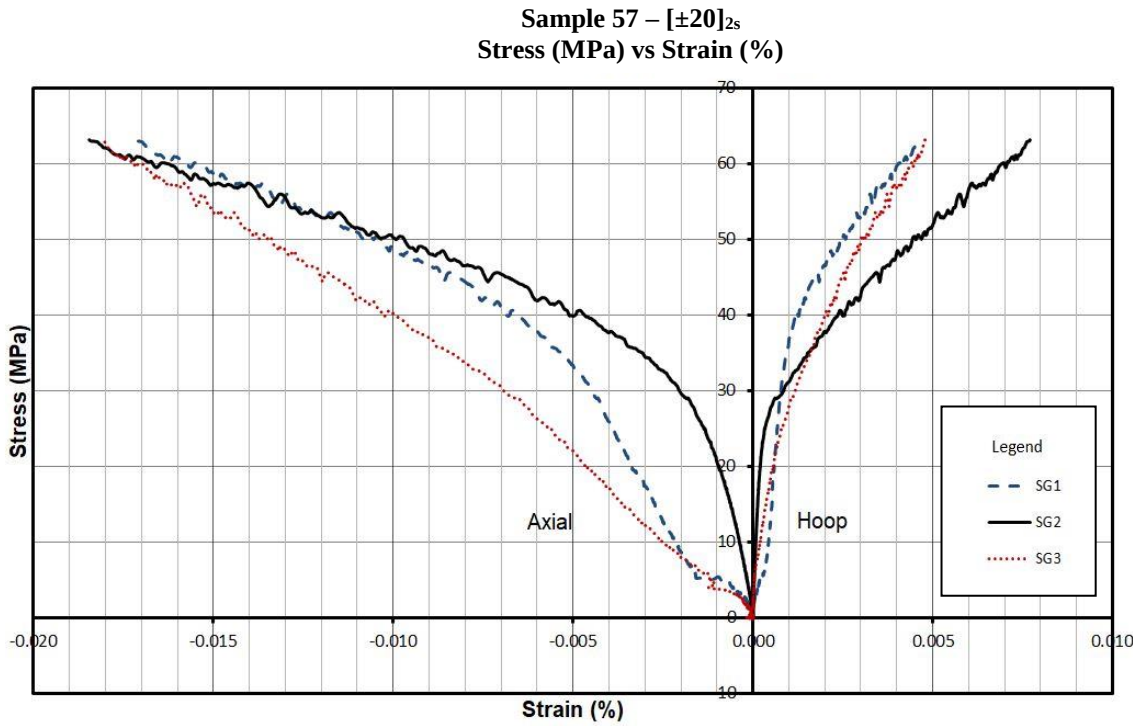

Figure B.30 – Stress (MPa) vs Strain (%) – Stacking Sequence $[\pm 20]_{2s}$ representing readings of Strain Gauges I, II & III for Sample 57.

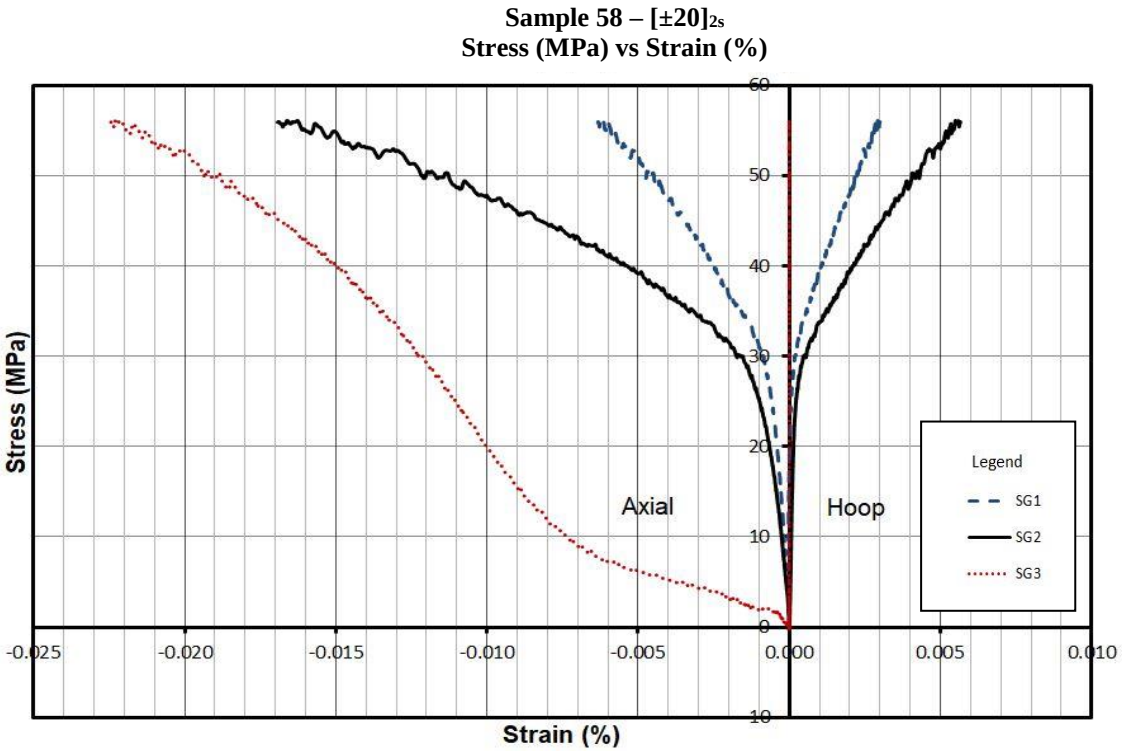

Figure B.31 – Stress (MPa) vs Strain (%) – Stacking Sequence $[\pm 20]_{2s}$ representing readings of Strain Gauges I, II & III for Sample 58.

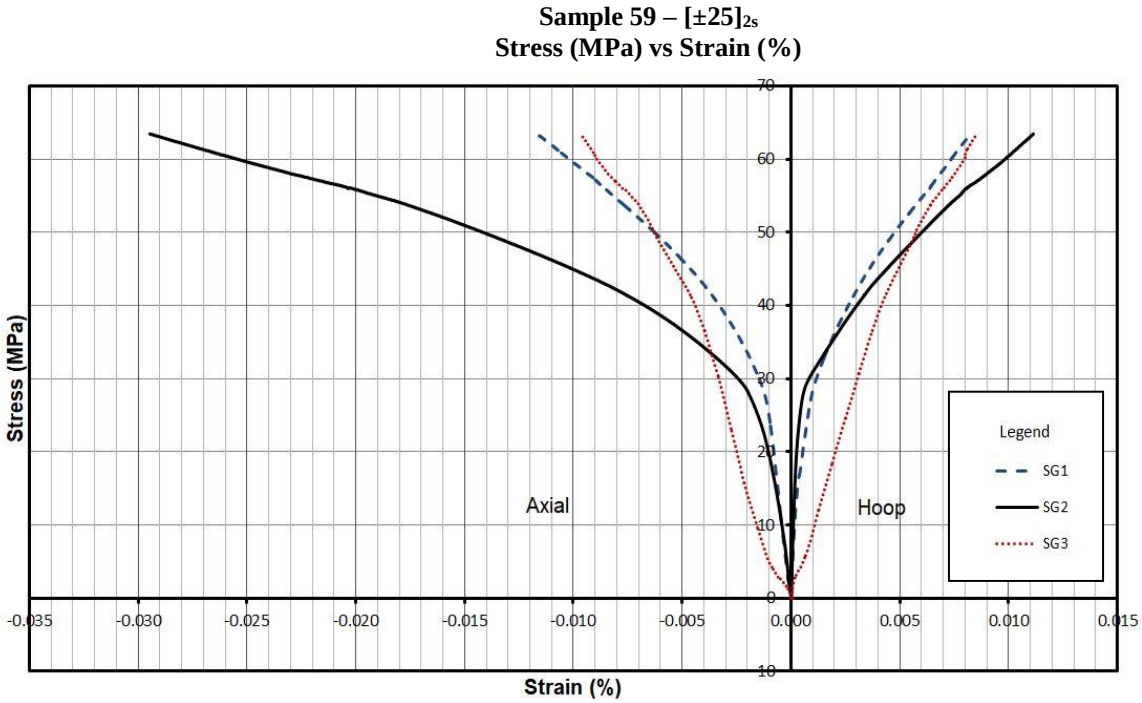

Figure B.32 – Stress (MPa) vs Strain (%) – Stacking Sequence $[\pm 25]_{2s}$ representing readings of Strain Gauges I, II & III for Sample 59.

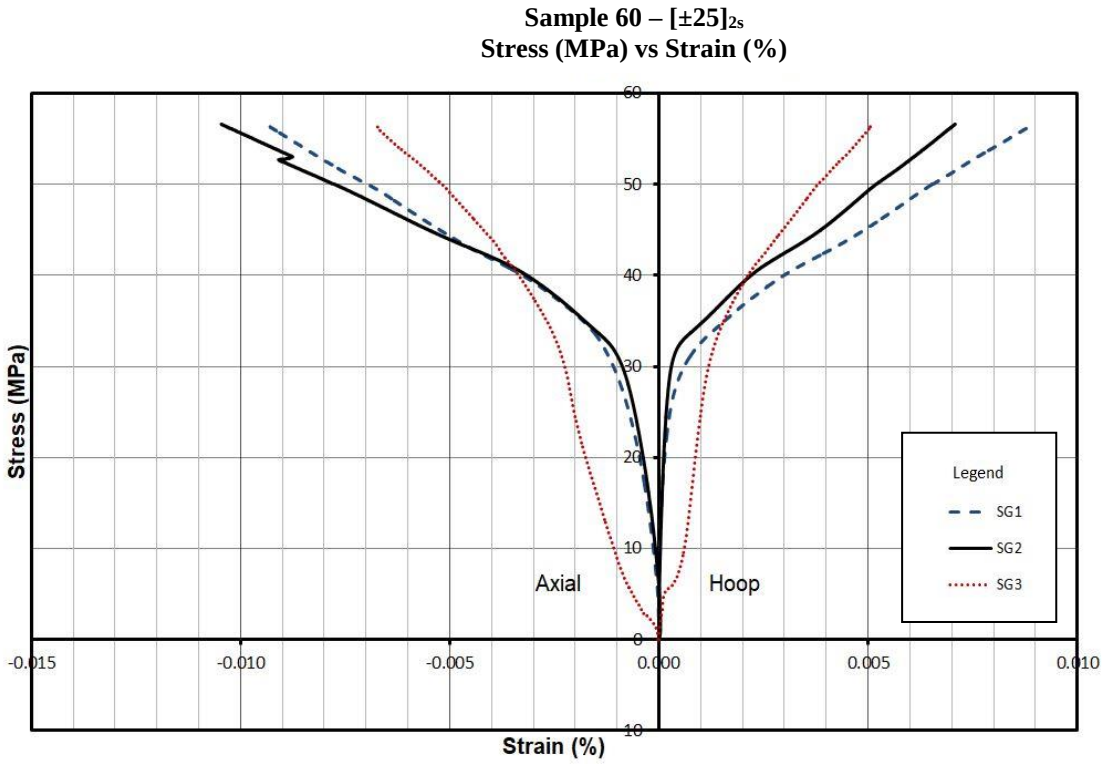

Figure B.33 – Stress (MPa) vs Strain (%) – Stacking Sequence $[\pm 25]_{2s}$ representing readings of Strain Gauges I, II & III for Sample 60.

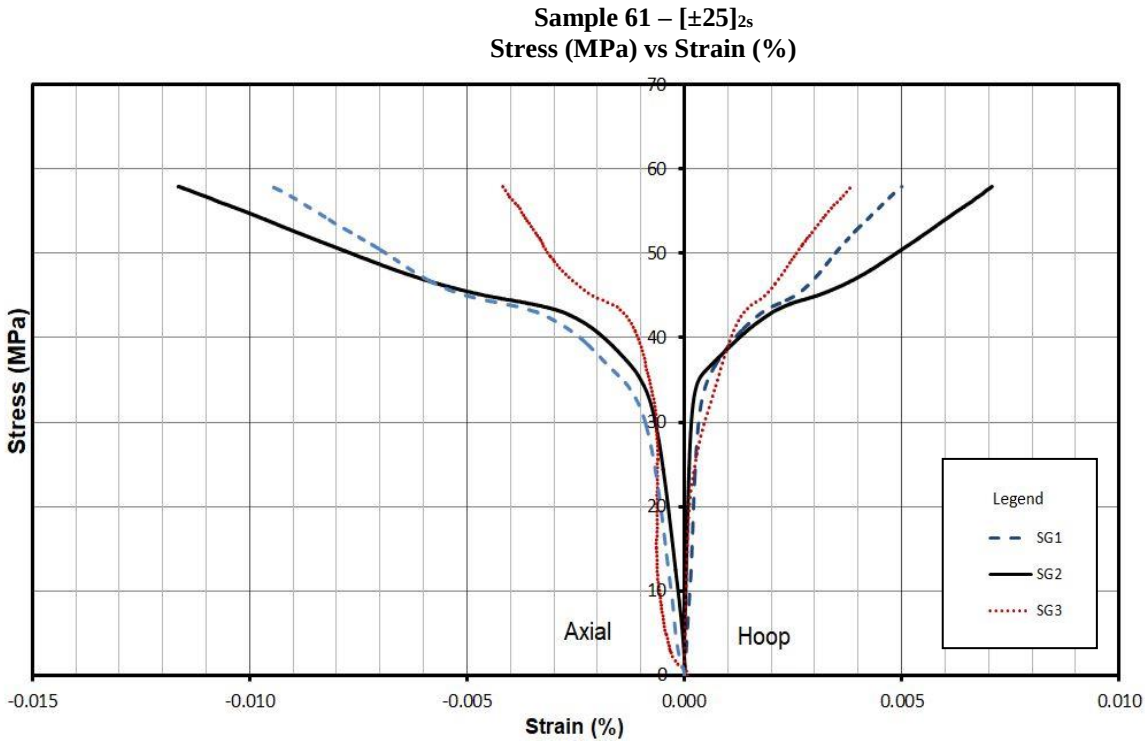

Figure B.34 – Stress (MPa) vs Strain (%) – Stacking Sequence $[\pm 25]_{2s}$ representing readings of Strain Gauges I, II & III for Sample 61.

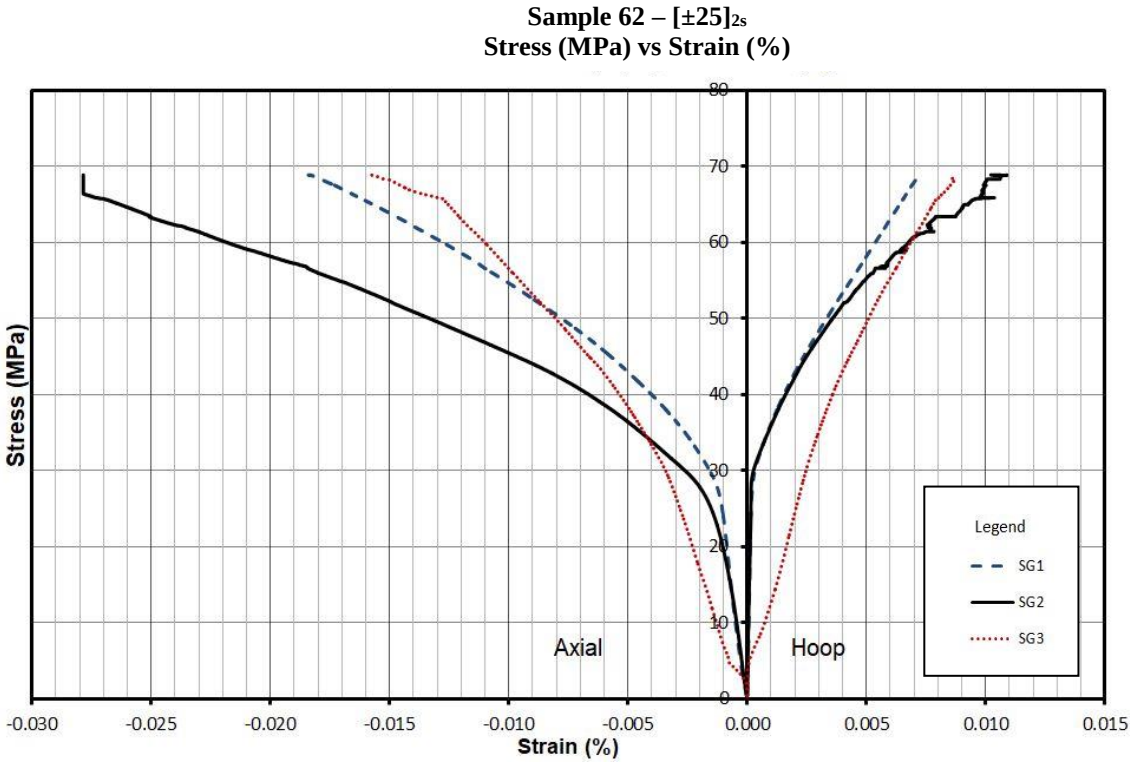

Figure B.35 – Stress (MPa) vs Strain (%) – Stacking Sequence $[\pm 25]_{2s}$ representing readings of Strain Gauges I, II & III for Sample 62.

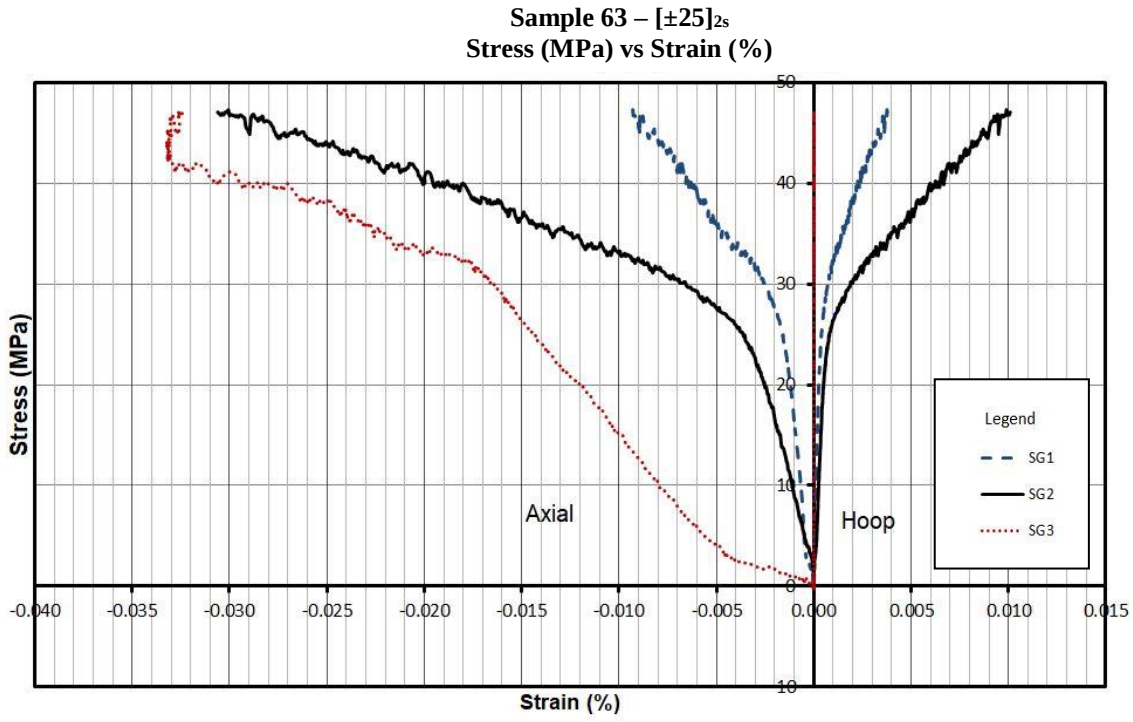

Figure B.36 – Stress (MPa) vs Strain (%) – Stacking Sequence $[\pm 25]_{2s}$ representing readings of Strain Gauges I, II & III for Sample 63.

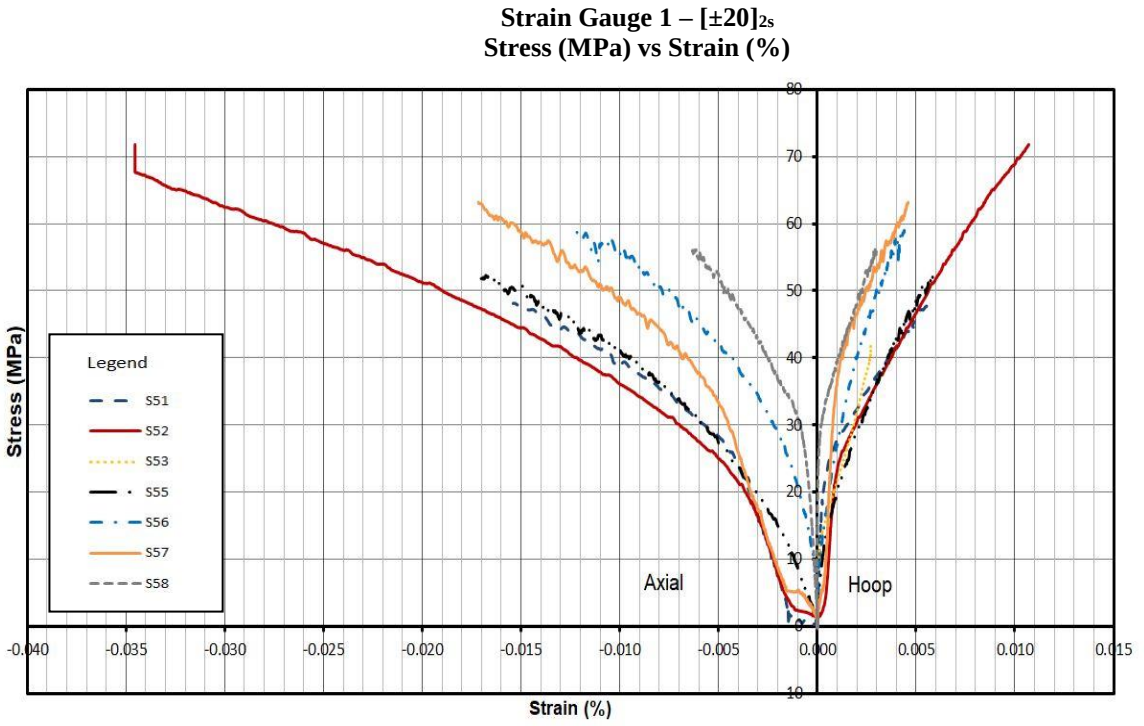

Figure B.37 – Stress (MPa) vs Strain (%) – Stacking Sequence $[\pm 20]_{2s}$ representing readings of Strain Gauge 1 for all cylinders tested – Cylinder Set I.

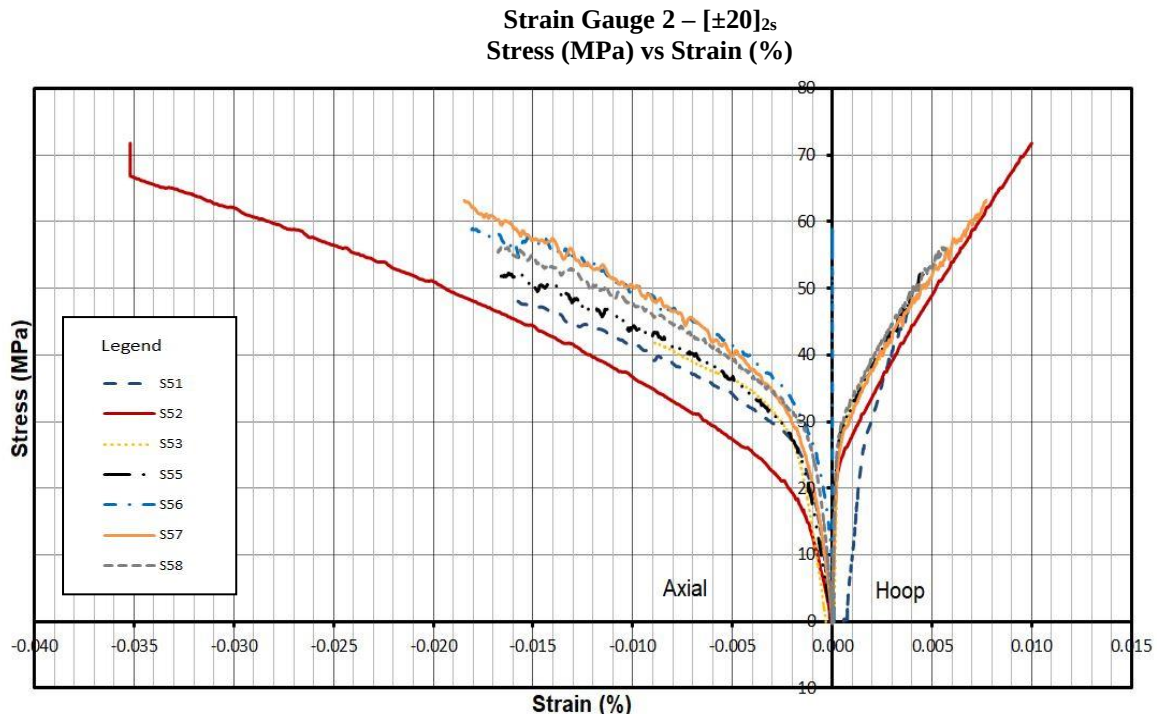

Figure B.38 – Stress (MPa) vs Strain (%) – Stacking Sequence $[\pm 20]_{2s}$ representing readings of Strain Gauge 2 for all cylinders tested – Cylinder Set I.

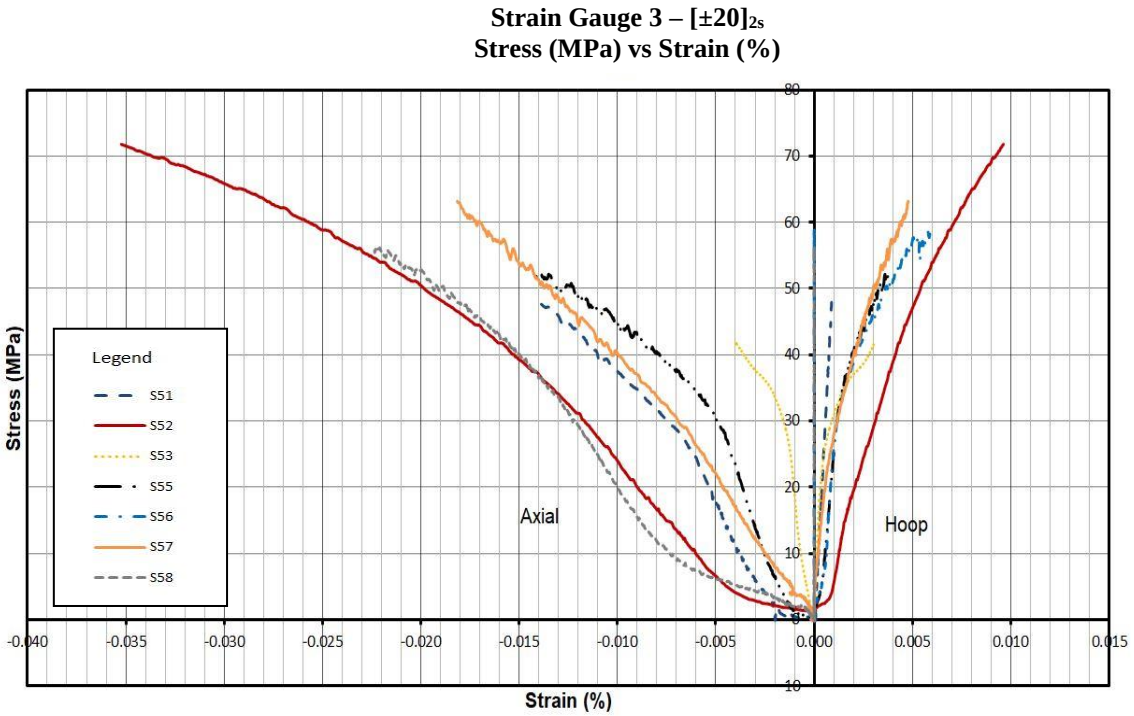

Figure B.39 – Stress (MPa) vs Strain (%) – Stacking Sequence $[\pm 20]_{2s}$ representing readings of Strain Gauge 3 for all cylinders tested – Cylinder Set I.

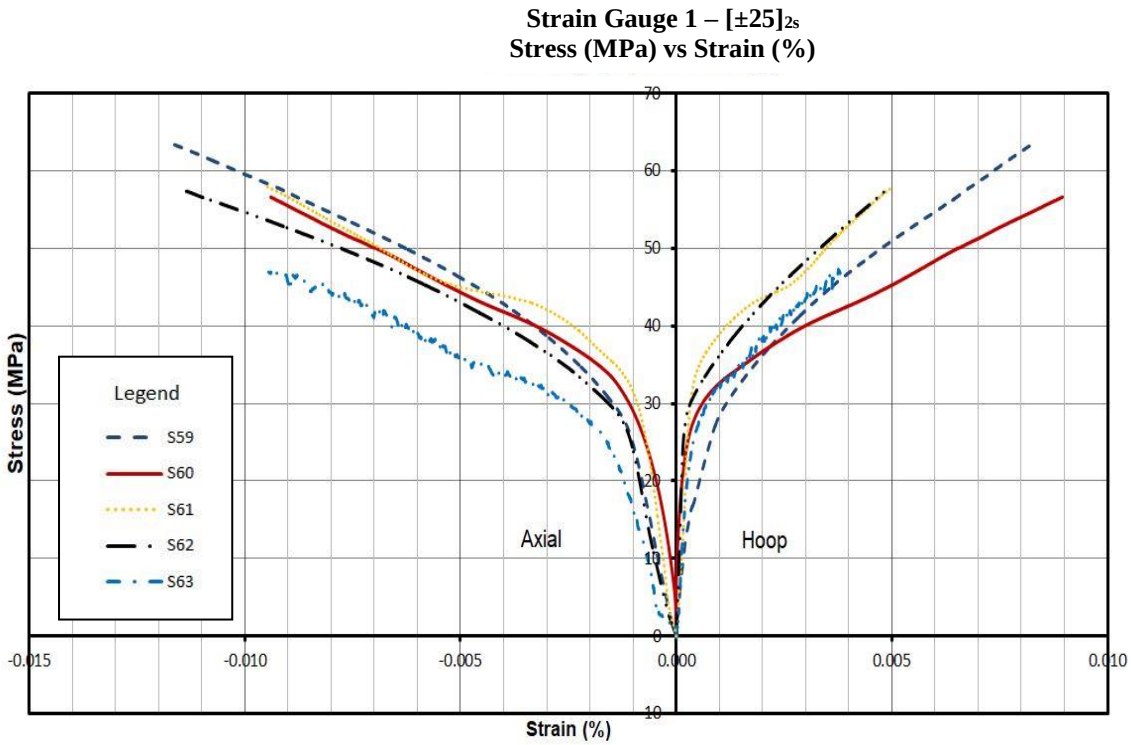

Figure B.40 – Stress (MPa) vs Strain (%) – Stacking Sequence $[\pm 25]_{2s}$ representing readings of Strain Gauge 1 for all cylinders tested – Cylinder Set I.

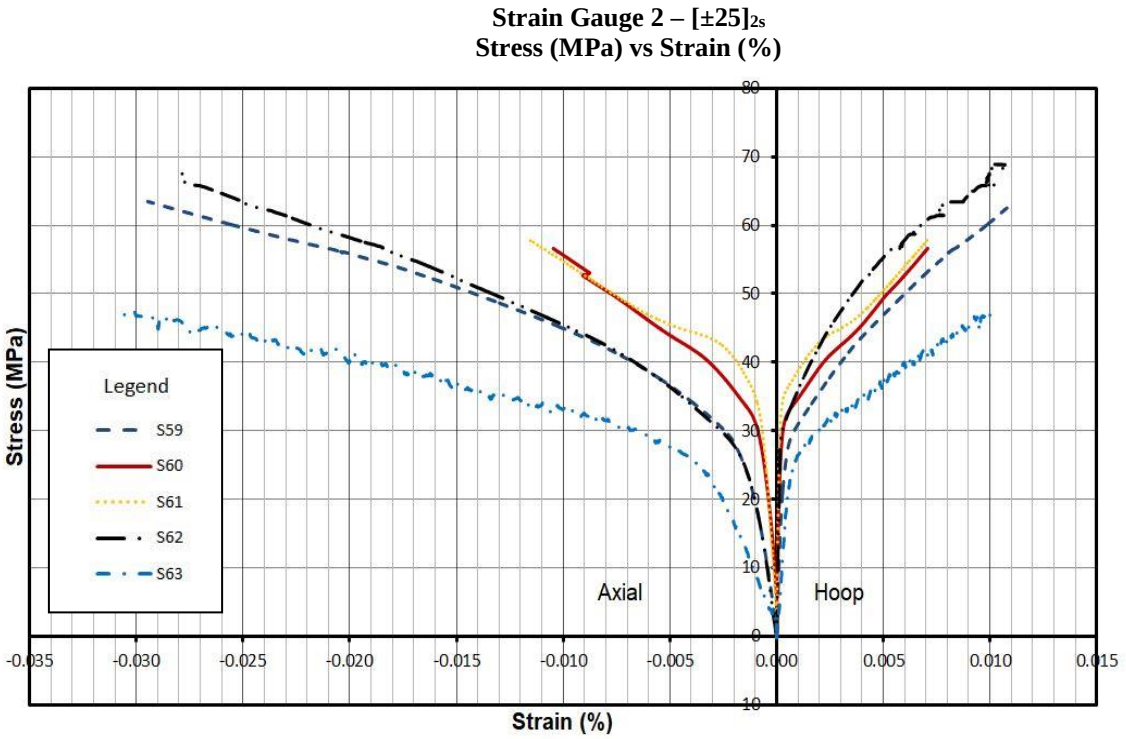

Figure B.41 – Stress (MPa) vs Strain (%) – Stacking Sequence $[\pm 25]_{2s}$ representing readings of Strain Gauge 2 for all cylinders tested – Cylinder Set I.

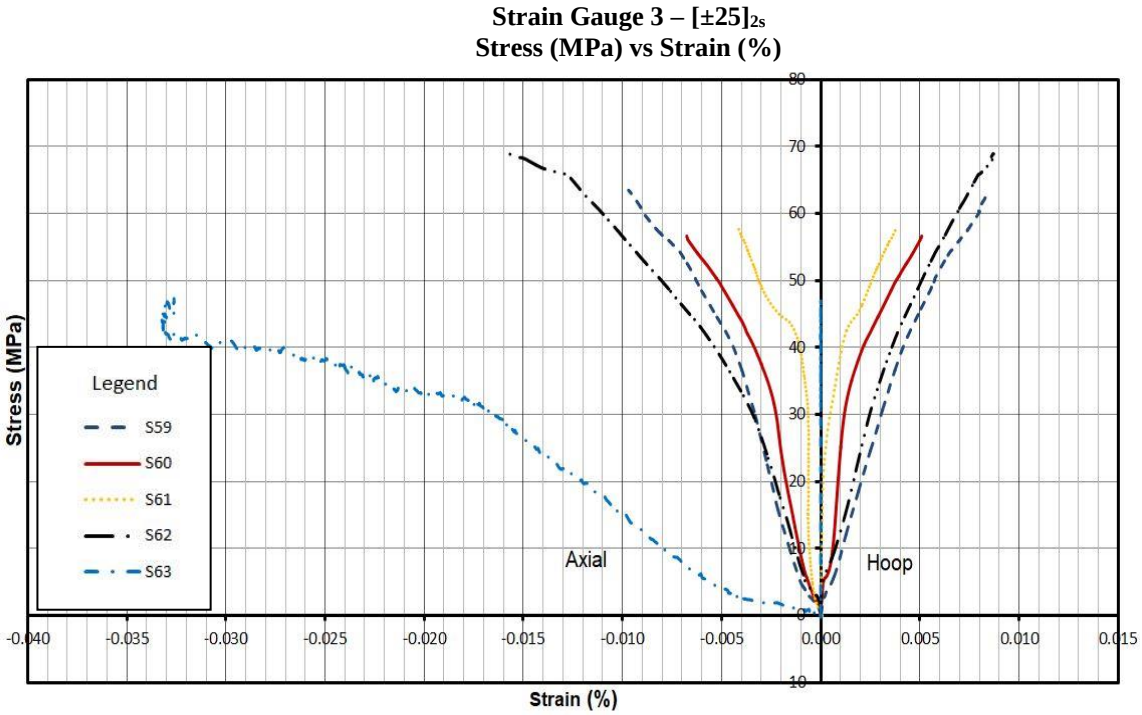

Figure B.42 – Stress (MPa) vs Strain (%) – Stacking Sequence $[\pm 25]_{2s}$ representing readings of Strain Gauge 3 for all cylinders tested – Cylinder Set I.

APPENDIX C

CYLINDER SETS I & II:
PHOTOGRAPHIC REPRESENTATION
OF FAILURE MODES
OF TESTED CYLINDERS

Concrete Cylinders Set I – Cylinders Not Heated

Figure C.1 Cylinder 1 Group A

Figure C.2 Cylinder 1 Group A

Figure C.3 Cylinder 2 Group A

Figure C.4 Cylinder 2 Group A

Figure C.5 Cylinder 3 Group B

Figure C.6 Cylinder 3 Group B

Figure C.7 Cylinder 4 Group B

Figure C.8 Cylinder 4 Group B

Figure C.9 Cylinder 5 Group C

Concrete Cylinders Set I – Cylinders Not Heated

Figure C.10 Cylinder 5 Group C

Figure C.11 Cylinder 6 Group C

Figure C.12 Cylinder 6 Group C

Figure C.13 Cylinder 7 Group D

Figure C.14 Cylinder 7 Group D

Figure C.15 Cylinder 8 Group D

Figure C.16 Cylinder 8 Group D

Figures C.1 – C.16 – The photos show the failure modes of the unheated and unwrapped concrete cylinders when compressed. Two cylinders per set were tested. The cylinders were loaded at a rate of 1kN/sec. Some failed by vertical cracks whereas others show diagonal fractures. Side fractures at time are also visible.

Concrete Cylinders Set I – Cylinders Heated

Figure C.17 Cylinder 9 Group A

Figure C.18 Cylinder 9 Group A

Figure C.19 Cylinder 10 Group A

Figure C.20 Cylinder 10 Group A

Figure C.21 Cylinder 11 Group B

Figure C.22 Cylinder 11 Group B

Figure C.23 Cylinder 12 Group B

Figure C.24 Cylinder 12 Group B

Figure C.25 Cylinder 13 Group C

Concrete Cylinders Set I – Cylinders Heated

Figure C.26 Cylinder 13 Group C

Figure C.27 Cylinder 14 Group C

Figure C.28 Cylinder 14 Group C

Figure C.29 Cylinder 15 Group D

Figure C.30 Cylinder 15 Group D

Figure C.31 Cylinder 16 Group D

Figure C.32 Cylinder 16 Group D

Figures C.17 – C.32 – The photos show the failure modes of the heated and unwrapped concrete cylinders when compressed. These concrete cylinders were heated at 70°C for 20 hours. Two cylinders per set were tested. The cylinders were loaded at a rate of 1kN/sec. Some failed by vertical cracks whereas others show diagonal fractures.

Cylinder 17
ST 1 – SET I

Figure C.33

Figure C.34

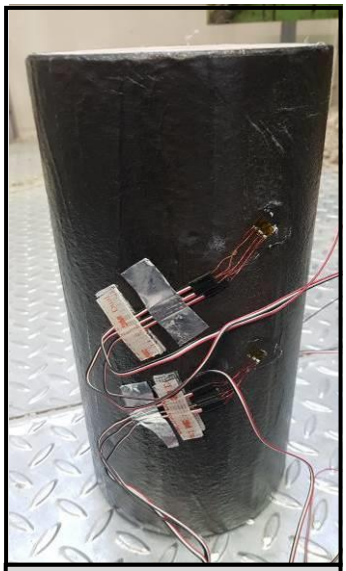

Figure C.35

Figure C.36

Figure C.37

Figure C.38

Figure C.39

Figure C.40

Figures C.33 – C.35 show Sample 17 prior to testing. The jacket has a smooth surface. No particular defects are visible.
Figures C.36 – C.40 depict the failure of the cylinder. An explosive failure occurred and the jacket ended up in parts. A vertical (i.e. axial failure) as well as fibre delamination was noted.

Cylinder 18
ST 1 – SET I

Figure C.41

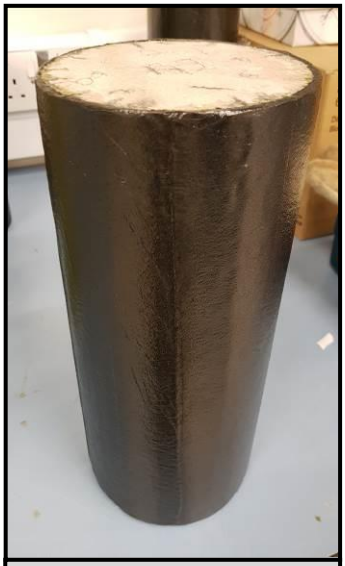

Figure C.42

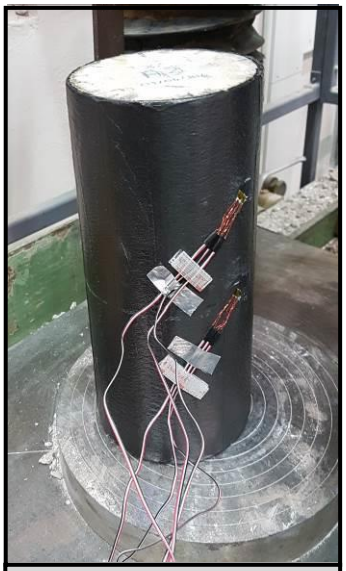

Figure C.43

Figure C.44

Figure C.45

Figure C.46

Figure C.47

Figure C.48

Figures C.41 – C.43 show Sample 18 prior to testing.

Figures C.44 – C.48 depict the presence of the back sheet that was erroneously not removed. The cylinder failed prematurely.

Cylinder 19
ST 1 – SET I

Figure C.49

Figure C.50

Figure C.51

Figure C.52

Figure C.53

Figure C.54

Figure C.55

Figure C.56

Figures C.49 – C.51 show Sample 19 prior to testing. A few vertical creases are visible.

Figures C.52 – C.56 depict the failure mode of the sample. A vertical failure is predominant. The failure was explosive.

Cylinder 20
ST 1 – SET I

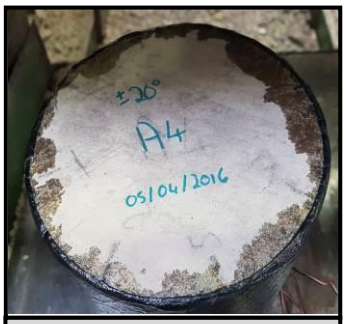

Figure C.57

Figure C.58

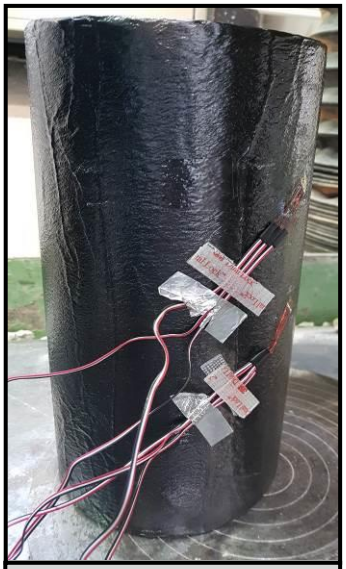

Figure C.59

Figure C.60

Figure C.61

Figure C.62

Figure C.63

Figure C.64

Figures C.57 – C.59 show Sample 20 prior to testing. A relatively smooth surface is visible. Yet, the presence of a few air bubbles was noted.

Figures C.60 – C.64 depict the explosive failure mode. An axial failure is visible. Fibre delaminations are seen.

Cylinder 21
ST 2 – SET I

Figure C.65

Figure C.66

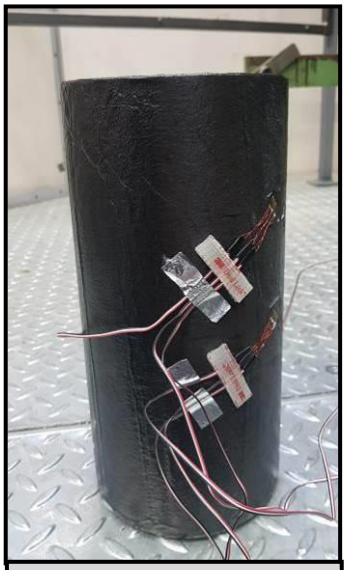

Figure C.67

Figure C.68

Figure C.69

Figure C.70

Figure C.71

Figure C.72

Figures C.65 – C.67 show Sample 21 prior to testing. A relatively smooth surface is visible.

Figures C.68 – C.72 depict the explosive failure mode. A predominant axial failure is noted. Fibre delaminations are noted.

Cylinder 22
ST 2 – SET I

Figure C.73

Figure C.74

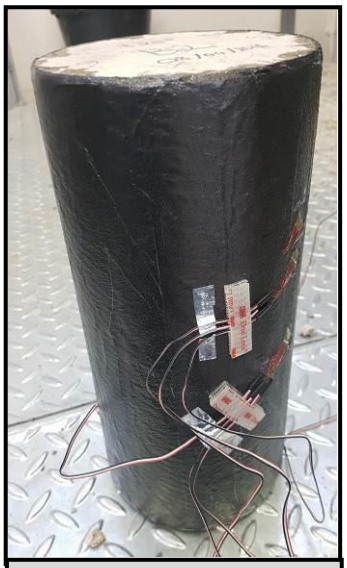

Figure C.75

Figure C.76

Figure C.77

Figure C.78

Figure C.79

Figure C.80

Figures C.73 – C.75 show Sample 22 prior to testing. A relatively smooth surface is visible.

Figures C.76 – C.80 depict the failure mode. Once again a predominant axial failure is noted and fibre delaminations are also visible.

Cylinder 23
ST 2 – SET I

Figure C.81

Figure C.82

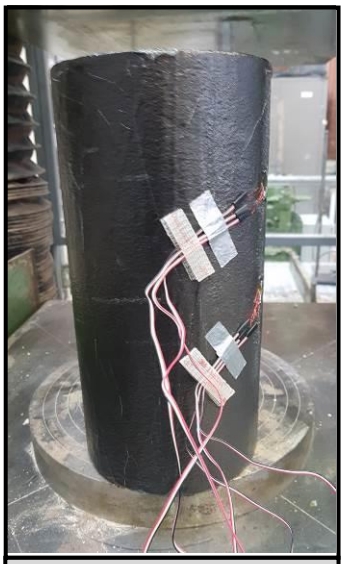

Figure C.83

Figure C.84

Figure C.85

Figure C.86

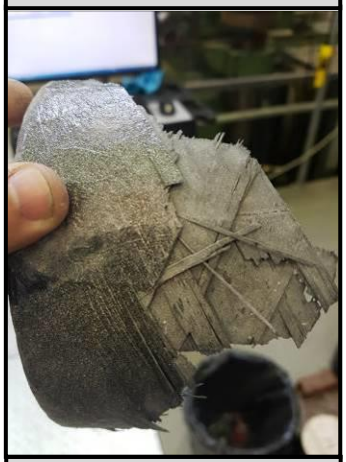

Figure C.87

Figure C.88

Figures C.81 – C.83 show Sample 23 prior to testing. A smooth surface is visible.

Figures C.84 – C.88 depict the explosive failure mode of the sample. The concrete is completely crushed. A predominant axial failure is noted and fibre delaminations are visible.

Cylinder 24
ST 2 – SET I

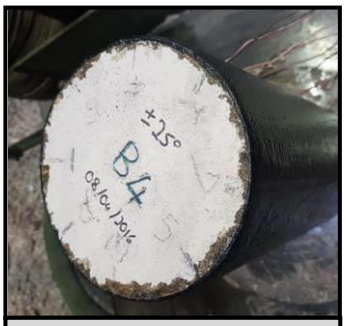

Figure C.89

Figure C.90

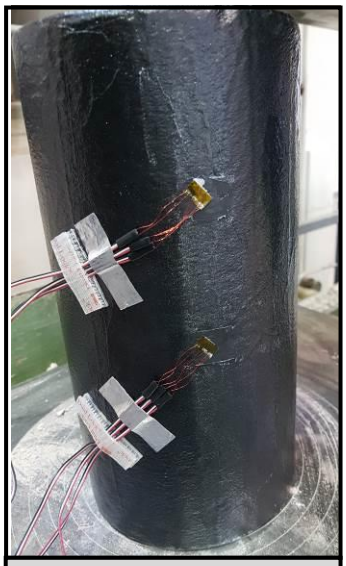

Figure C.91

Figure C.92

Figure C.93

Figure C.94

Figure C.95

Figure C.96

Figures C.89 – C.91 show Sample 24 prior to testing. A few vertical creases are visible.

Figures C.92 – C.96 depict the explosive failure mode of the sample. The concrete is completely crushed. A predominant axial failure is noted and fibre delaminations are visible.

Cylinder 25
ST 5 – SET I

Figure C.97

Figure C.98

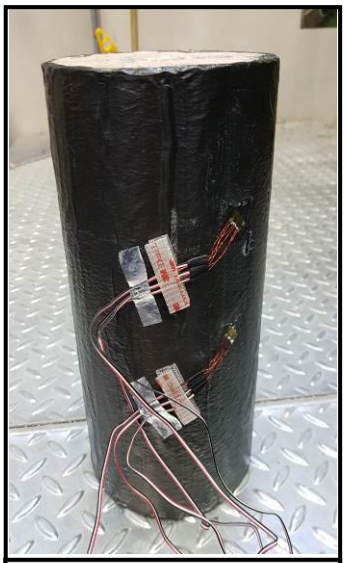

Figure C.99

Figure C.100

Figure C.101

Figure C.102

Figure C.103

Figure C.104

Figures C.97 – C.99 show Sample 25 prior to testing. A few vertical creases are visible.

Figures C.100 – C.104 depict the failure mode of the sample. A vertical axial failure is noted and seemed to happen in the crease.

Cylinder 26
ST 5 – SET I

Figure C.105

Figure C.106

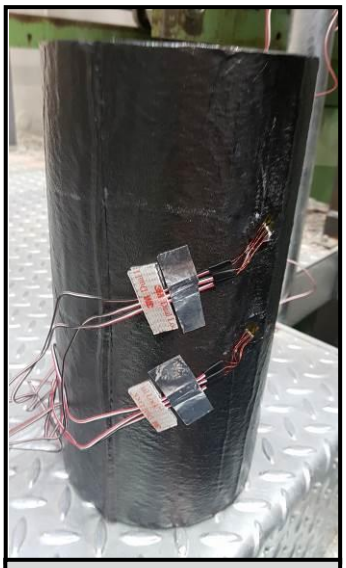

Figure C.107

Figure C.108

Figure C.109

Figure C.110

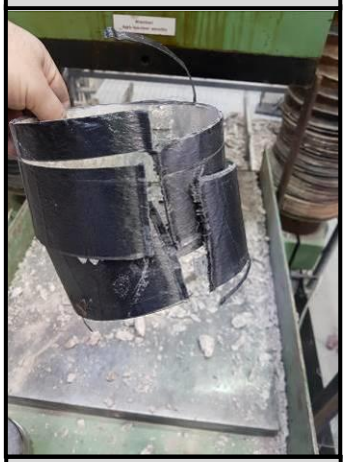

FigureC.111

Figure C.112

Figures C.105 – C.107 show Sample 26 prior to testing. A relatively smooth surface is visible.

Figures C.108 – C.112 depict the failure mode of the sample. The concrete cylinder is crushed and an axial failure is visible.

Cylinder 27
ST 5 – SET I

Figure C.113

Figure C.114

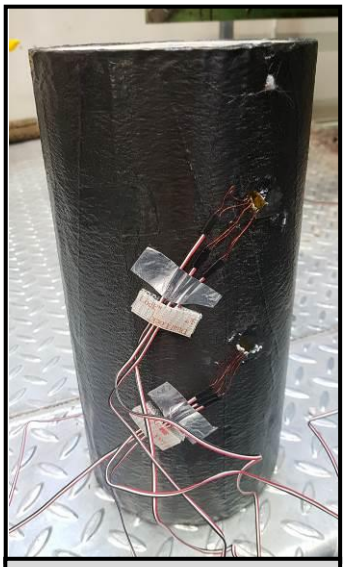

Figure C.115

Figure C.116

Figure C.117

Figure C.118

Figure C.119

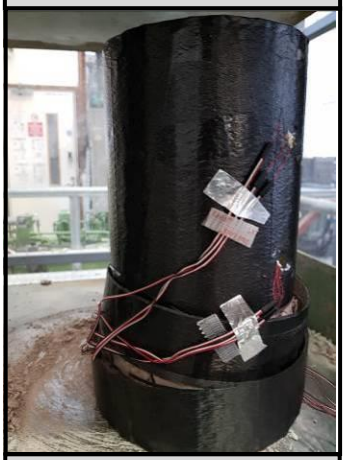

Figure C.120

Figures C.113 – C.115 show Sample 27 prior to testing. A few vertical creases are noted.

Figures C.116 – C.120 depict the failure mode of the sample. The failure occurred in the bottom third of the cylinder and consequently the crushed concrete fell out.

Cylinder 28
ST 5 – SET I

Figure C.121

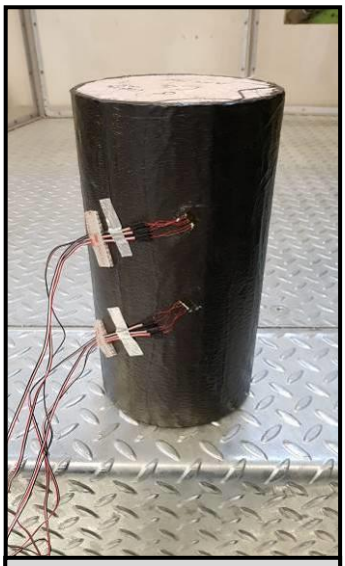

Figure C.122

Figure C.123

Figure C.124

Figure C.125

Figure C.126

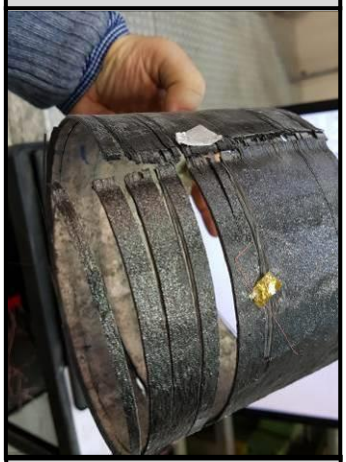

Figure C.127

Figure C.128

Figures C.121 – C.123 show Sample 28 prior to testing. A relatively smooth surface is visible

Figures C.124 – C.128 depict the failure mode of the sample. A similar failure as Sample 27 occurred. Yet, this time the failure occurred in the top third of the jacket.

Cylinder 29
ST 5 – SET I

Figure C.129

Figure C.130

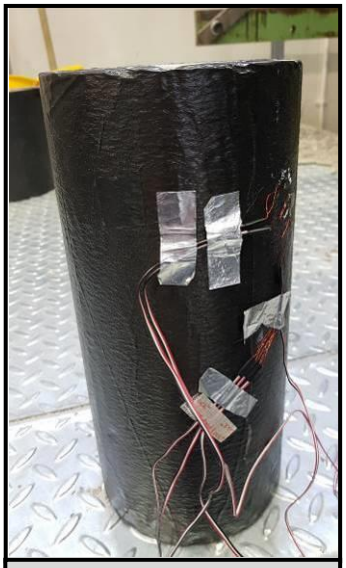

Figure C.131

Figure C.132

Figure C.133

Figure C.134

Figure C.135

Figure C.136

Figures C.129 – C.131 show Sample 29 prior to testing. A smooth surface is visible.

Figures C.132 – C.136 depict the failure mode of the sample. As shown in Figure C.133, there is an axial failure. Concentric failures in the direction of the fibres are visible.

Cylinder 30
ST 6 – SET I

Figure C.137

Figure C.138

Figure C.139

Figure C.140

Figure C.141

Figure C.142

Figure C.143

Figure C.144

Figures C.137 – C.139 show Sample 30 prior to testing. A smooth surface is noted.

Figures C.140 – C.144 depict the failure mode of the sample. A vertical failure in the direction of the fibre was noted. Failure occurred before the actual failure of the concrete.

Cylinder 31
ST 6 – SET I

Figure C.145

Figure C.146

Figure C.147

Figure C.148

Figure C.149

Figure C.150

Figure C.151

Figure C.152

Figures C.145 – C.147 show Sample 31 prior to testing. A smooth surface is noted.

Figures C.148 – C.152 depict the failure mode of the sample. A clear vertical failure in the direction of the fibre is noted. Failure occurred before the actual failure of the concrete.

Cylinder 32
ST 6 – SET I

Figure C.153

Figure C.154

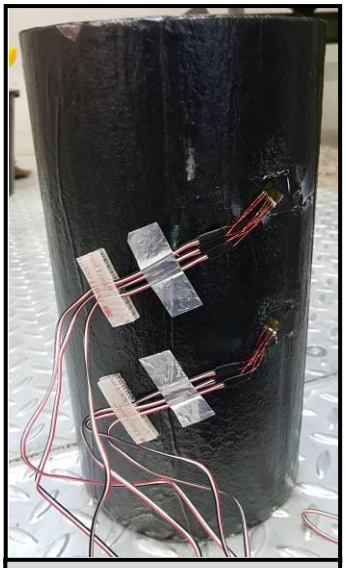

Figure C.155

Figure C.156

Figure C.157

Figure C.158

Figure C.159

Figure C.160

Figures C.153 – C.155 show Sample 32 prior to testing. A smooth surface is noted.

Figs C.156 – C.160 depict the failure mode of the sample. Failure occurred in the direction of the fibre.

Cylinder 33
ST 6 – SET I

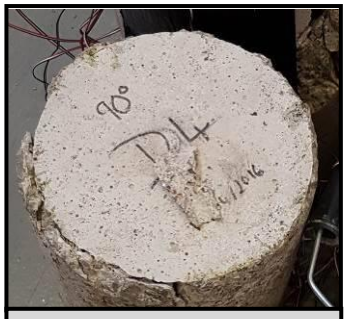

Figure C.161

Figure C.162

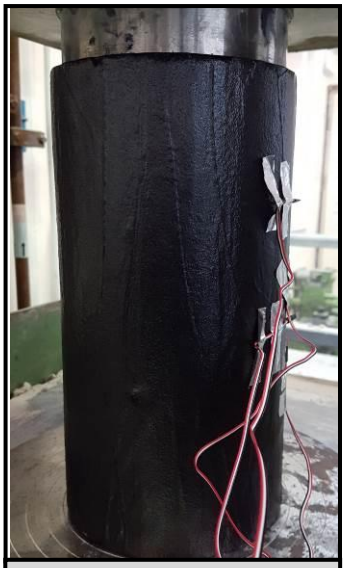

Figure C.163

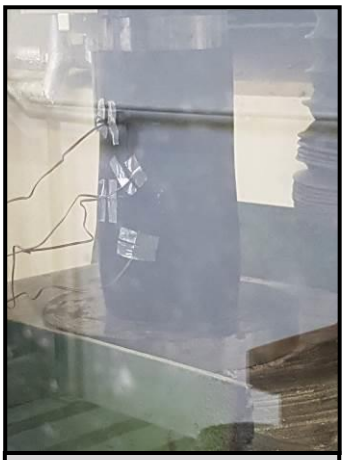

Figure C.164

Figure C.165

Figure C.166

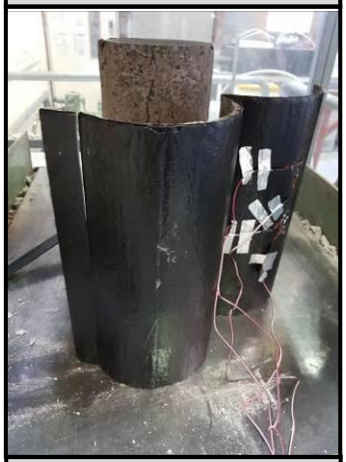

Figure C.167

Figure C.168

Figures C.161 – C.163 show Sample 33 prior to testing. A smooth surface is noted.

Figures C.164 – C.168 depict the failure mode of the sample. The angles of the fibre are in the same direction as the applied force. So, as visible failure occurred in the direction of the fibre.

Cylinder 34
ST 6 – SET I

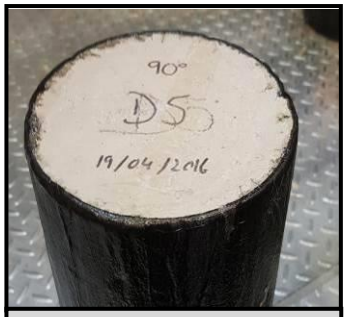

Figure C.169

Figure C.170

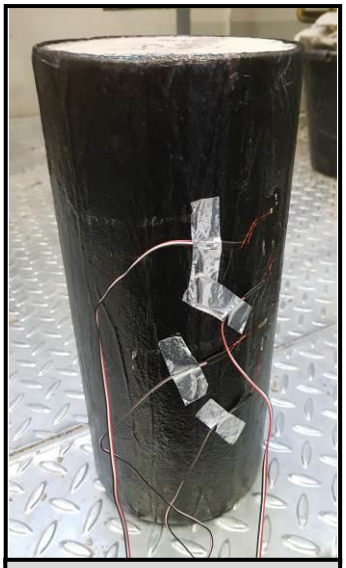

Figure C.171

Figure C.172

Figure C.173

Figure C.174

Figures C.169 – C.171 show Sample 34 prior to testing. A smooth surface is noted.

Figures C.172– C.174 depict the failure mode of the sample. The angles of the fibre are in the same direction as the applied force. As shown in Figure C.172, the jacket follows the shape of the concrete until failure.

Cylinder 35
ST 3 – SET I

Figure C.175

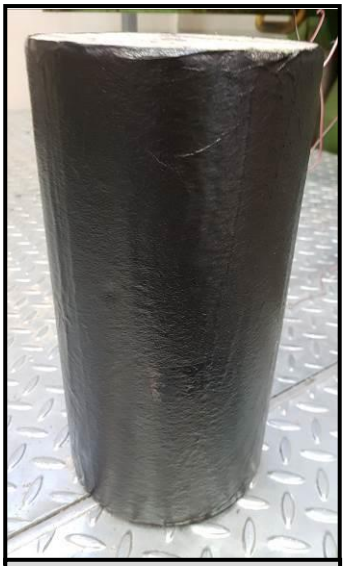

Figure C.176

Figure C.177

Figure C.178

Figure C.179

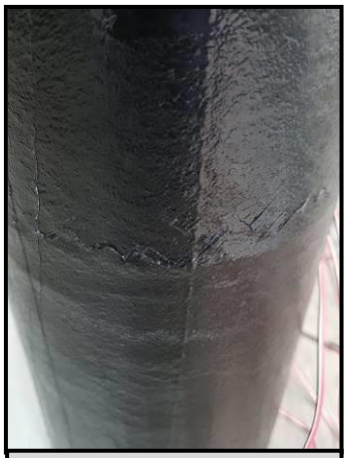

Figure C.180

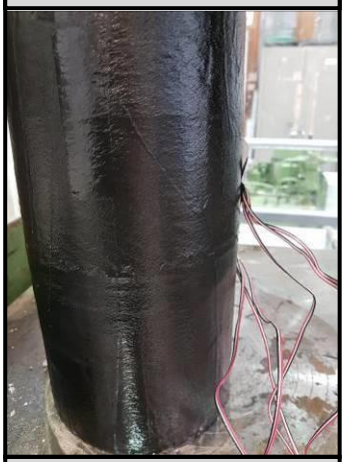

Figure C.181

Figure .C.182

Figures C.175 – C.177 show Sample 35 prior to testing. No creases are visible in the jacket.

Figures C.178 – C.182 depict the failure of the sample. As shown in Figure C.181, there was an axial failure that occurred at the bottom of the cylinder.

Cylinder 36
ST 3 – SET I

Figure C.183

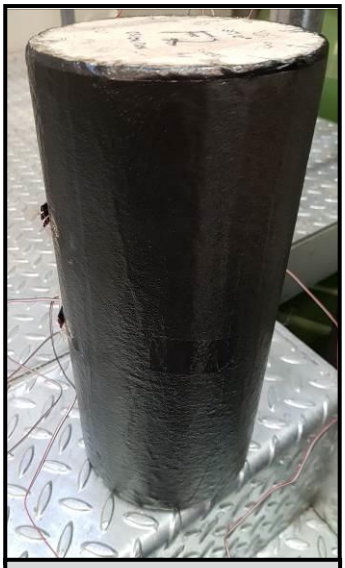

Figure C.184

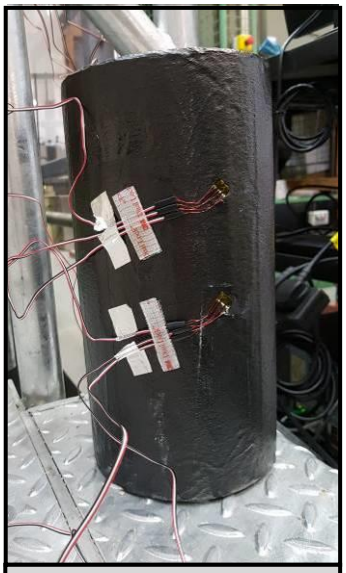

Figure C.185

Figure C.186

Figure C.187

Figure C.188

Figure C.189

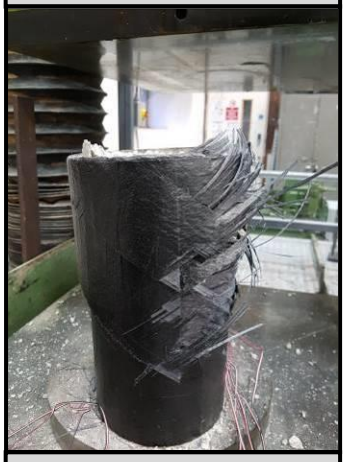

Figure C.190

Figures C.183 – C.185 show Sample 36 prior to testing. Minor creases are visible in the jacket.

Figures C.186 – C.190 depict the failure of the sample. The jacket failed abruptly once the maximum strength was reached.

Cylinder 37
ST 3 – SET I

Figure C.191

Figure C.192

Figure C.193

Figure C.194

Figure C.195

Figure C.196

Figure C.197

Figure C.198

Figures C.191 – C.193 show Sample 37 prior to testing. Minor creases are visible in the jacket.

Figures C.194– C.198 depict the failure of the sample. As depicted in Figures C.194 and C.195, failure occurred in the centre of the jacket. Fibre detachments are visible.

Cylinder 38
ST 4 – SET I

Figure C.199

Figure C.200

Figure C.201

Figure C.202

Figure C.203

Figure C.204

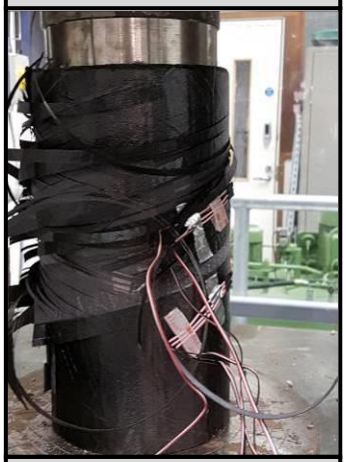

Figure C.205

Figure C.206

Figures C.199 – C.201 show Sample 38 prior to testing. A smooth surface is visible.

Figures C.202 – C.206 depict the failure of the sample. Complete fibre detachment is noted.

Cylinder 39
ST 4 – SET I

Figure C.207

Figure C.208

Figure C.209

Figure C.210

Figure C.211

Figure C.212

Figure C.213

Figure C.214

Figures C.207 – C.209 show Sample 39 prior to testing. Minor creases are visible on the surface.

Figures C.210 – C.214 depict the failure of the sample. An axial failure and fibre detachment is noted.

Cylinder 40
ST 4 – SET I

Figure C.215

Figure C.216

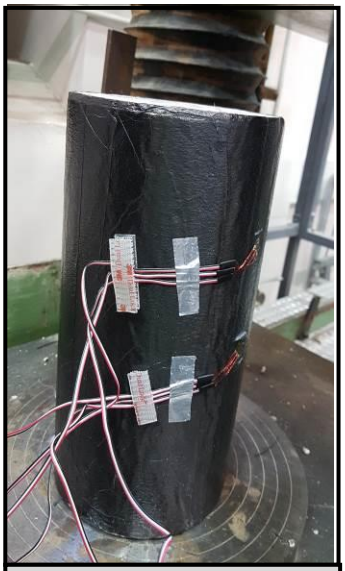

Figure C.217

Figure C.218

Figure C.219

Figure C.220

Figure C.221

Figure C.222

Figures C.215 – C.217 show Sample 40 prior to testing. A smooth surface is visible.

Figures C.218 – C.222 depict the failure of the sample. An axial failure is seen in Fig . C.219. Fibre detachments are also noted.

Concrete Cylinders Set II – Cylinders Not Heated

Figure C.223 Cylinder 41 Group F

Figure C.224 Cylinder 42 Group F

Figure C.225 Cylinder 43 Group G

Figure C.226 Cylinder 43 Group G

Figure C.227 Cylinder 44 Group G

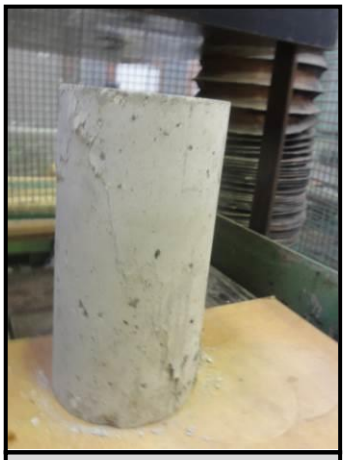

Figure C.228 Cylinder 44 Group G

Figure C.229 Cylinder 45 Group G

Figure C.230 Cylinder 45 Group G

Figures C.223 – C.230 – The photos show the failure modes of the non heated and unwrapped concrete cylinders when compressed. A total of 5 cylinders were tested.

Concrete Cylinders Set II – Cylinders Heated

Figure C.231 Cylinder 46 Group E

Figure C.232 Cylinder 47 Group E

Figure C.233 Cylinder 48 Group E

Figure C.234 Cylinder 48 Group E

Figure C.235 Cylinder 49 Group G

Figure C.236 Cylinder 49 Group G

Figure C.237 Cylinder 50 Group G

Figure C.238 Cylinder 50 Group G

Figures C.231 – C.238 – The photos show the failure of the heated and unwrapped concrete cylinders when compressed. These concrete cylinders were heated at 70°C for 20 hours. A total of 5 cylinders were tested.

Cylinder 51
ST1 - SETII

Figures C.239 & C.240 – show that the jacket has failed in the vertical crease due to the defects in the manufacturing process.

Figure C.239

Figure C.240

Cylinder 52
ST1 - SETII

Figures C.241 & C.242 – show that the jacket has failed in the vertical crease due to the defects in the manufacturing process.

Figure C.241

Figure C.242

Cylinder 53
ST1 –SET II

Figures C.243 & C.244 – show that the jacket has failed in the vertical crease due to the defects in the manufacturing process

Figure C.243

Figure C.244

Cylinder 54
ST1 – SET II

Figures C.245 & C.246 – show that the jacket has failed in the vertical crease due to the defects in the manufacturing process.

Figure C.245

Figure C.246

Cylinder 55
ST1 – SET II

Figures C.247 & C.248 – show that the jacket has failed in the vertical crease due to the defects in the manufacturing process.

Figure C.247

Figure C.248

Cylinder 56
ST1 – SET II

Figures C.249 & C.250 – show that the jacket has failed in the vertical crease due to the defects in the manufacturing process.

Figure C.249

Figure C.250

Cylinder 57
ST1 – SET II

Figures C.251 & C.252 – show that the jacket has failed in the vertical crease due to the defects in the manufacturing process.

Figure C.251

Figure C.252

Cylinder 58
ST1 – SET II

Figures C.253 & C.254 – show that the jacket has failed in the vertical crease due to the defects in the manufacturing process.

Figure C.253

Figure C.254

Cylinder 59
ST 2 – SET II

Figures C.255 & C.256 – show that the jacket has failed in the vertical crease due to the defects in the manufacturing process.

Figure C.255

Figure C.256

Cylinder 60
ST 2 – SET II

Figures C.257 & C.258 – show that the jacket has failed in the vertical crease due to the defects in the manufacturing process.

Figure C.257

Figure C.258

Cylinder 61
ST 2 – SET II

Figures C.259 & C.260 – show that the jacket has failed in the vertical crease due to the defects in the manufacturing process.

Figure C.259

Figure C.260

Cylinder 62
ST 2 – SET II

Figures C.261 & C.262 – show that the jacket has failed in the vertical crease due to the defects in the manufacturing process.

Figure C.261

Figure C.262

Cylinder 63
ST 2 – SET II

Figures C.263 & C.264 – show that the jacket has failed in the vertical crease due to the defects in the manufacturing process.

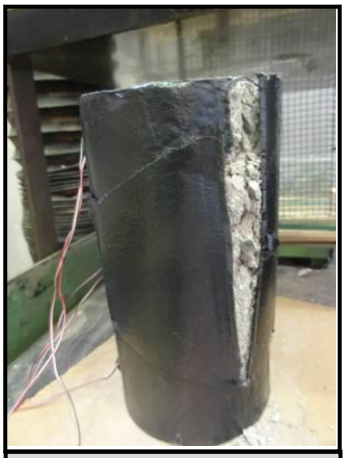

Figure C.263

Figure C.264

Cylinder 64
ST 2 – SET II

Figures C.265 & C.266 – show that the jacket has failed in the vertical crease due to the defects in the manufacturing process.

Figure C.265

Figure C.266

Cylinder 65
ST1 – SET II

Figures C.267 & C.268 – show that the jacket has failed in the vertical crease due to the defects in the manufacturing process.

Figure C.267

Figure C.268

Cylinder 66

ST1 – SET II

Figures C.269 & C.270 – show that the jacket has failed in the vertical crease due to the defects in the manufacturing process.

Figure C.269

Figure C.270